Department Of Physics
Aligarh Muslim University
India

Low And Medium Energy Weak Quasielastic And Pion Production Processes From Nuclei

Thesis
Doctor Of Philosophy

Shakeb Ahmad
2006

Abstract

Of The Thesis Entitled

Low And Medium Energy Weak Quasielastic And Pion Production Processes From Nuclei

Submitted
To
Department Of Physics
Aligarh Muslim University
Aligarh - 202 002, India

In Partial Fulfilment Of The Requirement
For The Degree Of
Doctor Of Philosophy In Physics

By
Shakeb Ahmad

Under The Supervision Of
Prof. S. K. Singh

2006

Contents

Chapter 1

Introduction

The study of weak quasielastic and pion production processes in the low and intermediate energy region is an interesting subject in itself, but the recent interest in the weak production of leptons and pions due to their importance in the neutrino oscillation experiments has started considerable activities in this field. The neutrino experiments done in last few years have given conclusive evidence for the existence of neutrino oscillations. These neutrino oscillation experiments are being performed in the low energy as well as in the intermediate energy region of neutrino energies using detectors which use materials with nuclei like ^{12}C, ^{16}O, ^{38}Ar, ^{56}Fe and ^{208}Pb etc., as targets. Even though most of these experiments are done in nuclei, no serious attempts have been made to study nuclear effects and their possible influence on the weak pion production cross section. In these energy regions, the processes which contribute to the lepton and pion production are quasielastic processes, inelastic processes where few resonances are excited and the deep inelastic processes. It is therefore, desirable, that nuclear effects in the neutrino(antineutrino) induced reactions at low and intermediate energies in these processes from nuclear targets be calculated.

Theoretically, there exist calculations in past where various nuclear effects in the quasielastic processes induced by neutrinos(antineutrinos) in nuclei in the low as well as in the intermediate energy region have been estimated. Various neutrino generators like NUANCE, NEUGEN, NEUT, NUX, GENEVE and FLUKA etc., which are being used to model neutrino nucleus interactions to analyze the various neutrino oscillation experiments do not include nuclear effects in the calculation of cross sections except for the quasielastic process calculated in nonrelativistic Fermi Gas Model (FGM). It is therefore, very important, that a detail study of nuclear effects in quasielastic as well as inelastic processes be made at low and intermediate energy neutrino scattering processes relevant for the study of neutrino oscillation experiments.

The major point of concern of this thesis is to study the effects of various nuclear effects in the neutrino(antineutrino) induced weak quasielastic and pion production processes at low

and intermediate energies. In this thesis, we have used a local Fermi gas (LFG) model to calculate neutrino induced quasielastic processes and inelastic processes (where one pion is produced). In the case of quasielastic reactions the nuclear effects like Pauli blocking, Fermi motion and nuclear binding are calculated using relativistic Lindhard function corresponding to particle-hole(ph) excitations in the nuclei. The effect of nuclear correlation is calculated by describing the interaction of particle-hole(ph) excitation, as it propagates through the nuclear medium using Random Phase Approximation(RPA). The effect of Coulomb distortion of the charged lepton in the final state is calculated using Fermi function at low electron energies and a modified effective momentum approximation at higher electron energies. The method has been applied to calculate low energy neutrino cross section for various nuclei like ^{12}C, ^{16}O, ^{38}Ar, ^{56}Fe and has been applied to pion decay at rest neutrinos and also for the case of supernova neutrinos.

In the case of inelastic reaction pion production is calculated through the excitation of Δ resonance which subsequently decays into nucleon and pion. The renormalization of Δ properties in the medium is included through the modification of Δ mass and width in the medium which is incorporated through the modification of Δ self-energy in the medium. Finally, the final state interaction of pion with the nucleus is taken into account using a Monte Carlo simulation of pion nucleus interaction for incoherent production of pions and a standard eikonal approximation for pion distortion for the case of coherent production. The optical model used in the eikonal approximation is determined from the self-energy of the pion calculated in the nuclear medium. Explicit calculations for coherent, and incoherent production of pions from ^{12}C, ^{16}O and ^{56}Fe nuclei have been made. These calculations have also been made for the neutrinos and antineutrinos spectra for β-beam neutrino(antineutrino).

The thesis comprises of six chapters including an introduction to the subject. The main formulation and results for the calculation of quasielastic process are given in chapter-2, while the formulation for the inelastic production of leptons and pions is given in chapters-3 and 4. In chapter-5, we present our results and discussions of inelastic production of leptons and pions. All our results have been summarized in chapter-6. In the following we give an abstract of various chapters contained in this thesis.

Chapter 2

Quasielastic Neutrino Reactions With Nucleons and Nuclei

In this chapter, we discuss the quasielastic neutrino/antineutrino reactions from nucleons and nuclei at low as well as at intermediate energy region of neutrino /antineutrino energies.

In the low energy region it is relevant for the neutrino processes initiated by supernova neutrinos as well as the laboratory neutrinos obtained by the decay of pions and muons at rest. The neutrino energy and the spectrum for these neutrinos is given by the Michel spectrum $\phi(E_\nu)$ which is given by

$$\phi(E_{\nu_e}) = \frac{12}{E_0^4} E_{\nu_e}^2 (E_0 - E_{\nu_e}), \quad E_0 = 52.8 \quad \text{MeV}$$

The energy distributions for supernova neutrinos is given by a thermal Fermi-Dirac distribution with an effective degeneracy parameter α (α=μ/T_ν, μ being the chemical potential and T_ν being the temperature of the neutrino gas) and is given by

$$\phi(E_\nu) = \frac{A}{{T_\nu}^3} \frac{E_\nu^2}{e^{(\frac{E_\nu}{T_\nu} - \alpha)} + 1},$$

where typical value of T_ν ~4-5 MeV and α is taken to be either 0 or 3.

In the intermediate energy region of $E_\nu \leq 1.0$ GeV, the charged current quasielastic reaction plays a crucial role in atmospheric and accelerator neutrino oscillation studies. Understanding charged current quasielastic interactions is necessary to accurately predict signal rates in neutrino oscillation experiments. Therefore, precision measurement of the cross section for this reaction, including its energy dependence for various target nuclei, is essential in order to interpret current and future neutrino oscillation experiments in this energy region.

In this chapter, we describe the formalism of free neutrino/antineutrino nucleon scattering and extend it to describe the inclusive quasielastic neutrino/antineutrino nucleus reactions. This has been done to investigate the effects of nuclear medium on the differential and the total cross sections. We first describe the neutrino (antineutrino) induced charged and neutral current quasielastic interactions with free nucleons,

$$\left.\begin{array}{l} \nu_l(k) + n(p) \rightarrow l^-(k') + p(p') \\ \bar{\nu}_l(k) + p(p) \rightarrow l^+(k') + n(p') \end{array}\right\} \quad \text{(Charged Current)}$$

$$\left.\begin{array}{l} \nu_l(k) + n(p) \rightarrow \nu_l(k') + n(p') \\ \nu_l(k) + p(p) \rightarrow \nu_l(k') + p(p') \\ \bar{\nu}_l(k) + n(p) \rightarrow \bar{\nu}_l(k') + n(p') \\ \bar{\nu}_l(k) + p(p) \rightarrow \bar{\nu}_l(k') + p(p') \end{array}\right\} \quad \text{(Neutral Current)}$$

where we have calculated the invariant matrix element and the cross section, using the weak interaction part of the standard model (SM) Lagrangian. The various nucleon vector and axial vector form factors have been discussed along with their parameterizations which have been used in recent years based on the fits to experimental data.

We have studied the inclusive quasielastic neutrino(antineutrino)-nucleus reactions,

$$\nu_l(k) + {}^A_Z Y(p) \rightarrow l^-(k') + X(p')$$

$$\bar{\nu}_l(k) + {}^A_Z Y(p) \rightarrow l^+(k') + X(p')$$

where the neutrino(antineutrino) scatters from a nucleon in the nucleus, the interactions become modified by the effects of various medium effects like Pauli blocking of the recoil nucleon, binding energy, Fermi motion, and renormalization of the weak coupling constants. To account for these medium effects, we have done the cross section calculations in the local density approximation (LDA). In the local density approximation, the cross section is evaluated as a function of local Fermi momentum, and integrated over the whole nucleus. Inside the nucleus various medium effects like Fermi motion and Pauli blocking effects in nuclei are taken into account through the imaginary part of the Lindhard function using relativistic kinematics for particle hole (p-h) excitations in the nuclear medium. The renormalization of weak transition strengths, which are quite substantial in the spin-isospin channel, are calculated in the random phase approximation (RPA) through the interaction of p-h excitations as they propagate in the nuclear medium using a nucleon-nucleon potential described by pion and rho exchanges. The effect of the Coulomb force on the outgoing charged lepton and Q_{th}-value of the reaction are also properly taken into account. The effect of Coulomb distortion of the lepton produced in charged current reactions is taken into account by using the Fermi function F(Z,E_e) at low electron energies, where Z is the atomic number and E_e is the outgoing lepton energy, as well as in a modified momentum approximation (MEMA) at higher lepton energies, where

the effect of Coulomb distortion is incorporated by modifying the momentum and energy of charged lepton in the Coulomb potential of the final nucleus We obtained the expressions for the total cross section and differential cross section in this approximation

The numerical results for charged current total cross section $\sigma(E_\nu)$ as a function of neutrino energy, in the low as well as intermediate energy region, for the inclusive quasielastic neutrino-nucleus reactions induced by ν_μ and ν_e on various nuclei have been presented, which are of present interest for atmospheric as well as accelerator neutrino experiments The calculations have been done for large number of nuclei in the low energy and in the intermediate energy region for ^{12}C, ^{16}O and ^{56}Fe We discuss separately the effects of various nuclear medium effects We see that

1 The reduction is larger in the total cross section for quasielastic reactions as compared to the Fermi gas model The energy dependence of the cross sections for ν_μ and ν_e are similar except for the threshold effects which are seen only at low energies (E_ν <500 MeV)

2 At low energies considered in this work the major suppression in the cross section comes due to the consideration of Q_{th}-values and Pauli blocking in the nuclear medium The reduction in the cross section $\sigma(E)$ due to these effects decreases with the increase of energy

3 In addition to the Pauli blocking, the consideration of RPA correlation in the nuclear medium gives rise to further reduction which increases with the mass number and decreases with the increase in energy.

4 The effect of the Coulomb distortion of the electron is to increase the total cross section which depends upon the incident energy of the neutrino and the charge of the final nucleus For a fixed Z, this increase in the cross section decreases with the increase in energy while for a fixed energy the inclusion of Coulomb distortion increases with the charge Z For high Z nuclei the Coulomb effect is very large and results in manifold increase in the cross sections.

5 The use of Fermi function to calculate the Coulomb distortion effects is not appropriate at higher electron energies Therefore, we use the modified effective momentum approximation(MEMA) It is seen that for low mass nuclei, the results for the cross sections in the two approximations are qualitatively similar but the MEMA gives slightly higher cross sections for the entire energy range considered in this thesis As Z increases the cross sections calculated with MEMA remain higher than the cross sections calculated with the Fermi function at lower energies but become lower than the cross sections obtained with the Fermi function at higher energies This crossover in the cross section for higher Z (Z>18) nuclei occurs at an energy E_c which depends upon Z

6. In the low energy region, we also present the results of the total cross sections $\langle\sigma\rangle$ averaged over Michel spectrum for various nuclei, calculated with RPA correlations without the Coulomb effect, with RPA correlations with Coulomb effect and without RPA correlations with the Coulomb effect. The results for ^{12}C, ^{16}O, ^{56}Fe and ^{208}Pb nuclei are compared with the available experimental and other theoretical results. We find that there are appreciable effects on the cross section due to various nuclear medium effects, and our results are in fair agreement with the experimental results and other theoretical calculations.

7. Based on the theoretical formalism discussed for inclusive quasielastic reactions, we have obtained the numerical results for the total scattering cross sections for charged current scattering cross section for supernova neutrino and antineutrino with ^{56}Fe nuclei, and are also compared with other results available in the literature.

8. In the intermediate energy region i.e. $E_\nu \leq 3$ GeV, we present the numerical results for the total cross sections as a function of energy for neutrino reactions on ^{12}C, ^{16}O and ^{56}Fe. We see that with the incorporation of various nuclear effects the total cross section is reduced. The reduction is energy dependent, and is large at lower energies but becomes small at higher energies.

Chapter 3

Weak Pion Production From Nucleons

This chapter is devoted mainly to the weak production of leptons and single pion from nucleon in the intermediate energy region in Δ dominance model, where we describe the charged current and neutral current induced weak production of Δ resonance from nucleons induced by neutrinos/antineutrinos, which subsequently decays into pions and nucleon.

$$\left.\begin{array}{llll} \nu_l\, p \to l^-\, \Delta^{++} \to l^-\, p\, \pi^+, & \bar{\nu}_l\, p \to l^+\, \Delta^+ \to l^+\, p\, \pi^0 \\ \nu_l\, n \to l^-\, \Delta^+ \to l^-\, n\, \pi^+, & \bar{\nu}_l\, p \to l^+\, \Delta^+ \to l^+\, n\, \pi^+ \\ \nu_l\, n \to l^-\, \Delta^+ \to l^-\, p\, \pi^0, & \bar{\nu}_l\, n \to l^+\, \Delta^- \to l^+\, n\, \pi^- \end{array}\right\}$$

$$\left.\begin{array}{llll} \nu_l\, p \to \nu_l\, \Delta^+ \to \nu_l\, p\, \pi^0, & \bar{\nu}_l\, p \to \bar{\nu}_l\, \Delta^+ \to \bar{\nu}_l\, p\, \pi^0 \\ \nu_l\, p \to \nu_l\, \Delta^+ \to \nu_l\, n\, \pi^+, & \bar{\nu}_l\, p \to \bar{\nu}_l\, \Delta^+ \to \bar{\nu}_l\, n\, \pi^+ \\ \nu_l\, n \to \nu_l\, \Delta^0 \to \nu_l\, n\, \pi^0, & \bar{\nu}_l\, n \to \bar{\nu}_l\, \Delta^0 \to \bar{\nu}_l\, n\, \pi^0 \\ \nu_l\, n \to \nu_l\, \Delta^0 \to \nu_l\, p\, \pi^-, & \bar{\nu}_l\, n \to \bar{\nu}_l\, \Delta^0 \to \bar{\nu}_l\, p\, \pi^- \end{array}\right\}$$

We discuss the weak production of pions in an effective Lagrangian formalism. We first write explicitly the effective Lagrangians for the different hadronic interactions for the weak production of pions. Following the basic weak interaction Lagrangians defined for charged current as well as neutral current interactions, we write down the matrix elements in case of nonresonant and resonant terms corresponding corresponding to the lowest order non vanishing Feynman diagrams contributing to the processes of pion production. For example, the matrix elements for N-Δ transition is written as

$$\langle \Delta^{++}|V^\mu|N\rangle = \sqrt{3}\,\bar{\psi}_\alpha(P)\left[\left(\frac{C_3^V(q^2)}{M}\,(g^{\alpha\mu}\not{q} - q^\alpha\gamma^\mu) + \frac{C_4^V(q^2)}{M^2}\,(g^{\alpha\mu}q\cdot P - q^\alpha P^\mu) + \frac{C_5^V(q^2)}{M^2}\,(g^{\alpha\mu}q\cdot p - q^\alpha p^\mu) + \frac{C_6^V(q^2)}{M^2}\,q^\alpha q^\mu\right)\gamma_5\right]u(p)$$

and

$$\langle \Delta^{++}|A^{\mu}|N\rangle = \sqrt{3}\,\bar{\psi}_{\alpha}(P)\left[\left(\frac{C_3^A(q^2)}{M}\,(g^{\alpha\mu}\not{q}-q^{\alpha}\gamma^{\mu})+\frac{C_4^A(q^2)}{M^2}\,(g^{\alpha\mu}q\cdot P - q^{\alpha}P^{\mu})+C_5^A(q^2)\,g^{\alpha\mu}+\frac{C_6^A(q^2)}{M^2}\,q^{\alpha}q^{\mu}\right)\right]u(p)$$

where $\psi_{\alpha}(P)$ and $u(p)$ are the Rarita-Schwinger and Dirac spinors for the Δ and the nucleon of momenta P and p respectively, $q(=P-p=k-k')$ is the momentum transfer and M is the mass of the nucleon. The following parameterizations have been used for the various N-Δ transition form factors. The expression for the cross section have been derived.

From the experimental data on these processes, the vector form factors are parametrized in a dipole form:

$$C_i^V(q^2) = C_i^V(0)\,\left(1-\frac{q^2}{M_V^2}\right)^{-2};\quad i=3,4,5.\ \Big\}\ \mathbf{A}$$

where M_V is the vector dipole mass. Other proposed modified forms of the form factors are given as·

$$C_i^V(q^2) = C_i^V(0)\,\left(1-\frac{q^2}{M_V^2}\right)^{-2}\mathcal{D}_i\ ,\quad i=3,4,5.\ \Big\}\ \mathbf{B}$$

where

$$\mathcal{D}_i=\left(1-\frac{q^2}{4M_V^2}\right)^{-1}\ \text{for}\ i=3,4,\quad \mathcal{D}_i=\left(1-\frac{q^2}{0.776M_V^2}\right)^{-1}\ \text{for}\ i=5$$

and

$$C_i^V(q^2) = C_i^V(0)\,\left(1-\frac{q^2}{M_V^2}\right)^{-2}\left(1-\frac{q^2}{4M_V^2}\right)^{-1}\ \Big\}\ \mathbf{C}$$

Along with these vector form factors the axial vector form factors have been used by various authors.

$$\left.\begin{array}{l} C_i^A(q^2) = C_i^A(0)\,\left(1-\frac{q^2}{M_A^2}\right)^{-2}\mathcal{D}_i\ ,\quad i=3,4,5. \\ \mathcal{D}_i = 1-\frac{a_i q^2}{(b_i-q^2)};\quad i=3,4,5;\qquad C_6^A(q^2)=C_5^A(q^2)\,\frac{M^2}{m_{\pi}^2-q^2} \end{array}\right\}\ \mathbf{A}$$

where $a_3=b_3=0$, $a_4=a_5=$ -1.21, $b_4=b_5=$2 GeV^2. Other forms of the axial vector form factors parameterizations are given as:

$$C_i^A(q^2) = C_i^A(0)\ (1-\frac{q^2}{M_A^2})^{-2}\,\mathcal{D}_i,\quad i=3,4,5;\quad \mathcal{D}_i=\left(1-\frac{q^2}{3M_A^2}\right)^{-1}\ \Big\}\ \mathbf{B\ \&\ C}$$

Table 3.1: Weak vector and axial vector couplings at $q^2 = 0$ and the values of M_V and M_A used in the literature, $W^2 = (p+q)^2$.

	$C_3^V(0)$	$C_4^V(0)$	$C_5^V(0)$	$C_3^A(0)$	$C_4^A(0)$	$C_5^A(0)$	M_V(GeV)	M_A(GeV)
A	2.05	$-\frac{M}{M_\Delta}$	0.0	0.0	-0.3	1.2	0.73	1.05
B	2.13	-1.51	0.48	0.0	-0.25	1.2	0.84	1.05
C	1.95	$-\frac{M}{W}$	0.0	0.0	-0.25	1.2	0.84	1.05

where M_A is the axial vector dipole mass and m_π is the pion mass. The values of $C_i^V(0)$ and $C_i^A(0)$ in various parameterizations **A, B and C** are given in table-3.1.

Chapter 4

Weak Pion Production From Nuclei

In this chapter, we discuss the weak production of leptons and pions from nuclei in the intermediate energy region using the formalism developed in chapter-3. There are two types of production processes from nuclear targets, known as coherent pion production and incoherent pion production depending upon the excitation energy of the residual nucleus. In a nucleus, the target nucleus can stay in the ground state leading to the coherent production of pions or can be excited and/or broken up leading to the incoherent production of pions.

We discuss separately the neutrino/antineutrino induced coherent and incoherent weak production of pions from nuclei assuming Δ-dominance. The calculations have been done assuming Δ-dominance model of one pion production because the contribution of higher resonances in the energy region of interest is sufficiently small. We have considered all the present available informations on the weak vector and axial vector form factors in the matrix elements of N-Δ transitions discussed in chapter-3. Nuclear pion production differ from pion production from free nucleon since the Δ produced inside the nuclear medium can decay through pionic decay i.e., $\Delta N \rightarrow NN\pi$ or non-mesonic decay through $\Delta N \rightarrow NN$, which is not available in case of free nucleon. In the excitation of Δ from nuclear targets, there is an additional model dependence due to strong interaction of Δ in the nuclear medium. Inside the nuclear medium Δ properties like its mass and decay width are both modified due to strong interactions. The nuclear effects in the Δ production are important to study the pion production from nuclei.

Inside the nuclear medium the modification in the mass and width of the Δ resonance is properly taken into account in terms of Δ self-energy Σ_Δ in nuclear medium in the local density approximation. The following modifications have been incorporated in the Δ self-energy

Σ_Δ:

$$\mathrm{Re}\Sigma_\Delta \simeq 40.0 \left(\frac{\rho}{\rho_0}\right) \mathrm{MeV}$$

$$-\mathrm{Im}\Sigma_\Delta = C_Q \left(\frac{\rho}{\rho_0}\right)^\alpha + C_{A2} \left(\frac{\rho}{\rho_0}\right)^\beta + C_{A3} \left(\frac{\rho}{\rho_0}\right)^\gamma$$

which is determined mainly by the one pion interactions in the nuclear medium. The different coefficients used above are parameterized in the range of energies $80 < T_\pi < 320 MeV$, where T_π is the pion kinetic energy, as:

$$C(T_\pi) = ax^2 + bx + c, \qquad x = \frac{T_\pi}{m_\pi}$$

where C stands for all the coefficients i.e. C_Q, C_{A2}, C_{A3}, α and $\beta(\gamma = 2\beta)$. The different coefficients used above are tabulated in table.4.1.

Table 4.1: Coefficients used for an analytical interpolation of $C(T_\pi)$.

	$C_Q(MeV)$	$C_{A2}(MeV)$	$C_{A3}(MeV)$	α	β
a	-5.19	1.06	-13.46	0.382	-0.038
b	15.35	-6.64	46.17	-1.322	0.204
c	2.06	22.66	-20.34	1.466	0.613

With these corrections in Σ_Δ, depending upon the medium, the mass and width have been modified to

$$M_\Delta \rightarrow \tilde{M}_\Delta = M_\Delta + \mathrm{Re}\Sigma_\Delta, \quad \text{and} \quad \Gamma \rightarrow \tilde{\Gamma} - 2\mathrm{Im}\Sigma_\Delta$$

where $\tilde{\Gamma}$ is the Pauli blocked width of Δ in the nuclear medium.

All these effects are taken into account in a local density approximation (LDA). We have also discussed the effect of final state interaction of pions with the residual nucleus. This has been discussed separately for the coherent and incoherent processes. The final state interaction in coherent production of pions is taken into account by replacing the plane wave pion by a distorted wave pion. The distortion of the pion is calculated in the eikonal approximation in which the distorted pion wave function is written as:

$$e^{i(\mathbf{q}-\mathbf{k}_\pi)\,\mathbf{r}} \rightarrow \exp\left[i(\mathbf{q}-\mathbf{k}_\pi)\cdot\mathbf{r} - \frac{i}{v}\int_{-\infty}^{z} V_{opt}(\mathbf{b}, z')dz'\right]$$

where $\mathbf{r} = (\mathbf{b}, z)$, $\mathbf{q}$ and $\mathbf{k}_\pi$ are the momentum transfer and the pion momentum, respectively. The pion optical potential V_{opt} is related with the pion self-energy Π as $\Pi = 2\omega\ V_{opt}$, where ω is the energy of the pion and $|\mathbf{v}| = |\mathbf{k}_\pi|/\omega$. The pion self-energy is calculated in local density approximation of the Δ-hole model and is given as

$$\Pi(\rho(\mathbf{b}, z')) = \frac{4}{9}\left(\frac{f_{\pi N\Delta}}{m_\pi}\right)^2 \frac{M^2}{\bar{s}}|\mathbf{k}_\pi|^2\ \rho(\mathbf{b}, z')\ G_{\Delta h}(\bar{s}, \rho)$$

where $\bar{s}$ is the center of mass energy in the Δ decay averaged over the Fermi sea and $G_{\Delta h}(\bar{s}, \rho)$ the Δ-hole propagator given by

$$G_{\Delta h}(s, \rho(\mathbf{b}, z')) = \frac{1}{\sqrt{\bar{s}} - M_\Delta + \frac{1}{2}i\bar{\Gamma}(\bar{s}, \rho) - i\mathrm{Im}\Sigma_\Delta(\bar{s}, \rho) - \mathrm{Re}\Sigma_\Delta(\bar{s}, \rho)}$$

We have calculated the charged current and neutral current induced coherent pion production from nuclei

$$\nu_l\ (\bar{\nu}_l)\ +\ \mathcal{N}\ \rightarrow\ l^{=}\ (\bar{\nu}_l)\ +\ \mathcal{N}\ +\ \pi^{\pm}(\pi^0)$$

including particle-hole (p-h) and Δ-h nuclear excitations with the relativistic description of Δ-resonance. We write the relativistic expression of matrix element for delta pole term in s-channel and u-channel processes by using the effective form of the $\Delta N\pi$ interactions vertices by taking the relativistic covariant form of the Δ propagator of the Rarita-Schwinger spinor for a $T = \frac{3}{2}$ particle.

$$\Delta^{\mu\nu} = \frac{\not{P} + M_\Delta}{P^2 - M_\Delta^2 + i\Gamma M_\Delta}\left[g^{\mu\nu} - \frac{1}{3}\gamma^\mu\gamma^\nu - \frac{2}{3M_\Delta^2}P^\mu P^\nu + \frac{(P^\mu\gamma^\nu - \gamma^\mu P^\nu)}{3M_\Delta}\right]$$

where P and M_Δ are the four momenta and mass of the delta, and Γ is the energy dependent P-wave decay width for the Δ resonance given as

$$\Gamma = \frac{1}{6\pi}\left(\frac{f_{\pi N\Delta}}{m_\pi}\right)^2 \frac{M}{W}|\mathbf{k}_\pi^{cm}|^3\Theta(W - M - m_\pi)$$

where

$$|\mathbf{k}_\pi^{cm}| = \frac{\sqrt{(W^2 - m_\pi^2 - M^2)^2 - 4m_\pi^2 M^2}}{2W}$$

The step function Θ denotes the fact that the width is zero for the invariant masses below the $N\pi$ threshold, W and M are the Δ invariant mass and nucleon mass respectively, and $|\mathbf{k}_\pi^{cm}|$ the pion momentum in the rest frame of the resonance.

We obtained the expressions for the differential cross sections for the coherent weak pion

production from nuclei, and the nuclear medium effects have been taken into account by using the nuclear form factor $\mathcal{F}(\mathbf{q}-\mathbf{k}_\pi)$ given as

$$\mathcal{F}(\mathbf{q}-\mathbf{k}_\pi) = \int d^3\mathbf{r}\ \rho(\mathbf{r})\ e^{-i(\mathbf{q}-\mathbf{k}_\pi).\mathbf{r}}$$

with $\rho(\mathbf{r})$ as the nuclear matter density as a function of nucleon relative coordinates.

Weak production of Δ has been studied in order to calculate the incoherent pion production from nuclei through charged and neutral current processes induced by neutrinos and antineutrinos, in which a Δ resonance is excited which give rise to pions as decay product through $\Delta \rightarrow N\pi$ channel, where only these pions are observed and no observation is made on other hadrons.

$$\begin{aligned} \nu_\mu(k) + p(p) &\rightarrow \mu^-(k') + \Delta^{++}(P) \\ &\qquad\qquad \searrow p + \pi^+ \end{aligned}$$

$$\begin{aligned} \nu_\mu(k) + n(p) &\rightarrow \mu^-(k') + \Delta^{+}(P) \\ &\qquad\qquad \searrow n + \pi^+ \ (\ p\ +\ \pi^0\ ) \end{aligned}$$

The calculations have been done assuming Δ-dominance model of one pion production in local density approximation using a relativistic description of Δ resonance following the standard Rarita-Schwinger formalism. In this work the nuclear effects on the Δ production in nuclei has been studied in the local density approximation (LDA) which takes into account the modification of mass and decay width of Δ in the nuclear medium.

The final state interaction of incoherent pions inside the nuclear medium is calculated through the Monte Carlo simulation using probabilities per unit length as the basic input. In this simulation, a pion of given momentum and charge is moved along the z-direction with a random impact parameter b, with $|\mathbf{b}| < R$, where R is the nuclear radius which is taken to be a point where nuclear density $\rho(R)$ falls to $10^{-3}\rho_0$, where ρ_0 is the central density. To start with, the pion is placed at a point $(\mathbf{b}, z_{in})$, where $z_{in} = -\sqrt{R^2 - |\mathbf{b}|^2}$ and then it is moved in small steps δl along the z-direction until it comes out of the nucleus or interact. If $P(p_\pi, r, \lambda)$ is the probability per unit length at the point r of a pion of momentum $\mathbf{p}_\pi$ and charge λ, then $P\delta l << 1$. A random number x is generated such that $x \in [0,1]$ and if $x > P\delta l$, then it is assumed that pion has not interacted while traveling a distance δl. however, if $x < P\delta l$ then the pion has interacted and depending upon the weight factor of each channel given by its cross section it is decided that whether the interaction was quasielastic, charge exchange reaction, pion production or pion absorption. For example, for the quasielastic scattering $P_{N(\pi^\lambda,\pi^{\lambda'})N'} = \sigma_{N(\pi^\lambda,\pi^{\lambda'})N'} \times \rho_N$ where N is a nucleon, ρ_N is its density and σ is the elementary cross section for the reaction $\pi^\lambda + N \rightarrow \pi^{\lambda'} + N'$ obtained from the phase shift analysis. For a pion to be absorbed, P is expressed in terms of the imaginary part of the pion self energy

Π i.e. $P_{abs} = -\frac{Im\Pi_{abs}(p_\pi)}{p_\pi}$, where the self energy Π is related to the pion optical potential V_{opt}.

The expressions for the cross section has been derived, and we see that all these nuclear effects and the final state interaction effects are found to give important effects on the coherent and incoherent weak pion production cross sections.

Chapter 5

Results and Discussions for Pion Production

In this chapter, we present all our numerical results for the neutrino induced charged current and neutral current coherent and incoherent production of leptons and pions from ^{12}C, ^{16}O and ^{56}Fe target at the intermediate neutrino energies The energy dependence of the total scattering cross sections for the charged current and neutral current coherent and incoherent pion production from ^{12}C and ^{16}O, induced by ν_μ is studied, where we have also studied the effect of the various weak N-Δ transition form factors used by various authors The nuclear medium effects and the final state interaction effect in the various observables of coherent pion spectrum like $\left(\frac{d\sigma^{CC}}{d\Omega_{\pi q}d\Omega_{\nu\mu}dE_\pi}\right)$, $\left(\frac{d\sigma^{CC}}{d\Omega_{\pi q}dE_\pi}\right)$, $\left(\frac{d\sigma^{CC}}{dk_\pi}\right)$ and $\left(\frac{d\sigma^{CC}}{d\cos\Theta_{\pi q}}\right)$ have been studied for charged current processes Similar to these, studied for the neutral current case has not been shown in the thesis We have also presented and discussed the effects of the nuclear medium effects and the final state interaction effect in the various observables of coherent lepton spectrum like $\left(\frac{d\sigma^{CC}}{d\Omega_{\nu\mu}dE_\mu}\right)$, $\left(\frac{d\sigma^{CC}}{dk'_\mu}\right)$ and $\left(\frac{d\sigma^{CC}}{d\cos\Theta_{\nu\mu}}\right)$ The Q^2-distribution $\left(\frac{d\sigma^{CC}}{dQ^2}\right)$ has been studied for coherent and incoherent processes from ^{12}C and ^{16}O The uncertainties in the cross sections due to the use of the various weak N-Δ transition form factors used in literature, has also been discussed

Specifically we have studied

A. Charged Current Coherent Pion Production

1 The differential cross section $\left(\frac{d\sigma^{CC}}{d\Omega_{\pi q}d\Omega_{\nu\mu}dE_\pi}\right)$ for the neutrino energy E_{ν_μ}=1 0 GeV as a function of the pion angle $\Theta_{\pi q}$ measured with respect to the momentum transfer (q) for lepton angle $\Theta_{\nu\mu}$=0^o with respect to the neutrino direction, at q_0=E_ν - E_μ=300 MeV in ^{12}C and ^{16}O

2. The differential cross section $\left(\frac{d\sigma^{CC}}{d\Omega_{\pi q}dE_\pi}\right)$ as a function of q_0 for the neutrino energy E_{ν_μ}=1.0 GeV and $\Theta_{\pi q} = 0^o$ from ^{12}C and ^{16}O.

3. The momentum distribution of pions $\left(\frac{d\sigma^{CC}}{dk_\pi}\right)$ as a function of $\mathbf{k}_\pi$ at E_{ν_μ}=1.0 GeV from ^{12}C and ^{16}O.

4. The angular distribution of pions $\left(\frac{d\sigma^{CC}}{d\cos\Theta_{\pi q}}\right)$ as a function of $\cos\Theta_{\pi q}$ at E_{ν_μ}=1.0 GeV from ^{12}C and ^{16}O.

B. Charged Current Coherent Lepton Production

1. The differential cross section $\left(\frac{d\sigma^{CC}}{d\Omega_{\nu_\mu}dE_\mu}\right)$ for $\Theta_{\nu\mu} = 0^o$ as a function of q_0 at E_{ν_μ}=1.0 GeV from ^{12}C and ^{16}O.

2. The momentum distribution of leptons $\left(\frac{d\sigma^{CC}}{dk'_\mu}\right)$ as a function of $\mathbf{k}'_\mu$ in ^{12}C nuclei at E_{ν_μ}=1.0 GeV.

3. The angular distribution of leptons $\left(\frac{d\sigma^{CC}}{d\cos\Theta_{\nu_\mu}}\right)$ as a function of $\cos\Theta_{\nu_\mu}$ in ^{12}C and ^{16}O nuclei at E_{ν_μ}=1.0 GeV.

C. Q^2-Distributions and The Total Cross Sections

1. The Q^2-distributions $\left(\frac{d\sigma^{CC}}{dQ^2}\right)$ in ^{12}C and ^{16}O nuclei, for charged current coherent pion production at neutrino energy E_{ν_μ}=1.0 GeV.

2. The total scattering cross section $\sigma^{CC}(E_{\nu_\mu})$ as a function of neutrino energy E_{ν_μ} for the coherent charged current reaction induced by ν_μ in ^{12}C and ^{16}O nuclei.

3. The total scattering cross section $\sigma^{NC}(E_{\nu_\mu})$ as a function of neutrino energy E_{ν_μ} for the coherent neutral current reaction induced by ν_μ in ^{12}C and ^{16}O nuclei.

4. The total scattering cross section $\sigma^{CC}(E_{\nu_\mu})$ as a function of neutrino energy E_{ν_μ} for the charged current incoherent one π^+ production induced by ν_μ in ^{12}C and ^{16}O nuclei.

5. The charged current incoherent one pion production cross section $\sigma^{CC}(E_{\nu_\mu})$ as a function of neutrino energy E_{ν_μ} induced by neutrinos on ^{12}C target. We have studied the uncertainty in the total cross sections due to the use of various parameterizations of the weak N-Δ transition form factors used in literature.

These results have been applied to the following β-beam neutrino(antineutrino) in ^{16}O nuclei, atmospheric neutrino(antineutrino) in ^{56}Fe nuclei, and accelerator neutrino(antineutrino) in ^{12}C and ^{16}O nuclei.

I. Application to β-beam neutrino(antineutrino) in ^{16}O:

We have studied the neutrino nucleus interaction cross sections in ^{16}O for β-beam neutrino(antineutrino) energies corresponding to the Lorentz boost factor γ in the range of 60< γ <250 (150). The energy spectrum of β-beam neutrinos(antineutrinos) from ^{18}Ne(^{6}He) ion source in the forward angle($\theta = 0^o$) geometry, corresponding to the Lorentz boost factor γ is given by:

$$\Phi_{lab}(E_\nu, \theta = 0) = \frac{\Phi_{cm}(E_\nu \gamma[1-\beta])}{\gamma[1-\beta]}$$
$$\Phi_{cm}(E_\nu) = bE_\nu^2 E_e p_e F(Z', E_e)\Theta(E_e - m_e)$$

where $b = ln2/m_e^5 f t_{1/2}$ and E_e, p_e are the energy and momentum of the outgoing electron. $F(Z', E_e)$ is the Fermi function.

We have presented the results of the flux averaged cross section $\langle\sigma\rangle$ for neutrino and antineutrino reactions for various values of the Lorentz boost factor γ where we can see the relative contributions of the cross sections for quasielastic and inelastic production of leptons along with the cross sections for neutral current induced production of neutral pions which is the major source of background to the quasielastic events at intermediate energies.

II. Application to atmospheric neutrino(antineutrino) in ^{56}Fe:

We have studied the neutrino nuclear cross section in ^{56}Fe nuclei which are relevant for the atmospheric neutrino experiments. The uncertainty in the nuclear production cross section of leptons from ^{56}Fe nuclei by the atmospheric neutrinos are discussed. The numerical results for the relative yield of muon over electron type events $R = R_{\mu/e} = \frac{Y_\mu + Y_{\bar{\mu}}}{Y_e + Y_{\bar{e}}}$ for quasielastic events, inelastic events and the total events have been presented. The lepton yields Y_l for lepton of flavor l we define as

$$Y_l = \int \Phi_{\nu_l}\, \sigma(E_{\nu_l})\, dE_{\nu_l}$$

where, Φ_{ν_l} is the atmospheric neutrino flux of ν_l by Honda et al. and Barr et al. for the Soudan site and the fluxes of Barr et al. and Plyaskin for the Gransasso site. We study the nuclear model dependence as well as the flux dependence of the relative yield.

We see that there is no appreciable nuclear model dependence on the ratio of total lepton yields for the production of muons and electrons. However, there is some dependence of the

ratio R on the atmospheric neutrino fluxes, which is mainly due to the quasielastic events.

We have also presented a quantitative estimate of the relative yield of inelastic events r_l defined by $r_l = \frac{Y_l^{\Delta}}{Y_l}$, where $Y_l^{\Delta} = Y_l^{\Delta} + Y_{\bar{l}}^{\Delta}$ is the lepton yield due to the inelastic events and Y_l is the total lepton yield due to the quasielastic and inelastic events i.e., $Y_l = Y_l^{q.e.} + Y_{\bar{l}}^{q.e.} + Y_l^{\Delta} + Y_{\bar{l}}^{\Delta}$.

III. Application to accelerator neutrino(antineutrino) in ^{12}C and ^{16}O:

The numerical results for ν_μ induced coherent and incoherent charged and neutral current lepton and pion production in ^{12}C and ^{16}O averaged over the K2K and the MiniBooNE neutrino spectra have been presented. We have also presented and discussed the results obtained by using different N-Δ transition form factors available in the literature.

We have presented and discussed

A. Momentum Distributions

1. The momentum distribution of coherent pions $\langle \frac{d\sigma^{CC}}{dk_\pi} \rangle$ as a function of the pion momentum k_π, averaged over the MiniBooNE and K2K spectra for ν_μ induced reaction in ^{12}C, and averaged over the K2K spectra for ν_μ induced reaction in ^{16}O.

2. The comparison of our final result which include both the nuclear medium modification and final state interaction effects, for the momentum distribution of coherent pions $\langle \frac{d\sigma^{CC}}{dk_\pi} \rangle$ averaged over the MiniBooNE spectrum for ν_μ induced reaction in ^{12}C, averaged over the K2K spectrum for ν_μ induced reaction in ^{12}C and averaged over the K2K spectrum for ν_μ induced reaction in ^{16}O.

3. The momentum distribution of leptons $\langle \frac{d\sigma}{dp_\mu} \rangle$ as a function of the lepton momentum p_μ, averaged over the MiniBooNE and the K2K neutrino spectra, for the incoherent charged current reactions induced by ν_μ in ^{12}C and ^{16}O, respectively.

4. The uncertainty in the momentum distribution of leptons $\langle \frac{d\sigma}{dp_\mu} \rangle$ as a function of the lepton momentum p_μ, averaged over the MiniBooNE and the K2K neutrino spectra, for the incoherent charged current reactions induced by ν_μ in ^{12}C and ^{16}O, respectively, due to use of the various weak N-Δ transition form factors used in the literature.

B. Angular Distributions

1. The angular distribution of coherent pions $\langle \frac{d\sigma^{CC}}{d\cos\Theta_{\pi q}} \rangle$ as a function of $\cos\Theta_{\pi q}$, averaged over the MiniBooNE and K2K spectra for ν_μ induced reaction in ^{12}C, and averaged over the

K2K spectrum for ν_μ induced reaction in ^{16}O.

2. The comparison of our final result which include both the nuclear medium modification and final state interaction effects, for the angular distribution of coherent pions $\langle \frac{d\sigma^{CC}}{d\cos\Theta_{\pi q}} \rangle$, averaged over the MiniBooNE spectrum for ν_μ induced reaction in ^{12}C, averaged over the K2K spectrum for ν_μ induced reaction in ^{12}C and averaged over the K2K spectrum for ν_μ induced reaction in ^{16}O.

3. The angular distribution of the leptons $\langle \frac{d\sigma^{CC}}{d\cos\Theta_{\nu_\mu}} \rangle$ as a function of $\cos\Theta_{\nu_\mu}$, averaged over the MiniBooNE and K2K spectra for ν_μ induced induced coherent charged current lepton production on ^{12}C and ^{16}O, respectively.

C. Q^2-Distributions

1. The differential cross sections $\langle \frac{d\sigma^{CC}}{dQ^2} \rangle$, averaged over the MiniBooNE and K2K spectra for ν_μ induced coherent charged current pion production on ^{12}C, and averaged over the K2K spectrum for ν_μ induced reaction in ^{16}O.

2. The comparison of our final result which include both the nuclear medium modification and final state interaction effects, for the differential cross sections $\langle \frac{d\sigma^{CC}}{dQ^2} \rangle$, averaged over the MiniBooNE spectrum in ^{12}C, averaged over the K2K spectrum in ^{12}C and averaged over the K2K spectrum in ^{16}O, for ν_μ induced coherent charged current pion production.

3. The differential cross sections $\langle \frac{d\sigma^{CC}}{dQ^2} \rangle$, averaged over the MiniBooNE and the K2K neutrino spectra, for the incoherent charged current reactions induced by ν_μ in ^{12}C and ^{16}O, respectively.

4. The uncertainty in the Q^2 distribution $\langle \frac{d\sigma^{CC}}{dQ^2} \rangle$, averaged over the MiniBooNE and the K2K neutrino spectra, for the incoherent charged current reactions induced by ν_μ in ^{12}C and ^{16}O, respectively, due to use of the various weak N-Δ transition form factors used in the literature.

D. Total Cross Sections

1. The charged current total cross section for coherent pion production from ^{12}C. We see that the various nuclear effects and the final state interaction give a large reduction in the total cross section. We have also presented the results for charged current total cross section for coherent pion production from ^{12}C when a cut of 450 MeV is applied on the muon momentum as done in the K2K experiment. We obtain a total cross section of $6.93\times10^{-40}cm^2$ in ^{12}C which corresponds to $0.578\times10^{-40}\frac{cm^2}{nucleon}$, and is consistent with the experimental result of

σ^{CC} <0.642×$10^{-40}\frac{cm^2}{nucleon}$ in ^{12}C reported by the K2K collaboration.

2. The total cross section for the neutral current induced π^0 production from ^{12}C, ^{16}O, ^{27}Al and CF_3Br (Freon), along with the some older experimental results and from the MiniBooNE collaboration. We see that the theoretical results for the neutral current induced coherent π^0 production are in reasonable agreement with presently available experimental results in the intermediate energy region.

3. The total cross section for ν_μ induced coherent and incoherent charged and neutral current pion production in ^{12}C and ^{16}O averaged over the K2K and the MiniBooNE neutrino spectra.

4. Specifically, we have presented the results for the total cross sections for $1\pi^+$ production from ^{12}C and studied the energy dependence of the ratio of single π^+ production to the quasielastic reaction. The results have been compared with some old experimental results and with the preliminary results available from MiniBooNE experiment. We see that the theoretical results for pion production are in reasonable agreement with presently available experimental results in the intermediate energy region.

5. The variation in the total cross section for the charged current $1\pi^+$ production for ν_μ induced reaction in ^{12}C due to the variation in the axial vector dipole mass M_A in the weak N-Δ transition form factors using the parametrization given in the literature. The results are shown for M_A=1.0 GeV, M_A=1.1 GeV and M_A=1.2 GeV.

6. The uncertainty in the total cross section for the charged current $1\pi^+$ production for ν_μ induced reaction in ^{12}C due to the use of the various weak N-Δ transition form factors used in the literature.

Chapter 6

Summary and Conclusions

This chapter contains the summary and conclusion of all our results for quasielastic inclusive lepton production, and for coherent and incoherent lepton and pion production. We find that

A. Quasielastic Inclusive Lepton Production:

1. The role of nuclear effects like Q_{th} value, Pauli blocking and Fermi motion is to reduce the cross sections. For a given Z, this reduction becomes smaller with the increase in energy. There is a further reduction of the cross section due to the renormalization of weak transition strengths in the nuclear medium. For a given Z, this reduction becomes smaller with the increase in neutrino energy, while for a given neutrino energy E_ν, this reduction increases with Z.

2. The effect of the Coulomb distortion of the final charged lepton in the total cross section is small except at very low energies and becomes negligible with increase in neutrino energy.

3. The two methods of treating the Coulomb distortion give similar results for low energy neutrinos in the case of low mass nuclei. For intermediate and heavy mass nuclei the cross sections with Fermi function are smaller than the cross sections with MEMA upto certain energy E_{ν_e} after which the the cross sections calculated with Fermi function become larger. At the energy E_{ν_e} where this cross over takes place changes with nuclei. For example it is around 40 MeV for nuclei like ^{56}Fe in the intermediate mass range and around 18 MeV for nuclei in the heavier mass range like ^{208}Pb.

4. The total cross sections averaged over the neutrino spectrum obtained from the muons decaying at rest is presented for all nuclei considered here. The results for ^{12}C, ^{16}O, ^{56}Fe and ^{208}Pb nuclei are compared with the available experimental results as well as different theoretical calculations. New results have been presented for many other nuclei.

5. The reduction is larger in the total cross section for quasielastic reactions as compared to the Fermi gas model. The energy dependence of this reduction in cross section is found to be different at threshold energy for ν_μ and ν_e neutrino reactions. However, for E$\geq$500 MeV, the energy dependence is similar in nature.

The numerical results for low energy region presented in this thesis can be a very useful benchmark for neutrino nucleus cross section measurements being proposed at SNS facilities using various nuclei as nuclear targets. The numerical results in the intermediate energy region are also useful to analyze the fully contained events of atmospheric neutrino oscillation experiments.

B. Coherent and Incoherent Production of Leptons and Pions:

1. The contribution to the cross section comes mainly from the s-channel diagram($>$ 90%) which is dominated by on shell Δ, thus making the off shell correction quite small. The inclusion of off shell effects by introducing a form factor at the πNΔ vertex leads to a reduction in the cross section which is estimated to be 4-6 % in the energy region of 1-2 GeV.

2. The contribution to the cross section from the vector current is negligibly small ($<$2 %) and the major contribution comes from the axial current only, leading to near equality of neutrino and antineutrino cross sections.

3. There is a large reduction due to nuclear effects in the coherent as well as incoherent production cross sections, and there is a further reduction in the cross sections due to the final state interaction of pions with the residual nucleus.

4. The total cross sections for neutrino induced π^+ production from free proton are closer to the π^+ production cross sections obtained by the ANL experiment and are smaller than the π^+ production cross sections obtained by the BNL experiment in the intermediate energy region. In this energy region, there is a $10-20\%$ theoretical uncertainty in the total cross section due to use of various parameterization of N-Δ transition form factors.

5. The total cross sections for $1\pi^+$ production is dominated by the incoherent process. The contribution of the coherent pion production is about 4-5% in the energy region of 0.7-1.4 GeV.

6. In the neutrino energy region of 0.7-1.4 GeV, the results for the ratio of cross section of $1\pi^+$ production to the quasielastic lepton production is described quite well for E_ν $<$1.0 GeV, when nuclear effects in both the processes are taken into account. However, for energies higher than E_ν $>$1.0 GeV, the theoretical value of the ratio underestimates the experimental value.

7. The role of nuclear medium and pion absorption effects is quite important in bringing out the good agreement between the theoretical and experimental results in the energy region of 1.0 GeV. The theoretical and experimental value of the ratio for the total cross sections for $1\pi^+$ production and quasielastic lepton production are in good agreement for neutrino energies upto 1.0 GeV. We also found that theoretical results for the neutral current induced coherent π^0 production are in reasonable agreement with presently available experimental results in the intermediate energy region.

8. The results for charged current and neutral current induced total cross sections in ^{12}C and ^{16}O averaged over K2K and MiniBooNE neutrino spectra have been presented for the coherent and incoherent pion production. We have also presented the momentum distribution, angular distribution and Q^2-distribution in ^{12}C and ^{16}O averaged over the MiniBooNE and K2K spectra for the incoherent and coherent charged current one pion production with various N-Δ transition form factors.

The method may be useful to analyze the neutrino induced pion production data at neutrino energies relevant for neutrino oscillation experiments being done by K2K, MiniBooNE and J-PARC collaborations.

List of Publications

I. List of Publications in Research Journals

1 *Nuclear Effects in Neutrino Induced Coherent Pion Production at K2K and MiniBooNE*
S K Singh, M Sajjad Athar and **Shakeb Ahmad**
Phys Rev Lett **96**, 241801 (2006).

2 *Neutrino Induced Charged Current $1\pi^+$ Production at Intermediate Energies*
Shakeb Ahmad, M. Sajjad Athar and S. K. Singh
Phys Rev **D 74**, 073008 (2006).

3 *Nuclear Cross Sections in ^{16}O for β beam neutrinos at Intermediate Energies*
S K Singh, M Sajjad Athar and **Shakeb Ahmad**
Phys Lett **B 641**, 159 (2006)

4 *Neutrino Nucleus Cross Sections for low Energy Neutrinos at SNS facilities*
M Sajjad Athar, **Shakeb Ahmad** and S K Singh
Nucl Phys **A 764**, 551 (2006)

5 *Weak Pion Production from Nuclei*
S K Singh, M Sajjad Athar and **Shakeb Ahmad**
Pramana J of Physics **66**, 689 (2006).

6 *Neutrino Induced Charged Current $1\pi^+$ Production from ^{12}C at Intermediate Energies*
M Sajjad Athar, **Shakeb Ahmad** and S K Singh
Nucl Phys **A** , (Accepted for Publication) (2006)

7 *Supernova Neutrino Induced Inclusive Reactions on ^{56}Fe in Terrestrial Detectors*
M Sajjad Athar, **Shakeb Ahmad** and S K Singh
Phys Rev **C 71**, 045501 (2005)

8 *Charged Current Lepton Production from Iron Induced by Atmospheric neutrinos*
M Sajjad Athar, **Shakeb Ahmad** and S K Singh
Eur Phys J **A 24**, 459 (2005)

9. *Coherent Pion Production in Electroweak Processes*
R. Husain, **S. Ahmad**, M. Sajjad Athar and S. K. Singh
Mesons and Quarks, Edited by A. B. Santra et al., Narosa Publication, New Delhi, Page 260-272 (2004).

10. Δ *Production Calculations with Nuclear Effects*
S. K. Singh, **S. Ahmad** and M. Sajjad Athar
NuInt02, university of california, Irvine, December 2002
http://www.ps.uci.edu/ nuint/.

11. *Antineutrino Induced Neutrino-Nucleus Reactions at Intermediate Energies*
Phys. Rev. **D** (To be submitted) (2006).

II. List of Papers in Conference/Symposium

1. *Photoproduction of Pions in* ^{12}C *Nuclei.*
R. Husain, **Shakeb Ahmad**, M. Sajjad Athar and S. K. Singh
DAE-BRNS Symposium on Nuclear Physics, Vol. **44B**, 344 (2001).

2. *Neutrino Magnetic Moment Effects in* $\nu + ^{16}O \rightarrow \nu + ^{16}O + \pi^0$.
R. Husain, **Shakeb Ahmad**, M. Sajjad Athar and S. K. Singh
DAE-BRNS Symposium on Nuclear Physics, Vol. **44B**, 334 (2001).

3. *Deuteron Effects in Pion Production from* νd *Reaction.*
Shakeb Ahmad, M. Sajjad Athar and S. K. Singh
DAE-BRNS Symposium on Nuclear Physics, Vol. **45B**, 308 (2002).

4. *Nuclear Medium Effects in Coherent Electroproduction of Pions from Nuclei.*
R. Husain, **Shakeb Ahmad**, M. Sajjad Athar and S. K. Singh
DAE-BRNS Symposium on Nuclear Physics, Vol. **45B**, 294 (2002).

5. *Nuclear Medium Effects in Coherent* $\nu_e + ^{16}O \rightarrow e^- + ^{16}O + \pi^+$ *Reaction.*
Shakeb Ahmad, M. Sajjad Athar and S. K. Singh
DAE-BRNS Symposium on Nuclear Physics, Vol. **46B**, 320 (2003).

6. *Inelastic lepton Production Induced by Neutrinos Relevant for MiniBooNE Energies.*
S. Chauhan, **Shakeb Ahmad**, M. Sajjad Athar and S. K. Singh
DAE-BRNS Symposium on Nuclear Physics, Vol. **47B**, 594 (2004).

7. *Neutrino Nucleus Cross Sections from Stopped Pion Neutrinos.*
Shakeb Ahmad, M. Sajjad Athar and S. K. Singh
DAE-BRNS Symposium on Nuclear Physics, Vol. **47B**, 596 (2004).

8. *Antineutrino Reactions from Nuclei at Intermediate Energies.*
Shakeb Ahmad, M. Sajjad Athar and S. K. Singh
DAE-BRNS Symposium on Nuclear Physics, (Accepted) (2006).

DEPARTMENT OF PHYSICS
ALIGARH MUSLIM UNIVERSITY
ALIGARH - 202002 (INDIA)

PH. : 91-571-2700984
PH. & FAX : 91-571-2701001

CERTIFICATE

Certified that the work reported in this thesis entitled " LOW AND MEDIUM ENERGY WEAK QUASIELASTIC AND PION PRODUCTION PROCESSES FROM NUCLEI", is the original work of **Mr. Shakeb Ahmad**, done under my supervision.

(**Prof. S. K. Singh**)

♣ ACKNOWLEDGEMENTS

It is my pleasure to express my sincere thanks and deep sense of gratitude to my supervisor, Prof. S. K. Singh for his patient guidance, continued interest and encouragement and support throughout this work. I am indebted to him for being tolerant of my personal shortcomings and professional limitations, for always helping me to remove my doubts and difficulties through many illuminating conversations and all the inspiration, I required, to take this work to completion. In fact to work with him was a most pleasurable, enriching and memorable experience of my life and I take this opportunity to pay my sincere thanks and best regards to him.

I feel obliged to Dr. M. Sajjad Athar, Reader, Department of Physics, Aligarh Muslim University, Aligarh for his valuable suggestions, comments and encouragement throughout this work which have helped me in improving the quality of this work, and with whom, in many conversations and discussions I learned a good deal of physics too.

I am thankful to Prof. M. Irfan, Chairman, Department of Physics, Aligarh Muslim University, Aligarh for providing the required infrastructure in the Department of Physics, Aligarh Muslim University, Aligarh to carry out my work without which nothing would have been feasible. He has always been a source of inspiration and great support to me whenever I needed, from the Department.

Thanks are also due to all my respected teachers of the Department of Physics, Aligarh Muslim University, Aligarh for their moral support and various suggestions during this period.

Thanks are also indebted to the office and seminar staffs of the Department of Physics, Aligarh Muslim University, Aligarh for their co-operation in providing the required official assistance and valuable literature.

I am indebted to all my good friends from the very beginning of this long, long process who always shared my joys and sorrows with equal willingness and made my stay at Aligarh, despite not very happy circumstances, pleasurable. Thank you for keeping me from quitting.

Financial assistance provided by the Council of Scientific and Industrial Research (India), is gratefully acknowledged.

Finally, I would not be who I am without my family and indeed I would not be at all without my parents. From an early age, my parents encouraged me to reach higher and satisfy my curiosity. My mother continued to influence me even after her passing. Words cannot express my indebtedness to my parents who through their love and affection, their wishes and prayers have given me the inspiration to do the work of my choice. I cannot thank you enough for the support (emotional and financial) and love that you have given without question over the years. In my family I was embraced by new members and have received much support from all of them. I give my thanks and my love to all of you. On a personal note, I express my special thanks to my beloved brothers and sisters whose blessings, boundless affection and encouragements helped me achieve this work successfully.

SHAKEB AHMAD

List of Publications

I. List of Publications in Research Journals

1 *Nuclear Effects in Neutrino Induced Coherent Pion Production at K2K and MiniBooNE*
S. K. Singh, M. Sajjad Athar and **Shakeb Ahmad**
Phys. Rev. Lett. **96**, 241801 (2006).

2 *Neutrino Induced Charged Current $1\pi^+$ Production at Intermediate Energies*
Shakeb Ahmad, M. Sajjad Athar and S. K. Singh
Phys. Rev. **D 74**, 073008 (2006)

3. *Nuclear Cross Sections in ^{16}O for β beam neutrinos at Intermediate Energies*
S. K. Singh, M. Sajjad Athar and **Shakeb Ahmad**
Phys. Lett **B 641**, 159 (2006).

4 *Neutrino Nucleus Cross Sections for low Energy Neutrinos at SNS facilities*
M. Sajjad Athar, **Shakeb Ahmad** and S. K. Singh
Nucl Phys **A 764**, 551 (2006)

5 *Weak Pion Production from Nuclei*
S K Singh, M Sajjad Athar and **Shakeb Ahmad**
Pramana J. of Physics **66**, 689 (2006)

6. *Neutrino Induced Charged Current $1\pi^+$ Production from ^{12}C at Intermediate Energies*
M. Sajjad Athar, **Shakeb Ahmad** and S. K. Singh
Nucl. Phys **A** , (Accepted for Publication) (2006).

7 *Supernova Neutrino Induced Inclusive Reactions on ^{56}Fe in Terrestrial Detectors*
M. Sajjad Athar, **Shakeb Ahmad** and S. K. Singh
Phys Rev. **C 71**, 045501 (2005).

8 *Charged Current Lepton Production from Iron Induced by Atmospheric neutrinos*
M. Sajjad Athar, **Shakeb Ahmad** and S. K. Singh
Eur. Phys. J. **A 24**, 459 (2005)

9 *Coherent Pion Production in Electroweak Processes*
R. Husain, **S. Ahmad**, M Sajjad Athar and S K. Singh
Mesons and Quarks, Edited by A B Santra et al , Narosa Publication, New Delhi, Page 260-272 (2004)

10 Δ *Production Calculations with Nuclear Effects*
S K Singh, **S. Ahmad** and M. Sajjad Athar
NuInt02, university of california, Irvine, December 2002
http.//www.ps uci.edu/ nuint/.

11 *Antineutrino Induced Neutrino-Nucleus Reactions at Intermediate Energies*
Phys. Rev. **D** (To be submitted) (2006)

II. List of Papers in Conference/Symposium

1 *Photoproduction of Pions in* ^{12}C *Nuclei.*
R Husain, **Shakeb Ahmad**, M. Sajjad Athar and S K Singh
DAE-BRNS Symposium on Nuclear Physics, Vol **44B**, 344 (2001).

2 *Neutrino Magnetic Moment Effects in* $\nu + ^{16}O \rightarrow \nu + ^{16}O + \pi^0$.
R. Husain, **Shakeb Ahmad**, M. Sajjad Athar and S. K Singh
DAE-BRNS Symposium on Nuclear Physics, Vol. **44B**, 334 (2001).

3 *Deuteron Effects in Pion Production fron* νd *Reaction.*
Shakeb Ahmad, M. Sajjad Athar and S K. Singh
DAE-BRNS Symposium on Nuclear Physics, Vol. **45B**, 308 (2002).

4. *Nuclear Medium Effects in Coherent Electroproduction of Pions from Nuclei.*
R. Husain, **Shakeb Ahmad**, M. Sajjad Athar and S. K. Singh
DAE-BRNS Symposium on Nuclear Physics, Vol. **45B**, 294 (2002).

5 *Nuclear Medium Effects in Coherent* $\nu_e + ^{16}O \rightarrow e^- + ^{16}O + \pi^+$ *Reaction.*
Shakeb Ahmad, M. Sajjad Athar and S. K. Singh
DAE-BRNS Symposium on Nuclear Physics, Vol **46B**, 320 (2003)

6. *Inelastic lepton Production Induced by Neutrinos Relevant for MiniBooNE Energies.*
S Chauhan, **Shakeb Ahmad**, M. Sajjad Athar and S K. Singh
DAE-BRNS Symposium on Nuclear Physics, Vol. **47B**, 594 (2004)

7 *Neutrino Nucleus Cross Sections from Stopped Pion Neutrinos*
Shakeb Ahmad, M Sajjad Athar and S K Singh
DAE-BRNS Symposium on Nuclear Physics, Vol **47B**, 596 (2004)

8 *Antineutrino Reactions from Nuclei at Intermediate Energies*
Shakeb Ahmad, M Sajjad Athar and S K Singh
DAE-BRNS Symposium on Nuclear Physics, (Accepted) (2006)

Contents

List of Figures

List of Tables

Chapter 1

Introduction

The neutrino experiments done in last few years have given conclusive evidence for the existence of neutrino oscillations. These experiments have been performed in the low energy as well as in the intermediate energy region of neutrino energies using detectors which use nuclear targets. In these energy regions, the major neutrino nuclear processes which are used to model neutrino cross sections are the quasielastic and inelastic neutrino processes in which leptons and pions are produced in neutrino-nuclear reactions. As the neutrino energy increases, the deep inelastic neutrino scattering processes also become important.

There are various neutrino generators which are used to simulate neutrino events in these experiments. The widely used neutrino generators are NUANCE [1], NEUGEN [2], NEUT [3], NUX [4], GENEVE [5] and FLUKA [6] which are being used in the analysis of various experiments. Most of these generators use quasielastic cross sections of Llewellyn Smith [7] with nuclear effects given by Smith and Moniz [8]. For inelastic reactions, where lepton production is accompanied by pions, the model of Rein and Sehgal [9] is used for coherent and incoherent processes. The deep inelastic scattering processes are modeled by using generalized parton distributions given by [10].

However, these generators differ in the specific details of the model used and do not include nuclear effects in the calculation of cross sections except for the quasielastic process. Even in these quasielastic processes, the nuclear effects due to nucleon correlation which have been shown to be very important for the low energy processes have not been included at intermediate energies. It is therefore, very important, that a detail study of nuclear effects in quasielastic as well as inelastic processes be made at low and intermediate energy neutrino scattering processes relevant for the study of neutrino oscillation experiments.

The low energy neutrino experiments have been done with solar neutrinos [11]-[19] and reactor antineutrinos [20]-[21], while the intermediate energy neutrino experiments have been done with atmospheric neutrinos [22]-[48] and accelerator neutrinos [49]-[65] to determine various parameters which enter in the phenomenological study of neutrino oscillations. The most simple model used to phenomenologically describe the physics of neutrino oscillations

assumes that these oscillations are described in terms of neutrino masses (through their mass squared differences Δm^2) and a 3×3 unitary matrix which is parametrized in terms of three mixing angles and a phase which is measure of CP violation. All these parameters, are not determined by the existing data from neutrino oscillation experiments. It has been, therefore, proposed to perform many new experiments in various energy regions, with very high neutrino flux, so that experimental data with high statistics is obtained from which these parameters can be determined.

Apart from the conventional sources of solar, reactor, and atmospheric neutrinos (antineutrinos) with which first experiments were done leading to the discovery of the phenomenon of neutrino oscillations, new neutrino sources are now being proposed to perform high statistics, precession experiments. For this, the conventional proton accelerators, have been used which provide neutrinos in various energy regions. The present ongoing and/or proposed experiments in intermediate and high energy regions by K2K, T2K, MiniBooNE, BooNE, NOνA, MINERVA, ICARUS, OPERA, NOMAD collaborations make use of such neutrino and antineutrino beams obtained from proton accelerator at KEK, Fermilab, J-PARC, and CERN. New neutrino sources, which can be obtained at neutrino factories [66]-[71], Superbeams [72]-[75] and β-beam neutrinos from heavy ion accelerators [76] have also been proposed. Out of these new sources, β-beam neutrinos are of special interest as they provide pure neutrino and antineutrino beams of $\nu_e(\bar{\nu}_e)$ type and have no contamination from $\nu_\mu(\bar{\nu}_\mu)$.

In the region of low energy, apart from solar neutrinos and reactor antineutrinos, the conventional neutrino beams from low energy proton accelerators have been used by LSND [77]-[78] and Karmen [79] collaborations. New neutrino beams with low energy have been proposed at Oak Ridge National Laboratory(ORNL) with low energy proton accelerator which is mainly used for producing Spallation Neutron Source(SNS) [80] and at heavy ion accelerators, which provide low energy β-beam neutrinos [81]-[90]. In the region of low energy, the neutrinos are mainly produced from the pions (muons) decaying at rest, the neutrino spectrum is given by Michel spectrum with $E_\nu^{max} \leq$52.8 MeV. The LSND collaboration also used neutrinos produced from low energy pion decaying in flight with $E_\nu^{max} \leq$300 MeV. In case of these low energy neutrinos which are given by Michel spectrum, the leptons are produced mainly through quasielastic reactions like $\nu_\mu + n \rightarrow \mu^- + p$, and $\nu_e + n \rightarrow e^- + p$ (and the corresponding reactions with antineutrinos) on nuclear targets. The neutrino-nuclear cross sections, which are studied in laboratory using various nuclear targets in this energy region are extremely important for the study of supernova simulations. Such an experimental program is proposed and approved to run very soon at Oak Ridge National Laboratory(ORNL) using iron and lead as targets in initial stage and planned to use various other nuclear targets like ^{12}C, ^{16}O, ^{38}Ar, ^{56}Fe, ^{208}Pb etc. in future.

In the intermediate energy region, neutrinos(antineutrinos) have been used/proposed to perform neutrino oscillation experiments using ^{12}C, ^{16}O, ^{38}Ar, ^{56}Fe and ^{208}Pb targets in Scintillator, Cerenkov, Liquid Argon TPC, iron Calorimeter and LANDD detectors. In the energy region E_ν <5 GeV, there are many processes which contribute to the lepton production. Among

them, the main processes which contribute to the lepton production are quasielastic processes, inelastic processes where few resonances are excited and the deep inelastic processes. It is therefore, desirable, that nuclear effects in the neutrino(antineutrino) induced reactions at low and intermediate energies in these nuclei be calculated.

Theoretically, calculations of nuclear effects in the inclusive quasielastic neutrino nucleus reactions have been studied by many authors using different nuclear models [7], [8], [91]-[121]. These calculations generally use a direct summation method (over many nuclear excited states) [91]-[97], a closure approximation [98], [99], Fermi gas model [7], [8], [100]-[107], relativistic mean field approximation [108], continuum random phase approximation (CRPA) [109]-[114] and local density approximation (LDA) [115]-[121]. Some of these methods have also been extended to compute pion production processes through the Δ dominance model [9], [122]-[148]. Recently the contribution of higher resonance excitations to the production of pions have also been calculated [137], [146]-[148].

In this thesis, we have used a local Fermi gas(LFG) model to calculate neutrino induced quasielastic processes and inelastic processes (where one pion is produced). In the case of quasielastic reactions the nuclear effects like Pauli blocking, Fermi motion and nuclear binding are calculated using relativistic Lindhard function corresponding to particle-hole(ph) excitations in the nuclei. The effect of nuclear correlation is calculated by describing the interaction of particle-hole(ph) excitation, as it propagates through the nuclear medium using Random Phase Approximation(RPA). The method has been earlier applied successfully to study the electromagnetic processes induced by photons and electrons and has been described in Refs. [115]-[118], [149]-[155] for application to weak processes. The effect of Coulomb distortion of the charged lepton in the final state is calculated using Fermi function at low electron energies and a modified effective momentum approximation at higher electron energies [116]-[119], [156]-[160]. The method has been applied to calculate low energy neutrino cross section for various nuclei like ^{12}C, ^{16}O, ^{38}Ar, ^{56}Fe and has been applied to pion decay at rest neutrinos relevant of ORNL proposal [119] and also for the case of supernova neutrinos [117], proposed to be studied at various laboratories [77]-[90].

In the case of inelastic reaction pion production is calculated through the excitation of Δ resonance which subsequently decays into nucleon and pion. The renormalization of Δ properties in the medium is included through the modification of Δ mass and width in the medium which is incorporated through the modification of Δ self-energy in the medium [161]-[173]. Finally, the final state interaction of pion with the nucleus is taken into account using a Monte Carlo simulation of pion nucleus interaction [174]-[176] for incoherent production of pions and a standard eikonal approximation for pion distortion for the case of coherent production [161], [162]. The optical model used in the eikonal approximation is determined from the self-energy of the pion calculated in the nuclear medium [161], [162], [169], [170]. Explicit calculations for coherent, and incoherent production of pions from ^{12}C, ^{16}O and ^{56}Fe nuclei have been made which are relevant for the neutrino oscillation experiments being done with Fermilab, KEK and CERN accelerator neutrino sources. These calculations have also been

made for the neutrinos and antineutrinos spectra for β-beam neutrino(antineutrino) which are relevant for the proposed SPL-FREJUS base-line experiments [177].

In the above introduction, we have presented the relevance and importance of low and medium energy weak quasielastic and pion production processes from nuclei. The detailed plan of the work presented here is the following:

In chapter-2., we study the quasielastic neutrino/antineutrino reactions from nucleons and nuclei at low as well as at intermediate energy region of neutrino/antineutrino energies. We first describe the formalism of free neutrino/antineutrino nucleon scattering and extend it to describe the inclusive quasielastic neutrino/antineutrino nucleus reactions. This has been done to investigate the effects of nuclear medium on the differential and the total cross sections. We have done the cross section calculations in the local density approximation (LDA). In local density approximation, the various nuclear medium effects like Pauli blocking, Fermi motion and the renormalization of the weak transition strengths due to the presence of the nuclear medium are taken into account. Also, the effect of coulomb distortion of the lepton produced in charged current reactions is taken into account by using the Fermi function at low electron energies and modified effective momentum approximation (MEMA) at higher electron/muon energies. The results for the calculations of quasielastic processes have been presented and discussed.

In chapter-3., we discuss the weak production of single pion from nucleon in the intermediate energy region in Δ dominance model, where we describe the weak production of Δ resonance from nucleons induced by neutrinos/antineutrinos, which subsequently decays into pions and nucleon. We discuss the weak production of pions in an effective Lagrangian formalism. We first write explicitly the effective Lagrangians for the different hadronic interactions for the weak production of pions and then write expressions for the matrix elements corresponding to the lowest order non vanishing Feynman diagrams contributing to the processes of pion production. We discuss briefly also the presently available N-Δ transition form factors, and write the differential cross section for the Δ production from free nucleon.

In chapter-4., we have taken up the weak production of single pion from nuclei in the intermediate energy region. We discuss the neutrino/antineutrino induced coherent and incoherent weak production of pions from nuclei assuming Δ-dominance. Nuclear pion production differ from pion production from free nucleon because of the various nuclear medium effects like Pauli blocking, Fermi motion of the initial nucleon and the renormalization of Δ properties in a nuclear medium that have to be taken into account. All these effects are taken into account in a local density approximation (LDA). In this chapter, we also discuss the effect of final state interaction of pions with the residual nucleus. This has been discussed separately for the coherent and incoherent processes.

In chapter-5., we present our results and discussion for coherent and incoherent production of leptons and pions. In section-5.1, the differential and total cross sections for the charged and neutral current coherent and incoherent production of pions and leptons have been presented and discussed. These results have been applied to the β-beam neutrino(antineutrino), atmospheric neutrino(antineutrino) and accelerator neutrino(antineutrino) in section-5.2, 5.3 and 5.4, respectively. The theoretical results have been compared with the experimental results and other available theoretical results wherever they are available.

Finally, we conclude and summarize our results in chapter-6. Many appendices (Appendices:A-H) are given at the end of the thesis, which give details of calculations, which have been used in the text.

==========********==========

Chapter 2

Quasielastic Neutrino Reactions With Nucleons and Nuclei

2.1 Introduction

The neutrino induced reactions from nucleons and nuclei at low and intermediate energies through different interaction channels, like elastic, quasielastic, single pion production, play an important role in the study of neutrino properties and their interaction with matter. The charged current quasielastic (CCQE) scattering cross section dominates the total neutrino nucleus cross sections in the energy region $E_\nu \leq 1.0$ GeV. The single charged lepton that is produced in this reaction carries almost all the neutrino energy and the cross section increases linearly at lower energy and then saturates around 1 GeV. In this energy region the charged current quasielastic reaction plays a crucial role in atmospheric and accelerator neutrino oscillation studies. Understanding charged current quasielastic interactions is necessary to accurately predict signal rates in neutrino oscillation experiments. The charged current quasielastic reactions taking place in nuclei i.e. inclusive quasielastic reactions dominates the fully contained events in the detectors of neutrino oscillation experiments with atmospheric neutrinos. Therefore, in the context of fully contained events in the neutrino oscillation experiments, a precise knowledge of the quasielastic inclusive cross section for intermediate energy neutrino nucleus scattering is highly desirable. Also, the nucleons form factors, such as $F_A(q^2)$ can be extracted from the charged current quasielastic differential cross section. Therefore, precession measurement of the cross section for this reaction, including its energy dependence and variation with target nuclei, is essential in order to interpret current and future neutrino oscillation experiments in this energy region.

Studies of quasielastic interactions were among the first ones made from bubble chamber neutrino exposures, and are the primary tool for studying the axial component of the weak nucleon current. The data were taken on both light nuclear (Hydrogen/Deuterium) and heavy nuclear (Neon/Propane/Freon) targets [178]-[188].

Theoretically, calculations of nuclear effects in the inclusive quasielastic neutrino nucleus reactions have been studied by many authors using different nuclear models [7], [8], [91]-[121]. These calculations generally use a direct summation method (over many nuclear excited states) [91]-[97], a closure approximation [98], [99], Fermi gas model [7], [8], [100]-[107], relativistic mean field approximation [108], continuum random phase approximation (CRPA) [109]-[114] and local density approximation (LDA) [115]-[121]. In this work we have studied the inclusive neutrino nucleus reaction using the local density approximation.

In this chapter we shall describe the quasielastic regime of charged current neutrino and antineutrino interactions from nucleons and nuclei. We first discuss the formalism of neutrino nucleon scattering in section-2.2. The inclusive quasielastic neutrino nucleus reaction have been discussed in section-2.3. The calculations have been done in local density approximation (LDA)(see section-2.4). The method has been successfully applied to study the various electromagnetic and weak processes in nuclei at low and intermediate energies [115]-[118], [149]-[155]. The Fermi motion and Pauli blocking effects in nuclei are taken into account through the imaginary part of the Lindhard function for particle hole (p-h) excitations in the nuclear medium. The renormalization of weak transition strengths, which are quite substantial in the spin-isospin channel, are calculated in the random phase approximation (RPA) through the interaction of p-h excitations as they propagate in the nuclear medium using a nucleon-nucleon potential described by pion and rho exchanges (see section-2.5). The effect of Coulomb distortion of the lepton produced in charged current reactions is taken into account by using the Fermi function F(Z,E_e), where Z is the atomic number and E_e is the outgoing lepton energy, as well as in a modified momentum approximation (MEMA) [116]-[119], [156]-[160], where the effect of Coulomb distortion is incorporated by modifying the momentum and energy of charged lepton in the Coulomb potential of the final nucleus (see section-2.6). In section-2.7, the results for the calculation of quasielastic processes have been presented and discussed.

2.2 Quasielastic Neutrino-Nucleon Reactions

2.2.1 Matrix Elements and Cross Section

Neutrinos (ν_l) and antineutrinos ($\bar{\nu}_l$), where $l(= e^{\pm}, \mu^{\pm})$ is the lepton interacts with free nucleons via charged as well as neutral current. Here we consider the neutrino and antineutrino induced charged and neutral current quasielastic interactions of the type

$$\left.\begin{array}{l} \nu_l(k) + n(p) \rightarrow l^-(k') + p(p') \\ \bar{\nu}_l(k) + p(p) \rightarrow l^+(k') + n(p') \end{array}\right\} \quad \text{(Charged Current)} \tag{2.1}$$

$$\left.\begin{array}{l} \nu_l(k) + n(p) \rightarrow \nu_l(k') + n(p') \\ \nu_l(k) + p(p) \rightarrow \nu_l(k') + p(p') \\ \bar{\nu}_l(k) + n(p) \rightarrow \bar{\nu}_l(k') + n(p') \\ \bar{\nu}_l(k) + p(p) \rightarrow \bar{\nu}_l(k') + p(p') \end{array}\right\} \quad \text{(Neutral Current)} \tag{2.2}$$

where k and k' are the four momenta of the neutrino and the corresponding charged lepton and p and p' are four momenta of the incoming and outgoing nucleons. In charged current interactions, a charged vector boson $W^{\pm}$ is exchanged, while in neutral current interactions a neutral vector boson Z^0 is exchanged. Feynman diagrams corresponding to reactions 2.1 and 2.2 are shown in Fig.2.1.

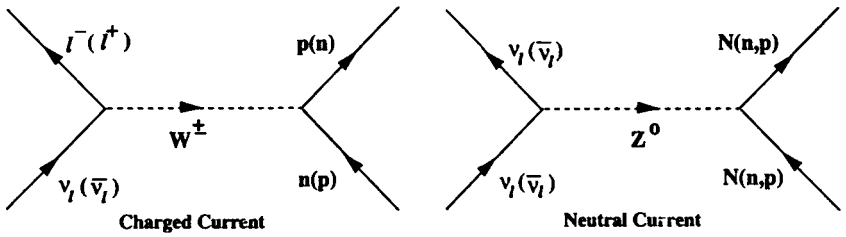

Figure 2.1: Feynman diagrams corresponding to $\nu(\bar{\nu})$-nucleon scattering.

Using the weak charged current interaction part of the standard model(SM) Lagrangian, the invariant matrix element for the charged current reaction of neutrino assuming that the reaction is mediated by charged vector boson W^+ can be written as

$$\begin{aligned} -i\mathcal{M} &= \left(\frac{-ig}{2\sqrt{2}}\right) l^{\mu} \left(\frac{ig_{\mu\nu}}{M_W^2}\right) \cdot \left(\frac{-ig}{2\sqrt{2}}\right) \langle p(p')|J^{\nu}(0)|n(p)\rangle \\ \mathcal{M} &= \frac{g^2}{8M_W^2} l^{\mu} \langle p(p')|J_{\mu}(0)|n(p)\rangle = \frac{G_F}{\sqrt{2}} l^{\mu} \langle p(p')|J_{\mu}(0)|n(p)\rangle \end{aligned} \tag{2.3}$$

where we have used the relation $g^2/8M_W^2 = G_F/\sqrt{2}$ for the scattering with low momentum transfer ($|q^2| << M_W^2$). G_F is the Fermi coupling constant (=1.16639×10^{-5}GeV^2) and M_W is the W-boson mass. $l^{\mu}(x)$ the leptonic weak current given by

$$l^{\mu} = \bar{\psi}_l(k')\gamma^{\mu}(1-\gamma^5)\psi_{\nu_l}(k) \tag{2.4}$$

The hadronic current $J_{\mu}(x)$ consist of vector and axial vector currents satisfying the Lorentz invariance is given as

$$J_{\mu}(x) = \cos\theta_C \langle p(p')|V_{\mu} - A_{\mu}|n(p)\rangle \tag{2.5}$$

where θ_C is the Cabibbo angle. The most general form of the hadronic current that is Lorentz invariant, constructed out of the four vectors p_{μ}, p'_{μ} and $q_{\mu} = p'_{\mu} - p_{\mu}$ is given as

$$J_{\mu} = \bar{u}(p') \left[F_1^V(q^2)\gamma_{\mu} + F_2^V(q^2)i\sigma_{\mu\nu}\frac{q^{\nu}}{2M} + F_A^V(q^2)\gamma_{\mu}\gamma_5 + F_P^V(q^2)q_{\mu}\gamma_5\right] u(p) \tag{2.6}$$

where, $Q^2 = -q^2 = (k-k')^2$ is the momentum transfer square and M is the nucleon mass. In this work we have taken neutron and proton mass to be same. $F_{1,2}^V(q^2)$ are the isovector

vector, and $F_A(q^2)$, $F_P(q^2)$ are the isovector axial vector and pseudoscalar form factors. These nucleon form factors have been discussed in subsection-2.2.2.

Using the leptonic and hadronic currents given in Eq.2.4 and Eq.2.6, respectively, we can write the matrix element square as:

$$|\mathcal{M}|^2 = \frac{G_F^2}{2}\cos^2\theta_C \; L^{\mu\nu} J_{\mu\nu} \tag{2.7}$$

with the leptonic tensor $L^{\mu\nu}$ calculated to be

$$\begin{aligned} L^{\mu\nu} = \bar{\Sigma}\Sigma l^{\mu\dagger} l^{\nu} &= \mathrm{Tr}\left[(\not{k} + m_\nu)\,\gamma^\mu(1-\gamma^5)(\not{k}' + m_l)\,\gamma^\nu(1-\gamma^5)\right] \\ &= L_S^{\mu\nu} + iL_A^{\mu\nu}, \quad \text{where} \qquad (2.8) \\ L_S^{\mu\nu} &= 8\left[k^\mu k'^\nu + k'^\mu k^\nu - g^{\mu\nu}\, k\cdot k'\right] \quad \text{and} \\ L_A^{\mu\nu} &= \cdot\, 8\,\epsilon^{\mu\nu\alpha\beta}\, k_\alpha k'_\beta \qquad (2.9) \end{aligned}$$

The subscript S and A refer to the symmetry under interchange of the Lorentz indices μ and ν. For antineutrino the antisymmetric part of the leptonic tensor gets a minus sign. In general we can write the leptonic tensor $L^{\mu\nu}$ to be

$$L^{\mu\nu} = L_S^{\mu\nu} \pm iL_A^{\mu\nu}, \quad (+ \text{ for } \nu, \text{ - for } \bar{\nu}) \tag{2.10}$$

The hadronic tensor $J_{\mu\nu}$ is given by:

$$\begin{aligned} J_{\mu\nu} &= \bar{\Sigma}\Sigma J_\mu^\dagger J_\nu \\ &= \frac{1}{2}\mathrm{Tr}\left[(\not{p}' + M)\Gamma_\mu(\not{p} + M)\tilde{\Gamma}_\nu\right] \qquad (2.11) \end{aligned}$$

where

$$\Gamma_\mu = \left[F_1^V(q^2)\gamma_\mu + F_2^V(q^2)i\sigma_{\mu\nu}\frac{q^\nu}{2M} + F_A^V(q^2)\gamma_\mu\gamma_5 + F_P^V(q^2)q_\mu\gamma_5\right] \tag{2.12}$$

and $\tilde{\Gamma}_\nu = \gamma_0\,\Gamma_\nu^\dagger\,\gamma_0$

The explicit expression for $J_{\mu\nu}$ is given in Eq.A.4 (Appendix-A). From this we obtain the differential cross section $d\sigma/dq^2$ for free neutrino-nucleon scattering given in Eq.2.1 in the laboratory system. In general the differential cross section for the reaction $\nu_l(k) + n(p) \rightarrow l^-(k') + p(p')$ can be written as

$$d\sigma = \left(\frac{G_F^2\cos^2\theta_C}{2}\right)\frac{(2\pi)^4\delta^4(k+p-p'-k')}{4\sqrt{(k\cdot k')^2 - m_\nu^2 M_n^2}}\frac{d^3\mathbf{k}'}{(2\pi)^3 2E_l}\frac{d^3\mathbf{p}'}{(2\pi)^3 2E_p}\prod_f (2m_f)|\mathcal{M}|^2 \tag{2.13}$$

where $|\mathcal{M}|^2 = L^{\mu\nu}J_{\mu\nu}$ and $k + p = k' + p'$, $q = k - k'$. Using the relations

$$4\sqrt{(k\cdot k')^2 - m_\nu^2 M_n^2} \;=\; 4p\cdot k \;=\; 4M_n E_\nu \tag{2.14}$$

$$d^3\mathbf{k}' = |\mathbf{k}'|^2\, d|\mathbf{k}|\, d\Omega_{k'} = E_{k'}\, |\mathbf{k}'|\, dE_{k'}\, d\Omega_{k'} \tag{2.15}$$

$$\int \frac{d^3\mathbf{p}'}{2E_{p'}}\delta^4(k+p-p'-k') = \frac{1}{2M_p}\delta\left(\nu + \frac{q^2}{2M_p}\right), \quad \nu = E_\nu - E_{k'} \tag{2.16}$$

and $|\mathcal{M}|^2$ from Appendix-A, the differential cross section is given as

$$\frac{d\sigma}{dq^2} = \frac{G_F^2 M^2 \cos^2\theta_C}{8\pi E_\nu^2}\left[A(q^2) \mp B(q^2)\,\frac{(s-u)}{M^2} + C(q^2)\,\frac{(s-u)^2}{M^4}\right] \tag{2.17}$$

where $M_p = M_n = M$ and $s - u = 4M_n E_\nu = q^2 - m_l^2$. The factors $A(q^2)$, $B(q^2)$ and $C(q^2)$ are given as:

$$\begin{aligned} A(q^2) &= \frac{m_l^2 - q^2}{4M^2}\left[\left(4 - \frac{q^2}{M^2}\right)F_A^2(q^2) - \left(4 + \frac{q^2}{M^2}\right)(F_1^V(q^2))^2 - \frac{q^2}{M^2}\left(1 + \frac{q^2}{4M^2}\right)\right. \\ &\quad (F_2^V(q^2))^2 - \frac{4q^2}{M^2}F_1^V(q^2)F_2^V(q^2) - \frac{m_l^2}{M^2}\left(\left(F_1^V(q^2) + F_2^V(q^2)\right)^2\right. \\ &\quad \left.\left. + \left(F_A(q^2) + 2F_p(q^2)\right)^2 + \left(\frac{q^2}{M^2} - 4\right)F_p^2(q^2)\right)\right] \end{aligned} \tag{2.18}$$

$$B(q^2) = -\frac{q^2}{M^2}F_A^2(q^2)\left[F_1^V(q^2) + F_2^V(q^2)\right] \tag{2.19}$$

$$C(q^2) = \frac{1}{4}\left[F_A^2(q^2) + (F_1^V(q^2))^2 - \frac{q^2}{4M^2}(F_2^V(q^2))^2\right] \tag{2.20}$$

The cross section is given in terms of the form factors $F_1^V(q^2)$, $F_2^V(q^2)$, $F_A(q^2)$ and $F_p(q^2)$. We can see that the pseudoscalar form factors is multiplied by m_l^2/M^2 so at relatively high neutrino energies where the experiments are performed, the lepton mass m_l can be neglected and then the pseudoscalar term does not contribute. In fact, the cross section is valid for all flavors of neutrino as it has dependence on the lepton mass, but the contribution of pseudoscalar term will be negligible for ν_e and ν_μ and is important for ν_τ. The negative (positive) sign in front of the $B(q^2)$ term refers to neutrino (antineutrino) scattering.

2.2.2 Nucleon Vector and Axial Form Factors

The hadronic current in Eq.2.6 contains two isovector form factors $F_{1,2}^V(q^2)$ of the nucleons, which can be related to the isovector combination of the Dirac and Pauli form factors of proton and neutron by the relation

$$F_{1,2}^V(q^2) = F_{1,2}^p(q^2) - F_{1,2}^n(q^2) \tag{2.21}$$

where $F_{1,2}^p(q^2)$ and $F_{1,2}^n(q^2)$ are the Dirac and Pauli form factors of proton and neutron. These Dirac and Pauli form factors further can be written in terms of the experimentally determined Sach's electric $G_E^{p,n}(q^2)$ and magnetic $G_M^{p,n}(q^2)$ form factors of the nucleons. These electric

and magnetic Sach's form factors by their pronounced Q^2-dependence, show clear evidence for the extended charge and current distributions of the nucleons, respectively.

$$G_M^{p,n}(q^2) = F_1^{p,n}(q^2) - F_2^{p,n}(q^2) \tag{2.22}$$

$$G_E^{p,n}(q^2) = F_1^{p,n}(q^2) + \frac{q^2}{4M^2} F_2^{p,n}(q^2) \tag{2.23}$$

With this, one gets the isovector form factors $F_{1,2}^V(q^2)$ in the form:

$$F_1^V(q^2) = \left(1 - \frac{q^2}{4M^2}\right)^{-1} \left[G_E^V(q^2) - \frac{q^2}{4M^2} G_M^V(q^2)\right] \tag{2.24}$$

$$F_2^V(q^2) = \left(1 - \frac{q^2}{4M^2}\right)^{-1} \left[G_M^V(q^2) - G_E^V(q^2)\right] \tag{2.25}$$

where $G_E^V(q^2)$ and $G_M^V(q^2)$ are the vector electric and magnetic form factors. Through the conserved vector current hypothesis (CVC), these vector electric and magnetic form factors are related to the elastic nucleon form factors $G_E^p(q^2)$, $G_E^n(q^2)$, $G_M^p(q^2)$ and $G_M^n(q^2)$ measured in electron scattering, given by

$$G_E^V(q^2) = G_E^p(q^2) - G_E^n(q^2) \quad \text{and} \quad G_M^V(q^2) = G_M^p(q^2) - G_M^n(q^2) \tag{2.26}$$

The axial part of the hadronic current given in Eq.2.6 has structure dependent form factors $F_A^V(q^2)$ and $F_P^V(q^2)$, known as the axial vector and pseudoscalar form factors, respectively. The axial vector form factor has been studied in considerable details, while the pseudoscalar form factor, is much harder to study, being negligible at the momentum transfer of β-decay. It is nevertheless very important.

The pseudoscalar form factor $F_p^V(q^2)$ is dominated by the pion pole and is given in terms of the Golberger-Treiman relation near $Q^2 = -q^2 \approx 0$ if partially conserved axial current (PCAC) are assumed. It is assumed that the same relation is valid for high q^2 as well and given as

$$F_p^V(q^2) = \frac{2M F_A^V(q^2)}{m_\pi^2 - q^2} \tag{2.27}$$

2.2.3 Form Factor Parameterizations

Now with four unknown form factors $F_{1,2}^V(q^2)$, $F_A(q^2)$ and $F_P(q^2)$, we are left with the electromagnetic Sach's form factors $G_E^{p,n}(q^2)$ and $G_M^{p,n}(q^2)$ of the nucleon which are known from electron scattering, and the axial form factors $F_A(q^2)$ which can only be determined through weak interaction processes.

These electromagnetic Sach's form factors are given as

$$G_E^p(q^2) = G_D(q^2), \quad G_E^n(q^2) = \mu_n \frac{\tau}{1 - A\tau} G_D(q^2), \quad \tau = \frac{q^2}{4M}. \tag{2.28}$$

$$G_M^p(q^2) = \mu_p\, G_D(q^2), \quad G_M^n(q^2) = \mu_n\, G_D(q^2) \tag{2.29}$$

with proton and neutron magnetic moments as μ_p=2.793μ_N and μ_n=-1.913μ_N, respectively given in units of the nuclear magneton, $\mu_N = e/2M_p$ and A=5.6. $G_D(q^2)$ is given as

$$G_D(q^2) = \left[1 - \frac{q^2}{M_V^2}\right]^{-2} \tag{2.30}$$

with the vector mass M_V^2=0.71 GeV^2. The above combination of form factors are known as dipole form factors. The axial form factor is parametrized as

$$F_A(q^2) = g_A(0)\ \left[1 - \frac{q^2}{M_A^2}\right]^{-2} \tag{2.31}$$

and is extracted from the quasielastic neutrino and antineutrino scattering. This form factor can also be extracted from pion electroproduction data. Previous neutrino experiments used the axial vector constant $g_A(0)$=-1.23, while the best current value is -1.267. The value of axial mass from the average of all neutrino scattering is M_A=1.026±0.020 GeV [189].

Many new parameterizations for these electromagnetic form factors have been developed in recent years based on fits to experimental data [190]-[194]. These days the best fit parameterizations are from Budd et al. [191] known as BBA-03 form factors and by Bradford et al. [194] known as BBBA-05 form factors. These parameterizations takes into account the recent electron scattering data at Jefferson Lab [195] to obtain updated values for the electromagnetic Sach's form factors with which they fitted gain the old neutrino data and updated also the axial mass which is the largest uncertainty in neutrino nucleon scattering.

In BBA-03 [191] parametrization, electron scattering data are fitted for each of the form factors to an inverse polynomials given as

$$G_{E,M}^N(Q^2) = \frac{G_{E,M}^N(0)}{1 + a_2Q^2 + a_4Q^4 + a_6Q^6 + a_8Q^8 + a_{10}Q^{10} + a_{12}Q^{12}} \tag{2.32}$$

Table 2.1: The coefficients of the inverse polynomial fits (Eq.2.32) for the $G_E^p(Q^2)$, $G_M^p(Q^2)$ and $G_M^n(Q^2)$ in BBA-03 parametrization.

Observables	a_2	a_4	a_6	a_8	a_{10}	a_{12}
$G_E^p(Q^2)$	3.253	1.422	0.08582	0.3318	-0.09371	0.01076
$G_M^p(Q^2)$	3.104	1.428	0.1112	-0.006981	0.0003705	-0.7063E-05
$G_M^n(Q^2)$	3.043	0.8548	0.6806	-0.1287	0.008912	-

Table.2.1 shows the parameters of the fit. $G_{E,M}^N(0)$ are those of the dipole form factors at Q^2=0. Their normalizations at Q^2=0 are given by the nucleon charges and magnetic moments:

$$\begin{aligned} &\text{Proton}: \quad G_E^p(0) = 1, \quad G_M^p(0) = \mu_p = 2.793 \\ &\text{Neutron}: \quad G_E^n(0) = 0, \quad G_M^n(0) = \mu_n = -1.913 \end{aligned} \tag{2.33}$$

Since the neutron has no charge, $G_E^n(Q^2)$ must be zero at Q^2=0, and previous neutrino experiments assumed $G_E^n(Q^2)$=0 for all Q^2 values. However, it is non zero away from Q^2=0. At intermediate Q^2, recent polarization transfer data give precise values of $G_E^n(Q^2)$. The parametrization used in BBA-03 analysis is of krutov et al. [196]:

$$G_E^n(Q^2) = -\mu_n \frac{a\tau}{1+b\tau} G_D(Q^2), \quad \tau = \frac{Q^2}{4M^2} \tag{2.34}$$

with a=0.942 and b=4.61. This parametrization is very similar to that of Galster et al. [197]. The axial form factor in BBA-03 analysis is of the same dipole form as in Eq.2.31 with updated value of axial mass M_A=1.00±0.020 GeV [191] which is in good agreement with the value obtained from pion electroproduction of M_A=1.014±0.016 GeV [189].

The BBBA-05 parametrization [194] is the updated parametrization of the earlier work [191], [193] developed by fitting a single functional form for all four elastic form factors. The functional form is given by

$$G_{E,M}^N(Q^2) = \frac{\sum_{k=o}^{n} a_k \tau^k}{1 + \sum_{k=1}^{n} b_k \tau^k}, \quad \tau = \frac{Q^2}{4M_p^2} \tag{2.35}$$

where n(=0,1,2) for parameter a and it is n(=1,2,3,4) for parameter b. The coefficients for the fit of the functional form in Eq.2.35 is given in Table.2.2

Table 2.2: The coefficients of the functional form fit (Eq.2.35) for the $G_E^p(Q^2)$, $G_E^n(Q^2)$, $G_M^p(Q^2)$ and $G_M^n(Q^2)$ in BBBA-05 parametrization.

Form Factors	a_0	a_1	a_2	b_1	b_2	b_3	b_4
$G_E^p(Q^2)$	1	-0.0578±0.166	-	11.1±0.217	13.6±1.39	33.0±8.95	-
$G_M^p(Q^2)$	1	0.150±0.312E-1	-	11.1±0.103	19.6±0.281	7.54±0.967	-
$G_E^n(Q^2)$	0	1.25±0.368	1.30 ±1.99	-9.86±6.46	305±28.6	-758±77.5	802 ±156
$G_M^n(Q^2)$	1	1.81±0.402	-	14.1±0.597	20.7±2.55	68.7±14.1	-

This form of the $G_{E,M}^N(Q^2)$ in Eq.2.35 has been used by other parameterizations in the past [193], which provides excellent fits to $G_E^p(Q^2)$, $G_M^p(Q^2)/\mu_p$ and $G_M^n(Q^2)/\mu_n$ using only four parameters each given in Table.2.3.

However, this approach is less successful for $G_E^n(Q^2)$ and for this Galster parametrization has been used [197] given as

$$G_E^n(Q^2) = \frac{A\tau}{1+B\tau} G_D(Q^2), \quad \tau = \frac{Q^2}{4M^2} \tag{2.36}$$

Table 2.3: The coefficients of the functional form fit (Eq.2.35) for the $G_E^p(Q^2)$, $G_M^p(Q^2)/\mu_p$ and $G_M^n(Q^2)/\mu_n$ in parametrization [193].

Observables	a_0	a_1	b_1	b_2	b_3
$G_E^p(Q^2)$	1	-0.24±0.12	10.98±0.19	12.82±1.1	21.97±6.8
$G_M^p(Q^2)/\mu_p$	1	0.12±0.04	10.97±0.11	18.86±0.28	6.55±1.2
$G_M^n(Q^2)/\mu_n$	1	2.33±1.4	14.72±1.7	24.20±9.8	84.1±41

with A=1.70±0.04 and B=3.30±0.32, and $G_D(Q^2)$ is the dipole form factor given in Eq.2.30.

Another parametrization is done by P. E. Bosted [190] fitting all three form factors $G_E^p(Q^2)$, $G_M^p(Q^2)/\mu_p$ and $G_M^n(Q^2)/\mu_n$ with a single function assuming form factor scaling. The functions are given as

$$G_E^p(Q^2) = \frac{1}{1+0.62Q+0.68Q62+2.80Q^3+0.83Q^4} \tag{2.37}$$

$$\frac{G_M^p(Q^2)}{\mu_p} = \frac{1}{1+0.35Q+2.44Q^2+0.50Q^3+1.04Q^4+0.34Q^5} \tag{2.38}$$

$$\frac{G_M^n Q^2)}{\mu_n} = \frac{1}{1-1.74Q+9.29Q^2-7.63Q^3+4.63Q^4} \tag{2.39}$$

with $G_E^p(0)$=1 and $G_M^p(0)/\mu_p$=1. The number of free parameters was increased until good fits were obtained. This fit for $G_E^p(Q^2)$ is only valid for Q^2=7 GeV^2. They also tried a fit assuming form factor scaling for the proton to obtain

$$G_E^p(Q^2) = \frac{G_M^p(Q^2)}{\mu_p} = \frac{1}{1+0.14Q+3.01Q^2+0.02Q^3+1.20Q^4+0.32Q^5} \tag{2.40}$$

the neutron electric form factor $G_E^n(Q^2)$ is given as

$$G_E^n(Q^2) = \frac{-a\mu_n\tau}{1+b\tau}\, G_D(Q^2), \quad \tau = \frac{Q^2}{4M^2} \tag{2.41}$$

with a=1.25±0.13 and b=18.3±3.4, and $G_D(Q^2)$ is the dipole form factor given in Eq.2.30.

2.3 Inclusive Quasielastic Neutrino-Nucleus Reactions

The study of weak processes in nuclei induced by neutrinos and antineutrinos has significant importance in current experimental studies of neutrino oscillations. The neutrino oscillation experiments use nuclei as targets in neutrino detectors so that the knowledge of reactions induced by neutrinos on nuclei are important for the interpretation of experiments on neutrino

oscillations. There are mainly two types of nuclear processes induced by neutrinos. First one is the exclusive reaction

$$\nu_l(k) + {}^{A}_{Z_i}X(p) \rightarrow l^-(k') + {}^{A}_{Z_f}Y(p'), \tag{2.42}$$

where $Z_i(Z_f)$ is the charge of initial(final) nucleus. In this case the final nucleus is left either in the ground state or in an excited state, which decays into some final states, which are observed individually. Second one is the inclusive reaction in which the final nucleus is left either in the ground state or many nuclear states are excited in the final nucleus and different particle production may take place. In these inclusive reactions only the energy and the scattering angle of the outgoing lepton are measured.

The process under consideration is the charged current neutrino and antineutrino induced quasielastic inclusive reactions

$$\nu_l(k) + {}^{A}_{Z}Y(p) \rightarrow l^-(k') + X(p') \tag{2.43}$$

$$\bar{\nu}_l(k) + {}^{A}_{Z}Y(p) \rightarrow l^+(k') + X(p') \tag{2.44}$$

in which a neutrino or antineutrino with four momentum k scatters from a nucleon inside the nucleus with four momentum p. The outgoing lepton has four momentum k' and the hadronic final state X is left with four momentum p'. X stands for the hadronic debris produced in the inclusive inelastic collision.

When the neutrino scatters from a nucleon in the nucleus, the interactions become modified by the effects of various medium effects like Pauli blocking of the recoil nucleon, binding energy, Fermi motion, and renormalization of the weak coupling constants. To account for these medium effects various methods are used [91]-[121]. Some of these methods are direct summation method (over many nuclear excited states) [91]-[97], a closure approximation [98], [99], Fermi gas model [7]-[8], relativistic mean field approximation [108], continuum random phase approximation (CRPA) [109]-[114] and local density approximation (LDA) [115]-[121]. In the present work local density approximation has been used, which has been briefly outlined below.

2.4 Local Density Approximation (LDA)

In the local density approximation, the cross section is evaluated as a function of local Fermi momentum, $p_F(r)$ and integrated over the whole nucleus. Inside the nucleus various medium effects like Fermi motion and Pauli blocking effects in nuclei are taken into account through the imaginary part of the Lindhard function using relativistic kinematics [198]-[202] for particle hole (p-h) excitations in the nuclear medium. The effect of the Coulomb force on the outgoing charged lepton and Q_{th}-value of the reaction are also properly taken into account. The renormalization of weak transition strengths, are calculated in the random phase approximation (RPA) through the interaction of p-h excitations as they propagate in the nuclear medium using a nucleon-nucleon potential described by pion and rho exchanges. We shall obtain the expressions for the total cross section and differential cross section in this approximation.

In a nucleus, the neutrino scatters from a neutron or a proton moving in the finite nucleus whose local density in the medium is $\rho_n(r)$ or $\rho_p(r)$ respectively with its corresponding Fermi momenta distribution. In the local density approximation, the local Fermi momenta of neutrons and protons are given by

$$p_{Fn} = \left[3\pi^2\rho_n(r)\right]^{1/3}; \quad p_{Fp} = \left[3\pi^2\rho_p(r)\right]^{1/3} \tag{2.45}$$

The scattering cross section, in the local density approximation is written as [115]-[116], [149]

$$\sigma(E_l, \theta_l) = \int \rho_n(r)\, d^3\mathbf{r}\, \sigma_0(E_l, \vartheta_l) \tag{2.46}$$

where $\sigma_0(E_l,\ \theta_l)$ is the double differential cross section for the charged current free neutrino-nucleon scattering (Eq.2.1) in the laboratory system given as

$$\sigma_0(E_l, \theta_l) = \frac{1}{4\pi^2}\, \frac{|\mathbf{p}_l|^2}{E_\nu E_l}\, \frac{M_n M_p}{E_n E_p}\, \bar{\sum}\sum |\mathcal{M}|^2\, \delta[q_0 + E_n - E_p] \tag{2.47}$$

where $\bar{\sum}\sum|\mathcal{M}|^2$ is the square modulus of the transition amplitude given in Eq.2.7, averaged over the initial and summed over the final spins of the nucleons calculated in Appendix-A.

In symmetric nuclear matter, each nucleon occupies a volume of $(2\pi\hbar)^3$. However, because of two possible spin orientations of nucleons, each unit cell in configuration space is occupied by two nucleons. Thus the number of nucleons in a certain volume is ($\hbar = 1$) [200]

$$N = 2V \int_0^{p_F} \frac{d^3p}{(2\pi)^3}, \quad \text{or} \quad \rho(r) = \frac{N}{V} = 2\int \frac{d^3p}{(2\pi)^3}\, n_n(\mathbf{p}, \mathbf{r}) \tag{2.48}$$

where $n_n(\mathbf{p}, \mathbf{r})$ is the local neutron occupation number. $n_n(\mathbf{p}, \mathbf{r})$=1 for $p \leq p_{F_n}$ and is equal to zero for $p > p_{F_n}$, where p_{F_n} is local Fermi momentum of neutron.

Hence,

$$\sigma_0(E_l, \theta_l) = 2\int d^3r\, \frac{d^3p}{(2\pi)^3}\, n_n(\mathbf{p}, \mathbf{r})\, \sigma_0(E_l, \theta_l) \tag{2.49}$$

$$= 2\int d^3r\, \frac{d^3p}{(2\pi)^3}\, n_n(\mathbf{p}, \mathbf{r})\, \frac{1}{4\pi^2}\, \frac{|\mathbf{p}_l|^2}{E_\nu E_l}\, \frac{M_n M_p}{E_n E_p}\, \bar{\Sigma}\Sigma|\mathcal{M}|^2\, \delta[q_0 + E_n - E_p] \tag{2.50}$$

To ensure that the reaction has taken place in the nucleus, there are several modifications that have to be done to the above formula. While integrating over the energy conserving δ function in Eq.2.50 it has to be kept in mind that the initial and final nucleons are no longer free. They are now moving in the Fermi sea of neutrons and protons in the initial and final nuclei.

The neutron energy E_n and proton energy E_p in the delta function are now function of momenta of neutron and proton in the nucleus, i.e., E_n and E_p are replaced by $E_n(|\mathbf{p}_n|)$ and

$E_p(|\mathbf{p}_n + \mathbf{q}|)$ where $\mathbf{p}_n$ is the momentum of the target neutron inside the nucleus. In the nucleus the neutrons and protons are not free and their momenta are constrained to satisfy the Pauli principle which is implemented in this model by requiring that the initial nucleon momentum $p_n < p_{F_n}$ and final nucleon momentum $p'_p(= |\mathbf{p}_n + \mathbf{q}|) > p_{F_p}$, where p_{F_n} and p_{F_p} are the local Fermi momenta of neutrons and protons at the interaction point in the nucleus defined in terms of their respective nuclear densities as given Eq.2.45. This constraint is the Pauli blocking condition and it is incorporated while performing the integration over the initial nucleon momentum in Eq.2.49 by replacing the factor

$$\int d^3r \, \frac{d^3p}{(2\pi)^3} \, n_n(\mathbf{p}, \mathbf{r}) \, \frac{M_n M_p}{E_n E_p} \, \delta[q_0 + E_n - E_p] \tag{2.51}$$

occurring in Eq.2.50 by $-(1/\pi)\mathrm{Im}U_N(q_0, \mathbf{q})$, where $U_N(q_0, \mathbf{q})$ is the Lindhard function corresponding to the particle hole(ph) excitations induced by weak interaction process through W-boson exchange shown in Fig.2.2(a). In the large mass limit of the W-boson, i.e. $M_W \to \infty$, Fig.2.2(a) is reduced to Fig.2.2(b) for which the Lindhard function is given by [198]-[202]

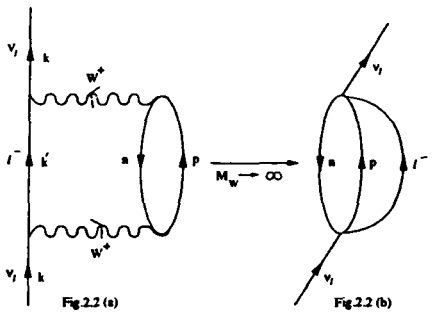

Figure 2.2: Diagrammatic representation of the neutrino self-energy diagram corresponding to the ph-excitation leading to $\nu_l + n \to l^- + p$ in nuclei. In the large mass limit of the IVB ($M_W \to \infty$) the diagram (a) is reduced to (b) which is used to calculate $|\mathcal{M}|^2$ in Eq.2.47.

$$U_N(q_0, \mathbf{q}) = 2 \int \frac{d^3p_n}{(2\pi)^3} \frac{M_n M_p}{E_n E_p} \frac{n_n(\mathbf{p}_n)\,[1 - n_p(\mathbf{p}_n + \mathbf{q})]}{q_0 + E_n(\mathbf{p}_n) - E_p(\mathbf{p}_n + \mathbf{q}) + i\epsilon} \tag{2.52}$$

where $q_0 = E_\nu - E_l$, $n_n(\mathbf{p}_n)$ and $n_p(\mathbf{p}_n + \mathbf{q})$ are occupation numbers for neutrons and protons, respectively, in the Fermi sea. To incorporate the conditions of Fermi motion and Pauli blocking, we take the imaginary part of the Lindhard function $U_N(q_0, \mathbf{q})$, expression for which has been obtained in Appendix-B. This is given by

$$\mathrm{Im}U_N(q_0, \mathbf{q}) = -\frac{1}{2\pi} \frac{M_p M_n}{|\mathbf{q}|} [E_{F_1} - A] \quad \text{with} \tag{2.53}$$

$$q^2 < 0, \quad E_{F_2} - q_0 < E_{F_1} \quad \text{and} \quad \frac{-q_0 + |\mathbf{q}|\sqrt{1 - \frac{4M^2}{q^2}}}{2} < E_{F_1} \tag{2.54}$$

where

$$E_{F_1} = \sqrt{{p_{F_n}}^2 + {M_n}^2}, \quad E_{F_2} = \sqrt{{p_{F_p}}^2 + {M_p}^2} \quad \text{and}$$
$$A = Max\left[M_n,\ E_{F_2} - q_0,\ \frac{-q_0 + |\vec{q}|\sqrt{1 - \frac{4M^2}{q^2}}}{2}\right]. \tag{2.55}$$

Otherwise, Im$U_N(q_0, \mathbf{q})$=0.

The energies E_n and E_p of the neutron and proton in the Lindhard function, refers to the local Fermi sea of the nucleons in the initial and final nucleus. Since in the Fermi sea, there is no energy gap for transition between the occupied and unoccupied states therefore, particle-hole(ph) excitations can be produced with an infinitesimal energy. However, in case of finite nuclei, this is not the case, there exists certain energy gap between ground state of initial and final nuclei. This is the minimum excitation excitation energy, needed for transition to the ground state of the final nucleus. This is the threshold energy Q_{th} of the reaction. Therefore, in nuclei the correction related to the threshold value of the reaction Q_{th} has to be taken into account in order to get a reliable value of the cross section for low energy neutrinos.

We have incorporated the threshold energy Q_{th} of the nuclear reactions in these calculations by replacing the energy conserving δ function i.e., $\delta[q_0 + E_n - E_p]$ in Eq.2.47 by $\delta[q_0 + E_n(\mathbf{p}) - E_p(\mathbf{p}+\mathbf{q}) - Q_{th}]$ and evaluating the Lindhard function in Eq.2.53 at $q_0 - Q_{th}$ instead of q_0. Also to account for the unequal Fermi sea for neutrons and protons for $N \neq Z$ nuclei the factor of $Q'_{th} = E_{Fn} - E_{Fp}$ is added to q_0 in the Lindhard function. Thus q_0 is replaced by $q_0 - Q_{th} + Q'_{th} = E_\nu - E_l - Q_{th} + Q'_{th}$ in the Lindhard function. Because of its nature, this method only applies to inclusive processes by summing over relatively many final states. Therefore, the implementation of this modification requires a reasonable choice for threshold value of the nuclear reaction Q_{th} to perform numerical evaluation of the cross sections. The threshold value of the energy, Q_{th}, for the neutrino reaction is taken to be the energy difference corresponding to the lowest allowed Fermi or Gamow-Teller transitions. However, in some cases the standard Q_{th} of the reaction corresponding to the ground state to ground state(gs-gs) transition is also taken [203], [204].

With inclusion of these nuclear effects the neutrino nuclear cross section $\sigma(E_\nu)$ is written as

$$\sigma(E_\nu) = -\frac{2G_F^2 \cos^2\theta_C}{\pi} \int_{r_{min}}^{r_{max}} r^2 dr \int_{p_l^{min}}^{p_l^{max}} {p_l}^2 dp_l \int_{-1}^{1} d(cos\theta) \frac{1}{E_{\nu_e} E_e}$$
$$\times \{L^{\mu\nu} J_{\mu\nu}\ \text{Im}U_N[E_\nu - E_l - Q_{th}, \mathbf{q}]\} \tag{2.56}$$

2.5 Nuclear Renormalization Effects

In the nucleus the strength of the electroweak couplings may change from their free nucleon values due to the presence of strongly interacting nucleons. Conservation of Vector Current (CVC) forbids any change in the charge coupling while magnetic and axial vector couplings are likely to change from their free nucleon values. This is so because axial current is related to the pion field due to PCAC and pion field is the mediator of strong interaction. Thus the effect of strong interaction in the nuclear medium changes the axial and pseudoscalar coupling constants. These changes are calculated by considering the interaction of particle-hole (ph) excitations in the nuclear medium. While propagating through the medium, the article-hole(ph) excitations interact through the nucleon-nucleon potential and create other particle-hole(ph) and Δh excitations as shown in Fig.2.3.

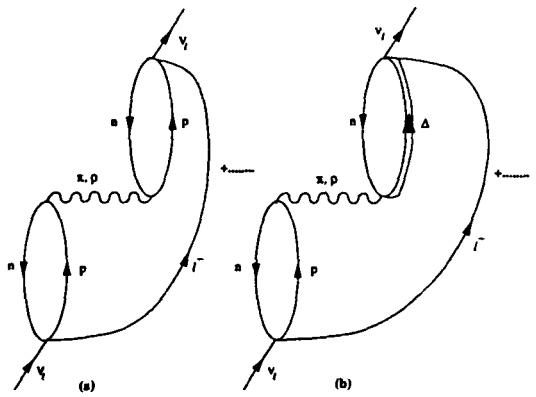

Figure 2.3: Many body Feynman diagrams (drawn in the limit $M_W \rightarrow \infty$) accounting for the medium polarization effects contributing to the process $\nu_l + n \rightarrow l^- + p$ transitions.

The effect of these excitations are calculated in Random Phase Approximation (RPA) which is described in Ref. [116], [149]. The diagram shown in Fig.2.3 simulates the effects of the strongly interacting nuclear medium at the weak vertex. The ph-ph interaction is shown by the wavy line in Fig.2.3 and is described by the π and ρ exchanges modulated by the effect of short range correlations.

The repulsive short range part of the strong interaction is described by π and ρ exchanges [198]. The πNN interaction gives longitudinal part of the interaction given as [205]

$$V_\pi(q) = \left(\frac{f_\pi^2}{m_\pi^2}\right) |\mathbf{q}|^2 \left[\frac{\hat{q}_i \hat{q}_j \sigma_i \sigma_j}{q_0^2 - \mathbf{q}^2 - m_\pi^2 + i\epsilon}\right] \vec{\tau} \cdot \vec{\tau} \tag{2.57}$$

and the ρNN interaction gives the transverse part of interaction which is given by [205]

$$V_\rho(q) = \left(\frac{f_\rho^2}{m_\rho^2}\right) |\mathbf{q}|^2 \left[\frac{(\delta_{ij} - \hat{q}_i \hat{q}_j)\sigma_i \sigma_j}{q_0^2 - \mathbf{q}^2 - m_\rho^2 + i\epsilon}\right] \vec{\tau} \cdot \vec{\tau} \tag{2.58}$$

$V_\pi(q)+V_\rho(q)$ provides the spin-isospin part of the nucleon-nucleon interaction in the meson exchange model. We also include vertex form factors to account for the off shell mesons. These are given by the monopole form for each πNN and ρNN vertices [198]:

$$F_i(q^2) = \frac{\Lambda_i^2 - m_i^2}{\Lambda_i^2 - q^2} \tag{2.59}$$

where, $q^2 = q_0^2 - \mathbf{q}^2$, Λ_π=1250 MeV and Λ_ρ=2500 MeV. The modification in the spin-isospin part of the nucleon-nucleon interaction due to the effect of short range correlations are taken into account by adding a term $g'(\sigma_1 \cdot \sigma_2)(\tau_1 \cdot \tau_2)$ to the potential $V_\pi + V_\rho$, where g' is the Landau-Migdal parameter taken to be 0.7 which has been used quite successfully to explain many electromagnetic and weak processes in nuclei [116], [150], [152], [153]. With all these effects the nucleon-nucleon potential in the momentum space is written as [198], [200]

$$V(q) = [V_l(q)(\delta_{ij} - \hat{q}_i\hat{q}_j) + V_t(q)\hat{q}_i\hat{q}_j](\sigma_i\sigma_j)(\vec{\tau}\cdot\vec{\tau}) \tag{2.60}$$

where

$$V_l(q) = \frac{f_\pi^2}{m_\pi^2}\left[\frac{|\mathbf{q}|^2}{q_0^2 - \mathbf{q}^2 - m_\pi^2}\left(\frac{\Lambda_\pi^2 - m_\pi^2}{\Lambda_\pi^2 - q^2}\right)^2 + g'\right] \tag{2.61}$$

$$V_t(q) = \frac{f_\pi^2}{m_\pi^2}\left[\frac{|\mathbf{q}|^2 c_\rho}{q_0^2 - \mathbf{q}^2 - m_\pi^2}\left(\frac{\Lambda_\rho^2 - m_\rho^2}{\Lambda_\rho^2 - q^2}\right)^2 + g'\right] \tag{2.62}$$

with g'=0.6-0.7, and

$$c_\rho = \left[\frac{f_\rho^2}{m_\rho^2}\right] / \left[\frac{f_\pi^2}{m_\pi^2}\right] \approx 2. \tag{2.63}$$

Here $V(q)$ is the ph-ph interaction mediated by π and ρ exchanges. V_l and V_t are the strength of the nucleon-nucleon potential in longitudinal and transverse channels, calculated with π and ρ exchanges and modulated by the landau Migdal parameter g' to take into account the short range correlation effects.

The effect of the Δ degrees of freedom in the nuclear medium is included in the calculation of the RPA response by considering the effect of ph-Δh and Δh-Δh excitations as shown in Fig.2.3. The ph-Δh or Δh-Δh interaction is obtained from Eqs.2.60-2.62 by substituting $\vec{\sigma} \rightarrow \vec{S}$, $\vec{\tau} \rightarrow \vec{T}$ and $f \rightarrow f^*$=2.15f for any Δ which replaces a nucleon line in the Fig.2.3. $\vec{S}$ and $\vec{T}$ are the spin, isospin NΔ transition operators.

Inclusion of the induced interaction driven by $V_\pi(q)$ and $V_\rho(q)$ leads to Fig.2.3 from Fig.2.2. The decomposition of the potential in longitudinal and transverse parts (Eq.2.60) helps in summing the geometric series in Fig.2.3 [198]. For example the contribution of Fig.2.3 is given by

$$\bar{U}(q) = [U(q)+U(q)V_{ij}(q)\sigma_i\sigma_j U(q)+U(q)V_{ik}(q)\sigma_i\sigma_k U(q)V_{kj}(q)\sigma_k\sigma_j U(q)+..]\vec{\tau}\cdot\vec{\tau} \tag{2.64}$$

where $V_{ij} = V_t(\delta_{ij} - \hat{q}_i\hat{q}_j) + V_l\hat{q}_i\hat{q}_j$. The longitudinal and transverse parts can be separated by using the following relationship.

$$\left.\begin{array}{l}(\delta_{ij} - \hat{q}_i\hat{q}_j)(\delta_{jl} - \hat{q}_j\hat{q}_l) = \delta_{il} - \hat{q}_i\hat{q}_l \\ \hat{q}_i\hat{q}_j\hat{q}_j\hat{q}_l = \hat{q}_i\hat{q}_l \\ (\delta_{ij} - \hat{q}_i\hat{q}_j)\hat{q}_j\hat{q}_l = 0\end{array}\right\} \tag{2.65}$$

Because of the last identity in Eq.2.65, there is no cross term of the longitudinal and transverse channels. We can write for example the longitudinal part of Eq.2.64 as

$$\begin{aligned}\bar{U}(q) &= [U(q) + U(q)V_l\hat{q}_i\hat{q}_j\sigma_i\sigma_j U(q) + U(q)V_l\hat{q}_i\hat{q}_k\sigma_i\sigma_k U(q)V_l\hat{q}_k\hat{q}_j\sigma_k\sigma_j U(q) + ...]\ \vec{\tau}\cdot\vec{\tau} \\ &= [U(q) + U(q)V_lU(q) + U(q)V_lU(q)V_lU(q) + ...]\ \hat{q}_i\hat{q}_j\ \sigma_i\sigma_j\ \vec{\tau}\cdot\vec{\tau} \\ &= U(q)[1 + V_lU(q) + (V_lU(q))^2 + ...]\ \hat{q}_i\hat{q}_j\ \sigma_i\sigma_j\ \vec{\tau}\cdot\vec{\tau} \\ &= \left[\frac{U(q)}{1 - U(q)V_l}\right]\ \hat{q}_i\hat{q}_j\ \sigma_i\sigma_j\ \vec{\tau}\cdot\vec{\tau}\end{aligned} \tag{2.66}$$

Similarly, the transverse part is given by

$$\bar{U}(q) = \left[\frac{U(q)}{1 - U(q)V_t}\right]\ (\delta_{ij} - \hat{q}_i\hat{q}_j)\ \sigma_i\sigma_j\ \vec{\tau}\cdot\vec{\tau} \tag{2.67}$$

Therefore, we can write Eq.2.64 as:

$$\bar{U}(q) = \left[\left(\frac{U(q)}{1 - U(q)V_t}\right)\ (\delta_{ij} - \hat{q}_i\hat{q}_j) + \left(\frac{U(q)}{1 - U(q)V_l}\right)\ \hat{q}_i\hat{q}_j\right]\ \vec{\sigma_i}\ \vec{\sigma_j}\vec{\tau}\cdot\vec{\tau} \tag{2.68}$$

where $U_N \rightarrow U = U_N + U_\Delta$, with U_N and U_Δ as the Lindhard function for particle-hole(ph) and Δh excitations, respectively, in the medium and the expressions for U_N and U_Δ are taken from [154]-[155]. The different couplings of N and Δ are incorporated in U_N and U_Δ and then the same interaction strengths $V_l(q)$ and $V_t(q)$ are used to calculate the RPA response. This is discussed in some detail in Ref. [149].

Now the renormalization of the various weak coupling constants can be calculated using the Feynman diagrams shown in Fig.2.3. The renormalization of these coupling constants is seen in the non-relativistic reduction of weak current [116]. The weak nucleon current described by Eq.2.6 gives, in nonrelativistic limit, terms like $F_A\vec{\sigma}\tau_+$ and $iF_2\frac{\vec{\sigma}\times\vec{q}}{2M}\tau_+$ (Appendix-C) which generate spin-isospin transitions in nuclei. While the term $iF_2\frac{\vec{\sigma}\times\vec{q}}{2M}\tau_+$ couples to the transverse excitations, the term $F_A\vec{\sigma}\tau_+$ couples to the transverse as well as longitudinal channels. These channels produce different RPA responses in the longitudinal and transverse channels when the diagrams of Fig.2.3 are summed over.

For example, consider the renormalization of the axial vector term of the hadronic current in Eq.2.6. The nonrelativistic reduction of the axial vector term written as

$$\begin{aligned}\bar{u}(p')F_A\gamma_\mu\gamma_5 u(p) &= (J_0,\ J_i) = F_A(q^2)\left[\bar{u}(p')\gamma_0\gamma_5 u(p),\ \bar{u}(p')\gamma_i\gamma_5 u(p)\right] \\ &= F_A(q^2)\left[\frac{\vec{\sigma}\cdot(\vec{p}+\vec{p'})}{2E},\quad \left(\vec{\sigma} - \frac{\sigma_i(\vec{\sigma}\cdot\vec{p})(\vec{\sigma}\cdot\vec{p'})}{4E^2}\right)\right]\end{aligned} \tag{2.69}$$

Note that it reads $F_A(q^2)\sigma_i$ in leading order (Eq.(C.6)). One of the contributions of this term to the hadronic tensor J_{ij} in the medium is proportional to $F_A^2(q^2)\delta_{ij}\mathrm{Im}U$ which is split between the longitudinal and transverse components as

$$F_A^2(q^2)\delta_{ij}\mathrm{Im}U \rightarrow F_A^2(q^2)\left[\hat{q}_i\hat{q}_j + (\delta_{ij} - \hat{q}_i\hat{q}_j)\right]\mathrm{Im}U \tag{2.70}$$

The RPA response of this term after summing the higher order diagrams like Fig.2.3 is modified and is given by J_{ij}^{RPA} (Appendix-D, section-D.2):

$$J_{ij} \rightarrow J_{ij}^{RPA} = F_A^2(q^2)\mathrm{Im}U\left[\frac{\hat{q}_i\hat{q}_j}{|1-UV_l|^2} + \frac{\delta_{ij} - \hat{q}_i\hat{q}_j}{|1-UV_t|^2}\right] \tag{2.71}$$

where V_l and V_t are the longitudinal and transverse part of the nucleon-nucleon potential calculated with π and ρ exchanges and are given in Eqs.2.61 and 2.62. Taking $\vec{q}$ along z-direction, Eq.2.71, implies that $F_A^2(q^2)\delta_{ij}$ contribution to the transverse (xx, yy) and longitudinal (zz) components of the hadronic tensor get renormalized by factors $1/|1-UV_l|^2$ versus $1/|1-UV_t|^2$. This modified tensor J_{ij}^{RPA} when contracted with the leptonic tensor L^{ij} gives the contribution of the $F_A^2(q^2)$ term to the RPA response (Appendix-D, section-D.3). All different contributions to the charged current hadronic tensor $J_{\mu\nu}$ have been examined and renormalized by summing up the RPA series in Fig.2.3. The terms upto $O(q/M)^2$ have been retained as shown in Appendix-D (section-D.2).

In this approach, an alternative way of including the RPA corrections in the hadronic tensor $J_{\mu\nu}$ has been recently given by Nieves et al. [151]. In this scheme, the hadronic tensor $J_{\mu\nu}$ given in Eq.A.4 (Appendix-A) has been expanded in longitudinal and transverse components with respect to $\vec{q}$ which has been taken along z-axis. Once this separation has been made, the RPA corrections have been incorporated in the longitudinal and transverse components by multiplying the longitudinal component with factor $C_L = 1/|1 - UV_l|^2$ and the transverse component by a factor $C_T = 1/|1 - UV_t|^2$, respectively in $J_{\mu\nu}$ coming from spin dependent components of J_μ. Similarly, the contribution of spin independent terms in J_μ to $J_{\mu\nu}$ is multiplied by a factor $C_N = 1/|1 - U_N V_N|^2$, where U_N is the Lindhard function for particle-hole(ph) excitation, and V_N is the potential in the spin independent isovector channel given in Ref. [151]. In this way the RPA corrections are incorporated upto $O(q/M)^2$, while the higher order terms like $(q_0 p/M^3)$ and $(q_0 q/M^3)$ etc., which are essentially $O(q/M)^3$ are retained without RPA corrections. This is an improvement over the method described earlier but the effect of additional terms is found to be quite small at the energies considered here. The results are given in Appendix-D.

2.6 Coulomb Effects

One of the important aspects of charge current neutrino interactions is the treatment of Coulomb distortion of the produced lepton in the Coulomb field of the final nucleus. At low energies of the electron relevant to β decays in nuclei the Coulomb distortion of electron in

the nuclear field is taken into account by multiplying the momentum distribution of lepton in Eq.2.56 by a Fermi function $F(Z, E_l)$, where $F(Z, E_l)$ is given by[206]:

$$F(Z, E_l) = \left[1 - \frac{2}{3}(1 - \gamma_0)\right]^{-1} f(Z, E_l) \tag{2.72}$$

where

$$f(Z, E_l) = 2(1 + \gamma_0)(2p_l R)^{-2(1-\gamma_0)} \frac{|\Gamma(\gamma_0 + i\eta)|^2}{(\Gamma(2\gamma_0 + 1))^2} \tag{2.73}$$

Here R is the nuclear radius and $\gamma_0 = \sqrt{1 - (\alpha Z)^2}$, $\eta = \alpha Zc/v$. This approximation works quite well at low energies, but it is not appropriate at higher energies, specially for high Z nuclei [156], [157]. Therefore, at higher lepton energies a different approach is needed to describe the Coulomb distortion effect of the lepton. For this purpose, we apply the methods of electron scattering where various approximations have been used to take into account the Coulomb distortion effects of the initial and final electron [207]-[213]. One of them is the Modified Effective Momentum Approximation(MEMA) in which the electron momentum and energy are modified by taking into account the Coulomb energy. We have used this approach in the case of charged current quasielastic neutrino scattering and the energy and momentum of the lepton present in the final state is modified in the Coulomb field of the final nucleus [150], [157]. In the local density approximation, the effective energy of the electron in the Coulomb field of the final nucleus is given by:

$$E_{eff} = E_l + V_c(r) \tag{2.74}$$

with $V_c(r)$ is the Coulomb potential taken to be of the form

$$V_c(r) = Z_i Z_f \alpha 4\pi \left(\frac{1}{r}\int_0^r \frac{\rho_p(r')}{Z_f} r'^2 dr' + \int_r^\infty \frac{\rho_p(r')}{Z_f} r' dr'\right) \tag{2.75}$$

where Z_i is the charge of the lepton produced in the reaction and $\rho_p(r)$ is the proton density in the final nucleus. This modification amounts to the evaluation of the Lindhard function in Eq.2.53 at $[q_0 - (Q_{th} + V_c(r)), \mathbf{q}]$ instead of $(q_0, \mathbf{q})$.

Thus, in presence of nuclear medium effects the total cross section $\sigma(E_\nu)$, with the inclusion of Coulomb distortion effects taken into account by Fermi function (MEMA), is written as

$$\begin{aligned}\sigma^{FF(MEMA)}(E_\nu) &= -\frac{2{G_F}^2 \cos^2\theta_c}{\pi} \int_{r_{min}}^{r_{max}} r^2 dr \int_{{p_l}^{min}}^{{p_l}^{max}} {p_l}^2 dp_l \int_{-1}^{1} d(cos\theta) \\ &\quad \times \frac{1}{E_\nu E_l} \left(L^{\mu\nu} J^{RPA}_{\mu\nu}\right) \ \mathrm{Im}U(q)^{FF(MEMA)}.\end{aligned} \tag{2.76}$$

where

$$\mathrm{Im}U^{FF}(q) = F(Z, E_l)\ \mathrm{Im}U[E_\nu - E_l - Q_{th},\ \mathbf{q}] \quad \text{and} \tag{2.77}$$

$$\mathrm{Im}U^{MEMA}(q) = \mathrm{Im}U[E_\nu - E_l - Q_{th} - V_c(r),\ \mathbf{q}] \tag{2.78}$$

2.7 Results and Discussions

2.7.1 Low Energy Neutrino-Nucleus Reactions

In this section, we present the numerical results for the charged current total cross section $\sigma(E_\nu)$ as a function of neutrino energy, in the low as well as intermediate energy region, for the quasielastic inclusive neutrino processes from various nuclei.

In the low energy region, we present the results for the total cross section $\sigma(E)$ as a function of energy and the flux averaged cross section $\langle\sigma\rangle$ for various nuclei which have been presently proposed to be studied at Spallation Neutron Source facility (SNS) at the Oak Ridge national laboratory (ORNL) using neutrinos from stopped muon decays [214]. The neutrino energy and the spectrum for these neutrinos is given by the Michel spectrum $\phi(E_\nu)$ which is written as

$$\phi(E_{\nu_e}) = \frac{12}{E_0^4} E_{\nu_e}^2 (E_0 - E_{\nu_e}), \quad E_0 = 52.8 MeV \tag{2.79}$$

and is shown in Fig.2.4. The cross sections have been calculated using Eq.2.76. For the

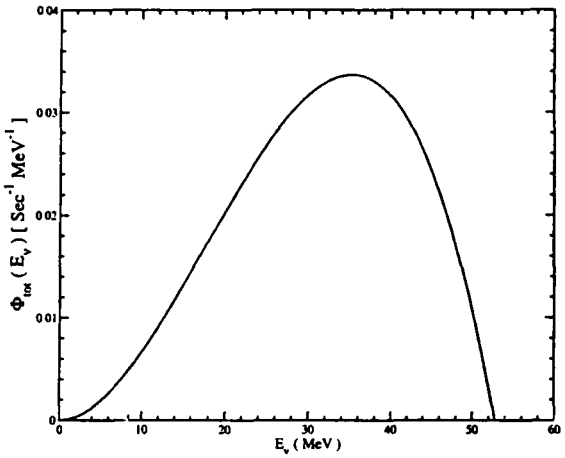

Figure 2.4: Michel spectrum for ν_e obtained from muon decay at rest.

numerical calculation of the cross section, we have classified the nuclei in three groups according to their nuclear densities used in the calculation which has been presented along with the Q_{th} value for the reaction in Tables-2.4-2.6.

In Table-2.4, we present the nuclear density parameters for ^{12}C, ^{14}N and ^{16}O nuclei using a 2-parameter harmonic oscillator(H.O.) density given by

$$\rho(r) = \rho_0 \left(1 + \alpha \left(\frac{r}{a}\right)^2\right) \exp\left(-\left(\frac{r}{a}\right)^2\right), \tag{2.80}$$

Table 2.4: Q_{th}-value and the density parameters used in the numerical evaluation of the cross sections. α and a are the parameters for H.O. density used in Eq.2.80.

Nucleus	Q_{th}(transition)(MeV)	α	a(fm)
^{12}C	17.84 ($0^+ \rightarrow 1^+$)	1.69	1.07
^{14}N	5.60 ($1^+ \rightarrow 0^+$)	1.76	1.23
^{16}O	19.76 ($0^+ \rightarrow 1^+$)	1.80	1.52

In Table-2.5 we present the nuclear density parameters for ^{19}F, ^{23}Na, ^{27}Al, ^{28}Si, ^{31}P, ^{37}Cl, ^{40}Ar, ^{51}V, ^{52}Cr, ^{55}Mn, ^{56}Fe, ^{59}Co, ^{71}Ga, ^{89}Y, ^{93}Nb, ^{98}Mo, ^{115}In, ^{127}I, ^{139}La, ^{181}Ta, ^{208}Pb and ^{209}Bi nuclei using a 2-parameter Fermi density (2pF) given by

$$\rho(r) = \frac{\rho_0}{(1 + exp((r - \alpha)/a))} \tag{2.81}$$

In Table-2.6, we present the nuclear density parameters for ^{32}S, ^{39}K and ^{40}Ca nuclei using a three parameter Fermi(3pF) density given by

$$\rho(r) = \frac{\rho_0 \left(1 + w \frac{r^2}{\alpha^2}\right)}{(1 + exp((r - \alpha)/a))}, \tag{2.82}$$

The parameters have been taken from de Vries et al. [215] except for ^{115}In and ^{127}I which have been taken from Ref. [115]. The Q_{th} values presented in these tables correspond to the lowest allowed Fermi or Gamow-Teller transitions for the above mentioned nuclei except for the case of ^{40}Ca and ^{98}Mo for which the Q_{th} value corresponding to the ground state to ground state transitions have been taken [203], [204].

2.7.2 Nuclear Medium Effects

When the reaction $\nu_e + n \rightarrow e^- + p$ takes place in the nucleus, the first consideration is the threshold energy Q_{th} which inhibits the reaction in the nucleus. This inhibition is quite substantial in the low energy region considered here for the nuclei like ^{12}C, ^{16}O, ^{28}Si, ^{32}S and ^{40}Ca for which the Q_{th} values are rather large (Q_{th} ≈13-20MeV). In addition to this, the effect of Pauli blocking which is taken into account through the imaginary part of the Lindhard function is to further reduce the cross section. Finally the renormalization of weak coupling constants which is generated in our model through RPA correlations and is taken into account by calculating the cross section with the modified hadronic tensor $J^{RPA}_{\mu\nu}$ defined in Eqs.D.40-D.44(Appendix-D) also reduces the cross sections. The total cross sections are calculated using Eq.2.56 without RPA. The effect of RPA is included through Eq.2.76. In Fig.2.5, we have shown the reduction due to these effects separately for some representative nuclei like

Table 2.5: Q_{th}-value and the density parameters used in the numerical evaluation of the cross sections. α and a are the parameters used in Eq.2.81 for 2pF density.

Nucleus	Q_{th}(transition)(MeV)	α	a(fm)
^{19}F	3.75 ($\frac{1}{2}^+ \rightarrow \frac{1}{2}^+$)	2.59	0.56
^{23}Na	4.56 ($\frac{3}{2}^+ \rightarrow \frac{3}{2}^+$)	2.81	0.54
^{27}Al	5.32 ($\frac{5}{2}^+ \rightarrow \frac{5}{2}^+$)	3.07	0.52
^{28}Si	14.80 ($0^+ \rightarrow 0^+$)	2.93	0.57
^{31}P	5.91 ($\frac{1}{2}^+ \rightarrow \frac{1}{2}^+$)	3.21	0.56
^{37}Cl	1.32 ($\frac{3}{2}^+ \rightarrow \frac{3}{2}^+$)	3.53	0.52
^{40}Ar	4.3 ($0^+ \rightarrow 1^+$)	3.39	0.61
^{51}V	1.26 ($\frac{7}{2}^- \rightarrow \frac{7}{2}^-$)	3.94	0.50
^{52}Cr	5.22 ($0^+ \rightarrow 1^+$)	4.01	0.50
^{55}Mn	0.74 ($\frac{5}{2}^- \rightarrow \frac{3}{2}^-$)	3.89	0.57
^{56}Fe	6.82 ($0^+ \rightarrow 1^+$)	3.97	0.59
^{59}Co	1.92 ($\frac{7}{2}^- \rightarrow \frac{5}{2}^-$)	4.08	0.57
^{71}Ga	0.74 ($\frac{3}{2}^- \rightarrow \frac{1}{2}^-$)	4.44	0.58
^{89}Y	4.44 ($\frac{1}{2}^- \rightarrow \frac{3}{2}^-$)	4.76	0.57
^{93}Nb	0.91 ($\frac{9}{2}^+ \rightarrow \frac{7}{2}^+$)	4.87	0.57
^{98}Mo	2.20($0^+ \rightarrow 6^+$)	5.10	0.57
^{115}In	0.008 ($\frac{9}{2}^+ \rightarrow \frac{7}{2}^+$)	5.36	0.56
^{127}I	1.42 ($\frac{5}{2}^+ \rightarrow \frac{3}{2}^+$)	5.40	0.55
^{139}La	0.78 ($\frac{7}{2}^+ \rightarrow \frac{9}{2}^+$)	5.71	0.53
^{181}Ta	0.70 ($\frac{7}{2}^- \rightarrow \frac{5}{2}^-$)	6.38	0.64
^{208}Pb	5.20 ($0^+ \rightarrow 1^+$)	6.62	0.50
^{209}Bi	3.80 ($\frac{9}{2}^- \rightarrow \frac{7}{2}^-$)	6.75	0.47

Table 2.6: Q_{th}-value and the density parameters used in the numerical evaluation of the cross sections. α, a and w are the parameters used in Eq.2.82 for the 3pF density.

Nucleus	Q_{th}(transition)(MeV)	α	a(fm)	w
^{32}S	13.20 ($0^+ \rightarrow 1^+$)	3.50	0.63	-0.25
^{39}K	7.04 ($\frac{3}{2}^+ \rightarrow \frac{3}{2}^+$)	3.74	0.58	-0.201
^{40}Ca	14.80($0^+ \rightarrow 4^-$)	3.67	0.58	-0.1017

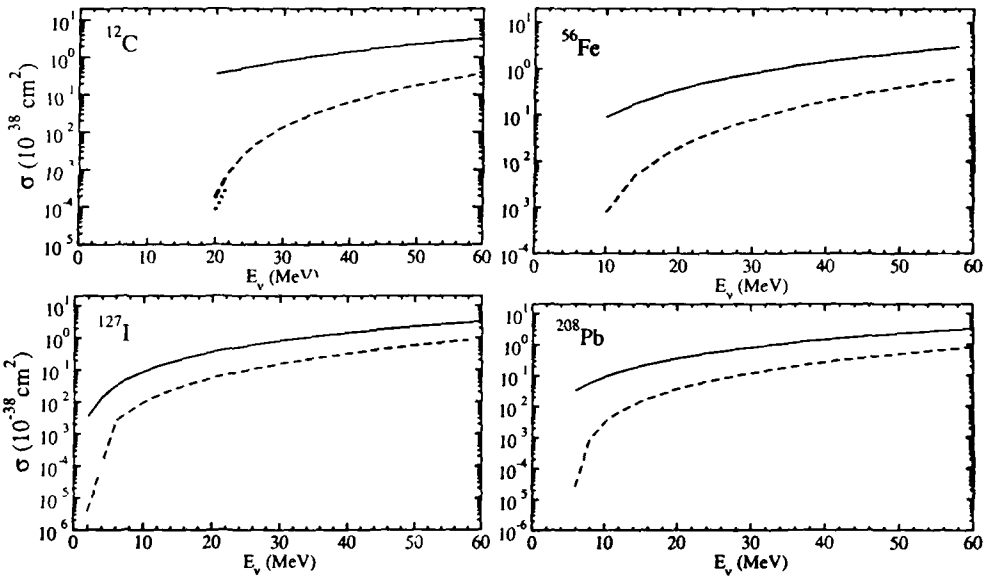

Figure 2 5 Quasielastic cross section $\sigma(E_\nu)$ vs E_ν for neutrino reaction in some nuclei. The dashed (dotted) lines represent neutrino nucleus cross section without (with) RPA correlations to be compared with the free nucleon cross section (solid lines)

^{12}C, ^{56}Fe, ^{127}I and ^{208}Pb in various mass ranges We see that at low energies considered in this work the major suppression in the cross section comes due to the consideration of Q_{th}-values and Pauli blocking in the nuclear medium The reduction in the cross section σ(E) due to these effects decreases with the increase of energy For example at E_ν=50 MeV, this suppression is $\approx$ 93% for ^{12}C and $\approx$ 75 – 77% for other nuclei like ^{56}Fe, ^{127}I and ^{208}Pb (compare the solid lines with the dashed line in Fig 2 5) This suppression reduces to 40 – 45% in all these nuclei at E_ν=200 MeV(not shown in Fig 2 5)

In addition to the Pauli blocking, the consideration of RPA correlation in the nuclear medium gives rise to further reduction which increases with the mass number and decreases with the increase in energy (compare the dashed line with the dotted line in Fig 2 5) For example at E_ν=50 MeV the RPA correlations give a further reduction of 50% for ^{12}C, 60% for ^{56}Fe and around 70% for ^{127}I and ^{208}Pb As the energy increases it becomes smaller and at E_ν=200 MeV the reduction is 35% for ^{12}C, 40% for ^{56}Fe and around 50% for ^{127}I and ^{208}Pb (not shown here) It should be noted that 40 – 60% reduction due to the medium polarisation effects calculated through the RPA correlations in our model is similar to using g_{eff}/g_A=0 7 in nuclear medium in some shell model calculations [102], [159], [216], [217]

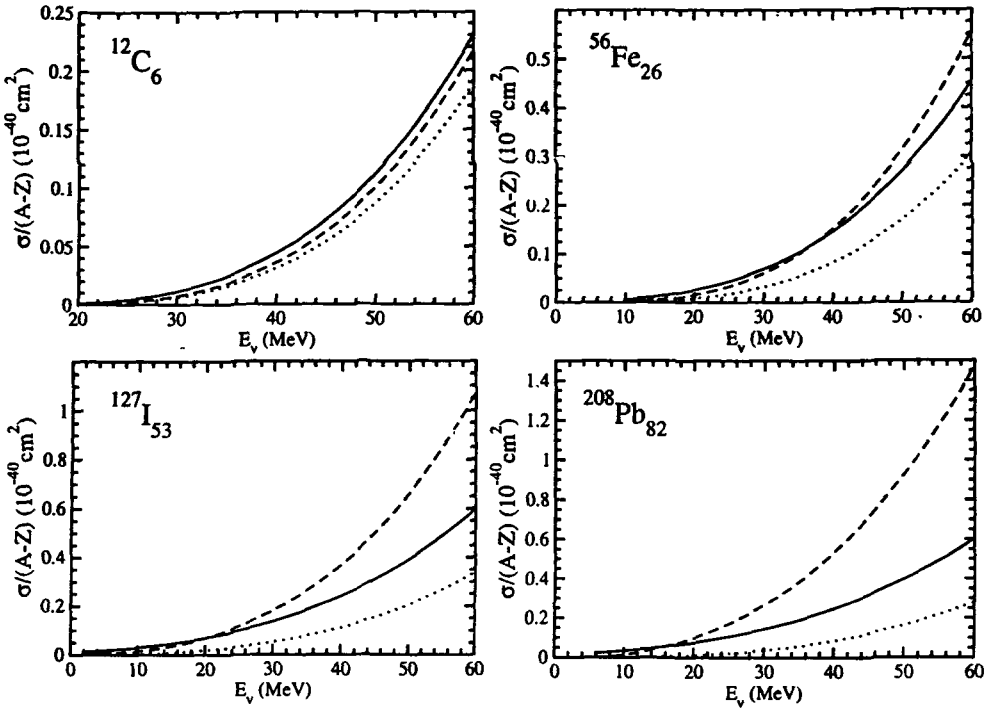

Figure 2.6: Quasielastic cross section $\sigma(E_\nu)$ vs E_ν for neutrino reaction in some nuclei. The dashed (solid) lines show the cross section calculated with RPA correlations and Coulomb effects using Fermi function (MEMA) to be compared with the cross section without Coulomb effects (dotted lines).

2.7.3 Effects of Coulomb distortion

The effect of Coulomb distortion is calculated using Fermi function $F(Z, E_e)$ as well as with the modified effective momentum approximation(MEMA). The results for some representative nuclei like ^{12}C, ^{56}Fe, ^{127}I and ^{208}Pb in various mass range are shown in Fig.2.6. The general effect of the Coulomb distortion of the electron is to increase the total cross section which depends upon the incident energy of the neutrino and the charge of the final nucleus.

For a fixed Z, this increase in the cross section decreases with the increase in energy while for a fixed energy the inclusion of Coulomb distortion increases with the charge Z. For example for ^{12}C this is 15% at E_ν=50 MeV which becomes 10% at E_ν=200 MeV. For high Z nuclei the Coulomb effect is very large and results in manifold increase in the cross sections. This can be seen by comparing the cross section without Coulomb effect shown by dotted lines and the cross sections with Coulomb effects using the Fermi function $F(Z, E_e)$ shown by dashed lines. For example in the case of ^{56}Fe nucleus the increase due to Coulomb distortion is 83% at E_ν=50

MeV which becomes 75% at E_ν−200 MeV. However, as discussed in Chapter-2, Section-2.6, the use of Fermi function to calculate the Coulomb distortion effects overestimates the cross sections and is not appropriate at higher electron energies. Therefore, we use the modified effective momentum approximation(MEMA) and present the results for σ(E) in Fig.2.6 with solid lines. It is seen that for ^{12}C, the results for the cross sections in the two approximations are qualititative similar but the MEMA gives slightly higher cross sections for the entire energy range presented here. This is also the case with other low Z nuclei, like ^{14}N, ^{16}O, ^{19}F and ^{23}Na studied in this work. As Z increases the cross sections calculated with MEMA remain higher than the cross sections calculated with the Fermi function at lower energies but become lower than the cross sections obtained with the Fermi function at higher energies. This crossover in the cross section for higher Z (Z>18) nuclei occurs at an energy E_c which depends upon Z. For example, the cross over energy E_c is 41 MeV, 21 MeV and 17 MeV for ^{56}Fe, ^{127}I and ^{208}Pb respectively as seen from Fig.2.6 It is observed that this energy E_c where the cross over takes place, decreases with Z but there are some exceptions which occur for nuclei like ^{28}Si, ^{39}K, ^{40}Ca, ^{208}Pb, etc. It is interesting to note that these are singly or doubly closed shell nuclei and this anomaly in the Z dependence of E_c may be related to the shell closure effects. A microscopic understanding of this dependence needs further study.

In the above discussions in this section, we have provided a quantitative description of the nuclear medium effects and Coulomb distortion. We now present our final results in Figs.2.7-2.10 for the total cross section $\sigma(E_\nu)$ as a function of neutrino energy E_ν for some representative nuclei from various mass ranges taken from Tables-2.4-2.6. In these figures the dashed lines show the cross sections without RPA correlations and dotted lines show the cross sections with RPA correlations using Fermi function for the Coulomb distortion. The solid lines show the cross section with RPA correlations where the Coulomb distortion effects are calculated with MEMA. In these figures a comparison of dashed lines and dotted lines shows the effect of RPA correlations while a comparison of dotted lines and solid lines shows the effect of Coulomb distortion calculated using Fermi function and MEMA.

2.7.4 Flux averaged cross sections in various nuclei applied to SNS neutrinos

We calculate the flux averaged cross section $\langle\sigma\rangle$ defined as

$$\langle\sigma\rangle = \int \phi(E_\nu)\sigma(E_\nu)dE_\nu \tag{2.83}$$

where $\phi(E_\nu)$ is given by Eq.2.79. The results for $\langle\sigma\rangle$ are presented in Tables-2.7 and 2.8, where we show by $\langle\sigma\rangle_{NC}^{RPA}$ the flux averaged cross sections with nuclear medium effects without any Coulomb distortion effects. When Coulomb distortion effects are taken into account the cross sections without RPA correlations are shown by $\langle\sigma\rangle_C^N$ and the results with RPA correlations are shown by $\langle\sigma\rangle_C^{RPA}$. We evaluate $\langle\sigma\rangle_C^N$ and $\langle\sigma\rangle_C^{RPA}$ in a hybrid model where at lower energies $\sigma(E_\nu)$ calculated with the Fermi function and at higher energies $\sigma(E_\nu)$ calculated

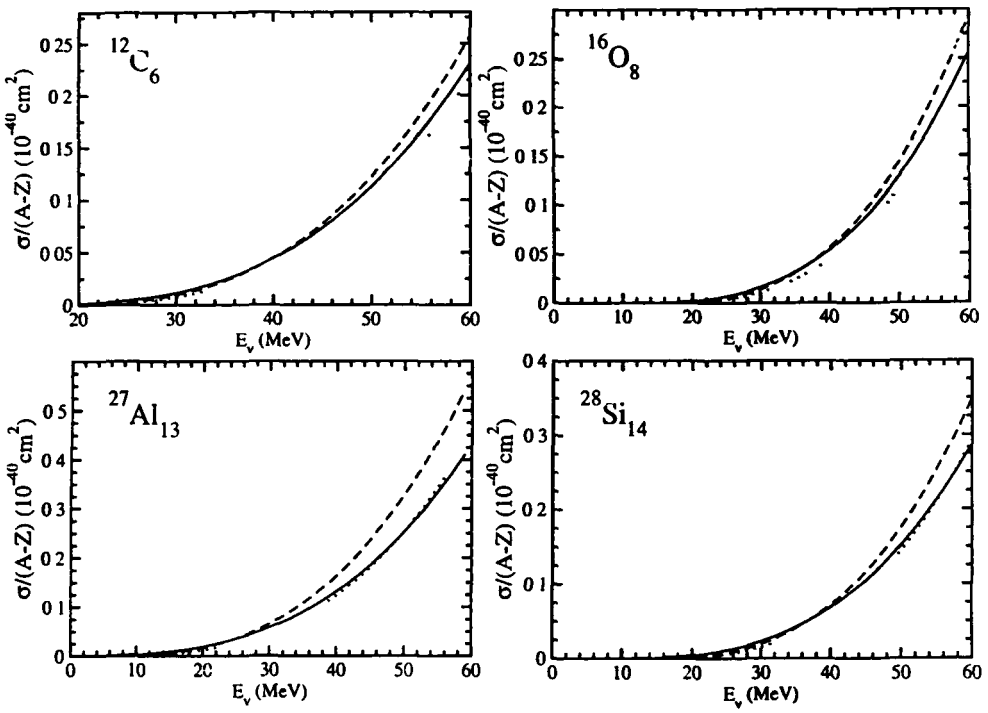

Figure 2 7 Quasielastic cross section $\sigma(E_\nu)$ vs E_ν for neutrino reaction in various nuclei. The dotted (solid) lines show the cross section calculated with RPA correlations and Coulomb effect using Fermi function (MEMA) to be compared with the cross section calculated with Coulomb effect using Fermi function and without RPA correlations (dashed lines-shown here after multiplying by 0 6)

with MEMA is used to perform the flux averaging in Eq.2.83 Thus, in hybrid model, it is the lower value of the cross section which is used for calculating $\langle\sigma\rangle$. For low Z nuclei like ^{12}C, ^{16}O, etc. considered here, the flux averaged cross sections evaluated with the cross section σ(E) calculated with the Fermi function for Coulomb effect has been used because these cross sections are always smaller than the cross sections calculated with the MEMA for the entire range of the Michel spectrum i e E_ν <52 8 MeV We see from this table that the effect of the Coulomb distortion is to increase the cross section and this increase is quite large for high Z nuclei like ^{56}Fe, ^{208}Pb, etc In case of ^{12}C, it is small but plays an important role in explaining the experimental result(Compare column 1 and column 3 in Tables-2.7 and 2 8) A comparison of column 2 and column 3 in this table shows the strong reduction due to RPA correlations which increases with mass number

In Table-2 9, we compare our results with the results of some other calculations In this energy region of the neutrinos, there are many theoretical calculations done for the inclusive

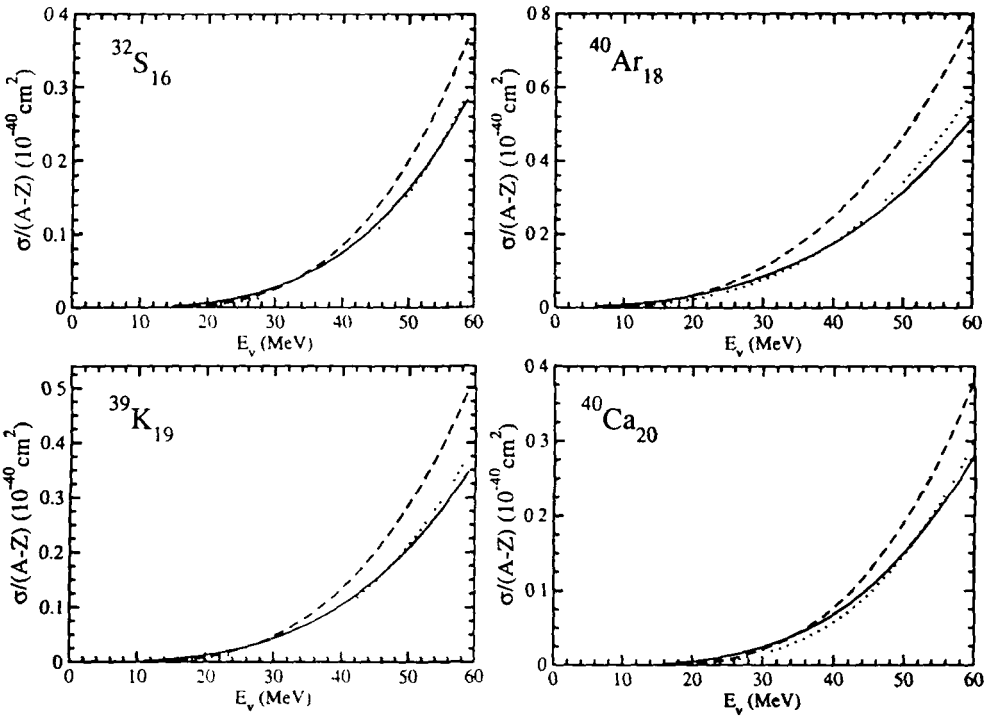

Figure 2.8: Quasielastic cross section $\sigma(E_\nu)$ vs E_ν for neutrino reaction in various nuclei. The dotted (solid) lines show the cross section calculated with RPA correlations and Coulomb effect using Fermi function (MEMA) to be compared with the cross section calculated with Coulomb effect using Fermi function and without RPA correlations (dashed lines-shown here after multiplying by 0.6).

neutrino reactions in ^{12}C [102], [110], [115]-[116], [150]-[151], [216], [218]-[220], while there are few calculations for ^{16}O [110], ^{56}Fe [159], [221] and ^{208}Pb [158]-[160], [217], [222]-[223] and some other nuclei [115] Some calculations are similar to the calculations presented in thesis [115], [151] while others make use of Shell Model [102], [216]-[217], random phase approximation(RPA) with pairing correlations [110], [158]-[160], [216], [218], [223] and elementary particle approach [221], [224]-[225]. We see that for ^{12}C and ^{56}Fe our results are in fair agreement with the experimental results and other theoretical calculations. For ^{208}Pb nucleus our results for $\langle\sigma\rangle$ is comparatively smaller than the results of Refs. ([159]-[160], [217], [222]). This is mainly due to the different approaches of taking into account the nuclear effects. However, among the different calculations of the inclusive cross section $\langle\sigma\rangle$ in ^{208}Pb, the results do not agree among themselves ([159]-[160], [217] [222]). Therefore, more work is needed for calculating the cross section in ^{208}Pb at low energies.

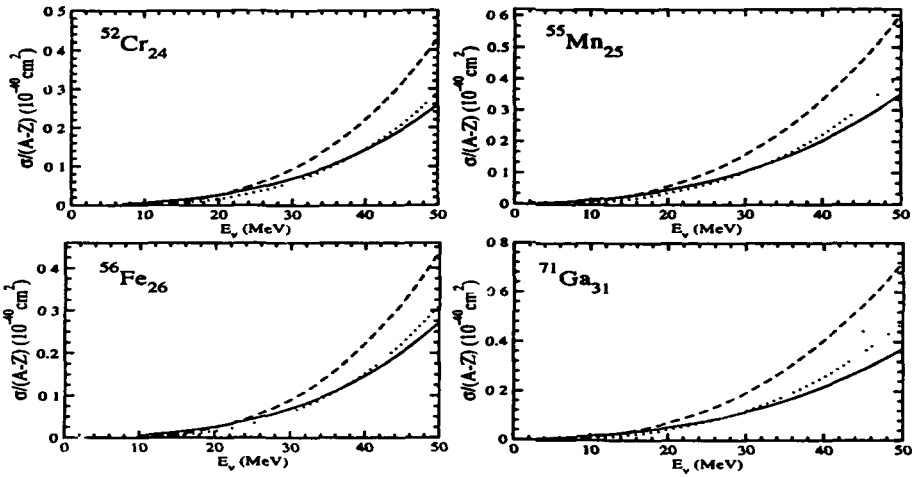

Figure 2.9: Quasielastic cross section $\sigma(E_\nu)$ vs E_ν for neutrino reaction in various nuclei. The dotted (solid) lines show the cross section calculated with RPA correlations and Coulomb effect using Fermi function (MEMA) to be compared with the cross section calculated with Coulomb effect using Fermi function and without RPA correlations (dashed lines-shown here after multiplying by 0.6).

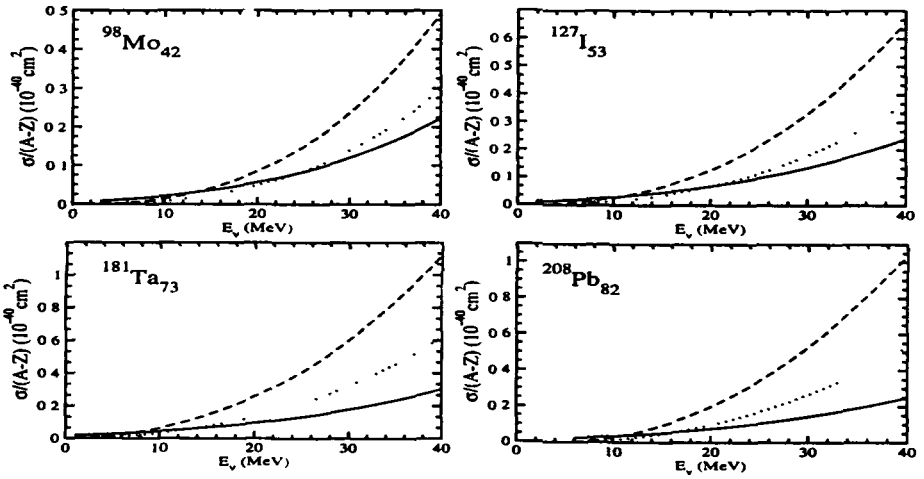

Figure 2.10: Quasielastic cross section $\sigma(E_\nu)$ vs E_ν for neutrino reaction in various nuclei. The dotted (solid) lines show the cross section calculated with RPA correlations and Coulomb effect using Fermi function (MEMA) to be compared with the cross section calculated with Coulomb effect using Fermi function and without RPA correlations (dashed lines-shown here after multiplying by 0.6).

Table 2.7: Total cross section $\langle\sigma\rangle$(in $10^{-42}cm^2$) averaged over the Michel spectrum. $\langle\sigma\rangle_{NC}^{RPA}$ is the averaged cross section calculated with RPA correlations without the Coulomb effect, $\langle\sigma\rangle_{C}^{RPA}$ is the averaged cross section calculated with RPA correlations with Coulomb effect and $\langle\sigma\rangle_{C}^{N}$ is the averaged cross section calculated without RPA correlations with the Coulomb effect.

Nucleus	$\langle\sigma\rangle_{NC}^{RPA}$	$\langle\sigma\rangle_{C}^{N}$	$\langle\sigma\rangle_{C}^{RPA}$
$^{12}_{6}$C	11.80	28.10	13.60
$^{14}_{7}$N	44.60	107.91	52.65
$^{16}_{8}$O	12.00	30.43	14.55
$^{19}_{9}$F	77.80	201.07	96.35
$^{23}_{11}$Na	94.70	263.50	120.50
$^{27}_{13}$Na	82.17	247.13	111.62
$^{28}_{14}$Si	33.17	95.18	46.25
$^{31}_{15}$P	89.34	276.60	127.10
$^{32}_{16}$S	44.10	141.38	64.40
$^{37}_{17}$Cl	154.70	531.18	216.00
$^{40}_{18}$Ar	166.50	560.49	228.00
$^{39}_{19}$K	78.80	285.14	123.55
$^{40}_{20}$Ca	38.00	135.32	61.25
$^{51}_{23}$V	198.40	879.18	323.20
$^{52}_{24}$Cr	157.10	643.18	254.70
$^{55}_{25}$Mn	250.40	1144.52	412.40
$^{56}_{26}$Fe	161.40	685.25	277.00
$^{59}_{27}$Co	244.70	1148.62	418.70
$^{71}_{31}$Ga	335.70	1762.91	596.00
$^{89}_{39}$Y	307.10	1912.11	633.50
$^{93}_{41}$Nb	370.00	2332.71	760.10
$^{98}_{42}$Mo	417.60	2661.25	854.00
$^{115}_{49}$In	516.60	3836.37	1133.00

Table 2.8: Total cross section $\langle\sigma\rangle$(in $10^{-42}cm^2$) averaged over the Michel spectrum. $\langle\sigma\rangle_{NC}^{RPA}$ is the averaged cross section calculated with RPA correlations without the Coulomb effect, $\langle\sigma\rangle_{C}^{RPA}$ is the averaged cross section calculated with RPA correlations with Coulomb effect and $\langle\sigma\rangle_{C}^{N}$ is the averaged cross section calculated without RPA correlations with the Coulomb effect.

Nucleus	$\langle\sigma\rangle_{NC}^{RPA}$	$\langle\sigma\rangle_{C}^{N}$	$\langle\sigma\rangle_{C}^{RPA}$
$^{127}_{53}$I	545.40	4262.30	1253.00
$^{139}_{57}$La	581.50	4787.43	1400.00
$^{181}_{73}$Ta	907.30	7912.80	2358.00
$^{208}_{82}$Pb	902.10	7857.37	2643.00
$^{209}_{83}$Bi	824.38	8257.85	2497.00

Table 2.9: $\langle\sigma\rangle(10^{-42}cm^2)$ for the inclusive reaction for some nuclei.

Nucleus	Experimental results	Theoretical results	Present calculation
		14.00 [115], 14.00 [151]	13.60
^{12}C	$13.2 \pm 0.5 \pm 1.3$ [78]	16.40 [216], 12.30 [102]	
	$14.8 \pm 0.7 \pm 1.4$ [219]	14.40 [218], 12.90, 17.60 [110]	
^{16}O		16.90, 17.20 [110]	14.55
^{56}Fe	$256 \pm 108 \pm 43$ [220]	240 [159], 214 [221]	277
^{208}Pb		4100 [222], 3620 [159], 2954, 3204 [217], 4439 [160]	2643

2.7.5 Application to Supernova Neutrino Cross Sections in ^{56}Fe

Based on the theoretical formalism discussed for inclusive quasielastic reactions, we have obtained the numerical results for the total scattering cross sections for charged current scattering cross section for supernova neutrino and antineutrino with ^{56}Fe nuclei. The energy distributions of these neutrinos shown in Fig.2.11 are well approximated by a thermal Fermi-Dirac distribution with an effective degeneracy parameter α (α=μ/T_ν, μ being the chemical potential and T_ν being the temperature of the neutrino gas) and is written as

$$\phi(E_\nu) = \frac{1}{{T_\nu}^3 F_2(\alpha)} \frac{E_\nu^2}{e^{(\frac{E_\nu}{T_\nu} - \alpha)} + 1}, \tag{2.84}$$

where $F_2(\alpha)$ is determined by the normalization factor given as

$$F_n(\alpha) = \int_0^\infty \frac{x^n dx}{e^{(x-\alpha)} + 1} \tag{2.85}$$

Using this expression, the average energy $\langle E_\nu \rangle$ is given by

$$\begin{aligned} \langle E_\nu \rangle &= \frac{F_3(\alpha)}{F_2(\alpha)} T_\nu \\ &= \left(3.1514 + 0.125\alpha + 0.0429\alpha^2 + ...\right) T_\nu \end{aligned} \tag{2.86}$$

For a given value of the degeneracy parameter α, the neutrino temperature T_ν is fixed using the relation between average neutrino energy $\langle E_\nu \rangle$ and T_ν given in Eq.2.86. The numerical simulations studies of supernova dynamics predict a hierarchal structure for average energies for various flavor of neutrino to be $\langle E_{\nu_e} \rangle \sim$ 10-11 MeV, $\langle E_{\bar{\nu}_e} \rangle \sim$ 15-16 MeV, and $\langle E_{\nu_x} \rangle \sim$ 23-25 MeV, where $x = e$, μ, τ [226]-[228].

The interaction of these supernova neutrinos with ^{56}Fe plays a very important role in the dynamics of supernova explosion and the process of nucleosynthesis. This is also of great importance as ^{56}Fe is proposed to be used as target material in number of experiments, like the proposed OMNIS detector [229] to be made out of steel and lead while large volume detector(LVD) in the INFN Gran Sasso National Laboratory consisting of iron and liquid scintillator [230]. Iron is also used in the MINOS experiment [2], [231] presently being done for neutrino oscillation studies, for very high energy neutrinos.

We have calculated the inclusive cross section for charged current neutrino and antineutrino reactions with the iron nuclei i.e., $\nu_e(\bar{\nu_e}) + ^{56}Fe \rightarrow e^-(e^+) + ^{56}Co^*$ ($^{56}Mn^*$).

The results for supernova neutrino and antineutrino with a neutrino spectrum given by Eq.2.84 corresponding to the various values of T and α which reproduce the correct average energies given in Eq.2.86 for neutrino and antineutrino of various flavors are shown in Table-2.10 and 2.11 for neutrinos and antineutrinos where they are also compared with other results available in the literature.

A comparison of the various results presented in Tables-2.10 and 2.11 show that our method predicts a value of $\langle \sigma \rangle$ for neutrino which is qualitatively in reasonable agreement with the

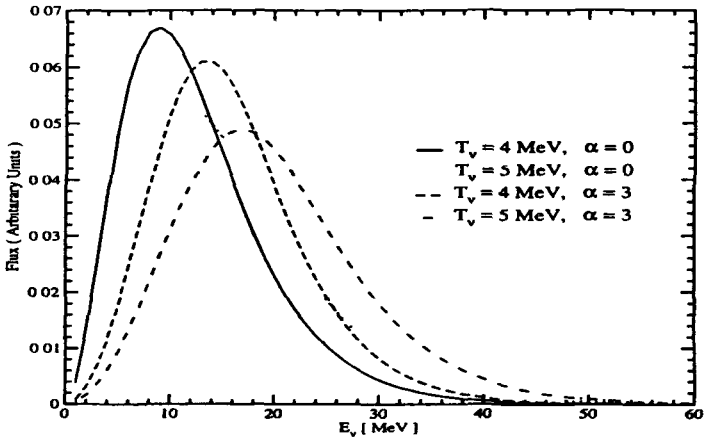

Figure 2.11: Supernova Spectrum

calculations of Kolbe and Langanke [159], [232] and Toivanen et al. [233]. However, there are some discrepancies with the results of Woosley et al. [234]. The results of Woosley et al [234] in general are always considerably larger as compared to our calculations and the calculations of Kolbe and Langanke [159], [232], and Toivanen et al. [233]. It is likely that in the calculations of Woosley et al. [234] where they use a shell model to calculate the GT transition and Goldhaber-Teller model for calculating other forbidden transitions, the effect of nuclear correlations in the weak transition strength is not taken into account adequately Moreover, they use Fermi function to calculate the Coulomb distortion which overestimates the cross section in the higher energy region. On the other hand the calculations of Kolbe and Langanke [159], [218] and Toivanen et al. [233] use shell model with quenched strength for GT transition and CRPA for other transitions to take into account the nuclear correlation effects and our results are in general in agreement with theirs.

The theoretical uncertainty present in these calculations comes due to the different nuclear models used as well as from the treatment of Coulomb distortion. In order to compare the theoretical uncertainty due to the nuclear model dependencies of $\langle\sigma\rangle$ alone, we have also calculated the inelastic cross section for the neutral current induced reactions in iron which are free from the Coulomb effect distortions, and are presented in ref. [117].

2.7.6 Intermediate Energy Neutrino-Nucleus Reactions in ^{12}C, ^{16}O and ^{56}Fe

In the intermediate energy region relevant to the fully contained events of atmospheric neutrinos i e $E_\nu \leq 3$ GeV, we present the numerical results for the total cross sections as a function of energy for neutrino reactions on ^{12}C, ^{16}O and ^{56}Fe

In Fig 2 12, we show the numerical result of the cross section for quasielastic charged lepton

Table 2.10: $\langle\sigma\rangle$ for $^{56}_{26}$Fe (ν_e, e^-) $^{56}_{27}$Co $(10^{-42}cm^2)$ averaged over ν_e spectrum (* For T=6.4)

$\alpha = 0$, T(MeV)	3.5	4	5	6	8	10
Woosely et al. [234]		35.0	72.2	122.6		
Kolbe & Langanke [159], [232]		16.0		74.0	200.0	410.0
Toivanen et al. [233]	11.0	19.0	45.0	111.0*	240.0	491.0
Present work	14.4	23.3	49.9	89.6	212.9	390.2
$\alpha = 3$, T(MeV)	2.75	3.5	4	5	6.26	8
Kolbe & Langanke [159], [232]			29.0		150.0	
Toivanen et al. [233]	7.0	19.0	33.0	78.0	191*	410.0
Present work	10.2	25.2	40.4	84.8	154.3	350.1

Table 2.11: $\langle\sigma\rangle$ for $^{56}_{26}$Fe $(\bar{\nu_e}, e^+)$ $^{56}_{25}$Mn $(10^{-42}cm^2)$ averaged over $\bar{\nu}_e$ spectrum (* For $T = 6.4$)

$\alpha = 0$, T(MeV)	3.5	4	5	6	8	10
Woosely et al. [234]		9.0	18.4	31.4		
Kolbe & Langanke [157]		3.9		15.0	39.0	79.0
Toivanen et al. [233]	2.0	4.0	9.0	21.0*	44.0	88.0
Present work	1.5	2.6	6.2	12.5	36.0	75.4
$\alpha = 3$, T(MeV)	3.5	4	5	6.26	8	10
Kolbe & Langanke [157]		6.6		29.0		
Toivanen et al. [233]	4.0	7.0	15.0	36.0*	74.0	147.0
Present work	2.7	4.6	11.0	28.0	61.9	128.0

production σ(E) in this model for the process $\nu_\mu + ^{12}C \rightarrow \mu^- + X$ using weak nucleon axial vector and vector form factors of BBBA05(Bradford, Bodek, Budd and Arrington) [194]. We see that with the incorporation of various nuclear effects the total cross section is reduced. The reduction is energy dependent, and is large at lower energies but becomes small at higher energies. We see that with the incorporation of the various nuclear effects and RPA, the total reduction in the cross section as compared to cross sections calculated without the nuclear medium modification effects is around 72% at E_{ν_μ}=200 MeV, 42% at E_{ν_μ}=400 MeV, 25% at E_{ν_μ}=0.8 GeV, 22% at E_{ν_μ}=1 GeV, 20% at E_{ν_μ}=1.5 GeV and around 19% at E_{ν_μ}=2.0 GeV. In the inset of Fig.2.12, we show the cross section for quasielastic charged lepton production induced by ν_e (dashed-dotted line) and ν_μ (solid line) with the incorporation of the various nuclear effects and RPA effect. The energy dependence of the cross sections for ν_μ and ν_e are

similar except for the threshold effects which are seen only at low energies (E_ν <500 MeV).

In Fig.2.13 and Fig.2.14, we show the result of the cross section for quasielastic charged lepton production induced by neutrinos on ^{16}O and ^{56}Fe nuclei. We found almost similar nature of the cross sections for ν_μ and ν_e as it is in case of ^{12}C nuclei. This reduction in σ(E) is due to Pauli blocking as well as due to the weak renormalization of transition strengths which have been separately shown in Fig.2.15, Fig.2.16 and Fig.2.17 for muon type neutrinos in ^{12}C, ^{16}O and ^{56}Fe nuclei, where we also show the results in the Fermi gas model given by Llewellyn Smith [7]. In all these figures, we plot the reduction factor $R = \frac{\sigma_{nuclear}(E)}{\sigma_{nucleon}(E)}$ vs E where $\sigma_{nuclear}$(E) is the cross section per neutron for neutrino reaction in the nuclear medium. The solid lines show the reduction factor R when taking into account the nuclear effects without RPA. This is almost similar to the results of Llewellyn Smith [7] in Fermi gas model shown by dashed lines. However, in our model we get further reduction due to renormalization of weak transition strengths in the nuclear medium when the effects of Fig.2.4 is included. These are shown by dotted lines in Figs.2.15, 2.16 and 2.17. The results for ν_e cross section are respectively similar to ν_μ reactions except for the threshold effects and are not shown here.

In Fig.2.18, we compare our results for $\sigma(E)$ with the results of some earlier experiments which contain nuclear targets like Carbon [182], Freon [184], [185], Freon-Propane [183] and Aluminum [186], where the experimental results for the deuteron targets [180], [235]-[236] are not included as they are not subject to the various nuclear effects discussed here. It should be kept in mind that the nuclear targets considered here (except for Br in Freon) are lighter than Fe. Therefore, the reduction in the total cross section due to nuclear effects will be slightly overestimated. In comparison to the neutrino nuclear cross section as obtained in the Fermi gas model of Llewellyn Smith [7] (shown by dashed lines in Fig.2.18) we get a smaller result for these cross section. This reduction in the total cross section leads to an improved agreement with the experimental results as compared to the Fermi gas model results. It should be emphasized that the Fermi gas model has no specific mechanism to estimate the renormalization of weak transition strengths in nuclei while in our model this is incorporated by taking into account the RPA correlations.

==========*******==========

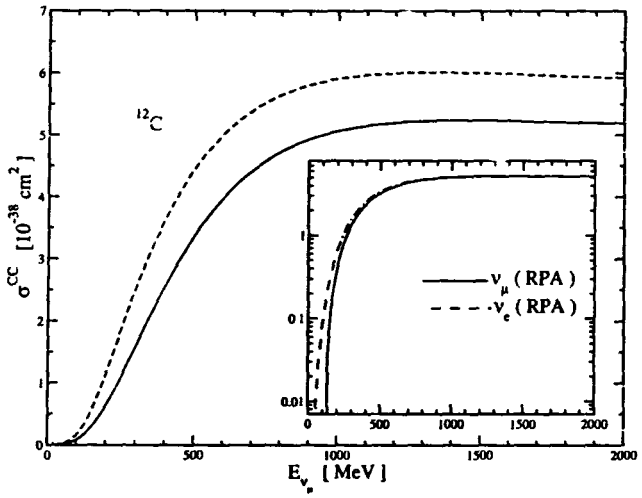

Figure 2.12: Quasielastic charged current lepton production cross section induced by neutrinos on ^{12}C target. The dotted line is the results for the free case and the solid line (dashed line) is the result with nuclear medium effects including RPA (without RPA).

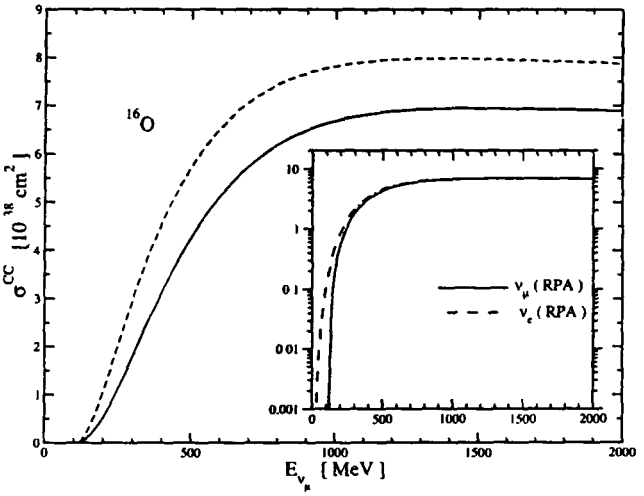

Figure 2.13: Quasielastic charged current lepton production cross section induced by neutrinos on ^{16}O target. The dotted line is the results for the free case and the solid line (dashed line) is the result with nuclear medium effects including RPA (without RPA).

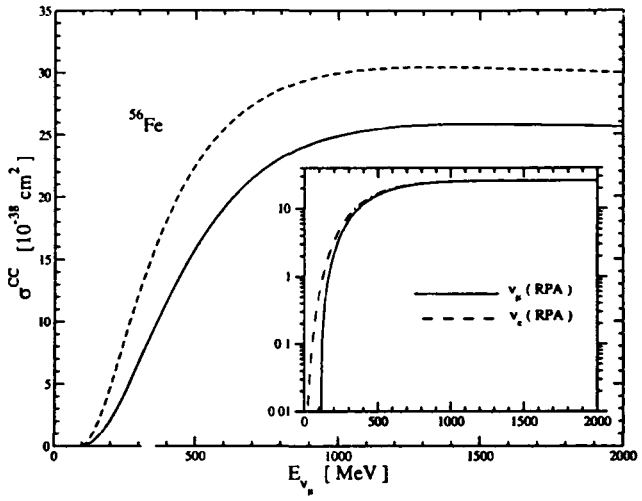

Figure 2 14· Quasielastic charged current lepton production cross section induced by neutrinos on ^{56}Fe target. The dotted line is the results for the free case and the solid line (dashed line) is the result with nuclear medium effects including RPA (without RPA).

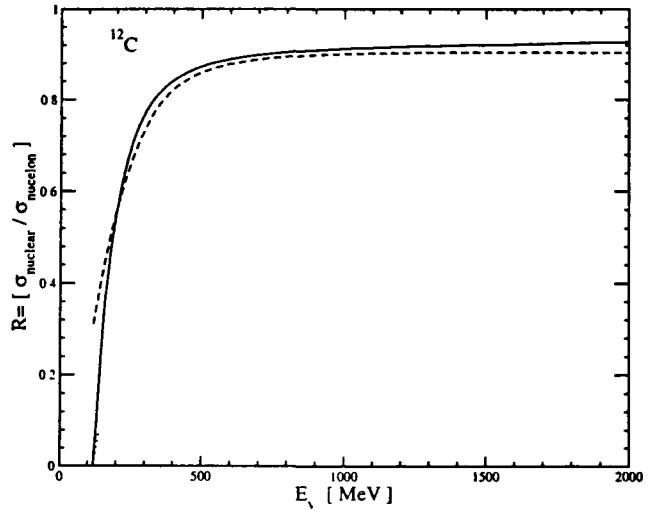

Figure 2.15 Ratio of the total cross section to the free neutrino nucleon cross section for the reactions $\nu_\mu + n \rightarrow \mu^- + p$ in ^{12}C nuclei in the present model without RPA (solid line) and with RPA (dotted line) and in the Fermi gas model (dashed line) [7].

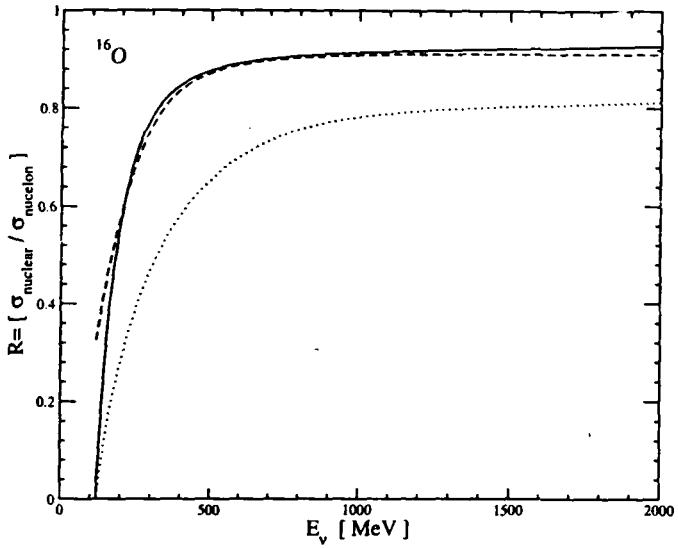

Figure 2.16: Ratio of the total cross section to the free neutrino nucleon cross section for the reactions $\nu_\mu + n \rightarrow \mu^- + p$ in ^{16}O nuclei in the present model without RPA (solid line) and with RPA (dotted line) and in the Fermi gas model (dashed line) [7].

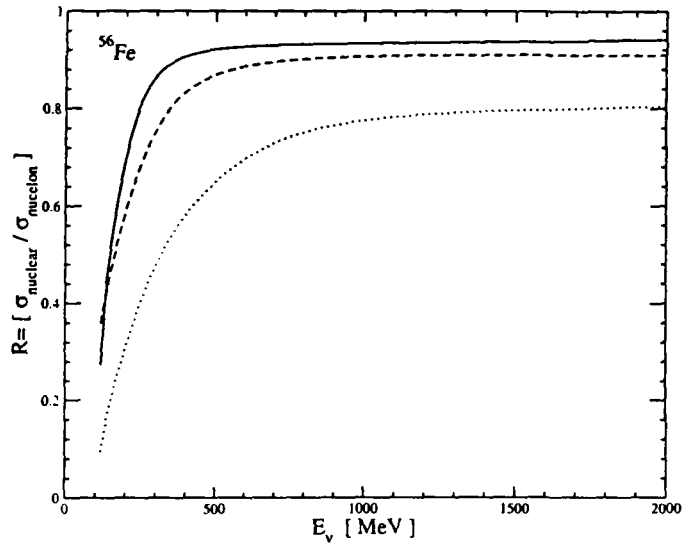

Figure 2.17: Ratio of the total cross section to the free neutrino nucleon cross section for the reactions $\nu_\mu + n \rightarrow \mu^- + p$ in ^{56}Fe nuclei in the present model without RPA (solid line) and with RPA (dotted line) and in the Fermi gas model (dashed line) [7].

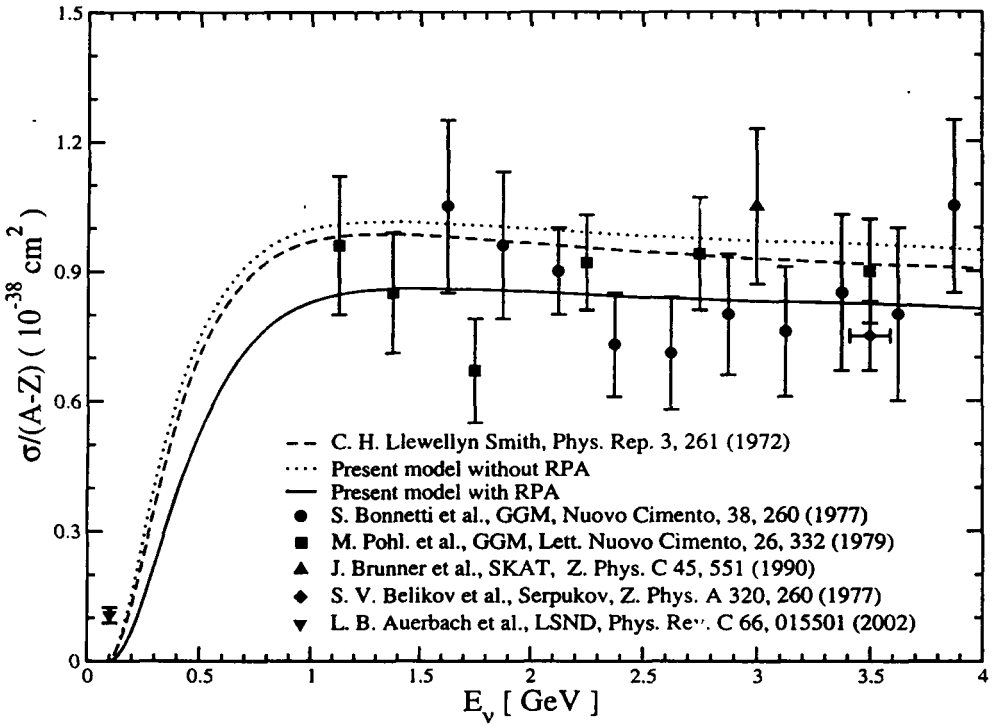

Figure 2.18: Neutrino quasielastic total cross section per nucleon in iron for $\nu_\mu + n \rightarrow p + \mu^-$ reaction. The data are from LSND [182](∇), Bonnetti et al. [184](o), SKAT collab. [185](△), Pohl et al. [183](□) and Belikov et al. [186](◇). The dashed line is the result of the cross section in the Fermi gas model [7] and dotted(solid) line is the result using the present model with nuclear effects without RPA(with RPA).

Chapter 3

Weak Pion Production From Nucleons

3.1 Introduction

In this chapter we shall be concerned mainly with the weak production of single pion from nucleons. In the intermediate energy region the most important process for neutrino induced pion production is through excitation of Δ resonance. The excitation of Δ resonance is the $I = \frac{3}{2}$, $J = \frac{3}{2}$ channel excitation of nucleon. In general, a Δ or N* resonance is excited which subsequently decays into pions and nucleon. In the following, we list the possible single pion production reactions induced by neutrinos and antineutrinos.

The neutrino and antineutrino induced channels for the charged current induced production of single pion on free nucleons are

$$\left.\begin{array}{llll} \nu_l\, p \rightarrow l^-\, \Delta^{++} \rightarrow l^-\, p\, \pi^+, & \bar{\nu}_l\, p \rightarrow l^+\, \Delta^+ \rightarrow l^+\, p\, \pi^0 \\ \nu_l\, n \rightarrow l^-\, \Delta^+ \rightarrow l^-\, n\, \pi^+, & \bar{\nu}_l\, p \rightarrow l^+\, \Delta^+ \rightarrow l^+\, n\, \pi^+ \\ \nu_l\, n \rightarrow l^-\, \Delta^+ \rightarrow l^-\, p\, \pi^0, & \bar{\nu}_l\, n \rightarrow l^+\, \Delta^- \rightarrow l^+\, n\, \pi^- \end{array}\right\} \tag{3.1}$$

Whereas, the neutrino and antineutrino induced channels for the neutral current induced production of single pion on free nucleon are

$$\left.\begin{array}{llll} \nu_l\, p \rightarrow \nu_l\, \Delta^+ \rightarrow \nu_l\, p\, \pi^0, & \bar{\nu}_l\, p \rightarrow \bar{\nu}_l\, \Delta^+ \rightarrow \bar{\nu}_l\, p\, \pi^0 \\ \nu_l\, p \rightarrow \nu_l\, \Delta^+ \rightarrow \nu_l\, n\, \pi^+, & \bar{\nu}_l\, p \rightarrow \bar{\nu}_l\, \Delta^+ \rightarrow \bar{\nu}_l\, n\, \pi^+ \\ \nu_l\, n \rightarrow \nu_l\, \Delta^0 \rightarrow \nu_l\, n\, \pi^0, & \bar{\nu}_l\, n \rightarrow \bar{\nu}_l\, \Delta^0 \rightarrow \bar{\nu}_l\, n\, \pi^0 \\ \nu_l\, n \rightarrow \nu_l\, \Delta^0 \rightarrow \nu_l\, p\, \pi^-, & \bar{\nu}_l\, n \rightarrow \bar{\nu}_l\, \Delta^0 \rightarrow \bar{\nu}_l\, p\, \pi^- \end{array}\right\} \tag{3.2}$$

In view of the basic importance of pion for our understanding of nucleons and the forces acting between them, the pion production processes are of considerable interest. These are also useful to determine the nucleon form factors, pion dynamics in the nuclear matter and to calculate the coupling strength of pion to the nucleons. Furthermore, nucleon excitation by weak interaction

with emission of pions is source of valuable information to understand neutrino interactions with nuclei and nuclear excitation mechanism. The neutrino induced weak pion production processes from nucleons and nuclei at intermediate energies are also important tools to study the hadronic structure. The dynamic models of the hadronic structure are used to calculate the various nucleon and transition form factors which are tested by using the experimental data on photo, electro and weak pion production processes on nucleons. The weak pion production along with the electro pion production from nucleon in the Δ-resonance region is used to determine various electroweak N-Δ transition form factors.

There exist data at low and high energy, for single pion production induced by charged current and neutral current interactions of neutrinos and antineutrinos on protons and neutrons [237]-[245]. These experiments are done in hydrogen and deuterium filled bubble chambers and are free from nuclear medium corrections. These experiments also have high statistics and provide reasonable estimates of the dominant form factors in N-Δ transitions. Theoretically, there have been many attempts in past to calculate the weak production of pions induced by neutrinos from free nucleons using various approaches like multipole analysis, effective Lagrangian and Quark model [7], [9], [122]-[133]. These approaches give a satisfactory description of these processes in terms of some parameters which are determined phenomenologically.

In next section-3.2, we describe the effective Lagrangians for different hadronic interactions contributing to weak processes with their coupling strengths. In section-3.3, the matrix elements for single pion production from free nucleons are written for different non-resonant and resonant channels, using the relativistic description of the interaction of leptons and hadrons in an effective Lagrangian field theory. In resonant production of pion, we have considered the Δ excitation, and the matrix element has been written using the information about the N-Δ transition form factors as determined from experiments. In section-3.4, we derive cross sections for the considered reactions.

3.2 The Effective Lagrangians

In the following we describe the effective Lagrangians for the different hadronic interactions used in calculation of charged current and neutral current induced processes mediated by a charged ($W^{\pm}$) and neutral (Z^0) intermediate vector bosons (IVB), shown in Fig.3.1.

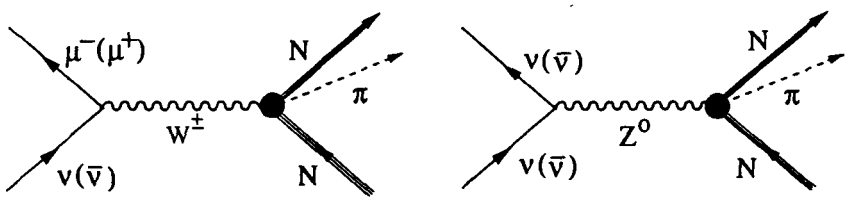

Figure 3.1: Diagrams considered for weak interaction

Specifically we give the effective Lagrangians for πNN, πNΔ, WNN, WNNπ and W$\pi\pi$ interaction in charged current induced production and ZNN, ZNNπ and Z$\pi\pi$ interaction in neutral current induced production in the following subsections.

3.2.1 Charged Current Interaction

The effective Lagrangians for charged current (CC) processes are ([126], [246])

$$\mathcal{L}_{\pi NN} = \left(\frac{f_{\pi NN}}{m_\pi}\right)\bar{\Psi}\gamma_\mu\gamma_5\tau\Psi\cdot\partial^\mu\Phi_\pi \tag{3.3}$$

$$\mathcal{L}_{\pi N\Delta} = i\left(\frac{f_{\pi N\Delta}}{m_\pi}\right)\bar{\Psi}^\mu_\Delta(\partial_\mu\Phi_\pi)\mathbf{T}\Psi + \text{h.c.} \tag{3.4}$$

$$\mathcal{L}^V_{WNN} = \frac{g}{2\sqrt{2}}\bar{\Psi}\left[F_1^V\gamma_\mu W^\mu + F_2^V\frac{\sigma_{\mu\nu}}{2M}\partial^\nu W^\mu\right]\frac{\tau_3}{2}\Psi \tag{3.5}$$

$$\mathcal{L}^A_{WNN} = -\frac{g}{2\sqrt{2}}\bar{\Psi}\left[G_A^V\gamma_\mu W^\mu + i\frac{G_P^V}{2M}\partial_\mu W^\mu\right]\frac{\tau_3}{2}\gamma_5\Psi \tag{3.6}$$

$$\mathcal{L}^V_{WNN\pi} = \frac{g}{2\sqrt{2}}\left(\frac{f_{\pi NN}}{m_\pi}\right)F_\pi(Q^2)\bar{\Psi}\left(\vec{\tau}\times\vec{\phi}_\pi\right)_3\gamma_\mu\gamma_5\Psi W^\mu \tag{3.7}$$

$$\mathcal{L}^A_{WNN\pi} = \frac{g}{2\sqrt{2}}\left(\frac{f_{\pi NN}}{m_\pi}\right)F_\pi(Q^2)\bar{\Psi}\left(\vec{\tau}\times\vec{\phi}_\pi\right)_3\left[F_1^V\gamma_\mu + F_2^V\frac{\sigma_{\mu\nu}}{2M}\partial^\nu\right]\Psi W^\mu \tag{3.8}$$

$$\mathcal{L}^V_{W\pi\pi} = \frac{g}{2\sqrt{2}}F_\pi(Q^2)\left\{\vec{\phi}_\pi\times\left(\partial_\mu\vec{\phi}_\pi\right)\right\}_3 W^\mu \tag{3.9}$$

3.2.2 Neutral Current Interaction

The effective Lagrangians for neutral current (NC) processes are ([127], [246])

$$\mathcal{L}^V_{ZNN} = \bar{\Psi}\frac{1}{2}\left[\left(\xi_V^{I=0}F_1^S + \xi_V^{I=1}\tau_3F_1^V\right)\gamma_\mu + \left(\xi_V^{I=0}\kappa_s F_2^S + \xi_V^{I=1}\kappa_v\tau_3F_2^V\right)\frac{\sigma_{\mu\nu}}{2M}\partial^\nu\right]Z^\mu\Psi \tag{3.10}$$

$$\begin{aligned}\mathcal{L}^A_{ZNN} &= \bar{\Psi}\frac{1}{2}\left[\left(\xi_A^{I=0}G_A^S + \xi_A^{I=1}\tau_3G_A^V\right)\gamma_\mu + \left(\xi_A^{I=0}G_P^S + \xi_A^{I=1}\tau_3G_P^V\right)\frac{i\partial_\mu}{2M}\right]Z^\mu\Psi \\ &= \xi_A^{I=1}\bar{\Psi}\left[G_A^V(Q^2)\gamma_\mu + G_P^V\frac{i\partial_\mu}{2M}\right]\frac{\tau_3}{2}Z^\mu\Psi\end{aligned} \tag{3.11}$$

$$\mathcal{L}^V_{Z\pi\pi} = \xi_V^{I=1}F_\pi(Q^2)\left\{\vec{\phi}_\pi\times\left(\partial_\mu\vec{\phi}_\pi\right)\right\}_3 Z^\mu \tag{3.12}$$

$$\mathcal{L}^V_{ZNN\pi} = \xi_V^{I=1}\left(\frac{f_{\pi NN}}{m_\pi}\right)F_\pi(Q^2)\bar{\Psi}\left(\vec{\tau}\times\vec{\phi}_\pi\right)_3\gamma_\mu\gamma_5\Psi Z^\mu \tag{3.13}$$

$$\mathcal{L}^A_{ZNN\pi} = \xi_A^{I=1}\left(\frac{f_{\pi NN}}{m_\pi}\right)F_\pi(Q^2)\bar{\Psi}\left(\vec{\tau}\times\vec{\phi}_\pi\right)_3\left[F_1^V\gamma_\mu W^\mu - \kappa_v F_2^V\frac{\sigma_{\mu\nu}}{2M}\partial^\nu Z^\mu\right]\Psi \tag{3.14}$$

With $\kappa_{(s,v)} = (\kappa_p \pm \kappa_n)$ and g the coupling constant for the weak-isospin group SU(2). The form factors F_1, F_2, F_A, F_π, G_A and G_p are functions of momentum transfer ($Q^2 = -q^2$), and have been discussed in the detail in Chapter-2. We take $f^2_{\pi N\Delta}/4\pi$=0.36 and $f^2_{\pi NN}/4\pi$=0.08 with $f_{\pi N\Delta}/f_{\pi NN}$=2.12, a value in between the factor 2.2 taken by [247] and the factor of 2 considered in [134]. In standard model (SM) the isospin factors $\xi^{I=0,1}_{V,A}$ are given as [246]:

$$\left.\begin{array}{ll} \xi_V^{I=1} = \frac{1}{2\sin\theta_W\cos\theta_W}\,(1-2\sin^2\theta_W), & \xi_A^{I=1} = -\frac{1}{2\sin\theta_W\cos\theta_W} \\ \xi_V^{I=0} = -\frac{1}{2\sin\theta_W\cos\theta_W}\,2\sin^2\theta_W, & \xi_A^{I=0} = 0 \end{array}\right\} \tag{3.15}$$

where θ_W is the Weinberg angle.

3.3 Matrix Elements

We construct the amplitude for the process shown in Fig.3.2, using the weak interaction Lagrangian described in section-3.2 for neutrino induced weak charged current (CC) and neutral current (NC) single pion production by the free nucleon, mediated by a charged ($W^\pm$) and neutral (Z^0) intermediate vector bosons (IVB) coupled to vector and axial vector hadronic currents. The basic weak interaction Lagrangian for charged current interaction is given as

$$\mathcal{L}_{int}^{weak} = -\frac{g}{2\sqrt{2}}\,J^\mu_{CC}(x)\,W^\dagger_\mu(x) + \text{Hermitian conjugate.} \tag{3.16}$$

where the weak charged current $J^\mu_{CC}(x)$ couples to the charged W-boson fields $W^\pm_\mu$. The current $J^\mu_{CC}(x)$ consist of leptonic and hadronic part as:

$$J^\mu_{CC}(x) = l^\mu_{lep}(x) + J^\mu_{had}(x) \tag{3.17}$$

with $l^\mu_{lep}(x)$ the leptonic weak current given by

$$l^\mu_{lep}(x) = \bar{\psi}_l(k')\gamma^\mu(1-\gamma^5)\psi_{\nu_l}(k) \tag{3.18}$$

and $J^{had}_\mu(x) = \cos\theta_C\,(J^V_\mu(x) + J^A_\mu(x))$ is the weak hadronic current divided into its vector and axial vector part, and θ_C is the Cabibbo angle. At low momentum transfer ($q^2 << M^2_W$) assuming that the weak interactions are mediated by an intermediate vector boson, the invariant matrix element for neutrino induced charged current reactions can be written as

$$\mathcal{M} = \frac{G}{\sqrt{2}}\,J^{\mu\dagger}_{had}(x)\,l^{lep}_\mu(x) + \text{Hermitian conjugate.} \tag{3.19}$$

where we have used the relation $g^2/8M^2_W = G/\sqrt{2}$. G is the Fermi coupling constant G=1.16639$\times10^{-5}$GeV^2 and M_W is the W-boson mass. The matrix element of the hadronic current is generally calculated using the nucleon and meson exchanges and the resonance excitation diagrams. However, it has been shown that in the intermediate energy region of about 1 GeV, the dominant contribution to the single pion production from nucleons comes from the

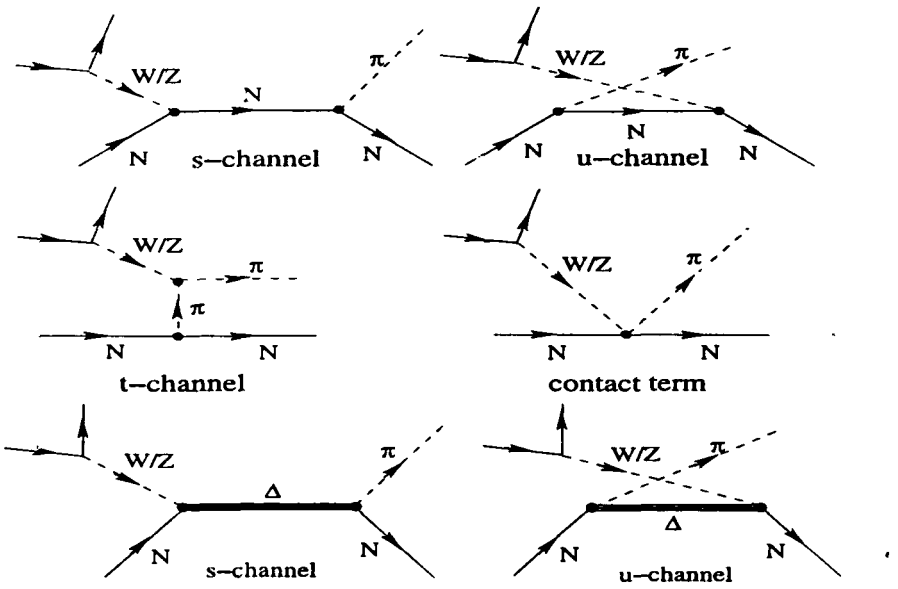

Figure 3.2: Feynman diagrams considered for weak pion production

Δ resonance due to very strong P wave pion nucleon coupling leading to Δ resonance. Furthermore, the angular distribution and the energy distribution of the pions is dominated by the Δ contribution while the other diagrams contribute to the tail region due to the interference of the nucleon and meson exchange diagrams with the Δ resonance diagram. Following the basic weak interaction Lagrangians defined in section-3.2 for charged current as well as neutral current interactions, we write down the matrix elements in case of nonresonant and resonant terms corresponding to the Feynman diagrams shown in Fig.3.2.

3.3.1 Non-Resonant Terms

The matrix elements in charged current(CC) channel corresponding to the considered Feynman diagrams in Fig.3.2 for nucleon direct(s), crossed(u), contact(c) and pion pole(t) term are as follows ([126], [246])

$$\mathcal{M}_s^N = \frac{G}{\sqrt{2}}\cos\theta_C\left(\frac{f_{\pi NN}}{m_\pi}\right)\bar{u}(\mathbf{p}')\gamma_5\, \not{k}_\pi\left(\frac{\not{p}+\not{q}+M}{s-M^2}\right)\times \left[\left(F_1^V(Q^2)\gamma_\mu+\frac{F_2^V(Q^2)}{2M}\sigma_{\mu\nu}\partial^\nu\right)-\left(G_A^V(Q^2)\gamma_\mu+i\frac{G_P^V(Q^2)}{2M}\partial_\mu\right)\right]u(\mathbf{p})l^\mu \tag{3.20}$$

$$\mathcal{M}_u^N = \frac{G}{\sqrt{2}}\cos\theta_C\left(\frac{f_{\pi NN}}{m_\pi}\right)\bar{u}(\mathbf{p}')\left[\left(F_1^V(Q^2)\gamma_\mu+\frac{F_2^V(Q^2)}{2M}\sigma_{\mu\nu}\partial^\nu\right)\right.$$

$$- \left(G_A^V(Q^2)\gamma_\mu + i\frac{G_P^V(Q^2)}{2M}\partial_\mu \right) \Big] \left(\frac{\not{p} - \not{k}_\pi + M}{u - M^2} \right) \gamma_5 \not{k}_\pi u(\mathbf{p}) l^\mu \tag{3.21}$$

$$\mathcal{M}_t^\pi = \frac{G}{\sqrt{2}} \cos\theta_C \left(\frac{f_{\pi NN}}{m_\pi} \right) \left(\frac{2k_\pi - q}{t - m_\pi^2} \right) 2M F_\pi(Q^2) \left[\bar{u}(\mathbf{p}')\gamma_5 u(\mathbf{p}) \right] l^\mu \tag{3.22}$$

$$\begin{aligned} \mathcal{M}_c = & \frac{G}{\sqrt{2}} \cos\theta_C \left(\frac{f_{\pi NN}}{m_\pi} \right) \bar{u}(\mathbf{p}') \left[F_\pi(Q^2)\gamma_\mu\gamma_5 \right. \\ & \left. - \left(F_1^V(Q^2)\gamma_\mu + i\frac{F_2^V(Q^2)}{2M}\sigma_{\mu\nu}\partial^\nu \right) \right] u(\mathbf{p}) l^\mu \end{aligned} \tag{3.23}$$

The matrix elements in neutral current(NC) channel corresponding to the considered Feynman diagrams in Fig.3.2 for nucleon direct(s), crossed(u), contact(c) and pion pole(t) term are given as ([127], [246])

$$\begin{aligned} \mathcal{M}_s^N = & \frac{G}{\sqrt{2}} \left(\frac{f_{\pi NN}}{m_\pi} \right) \bar{u}(\mathbf{p}')\gamma_5 \not{k}_\pi \left(\frac{\not{p} + \not{q} + M}{s - M^2} \right) \times \\ & \left[\xi_V^{I=1} \left(I_s^D \gamma_\mu + i I_s^P \frac{\sigma_{\mu\nu}}{2M} q^\nu \right) + \xi_A^{I=1} \left(I_s^A \gamma_\mu - I_s^I \frac{q_\mu}{2M} \right) \right] u(\mathbf{p}) l^\mu \end{aligned} \tag{3.24}$$

$$\begin{aligned} \mathcal{M}_u^N = & \frac{G}{\sqrt{2}} \left(\frac{f_{\pi NN}}{m_\pi} \right) \bar{u}(\mathbf{p}') \left[\xi_V^{I=1} \left(I_s^D \gamma_\mu + i I_s^P \frac{\sigma_{\mu\nu}}{2M} q^\nu \right) \right. \\ & \left. + \xi_A^{I=1} \left(I_s^A \gamma_\mu - I_s^I \frac{q_\mu}{2M} \right) \right] \gamma_5 \not{k}_\pi \left(\frac{\not{p} + \not{q} + M}{s - M^2} \right) u(\mathbf{p}) l^\mu \end{aligned} \tag{3.25}$$

$$\mathcal{M}_t^\pi = \frac{G}{\sqrt{2}} \left(\frac{f_{\pi NN}}{m_\pi} \right) \xi_V^{I=1} \left(\frac{2k_\pi - q}{t - m_\pi^2} \right) 2M I_t F_\pi(Q^2) \left[\bar{u}(\mathbf{p}')\gamma_5 u(\mathbf{p}) \right] l^\mu \tag{3.26}$$

$$\begin{aligned} \mathcal{M}_c = & \frac{G}{\sqrt{2}} \left(\frac{f_{\pi NN}}{m_\pi} \right) I_t \bar{u}(\mathbf{p}') \left[\xi_V^{I=1} F_\pi(Q^2)\gamma_\mu\gamma_5 \right. \\ & \left. - \xi_A^{I=1} \left(F_1^V \gamma_\mu + i\frac{F_2^V}{2M}\sigma_{\mu\nu} q^\nu \right) \right] u(\mathbf{P_i}) l^\mu \end{aligned} \tag{3.27}$$

where the following abbreviations for the isospin matrix elements have been used in above expressions [246]

$$\begin{aligned} I_{(s,u)}^D &= \frac{1}{2} \left[\frac{\xi_V^{I=0}}{\xi_V^{I=1}} F_1^S I^0 + F_1^V (I^+ \pm I^-) \right], \quad I_{(s,u)}^P = \frac{1}{2} \left[\frac{\xi_V^{I=0}}{\xi_V^{I=1}} F_2^S I^0 + F_2^V (I^+ \pm I^-) \right] \\ I_{(s,u)}^A &= \frac{1}{2} \left[\frac{\xi_A^{I=0}}{\xi_A^{I=1}} G_A^S I^0 + G_A^V (I^+ \pm I^-) \right], \quad I_{(s,u)}^I = \frac{1}{2} \left[\frac{\xi_A^{I=0}}{\xi_A^{I=1}} G_P^S I^0 + G_P^V (I^+ \pm I^-) \right] \\ I_t &= I^- \end{aligned} \tag{3.28}$$

with

$$I^0 = \chi_f^\dagger \tau_\pi \chi_i, \quad I^+ = \chi_f^\dagger \frac{1}{2} \{\tau_\pi, \tau_3\} \chi_i, \quad I^- = \chi_f^\dagger \frac{1}{2} [\tau_\pi, \tau_3] \chi_i \tag{3.29}$$

$\chi_{f(i)}$ is the final(initial) nucleon iso-spin function, τ_3 is the Pauli iso-spin matrix.

3.3.2 Resonant Terms

In the intermediate energy region, contribution to the single pion production comes through the excitation of the low mass resonances. The dominant contribution to the cross section comes from the production and subsequent decay of the $\Delta(1232)$ resonance which is the most important resonance observed in the πN scattering system, driven by the strong P-wave attraction. Beside this some of the channels have a non-negligible contribution from the isospin 1/2 resonances. We have done the calculations assuming Δ dominance of single pion production. In this model of the Δ dominance, we follow the standard Rarita-Schwinger formalism [124], [126], [133], [135]-[137] for the neutrino induced charged current Δ production

$$\nu_l(k) + p(p) \rightarrow l^-(k') + \Delta^{++}(P) \tag{3.30}$$

$$\nu_l(k) + n(p) \rightarrow l^-(k') + \Delta^{+}(P) \tag{3.31}$$

The matrix element for Δ production (Eq.3.30) is written as

$$\langle l^- \Delta^{++}|\mathcal{M}\ \nu_l\ p\rangle = \frac{G}{\sqrt{2}} \cos\theta_C\ l_\mu^{lep}\ \langle \Delta^{++}|V^\mu - A^\mu|p\rangle \tag{3.32}$$

where l_μ^{lep} is the invariant matrix element of the leptonic weak current given by Eq.3.18. The matrix elements $\langle \Delta^{++}|V^\mu|p\rangle$ and $\langle \Delta^{++}|A^\mu|p\rangle$ corresponds to the N-Δ transition matrix elements of the vector V^μ and axial vector A^μ transition hadronic current between N and Δ states for the charged current interaction. From the conservation of vector current(CVC)(isotriplet vector current hypothesis) we know that the matrix elements of the weak strangeness conserving hadronic vector current are related by isospin Clebsch-Gordon coefficients to the matrix elements of the I=1 electromagnetic current measured in electroproduction of pions. Since in electroproduction of the Δ, the I=0 component of the electromagnetic current does not contribute so that the relationship becomes simply [7], [124], [248].

$$\langle\ \Delta^{++}\ |\ V^\alpha\ \ p\ \rangle = \sqrt{3}\ \langle\ \Delta^{+}\ |\ V_{em}^\alpha\ |\ p\ \rangle \tag{3.33}$$

The most general form of the matrix elements of the hadronic transition currents for the Δ excitation from proton target $p \rightarrow \Delta^{++}$ in the s-channel are written as ([7], [9], [122], [124], [126]-[127], [135]-[139], [243]-[244]):

$$\langle \Delta^{++}|V^\mu|p\rangle = \sqrt{3}\ \bar{\upsilon}_\alpha(P)\left[\left(\frac{C_3^V(q^2)}{M}\ (g^{\alpha\mu}\not{q} - q^\alpha\gamma^\mu) + \frac{C_4^V(q^2)}{M^2}\ (g^{\alpha\mu}q\cdot P - q^\alpha P^\mu) + \frac{C_5^V(q^2)}{M^2}\ (g^{\alpha\mu}q\cdot p - q^\alpha p^\mu) + \frac{C_6^V(q^2)}{M^2}\ q^\alpha q^\mu\right)\gamma_5\right] u(p) \tag{3.34}$$

and

$$\langle \Delta^{++}|A^{\mu}|p\rangle = \sqrt{3}\,\bar{\psi}_{\alpha}(P)\left[\left(\frac{C_3^A(q^2)}{M}\,(g^{\alpha\mu}\not{q} - q^{\alpha}\gamma^{\mu}) + \frac{C_4^A(q^2)}{M^2}\,(g^{\alpha\mu}q\cdot P - q^{\alpha}P^{\mu}) + C_5^A(q^2)\,g^{\alpha\mu} + \frac{C_6^A(q^2)}{M^2}\,q^{\alpha}q^{\mu}\right)\right]u(p) \tag{3.35}$$

Here $\psi_{\alpha}(P)$ and $u(p)$ are the Rarita-Schwinger and Dirac spinors for the Δ and the nucleon of momenta P and p respectively, $q(= P - p = k - k')$ is the momentum transfer and M is the mass of the nucleon. $C_i^V(i = 3-6)$ are the vector and $C_i^A(i = 3-6)$ are the axial vector transition form factors. The factor of $\sqrt{3}$ in the matrix element is according to the relation in Eq.3.33, so that, the $C_i^V(i = 3-6)$ are just those measured in the $p \rightarrow \Delta^+$ photoproduction and electroproduction experiments.

3.3.3 N-Δ Transition Form Factors

The two basic approaches have been extensively described in the literature for the N-Δ transition form factors $C_i^V(i = 3-6)$ and $C_i^A(i = 3-6)$ relevant to the weak transition current. They are phenomenological with parameters extracted from the analysis of neutrino and electron scattering experimental data [7], [122]-[124], [126], [135], [249]-[252] or using quark model calculations without and with pion dynamics [253]-[254]. Early attempts for the later are reviewed in Ref. [124] and more recent ones are summarized in Ref. [255]. In the model of resonance production, Rein and Sehgal [9] adopted the quark model of Feynman, Kislinger and Ravndal [256]. A more recent calculation was done by Liu et al. [255] who applied the Isgur-Karl quark model and by Sato et al. [132] who developed a dynamical model including pion cloud effects. In the following sections we describe in some detail, about these form factors used in the present calculation.

A. Vector form factors

In section-3.3.2, Eq.3.34, there are four weak vector form factors $C_i^V(i = 3-6)$ occurring in the transition. The conserved vector current (CVC) hypothesis which in momentum space reads $q_{\mu}V^{\mu}$ implies $C_6^V(q^2)$=0. The other form factors $C_i^V(i = 3-5)$ are related in terms of the isovector electromagnetic form factors of the $p \rightarrow \Delta^+$ electromagnetic transition, and are determined from the analysis of photoproduction and electroproduction data of Δ which is done in terms of the multipole amplitudes [257]-[262]. Assuming M1 dominance, these form factors $C_i^V(q^2)$ satisfy the relations:

$$C_5^V(q^2) = 0, \quad C_4^V(q^2) = -\frac{M}{M_{\Delta}}\,C_3^V(q^2) \tag{3.36}$$

where M_Δ is the invariant mass of the πN system and we use a fixed Δ mass, $M_\Delta = 1.232$GeV and the electroproduction data in the Δ-region is well fitted with

$$C_3^V(q^2) = \frac{2.05}{(1 - q^2/0.54GeV^2)^2} \tag{3.37}$$

In general these are parametrized in a dipole form [124]

$$C_i^V(q^2) = C_i^V(0) \left(1 - \frac{q^2}{M_V^2}\right)^{-2} ; \quad i = 3, 4, 5. \tag{3.38}$$

where M_V is the vector dipole mass. Recently, there are other proposed modified forms of these form factors, parametrized in dipole form and in quark model calculations without or with pion dynamics [9], [132], [146]-[147], [263]. In the case of dipole form factors various modifications have been proposed. For example, Lalakulich et al. [147] use

$$C_i^V(q^2) = C_i^V(0) \left(1 - \frac{q^2}{M_V^2}\right)^{-2} \mathcal{D}_i \ , \quad i = 3, 4, 5. \tag{3.39}$$

where

$$\begin{aligned} \mathcal{D}_i &= \left(1 - \frac{q^2}{4M_V^2}\right)^{-1} \quad \text{for} \quad i = 3, 4 \\ \mathcal{D}_i &= \left(1 - \frac{q^2}{0.776M_V^2}\right)^{-1} \quad \text{for} \quad i = 5. \end{aligned} \tag{3.40}$$

While Paschos et al. [146] and Leitner et al. [263] use

$$C_6^V(q^2) = 0, \quad C_5^V(q^2) = 0, \quad \text{and} \quad C_4^V(q^2) = -\frac{M}{W} C_3^V(q^2) \tag{3.41}$$

and

$$C_3^V(q^2) = C_3^V(0) \left(1 - \frac{q^2}{M_V^2}\right)^{-2} \left(1 - \frac{q^2}{4M_V^2}\right)^{-1} \tag{3.42}$$

W is the center of mass energy i.e. $W = \sqrt{(p+q)^2}$ and M_Δ is the mass of Δ. Various parameters occurring in these form factors used by these authors are summarized in table-3.1.

B. Axial vector form factors

In the case of axial vector matrix element, partially conserved axial vector current (PCAC) hypothesis implies that its divergence should vanish in the limit when pion mass goes to zero. In practical terms this means that the matrix element of $\partial_\mu A^\mu$ or in momentum space $q_\mu A^\mu$

should be proportional to the square of pion mass m_π^2 and so vanish in the limit $m_\pi^2 \to 0$. From Eq.3.35, it may be seen that

$$\begin{aligned}\langle \Delta^{++}|i\partial_\mu A^\mu|p\rangle &= \sqrt{3}\,\bar{\psi}_\alpha(P)\,q_\mu\left(C_5^A(q^2)\,g^{\alpha\mu}+\frac{C_6^A(q^2)}{M^2}\,q^\alpha q^\mu\right)u(p)\\ &= \sqrt{3}\,\bar{\psi}_\alpha(P)\,q^\alpha\left(C_5^A(q^2)+\frac{C_6^A(q^2)}{M^2}\,q^2\right)u(p)\end{aligned} \tag{3.43}$$

Pion pole dominance implies that the induced pseudoscalar form factor $C_6^V(q^2)$ must have a pion pole [124]:

$$C_6^A(q^2)(\text{pole}) \approx \frac{g_{\pi N\Delta} f_\pi}{2\sqrt{3}M}\,\frac{M^2}{m_\pi^2 - q^2} \tag{3.44}$$

where $g_{\pi N\Delta} = 28.6$ is the $\Delta^{++} \to p\pi^+$ coupling constant and $f_\pi = 0.97 m_\pi$ is the pion decay constant. Using this relation in Eq.3.43, we see that when $m_\pi^2 = 0$, this pole will give a non vanishing contribution to the matrix element of the divergence even as $q^2 \to 0$.

$$\langle \Delta^{++}|i\partial_\mu A^\mu|p\rangle \xrightarrow[q^2\to 0.]{m_\pi = 0.} \sqrt{3}\,\bar{\psi}_\alpha(P)\,q^\alpha\left(C_5^A(0) - \frac{g_{\pi N\Delta} f_\pi}{2\sqrt{3}M}\right)u(p) \tag{3.45}$$

This leads to the connection between $C_5^A(q^2)$ and $C_6^A(q^2)$ in the axial current as

$$C_6^A(q^2) = C_5^A(q^2)\,\frac{M^2}{m_\pi^2 - q^2} \tag{3.46}$$

If the coupling constants $g_{\pi N\Delta}$, f_π and mass M do not vary much from their physical values as the pion mass goes to zero ($m_\pi^2 = 0$) and $q^2 = 0$, we obtain the off-diagonal Goldberger-Treiman relation as

$$C_5^A(0) = \frac{g_{\pi N\Delta} f_\pi}{2\sqrt{3}M} \approx 1.2 \tag{3.47}$$

This coupling was extracted from the BNL data in Ref. [264] and found to be consistent with the PCAC prediction.

The remaining axial vector form factor $C_i^A (i = 3-5)$ are taken from the experimental analysis of the neutrino experiments producing Δ's in proton and deuteron targets [239], [243]-[245]. These form factors are not uniquely determined but they are in general parametrized in the dipole form giving a satisfactory fit to the data, and are given as

$$\begin{aligned}C_i^A(q^2) &= C_i^A(0)\left(1 - \frac{q^2}{M_A^2}\right)^{-2}\mathcal{D}_i\ , \quad i = 3,4,5.\\ \mathcal{D}_i &= 1 - \frac{a_i q^2}{(b_i - q^2)};\ i = 3,4,5\end{aligned} \tag{3.48}$$

where $C_i^A(0)$ and a_i, b_i are the model dependent axial vector form factor parameters determined for the Adler model [124], [265] with $C_3^A(0) = 0$, $C_4^A(0) = -0.3$, $C_5^A(0) = 1.2$, $a_3 = b_3 = 0$, $a_4 = a_5 = -1.21$, $b_4 = b_5 = 2$ GeV^2, $M_A = 1.05$ GeV.

Recently, these form factors have been given by Paschos et al. [146], Lalakulich et al. [147] and Leitner et al. [263] having the form

$$
\begin{aligned}
C_i^A(q^2) &= C_i^A(0)\ (1 - \frac{q^2}{M_A^2})^{-2}\,\mathcal{D}_i\ , \quad i = 3,4,5. \\
\mathcal{D}_i &= \left(1 - \frac{q^2}{3M_A^2}\right)^{-1}
\end{aligned}
\tag{3.49}
$$

where M_A is the axial vector dipole mass and m_π is the pion mass.

Various parameters occurring in these form factors used by these authors are summarized in table-3.1.

Table 3.1: Weak vector and axial vector couplings at $q^2 = 0$ and the values of M_V and M_A used in the literature.

References	C_3^V	C_4^V	C_5^V	C_3^A	C_4^A	C_5^A	M_V(GeV)	M_A(GeV)
Schreiner and von Hippel [124]	2.05	$-\frac{M}{M_\Delta}$	0.0	0.0	-0.3	1.2	0.73	1.05
Singh et al. [135]	2.05	$-\frac{M}{M_\Delta}$	0.0	0.0	-0.3	1.2	0.73	1.05
Paschos et al. [146]	1.95	$-\frac{M}{W}$	0.0	0.0	-0.25	1.2	0.84	1.05
Lalakulich et al. [147]	2.13	-1.51	0.48	0.0	-0.25	1.2	0.84	1.05
Leitner et al. [263]	1.95	$-\frac{M}{W}$	0.0	0.0	-0.25	1.2	0.84	1.05

3.4 Cross Sections

The differential cross section for the production of Δ from free nucleon i.e., $\nu(k) + p(p) \rightarrow \mu^-(k') + \Delta^{++}(p')$ can be written as

$$
d\sigma = \frac{(2\pi)^4\delta^4(k+p-p'-k')}{4\sqrt{(k\cdot k')^2 - m_\nu^2 M^2}}\,\frac{d^3\mathbf{k}'}{(2\pi)^3 2E_{k'}}\,\frac{d^3\mathbf{p}'}{(2\pi)^3 2E_{p'}}\left\{\frac{G^2\cos^2\theta_C}{2}\,L_{\mu\nu}J^{\mu\nu}\right\} \tag{3.50}
$$

where $k + p = k' + p'$, and $q = k - k'$. Using the relations

$$
4\sqrt{(k\cdot k')^2 - m_\nu^2 M^2} = 4p\cdot k = 4ME_\nu \tag{3.51}
$$

$$
d^3\mathbf{k}' = |\mathbf{k}'|^2\, d|\mathbf{k}|\, d\Omega_{k'} = E_{k'}\,|\mathbf{k}'|\, dE_{k'} \tag{3.52}
$$

and performing the $d^3\mathbf{p}'$ integration, we get

$$\frac{d^2\sigma}{dE_{k'}d\Omega_{k'}} = \frac{1}{64\pi^2}\frac{1}{ME_\nu}\frac{|\mathbf{k}'|}{E'_p}\,\delta(E_p+q_0-E_{p'})\left\{\frac{G^2\cos^2\theta_C}{2}\,L_{\mu\nu}J^{\mu\nu}\right\} \tag{3.53}$$

The leptonic tensor $L_{\mu\nu}$ in Eq.3.53 is defined as

$$\begin{aligned} L_{\mu\nu} = \bar{\Sigma}\Sigma l_\mu{}^\dagger l_\nu &= \mathrm{Tr}\left[(\not{k}+m_\nu)\,\gamma_\mu(1-\gamma_5)(\not{k}'+m_l)\,\gamma_\nu(1-\gamma_5)\right] \\ &= 8\,(k_\mu k'_\nu + k'_\mu k_\nu - g_{\mu\nu}\,k\cdot k' + i\epsilon_{\mu\nu\alpha\beta}\,k^\alpha k'^\beta) \end{aligned} \tag{3.54}$$

and the hadronic tensor $J^{\mu\nu}$ is given as

$$\begin{aligned} J^{\mu\nu} &= \bar{\Sigma}\Sigma J^{\mu\dagger}J^\nu \\ &= \mathrm{Tr}\left[(\not{p}+M)\,\tilde{\mathcal{O}}^{\mu\alpha}\,\mathcal{P}^{3/2}_{\alpha\beta}\,\mathcal{O}^{\beta\nu}\right] \end{aligned} \tag{3.55}$$

where $\mathcal{O}^{\mu\alpha}$ is the weak N-Δ transition vertex given as the sum of vector (V^μ) and axial vector (A^μ) part using Eq.3.34 and Eq.3.35 given as

$$\begin{aligned} \mathcal{O}^{\mu\alpha} = &\left[\frac{C_3^V}{M}(g^{\mu\alpha}\,\not{q}-q^\mu\gamma^\alpha)+\frac{C_4^V}{M^2}(g^{\mu\alpha}q\cdot P-q^\mu P^\alpha)+\frac{C_5^V}{M^2}(g^{\mu\alpha}q\cdot p-q^\mu p^\alpha)\right]\gamma^5 \\ &+\left[\frac{C_3^A}{M}(g^{\mu\alpha}\,\not{q}-q^\mu\gamma^\alpha)+\frac{C_4^A}{M^2}(g^{\mu\alpha}q\cdot P-q^\mu P^\alpha)+C_5^A g^{\mu\alpha}+\frac{C_6^V}{M^2}q^\mu q^\alpha\right] \end{aligned} \tag{3.56}$$

with the Rarita Schwinger spin-$\frac{3}{2}$ projection operator $\mathcal{P}^{3/2}_{\alpha\beta}(P)$ (see Appendix J [266]

$$\mathcal{P}^{3/2}_{\alpha\beta}(P) = -\frac{\not{P}+M_\Delta}{2M_\Delta}\left[g_{\alpha\beta}-\frac{1}{3}\gamma_\alpha\gamma_\beta-\frac{2P_\alpha P_\beta}{3M_\Delta^2}+\frac{P_\alpha\gamma_\beta-P_\beta\gamma_\alpha}{3M_\Delta}\right] \tag{3.57}$$

In order to take into account the width of the Δ, we must replace in Eq.3.53

$$\delta(E_p+q_0-E_\Delta) \to -\frac{1}{\pi}\,\mathrm{Im}\left[\frac{1}{E_p+q_0-E_\Delta+i\frac{\Gamma}{2}}\right] \tag{3.58}$$

where we have used the relation

$$\frac{1}{x-x_0\mp i\epsilon} = P\frac{1}{x-x_0}\pm i\pi\delta(x-x_0) \tag{3.59}$$

and then

$$\frac{M_\Delta}{E_\Delta}\,\delta(p^0_\Delta-E_\Delta) \;\to\; -\frac{1}{\pi}\,\mathrm{Im}\left[\frac{1}{W-M_\Delta+i\frac{1}{2}\Gamma(W)}\right] \to \frac{1}{\pi}\left[\frac{\frac{\Gamma(W)}{2}}{(W-M_\Delta)^2+\frac{\Gamma^2(W)}{4}}\right] \tag{3.60}$$

using

$$\delta(W - M_\Delta) = \frac{1}{p_\Delta^0/W}\delta(p_\Delta^0 - E_\Delta) \simeq \frac{M_\Delta}{E_\Delta}\delta(p_\Delta^0 - E_\Delta) \tag{3.61}$$

where $W = \sqrt{p'^2} = \sqrt{{p_\Delta^0}^2 - \vec{p}_\Delta^2}$ is the invariant mass of Δ and $\Gamma(W)$ is the rest width of Δ. Using Eq.3.60 in Eq.3.53, we get

$$\frac{d^2\sigma}{dE_{k'}d\Omega_{k'}} = \frac{1}{64\pi^3}\frac{1}{MM_\Delta}\frac{|\mathbf{k}'|}{E_k}\left[\frac{\frac{\Gamma(W)}{2}}{(W - M_\Delta)^2 + \frac{\Gamma^2(W)}{4}}\right]\left\{\frac{G^2\cos^2\theta_C}{2}\, L_{\mu\nu}J^{\mu\nu}\right\} \tag{3.62}$$

The Δ decay width $\Gamma(W)$ is taken to be the energy dependent P-wave decay width for the Δ resonance. Around the decay threshold the energy dependence of the decay width is determined by the orbital angular momentum [267], [268]:

$$\Gamma(W) \sim |\mathbf{k}_\pi^{cm}|^{2l+1} \tag{3.63}$$

where $|\mathbf{k}_\pi^{cm}|$ is the pion momentum in the rest frame of the resonance. The Δ resonance has the quantum numbers P_{33} ($I = \frac{3}{2}$, $J = \frac{3}{2}$), therefore, $\Gamma(W) \sim |\mathbf{k}_\pi^{cm}|^3$ is required i.e. a P-wave width. In earlier analysis of Δ production from deuteron, S-wave decay width for Δ resonance has been used by many authors [124], [243]-[245]. But most new calculations use the correct P-wave width [133], [135]-[139]. Therefore, it is more appropriate to use a P-wave decay width for the Δ resonance given as

$$\Gamma(W) = \frac{1}{6\pi}\left(\frac{f_{\pi N\Delta}}{m_\pi}\right)^2\frac{M}{W}|\mathbf{k}_\pi^{cm}|^3\Theta(W - M - m_\pi) \tag{3.64}$$

where

$$|\mathbf{k}_\pi^{cm}| = \frac{\sqrt{(W^2 - m_\pi^2 - M^2)^2 - 4m_\pi^2M^2}}{2W} \tag{3.65}$$

The step function Θ denotes the fact that the width is zero for the invariant masses below the Nπ threshold, W and M are the Δ invariant mass and nucleon mass respectively, and $|\mathbf{k}_\pi^{cm}|$ the pion momentum in the rest frame of the resonance.

==========*******==========

Chapter 4

Weak Pion Production From Nuclei

4.1 Introduction

The pion production processes described in Eqs.3.1 and 3.2 take place on free nucleons. When these processes take place in nuclei then, there are two types of processes, known as coherent pion production and incoherent pion production depending upon the excitation energy of the residual nucleus. In a nucleus, the target nucleus can stay in the ground state leading to the coherent production of pions or can be excited and/or broken up leading to the incoherent production of pions.

It is well known that in the energy region of low and intermediate neutrino energies, the dominant mechanism of single pion production from the nucleon arises through the excitation of a baryon resonance which then decays into a nucleon and a pion. Similarly, this is expected to be true in the case of nuclei also where baryon resonance is produced within the nucleus and it propagates in the nuclear medium before it decays. The excitation of the Δ is the dominant resonance excitation at these energies contributing to one pion production and many authors have used the delta dominance model to calculate the one pion production.

In nuclear pion production processes the modification of the elementary production operator inside the nuclear medium should be properly taken into account, since the Δ produced inside the nuclear medium can decay through pionic decay i.e., $\Delta N \rightarrow NN\pi$ or non-mesonic decay through $\Delta N \rightarrow NN$, which is not available in case of free nucleon. Furthermore, the nuclear structure, the final state interaction of the outgoing pions with the nucleus, the Fermi motion of the nucleons and Pauli blocking effect should be kept in mind while doing such calculations. Various theoretical models aim at a unified description of neutrino and pion interaction in the region of Δ-hole excitation, where intermediate Δ-isobar can decay independent of the production mechanism, Δ modification in the nuclear medium has been incorporated in one way or other. It has been found that the propagation of Δ in the nuclear medium not only

affects the pion propagation through the nucleus but it also modifies the transition amplitude. But there are discrepancy between different theories. Hence the precise theoretical calculations are required.

Experimentally, neutrinos and antineutrinos induced pion production reactions from nuclei were studied at CERN, ANL, BNL and SKAT collaboration [269]-[286], and have been analyzed to obtain informations on various N-Δ transition form factors. These experiments done with the bubble chambers filled with heavy nuclear targets like propane and freon have low statistics and their analysis have uncertainties related to nuclear corrections. However, with the availability of the new neutrino beams in intermediate energies at K2K [52]-[60] and MiniBooNE [61]-[65], it is possible that various N*-N weak transition form factors are determined for low lying nuclear resonances like $\Delta(1232)$, N*(1440), N*(1535), etc. There is a considerable activity in this field, specially, in the determination of electromagnetic transition form factors using the photo and electroproduction data from MAINZ, BONN and TJNAF laboratories [287]. It is desirable that such attempts be extended to the determination of weak transition form factors also.

These days, the weak pion production processes at intermediate energies have become very important in the analysis of the neutrino oscillation experiments with atmospheric and accelerator neutrinos. The weak charged current as well as the neutral current weak pion production processes contribute a major source of uncertainty in the identification of quasielastic electron and muon events. In particular, the neutral current π^0 production contributes to the background of $e^{\pm}$ production while $\pi^{\pm}$ production contributes to the background of $\mu^{\pm}$ production. This is because both the particles i.e. π^0 and $e^{\pm}$ are identified through the detection of photons and $\pi^{\pm}$ and $\mu^{\pm}$ are identified through single track events in the detection of neutrino oscillation experiments. Moreover, the neutral current π^0 production plays very important role in distinguishing between the two oscillation mechanisms $\nu_\mu \rightarrow \nu_\tau$ and $\nu_\mu \rightarrow \nu_s$ [288].

The neutrino oscillation experiments are generally performed with detectors which use materials with nuclei like ^{12}C, ^{16}O, ^{56}Fe etc. as targets. Even though most of these experiments were done in nuclei, no serious attempts were made to study nuclear effects and their possible influence on the weak pion production cross section, or in the determination of electroweak N-Δ transition form factors in the region of Δ dominance. Recently a great interest in the study of these processes has been generated by the ongoing neutrino oscillation experiments being performed at the intermediate neutrino energies by the MiniBooNE and the K2K collaborations using ^{12}C and ^{16}O as the nuclear targets in the detector [52]-[65]. These experiments are designed to search for neutrino oscillations in ν_μ disappearance and ν_e appearance channels. In these experiments, the ν_μ-spectrum is determined by the observed energy spectrum of muons which are predominantly produced in forward direction through the charged current quasielastic reactions induced by ν_μ. In this kinematic region the major background to these events come from the non quasielastic events in which pions are produced through coherent and incoherent processes induced by charged and neutral weak currents in neutrino nucleus interactions. The neutral current induced π^0 production is of particular importance as it constitutes a major

background to the electron signal in ν_e appearance channel. The analysis of neutrino oscillation experiments, therefore, requires a better understanding of pion production processes in neutrino nucleus interaction and many experiments are being done to study neutrino induced coherent and incoherent production of pions from nuclei. Furthermore, many high precision neutrino experiments in the intermediate energy region of 1-3 GeV using neutrino beams from neutrino factories, superbeams and β-beams have been proposed [66]-[76], [289]-[301]. These experiments are planned to be performed with nuclear targets like ^{12}C, ^{16}O, ^{40}Ar, ^{56}Fe, etc. In order to analyze these neutrino oscillation experiments the study of pion production from the nuclei are very important. It is, therefore, required that the various nuclear effects in the weak pion production processes induced by neutrinos be studied in the energy region of these experiments.

Theoretically, there exist calculations in past where various nuclear effects in the weak pion production processes induced by neutrinos in nuclei in the intermediate energy region have been estimated [134], [135], [140]-[142]. In view of the recent data on some weak pion production processes already available [61]-[62] and new data to be expected soon from MiniBooNE and K2K collaborations, the subject has attracted some attention and many calculations have been made for these processes [136], [143]-[146], [263]. However, neutrino generators like NUANCE and NEUGEN which are used to model low energy neutrino nucleus interactions to analyze the neutrino oscillation experiments, beside Δ resonance, include higher resonance states as well [1]-[2]. However, these generators do not use any nuclear effects in their resonance production model for the single pion production and take in some adhoc way the pion absorption effects. For example in the NUANCE Monte Carlo event generator a 10% suppression is considered for $I=\frac{3}{2}$ channel processes for pion absorption [1]. These nuclear effects are quite important in the energy region of 1 GeV, corresponding to K2K and MiniBooNE experiments. This can be studied in a Δ-dominance model, using modification of Δ properties which has been extensively studied in the various electromagnetic and strong interaction processes [161]-[163].

In this chapter, we have studied the neutrino induced coherent and incoherent weak production of leptons and pions from nuclei assuming Δ-dominance. The effect of Pauli blocking, Fermi motion of the nucleon and the renormalization of Δ properties in a nuclear medium are taken into account in a local density approximation (LDA). The effect of final state interaction of pions with the residual nucleus has also been treated separately for the coherent and incoherent processes.

4.2 Coherent Production of Pions

4.2.1 Introduction

Coherent pion production processes induced by neutrinos and antineutrinos on nuclei via. charged or neutral currents, were the subject of intense studies in the last few years. The

coherent pion production process

$$\nu_l\ (\bar{\nu}_l)\ +\ \mathcal{N}\ \rightarrow\ l^{\pm}\ (\bar{\nu}_l)\ +\ \mathcal{N}\ +\ \pi^{\pm}(\pi^0) \tag{4.1}$$

can be qualitatively interpreted as the emission of a virtual pion from the projectile neutrino followed by the elastic scattering of this off-shell pion with the target nucleus, till it becomes a real pion with the target nucleus left in the ground state. In the coherent interactions on nuclei the overall scattering amplitude is given as the sum of the constructive interferences between the scattering amplitudes of the incident wave on the various nucleons in the target nucleus, which implies that all the nucleons in the nucleus must react in phase in order to have the maximum constructive interferences for enhanced cross section. Thus, the distortion of the incident wave must be small enough, which means, the momentum transferred ($|\mathbf{k}|$) to any nucleons in a nucleus of radius (R) must thus be small enough so that the condition

$$|\mathbf{k}|R\ <\ 1. \quad (\hbar\ =\ c\ =\ 1.) \tag{4.2}$$

gets fulfilled, implying that the nucleons remains bound in the nucleus.

Coherent reactions are also characterized by the fact that the target nucleus recoils as a whole without breakup with very little recoil energy, since the effect of the incident wave is approximately same on all the nucleons, otherwise, the coherence would disappear. In the coherent interactions the enhanced cross section can occur due to coherence effect as long as no charge, spin, isospin or any other additive quantum number is transferred to the target nucleus. If any of these are forbidden, then this would single out a specific nucleon, and destroy the coherence. For example, the total isospin (I) of the exchanged state must be zero. Indeed, the operator I_3 (third component of the isospin) induced amplitude for protons and neutrons would have opposite sign, resulting in a small effect on nuclei with total isospin I=0. As in the case of nuclei with a neutron number slightly more than the proton number, process with isospin exchanged are suppresses in compare with zero isospin exchange. Similar, is the case if the nucleus has spin, spin term in the coherent amplitude are suppressed in comparison to total spin zero nuclei. Also, the emission of scattered particles in forward direction, which is generally the case, implies that the coherent interactions conserve helicity.

Coherent production of pion induced by neutrinos and antineutrinos on nuclei have been reported in four possible charged as well as neutral current channels:

$$\left.\begin{array}{l}\nu_\mu\ +\ \mathcal{N}\ \rightarrow\ \mu^-\ +\ \mathcal{N}\ +\ \pi^+\\ \bar{\nu}_\mu\ +\ \mathcal{N}\ \rightarrow\ \mu^+\ +\ \mathcal{N}\ +\ \pi^-\end{array}\right\}\ \text{(Charged Current)} \tag{4.3}$$

$$\left.\begin{array}{l}\nu_\mu\ +\ \mathcal{N}\ \rightarrow\ \nu_\mu\ +\ \mathcal{N}\ +\ \pi^0\\ \bar{\nu}_\mu\ +\ \mathcal{N}\ \rightarrow\ \bar{\nu}_\mu\ +\ \mathcal{N}\ +\ \pi^0\end{array}\right\}\ \text{(Neutral Current)} \tag{4.4}$$

These processes could be studied in detail and with relatively large statistics and small background, as the kinematical situation in coherent processes are different from other interaction processes and also due to the small pion mass and the simple geometry. Experimentally,

the coherent charged current as well as neutral current pion production induced by neutrinos and antineutrinos have been observed on various nuclei using different techniques like bubble chambers and counters [274]-[286]. The events are characterized by the small four momentum transfer to the nucleus and the exponential fall of the cross section with $|t|$. The latter can not be measured directly, since the nucleus remains undetected experimentally, but it can be estimated from the measurement of the muon and meson momenta, neglecting the recoil of the nucleus, one finds [302]-[303]

$$|t| = \left[\sum_i E_i - k_i^L\right]^2 + \left[\sum_i k_i^T\right]^2 \qquad i = \mu,\ \pi \qquad (4.5)$$

where E_i, k_i^L and k_i^T are the energy, the longitudinal and the transverse momenta of the muon and pion relative to the incident neutrino direction, both of which are detectable in the experiment. In addition to $|t|$ dependence, coherent scattering also depends on the square of the four momentum (Q^2) transferred between the leptons. Experimentally it has also been established that the coherent scattering cross section, peaks at low $Q^2 \leq 0.1$ GeV^2 and the cross section rises as a function of neutrino energy which becomes logarithmic at large neutrino energies.

In this sense the neutrino induced coherent pion production reaction is an advantage over other existing reactions, which can enrich our understanding of the nuclear excitation mechanism, and it allows the study of the longitudinal axial current for very small Q^2 values, providing the most detailed test of the PCAC hypothesis at high energy. A good knowledge of coherent pion production induced by neutrinos and antineutrinos is also important for practical purposes, especially to understand the background to the quasielastic lepton production in forward direction in the analysis of neutrino oscillation experiments with atmospheric neutrinos and accelerator neutrino beams in intermediate energies.

Coherent pion production in the nuclei is considered to be an independent test of the Δ-hole model, also to investigate the properties of the pion-nucleus interaction and to obtain the information about the behavior of pion in nuclear medium. On the other hand, since the description of the nuclear ground state is well under control, the coherent process is then suitable for analyzing the medium effects in the production and propagation of Δ resonance.

The coherent production of charged pions from ^{12}C has been recently studied by the K2K collaboration [57]. The coherent production of neutral pions has been studied by the K2K collaboration for ^{16}O [55], [60] and by the MiniBooNE collaboration for ^{12}C [61]-[65]. In the intermediate energy region, recently, an upper limit on the contribution of charged current coherent pion production by ν_μ with average neutrino energy $\langle E_\nu \rangle$=1.3 GeV has been reported in a long base line neutrino oscillation experiment KEK to K2K [57]. This limit has been found out to be far below the theoretical expectations. At very high energies, the coherent pion production has been studied theoretically using Adler's PCAC theorem to predict the total cross section for neutrino reaction for forward production and extrapolating the results to non zero Q^2 [302]-[305], which overestimate the experimental cross sections at low energies.

Recently these calculations have been updated by Paschos, Kartavtsev and Gounaris [306] using a generalized PCAC. In these calculations the nuclear medium effects are included only through the final state interaction of the outgoing pions with the nucleus using a model of pion nucleus scattering. A theoretical framework for treating the nuclear medium effects in the neutrino production of coherent pions using some model of nuclear structure has been recently discussed by some groups [141], [142], [307] but no definite predictions are made for the kinematics of the neutrino oscillation experiments of present interest.

In the following sections we discuss the calculation of the neutrino induced production of coherent pion from nuclei at intermediate neutrino energy in charged current as well as neutral current interactions. We apply the relativistic approach to calculate the matrix elements and differential cross sections by using the effective Lagrangians defined in chapter-4. The nuclear medium effects are taken into account in the weak production process as well as in the final state interaction of the outgoing pions with the nucleus. The calculation uses the local density approximation to the Δ-hole model which has been used earlier to study photo and electro production of pions from nuclei [163], [164]. The final state interaction of pions has been treated in eikonal approximation with the pion optical potential described in terms of the self energy of a pion in a nuclear medium calculated in this model [161]-[162].

4.2.2 Matrix Elements

It is well known that in the kinematical region between threshold and few hundred MeV excitation energy relevant for the production of pions, the coherent pion production induced by neutrinos and antineutrinos is dominated Δ-isobar excitation in the intermediate energy. An additional contribution comes from the production of higher resonances. In literature the production of higher mass resonances is covered by some authors. The model of Fogli and Nardulli [126] has been extended by Paschos et al. [146] where they included, besides the Δ, the resonances N*(1440) and N*(1535). The model of Rein and Sehgal [9] includes all resonances up to an invariant mass of 2 GeV using old quark model calculations. Finally, the N*(1440) was studied by Alvarez-Ruso et al. [137]. All these studies show that at intermediate energies, the Δ resonance is dominant contributing part than other resonance with the Δ being well separated from other resonances. In addition, the theoretical description and the form factors for higher resonances contain much more uncertainties than for the Δ resonance.

Therefore, in this energy region of neutrino of our interest, we have calculated the charged current and neutral current induced coherent pion production from nuclei including particle-hole (p-h) and Δ-h nuclear excitations with the relativistic description of Δ-resonance. As shown in Fig.4.1, the incoming neutrino interacts weakly with the nucleus exciting an intermediate Δ-h state. The vertex of the weak interaction contains vector and axial vector parts while the $\pi N\Delta$ vertex, on the other hand, involves only the axial vector part contracted with a pion four momentum k_π. We write the relativistic expression of matrix element for delta pole term in s-channel and u-channel processes by using the effective form of the $\Delta N\pi$ interactions vertices by taking the relativistic covariant form of the Δ propagator of the Rarita-Schwinger spinor

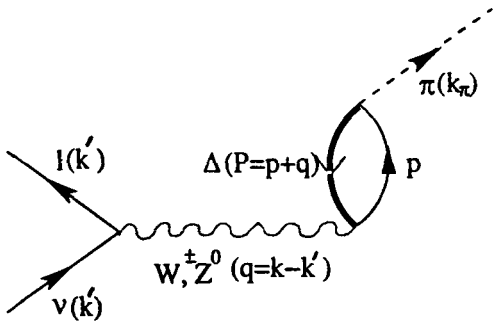

Figure 4.1: Scattering diagram considered for coherent pion production through Δ-h excitations. In the charged current reaction, k' is the four momentum of the muon or electron, and q is the four momentum of the $W^{\pm}$ boson. In the neutral current reaction, k' is the momentum of the scattered neutrino and q is the momentum of the exchanged Z^0.

for a $T = \frac{3}{2}$ particle of the form [308], [309]

$$u_s^{\mu}(P) = \sqrt{\frac{E_\Delta + M_\Delta}{2M_\Delta}}\, L^{(1)}(P)_\nu^\mu \begin{pmatrix} \mathbf{I} \\ \frac{\sigma.\mathbf{P}}{E_\Delta + M_\Delta} \end{pmatrix} S_{\Delta N}^{\nu\dagger}\, \chi_s \tag{4.6}$$

where $L^{(1)}(P)_\nu^\mu$ is the Lorentz boost operator for spin-1 particle, χ_s is the four components Pauli spinor for spin-$\frac{3}{2}$ particle and $S_{\Delta N}^{\nu\dagger}$ is the four components of the transition spin operator. The Rarita-Schwinger spinors obey a completeness relation:

$$\sum_s u_s^{\mu}(P)\bar{u}_s^{\nu}(P) = -\frac{\not{P} + M_\Delta}{2M_\Delta}\left(g^{\mu\nu} - \frac{1}{3}\gamma^\mu\gamma^\nu - \frac{2P^\mu P^\nu}{3M_\Delta^2} + \frac{P^\mu\gamma^\nu - \gamma^\mu P^\nu}{3M_\Delta}\right) \tag{4.7}$$

In general spin-$\frac{3}{2}$ Projection operator for the Δ is defined as [266](Appendix-E):

$$\Lambda^{\mu\nu} = \sum_{-\frac{3}{2}}^{\frac{3}{2}} u_s^{\mu}(P)\bar{u}_s^{\nu}(P) = -\frac{\not{P} + M_\Delta}{2M_\Delta}\left(g^{\mu\nu} - \frac{1}{3}\gamma^\mu\gamma^\nu - \frac{2P^\mu P^\nu}{3M_\Delta^2} + \frac{P^\mu\gamma^\nu - \gamma^\mu P^\nu}{3M_\Delta}\right) \tag{4.8}$$

and on mass shell state with $P^2 = M_\Delta$ the Δ-propagator is written as

$$\Delta^{\mu\nu} = \frac{2M_\Delta\, \Lambda^{\mu\nu}(P)}{P^2 - M_\Delta^2} \tag{4.9}$$

Introducing the Δ width this modifies to

$$\Delta^{\mu\nu} = \frac{\not{P} + M_\Delta}{P^2 - M_\Delta^2 + i\Gamma M_\Delta}\left[g^{\mu\nu} - \frac{1}{3}\gamma^\mu\gamma^\nu - \frac{2}{3M_\Delta^2}P^\mu P^\nu + \frac{(P^\mu\gamma^\nu - \gamma^\mu P^\nu)}{3M_\Delta}\right] \tag{4.10}$$

where P and M_Δ are the four momenta and mass of the delta, and Γ is the energy dependent P-wave decay width for the Δ resonance given in Eq.3.64. We use

$$\mathcal{L}^{int}_{\pi N\Delta} = \frac{f_{\pi N\Delta}}{m_\pi}\,\bar{\Psi}_\mu \partial^\mu \phi \Psi + \text{h.c.} \tag{4.11}$$

with $\frac{f^2_{\pi N\Delta}}{4\pi}$=0.36 to describe the on shell πNΔ interaction [267]-[268] and the standard model of weak interactions to describe the Δ-N isovector charge and neutral transition currents corresponding to $W^\pm$ and Z^0 exchanges. While we use the on-shell form of the Δ propagator, the off-shell effects at πNΔ vertex has been studied using

$$f_{\pi N\Delta}(P^2) = \frac{\Lambda^4}{\Lambda^4 + (P^2 - M^2_\Delta)^2}\, f_{\pi N\Delta} \tag{4.12}$$

with Λ=1.0 GeV [267]-[268].

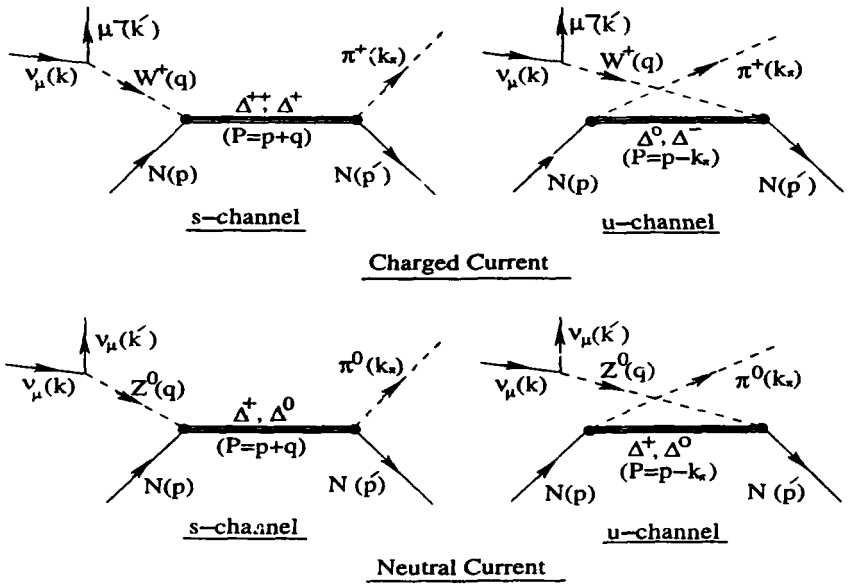

Figure 4.2: Feynman diagrams considered for neutrino induced weak coherent pion production for Δ-resonance.

The amplitude of the reaction (Eq.4.1) for charged current interaction is calculated using the Feynman diagram shown in Fig.4.2, and in general written as

$$\mathcal{A} = \frac{G}{\sqrt{2}} \cos\theta_C\, l^\mu\, \mathcal{J}_\mu\, \mathcal{F}(\mathbf{q} - \mathbf{k}_\pi) \tag{4.13}$$

where G is the Fermi coupling constant of weak interactions $G = 1.166\times10^{-5}\text{GeV}^2$ and $\mathcal{F}(\mathbf{q} - \mathbf{k}_\pi)$ is the nuclear form factor modulated by the isospin factors, will be discussed later.

l^μ is the leptonic current given in Eq.3.18 and the hadronic current $\mathcal{J}_\mu = (J^s_\mu + J^u_\mu)$ is the sum of direct (s-channel) and crossed (u-channel) diagram, each has been separated into its vector (V^μ) and axial vector part (A^μ) as $J^s_\mu = (V^s_\mu + A^s_\mu)$ and $J^u_\mu = (V^u_\mu + A^u_\mu)$, given as

$$\mathcal{J}_\mu = J^s_\mu + J^u_\mu \tag{4.14}$$

$$= \sqrt{3}\,\frac{f_{\pi N\Delta}}{m_\pi} \sum_s \bar{\Psi}^s(p') \left[k_{\pi\sigma}\, \Delta^{\sigma\lambda}\, \mathcal{O}_{\lambda\mu} + k_{\pi\sigma}\, \mathcal{O}^{\sigma\lambda}\, \Delta_{\lambda\mu}\right] \Psi^s(p) \tag{4.15}$$

where $\Delta^{\sigma\lambda}$ or $\Delta_{\lambda\mu}$ is the relativistic Δ propagator modified by a phenomenological decay width given as in Eq.4.10 and $\mathcal{O}^{\sigma\lambda}$ or $\mathcal{O}_{\lambda\mu}$ is the weak N-Δ transition vertex given as the sum of vector(V^μ) and axial part (A^μ) in Eq.3.56. The first term in the bracket (Eq.4.15) is for the direct diagram (s-channel) and the second term for the crossed (u-channel) diagram shown in Fig.4.2.

Similarly in the neutral current case the amplitude for the direct (s-channel) and crossed (u-channel) Δ-resonance term is written with lepton mass replaced by zero and $\cos\theta_C$ by one along with the isospin factors $\xi_V^{I=1}$ and $\xi_A^{I=1}$ as defined in Eq.3.15 with vector and axial part respectively. The weak N-Δ transition vertex in case of neutral current is written as:

$$\mathcal{O}^{\lambda\mu}_{NC} = \xi_V^{I=1}\left[\frac{C_3^V}{M}(g^{\lambda\mu}\not{q} - q^\lambda\gamma^\mu) + \frac{C_4^V}{M^2}(g^{\lambda\mu}q\cdot P - q^\lambda P^\mu) + \frac{C_5^V}{M^2}(g^{\lambda\mu}q\cdot p - q^\lambda p^\mu)\right]\gamma^5$$
$$+ \xi_A^{I=1}\left[\frac{C_3^A}{M}(g^{\lambda\mu}\not{q} - q^\lambda\gamma^\mu) + \frac{C_4^A}{M^2}(g^{\lambda\mu}q\cdot P - q^\lambda P^\mu) + C_5^A g^{\lambda\mu} + \frac{C_6^V}{M^2}q^\lambda q^\mu\right] \tag{4.16}$$

After squaring the amplitude $\mathcal{A}$ and taking the average over the initial spin states and the sum over the final states, one has

$$|\bar{\mathcal{A}}|^2 = \frac{G^2}{2}\cos^2\theta_C\, \mathcal{L}^{\mu\nu}\mathcal{J}_{\mu\nu}\, |\mathcal{F}(\mathbf{q} - \mathbf{k}_\pi)|^2 \tag{4.17}$$

In case of neutral current interaction $\cos^2\theta_C$ is taken to be unity. Expressions for the leptonic tensor $\mathcal{L}^{\mu\nu}$ and hadronic tensor $\mathcal{J}_{\mu\nu}$ are given in Eq.F.3 and Eq.F.4, respectively (Appendix-F). The hadronic tensor $\mathcal{J}_{\mu\nu}$ contains the tensors $V_{\mu\nu}$, $A_{\mu\nu}$ and $W_{\mu\nu}$ corresponds, respectively, to the contributions of the vector current, of the axial current, and of their interference in s-channel as well as in u-channel diagrams.

We have calculated the amplitude square $|\mathcal{A}|^2$ for the coherent charged current and neutral current processes for the direct and crossed Δ diagrams. The square of the amplitude for the coherent charged current induced pion production from a nucleus is obtained by summing over all the occupied nucleons in the amplitude and is written as (Appendix-F):

$$\bar{\sum}\sum |\mathcal{A}_\Delta|^2_{CC} = \bar{\sum}\sum \left(|\mathcal{A}^s_\Delta|^2 + |\mathcal{A}^u_\Delta|^2 + |\mathcal{A}^s_\Delta \mathcal{A}^{u\,\dagger}_\Delta| + |\mathcal{A}^u_\Delta \mathcal{A}^{s\,\dagger}_\Delta|\right) \tag{4.18}$$

The matrix element square in the neutral current process for Δ-direct (s-channel) and crossed (u-channel) diagrams are directly related with the charged current matrix elements through the isospin factors given in Eq.3.15 (Appendix-F).

The nuclear form factor $\mathcal{F}(\mathbf{q}-\mathbf{k}_\pi)$ in Eq.4.13 is given as

$$\mathcal{F}(\mathbf{q}-\mathbf{k}_\pi) = \int d^3\mathbf{r}\ \rho(\mathbf{r})\ e^{-i(\mathbf{q}-\mathbf{k}_\pi).\mathbf{r}} \tag{4.19}$$

with $\rho(\mathbf{r})$ as the nuclear matter density as a function of nucleon relative coordinates. For production from nuclear targets, it is the linear combination of proton and neutron densities incorporating the isospin factors for charged and neutral pion production from proton and neutron targets corresponding to $W^{\pm}$ and Z^0 exchange diagrams in s-channel and u-channel. It is written as

$$\mathcal{F}(\mathbf{q}-\mathbf{k}_\pi) = \int d^3\mathbf{r}\,[a\rho_p(\mathbf{r}) + b\rho_n(\mathbf{r})]\,e^{-i(\mathbf{q}-\mathbf{k}_\pi).\mathbf{r}} \tag{4.20}$$

where a and b are the numerical factors and depends upon the charge state of pion produced in charged or neutral current process. For example, inside the nucleus the production of neutral pion takes place from both proton and neutron targets through the reaction $\nu + p \rightarrow \Delta^+ \rightarrow p+\pi^0$ and $\nu+n \rightarrow \Delta^0 \rightarrow n+\pi^0$. The isospin consideration give a factor of $\frac{2}{3}$ for both protons and neutrons at the respective vertices. Therefore, the density $\rho(\mathbf{r})$ in the nuclei should be replaced by $\frac{2}{3}[\rho_p(\mathbf{r}) + \rho_n(\mathbf{r})]$. We have considered the proper isospin factor for the different vertices of the Feynman diagrams Fig.4.2 considered. In case of neutrino induced charged current reactions the factors are as follows

$$\begin{aligned} a &= 1,\ b = \frac{1}{3} \quad \text{for s-channel} \\ a &= \frac{1}{6},\ b = \frac{1}{2} \quad \text{for u-channel} \end{aligned} \tag{4.21}$$

Similarly, in case of neutral current we have the factors as

$$\begin{aligned} a &= \frac{2}{3},\ b = \frac{2}{3} \quad \text{for s-channel} \\ a &= \frac{1}{3},\ b = \frac{1}{3} \quad \text{for u-channel} \end{aligned} \tag{4.22}$$

In case of antineutrino reactions the role of $\rho_p(\mathbf{r})$ and $\rho_n(\mathbf{r})$ are interchanged. For our numerical calculation we use the proton density as $\rho_p(\mathbf{r}) = \frac{Z}{A}\rho(\mathbf{r})$ and the neutron density as $\rho_n(\mathbf{r}) = \frac{A-Z}{A}\rho(\mathbf{r})$, where for the nuclear density profile, we adopted the modified harmonic oscillator (M.H.O) model in case of ^{12}C nuclei and the three parameter Fermi (3pF) model for ^{16}O nuclei, normalized to the number of nucleons i.e. $\int d^3(\mathbf{r})\ \rho(\mathbf{r}) = A$ and are given as [215]

$$\rho(\mathbf{r})_{H.O} = \rho_0 \left[1+\alpha\left(\frac{r}{a}\right)^2\right] \exp\left[-\left(\frac{r}{a}\right)^2\right] \tag{4.23}$$

$$\rho(\mathbf{r})_{3pF} = \rho_0 \left[1+\omega\left(\frac{r^2}{c^2}\right)\right] / \left[1+\exp\left(\frac{r-c}{z}\right)\right] \tag{4.24}$$

with α=1.150 fm, a=1.672 fm, ω=-0.051, c=2.608 fm and z=0.513 fm.

4.2.3 Cross Section

In general the differential cross section for a pion produced in charged current weak production process induced by neutrino (Eq.4.1) can be written as

$$d^9\sigma = \frac{(2\pi)^4\delta^4(q+p-p'-k_\pi)}{4\sqrt{(k\cdot k')^2-m_l^2M^2}}\frac{d^3\mathbf{k}'}{(2\pi)^3 2E_{l'}}\frac{d^3\mathbf{p}'}{(2\pi)^3 2E_{p'}}\frac{d^3\mathbf{k}_\pi}{(2\pi)^3 2E_\pi}\Pi_f(2m_f)\bar{\sum}\sum|\mathcal{A}|^2 \tag{4.25}$$

On integrating over the final nucleon momentum and taking a factor of $2M^2$ outside from the matrix element square $|\mathcal{A}|^2$ the differential cross section reduces to

$$d^6\sigma = \frac{1}{(2\pi)^5}\frac{M}{E_l}\frac{1}{2E_{p'}}\frac{d^3\mathbf{k}'}{2E_l'}\frac{d^3\mathbf{k}_\pi}{2E_\pi}\delta^0(q_0+p_0-p_0'-k_\pi^0)\bar{\sum}\sum|\mathcal{A}|^2 \tag{4.26}$$

Using the following relations

$$d^3\mathbf{k}' = |\mathbf{k}'|^2\, d|\mathbf{k}|\, d\Omega_{ll'} = E_{l'}\,|\mathbf{k}'|\, dE_{l'}\, d\Omega_{ll'} \tag{4.27}$$

$$d^3\mathbf{k}_\pi = |\mathbf{k}_\pi|^2\, d|\mathbf{k}_\pi|\, d\Omega_{\pi q} = E_\pi\,|\mathbf{k}_\pi|\, dE_\pi\, d\Omega_{\pi q} \tag{4.28}$$

we get

$$\frac{d^5\sigma}{dE_\pi\, d\Omega_\pi\, d\Omega_{ll'}} = \frac{1}{8}\frac{1}{(2\pi)^5}\frac{M}{E_l}\frac{|\mathbf{k}_\pi|}{E_{p'}}|\mathbf{k}'|\, dE_{l'}\,\delta^0(M+q_0-E_{p'}-E_\pi)\bar{\sum}\sum|\mathcal{A}|^2 \tag{4.29}$$

Now doing the energy integration over $dE_{l'}$ i.e. $\int dE_{l'}\,\delta^0(M+q_0-E_{p'}-E_\pi)$ and using the property of standard delta function defined as

$$\delta(f(x)) = \sum_i \delta(x-x_i)/\left|\frac{\partial f}{\partial x}\right|_{x=x_i} \tag{4.30}$$

the differential cross section comes out to be (Appendix-G)

$$\left[\frac{d^5\sigma}{dE_\pi d\Omega_\pi d\Omega_{ll'}}\right]_{CC} = \frac{1}{8}\frac{1}{(2\pi)^5}\frac{M}{E_l}|\,\mathbf{k}'|\,|\,\mathbf{k}_\pi|\,\frac{1}{\mathcal{R}}\bar{\sum}\sum|\mathcal{A}|^2 \tag{4.31}$$

and

$$\left[\frac{d^5\sigma}{dE_\pi d\Omega_\pi dQ^2}\right]_{CC} = \frac{\pi}{8}\frac{1}{(2\pi)^5}\frac{M}{E_l^2}\,|\,\mathbf{k}_\pi|\,\frac{1}{\mathcal{R}}\bar{\sum}\sum|\mathcal{A}|^2 \tag{4.32}$$

where

$$\mathcal{R} = \left[(E_{p'}+E_{l'}-E_l\cos\theta_{ll'})-\frac{|\mathbf{k}_\pi|}{|\mathbf{q}|}(E_{l'}-E_l\cos\theta_{ll'})\cos\theta_{\pi q}\right] \tag{4.33}$$

is a kinematical factor incorporating the recoil effects, which is very close to unity for low $Q^2(=-q^2)$, relevant for the coherent reactions. We have also calculated the differential cross section for the charged current weak pion production where the recoil of the nucleus has been neglected i.e. $E_{p'} = M$ and keeping in mind that in the coherent reaction the energy transfer to the nucleus is directly taken away by the emitted pion i.e. $q_0 = E_l - E_{l'} = E_\pi$ and is found to be in the following form

$$\left[\frac{d^5\sigma}{dE_\pi d\Omega_\pi d\Omega_{ll'}}\right]_{CC} = \frac{1}{8}\frac{1}{(2\pi)^5}\frac{|\mathbf{k}'|}{E_l}|\mathbf{k}_\pi|\bar{\sum}\sum|\mathcal{A}|^2 \tag{4.34}$$

We find that considering the recoil of the nucleus gives less than $(3-4\%)$ correction in the energy region of our interest. In the charged current weak reaction we could also measure the energy and the momentum of the muons. It also allows an approximative separation of the coherent cross section from the non-coherent background. We can measure the differential cross section for the charged lepton production, and is found to be

$$\left[\frac{d^5\sigma}{d\Omega_\pi d\Omega_{ll'} dE_{l'}}\right]_{CC} = \frac{1}{8}\frac{1}{(2\pi)^5}\frac{|\mathbf{k}'||\mathbf{k}_\pi|}{E_l}\mathcal{R}\bar{\sum}\sum|\mathcal{A}|^2 \tag{4.35}$$

where

$$\mathcal{R} = \left[\frac{M|\mathbf{k}_\pi|}{E_{p'}|\mathbf{k}_\pi| + E_\pi(|\mathbf{k}_\pi| - |\mathbf{q}|\cos\theta_\pi)}\right] \tag{4.36}$$

We have also calculated the differential cross section for the neutral current weak pion production where the recoil of the nucleus has been neglected and is found to be in the following form (Appendix-G):

$$\left[\frac{d^5\sigma}{d\Omega_\pi dE_\pi d\Omega_{\nu\nu'}}\right]_{NC} = \frac{1}{8}\frac{1}{(2\pi)^5}\left(1-\frac{E_\pi}{E_\nu}\right)|\mathbf{k}_\pi|\bar{\sum}\sum|\mathcal{A}|^2 \tag{4.37}$$

Integrating over the respective lepton and pion solid angles, we can find the double differential cross sections. We have calculated the momentum and angular distributions of pions and muons along with the Q^2 distribution. Finally, integrating over the respective energies we have calculated the total cross sections for charged current as well as neutral current induced weak production of pions.

4.3 Incoherent Production of Pion

4.3.1 Introduction

In nuclear pion production, if the final nucleus goes to excited state which decays to ground state by further emission of particles and/or radiation, accompanied by pion, then the process is known as incoherent production. Weak production of Δ has been studied in order to calculate

the pion production from nuclei. As discussed earlier that the reaction given in Eqs.3.1 and 3.2 taking place in the nucleus produces Δ which give rise to pions as decay product through $\Delta \rightarrow N\pi$ channel. In the incoherent pion production process only these pions are observed and no observation is made on other hadrons.

We want to study the weak production of Δ through charged and neutral current processes induced by neutrinos and antineutrinos, in which a Δ resonance is excited which subsequently decays into a pion and a nucleon. In the excitation of Δ from nuclear targets, there is an additional model dependence due to strong interaction of Δ in the nuclear medium. Inside the nuclear medium Δ properties like its mass and decay width are both modified due to strong interactions. The nuclear effects in the Δ production are important to study the pion production from nuclei. Weak production of Δ has been studied in order to calculate the pion production from nuclei by many authors [134]-[136], [140]-[146], [263], which discuss the various nuclear effects in weak production of Δ. In this work the nuclear effects on the Δ production in nuclei has been studied in the local density approximation (LDA) which takes into account the modification of mass and decay width. The various nuclear effects have been discussed in section-4.4. The calculations have been done assuming Δ-dominance model of one pion production because the contribution of higher resonances in the energy region of interest is sufficiently small. We have considered all the present available informations on the weak vector and axial vector form factors in the matrix elements of N-Δ transitions, discussed in Chapter-3. In addition, inside the nuclear medium the modification in the mass and width of the Δ resonance is properly taken into account and is found to give important effects on the differential cross section. The final state interaction of pions inside the nuclear medium is calculated through the Monte Carlo simulation using probabilities per unit length as the basic input. Next, we describe the matrix element for the production of Δ and derive the expressions for the cross sections.

4.3.2 Matrix Element and Cross section

In this section, we describe the nuclear excitation of Δ resonance. We have calculated the charged and neutral current induced neutrino interactions for nuclear excitation of Δ resonance which subsequently decays into a pion and a nucleon. The calculations have been done in local density approximation using a relativistic description of Δ resonance following the standard Rarita-Schwinger formalism [124], [126], [133], [135], [137]. The matrix element is calculated using the Feynman diagrams shown in Fig.4.3 for the following charged current neutrino induced reactions:

$$\nu_\mu(k) + p(p) \rightarrow \mu^-(k') + \Delta^{++}(P) \qquad (4.38)$$
$$\searrow p + \pi^+$$

$$\nu_\mu(k) + n(p) \rightarrow \mu^-(k') + \Delta^{+}(P) \qquad (4.39)$$
$$\searrow n + \pi^+ \ (\ p \ + \ \pi^0\ ) \qquad (4.40)$$

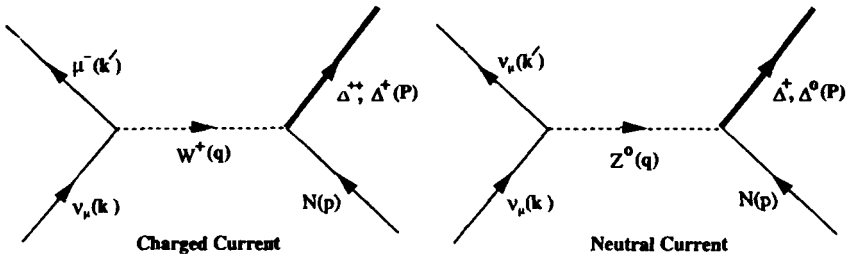

Figure 4.3: Feynman diagrams for neutrino induced weak production of Δ-resonance.

Following the Lagrangian in the standard model given in Eq.3.16, the matrix element for the process (Eq.4.38) is then written as the product of the leptonic and hadronic currents as given in Eq.3.19. The hadronic current for the reaction (Eq.4.38) is given by:

$$J^{\mu}_{had} = \langle \Delta^{++}|V^{\mu} - A^{\mu}|p\rangle = \cos\theta_C\ \bar{\psi}_{\alpha}(P)\ \mathcal{O}^{\alpha\mu}\ u(p), \tag{4.41}$$

where $\mathcal{O}^{\alpha\mu}$ is the weak N-Δ transition vertex given in Eq.3.56. For neutral current interaction $\mathcal{O}^{\alpha\mu}$ is given in Eq.4.16, and $\cos\theta_C$ is one.

When the reactions given by Eq.4.38 or 4.39 take place in the nucleus, the neutrino interacts with a nucleon moving inside the nucleus of density $\rho(r)$ with its corresponding momentum $\vec{p}$ constrained to be below its Fermi momentum $k_{F_{n,p}}(r) = \left[3\pi^2\rho_{n,p}(r)\right]^{\frac{1}{3}}$, where $\rho_n(r)$ and $\rho_p(r)$ are the neutron and proton nuclear densities. In the local density approximation, the scattering cross section is evaluated as a function of local Fermi momentum and integrated over the whole nucleus. Therefore, the differential cross section for Δ production in local density approximation is written as

$$\begin{aligned}\frac{d^2\sigma}{dE_{k'}d\Omega_{k'}} &= \int \rho(\mathbf{r})\ d^3\mathbf{r}\left[\frac{d^2\sigma}{dE_{k'}d\Omega_{k'}}\right]_{free} \\ &= \frac{G^2\cos^2\theta_C}{128\pi^3}\int d^3\mathbf{r}\rho(\mathbf{r})\frac{|\mathbf{k}'|}{E_k}\frac{1}{MM_{\Delta}}\left[\frac{\frac{\Gamma(W)}{2}}{(W-M_{\Delta})^2+\frac{\Gamma^2(W)}{4}}\right](L_{\mu\nu}J^{\mu\nu})\end{aligned} \tag{4.42}$$

where $\left[\frac{d^2\sigma}{dE_{k'}d\Omega_{k'}}\right]_{free}$ is the differential cross section for Δ production from free nucleon given in Eq.3.62. For our numerical calculations we take the proton $\rho_p(\mathbf{r})$ and the neutron $\rho_n(\mathbf{r})$ density as given in section-4.2.2. The nuclear density $\rho(\mathbf{r})$ have been taken as 3-parameter Fermi (3pF) density for ^{12}C and ^{16}O nuclei given in Eq.4.24, and the density parameters c=2.355fm, z=0.5224fm and w=-0.149 for ^{12}C and c=2.608fm, z=0.513fm and w=-0.051 for ^{16}O are taken from Ref. [215].

4.4 Nuclear Effects

We obtained the expressions for the differential cross sections for the coherent and incoherent weak pion production from nuclei. Inside the nucleus, in coherent weak pion production, the effect of nuclear medium has to be taken into account by using the nuclear form factor $\mathcal{F}(\mathbf{q}-\mathbf{k}_\pi)$. The nuclear effects in Δ production are important to study the pion production from nuclei, since inside the nuclear medium the mass (M_Δ) and decay width (Γ_Δ) of the intermediate Δ produced are both modified due to strong interactions. In the medium there will be important corrections to the free space value of the Δ decay width and mass from Pauli blocking and binding energy effect and N-Δ interactions.

The effect of nuclear medium has been recently calculated in a relativistic mean field approximation [134], [141] where a modified mass for nucleon and Δ has been used but a constant decay width for the Δ has been taken to calculate the pion production. In nuclear medium, the effect of modified mass (M_Δ) and decay width (Γ) of Δ has been calculated by Kelkar et al. [307] in a non-relativistic approach in local density approximation. They have taken into account the renormalization of the Δ and pion properties in the medium and observed that the cross section was quite sensitive to these medium effects, and their inclusion in the calculation decreased the cross section appreciably with respect to the impulse approximation.

We have considered the nuclear effect in term of Δ self-energy (Σ_Δ) in nuclear medium in the local density approximation (LDA) [135], [138], [139] which takes into account the modification of mass and decay width. The method has been used in past to calculate some electromagnetic and strong reactions in nuclei in the region of Δ dominance ([126]-[127], [161]-[173]).

We treat the nucleus as a collection of independent nucleons which are distributed in space accordingly to a density profile determined through the electron nuclei scattering experiments. Inside the nucleus we visualize the reaction as a two step process with the lepton interacting with individual nucleons producing single pions and the final nucleus. The production process is influenced by the Pauli principle and the Fermi-motion of the individual nucleons. In local density approximation the incoming neutrino interacts with the the nucleons moving inside the nucleus of density $\rho(\mathbf{r})$ with the corresponding momentum $\mathbf{p}_{n,p}$ are constrained to be within the Fermi sea and is therefore bounded by the local Fermi momentum

$$\mathbf{k}_{F_{n,p}}(\mathbf{r}) = \left[3\pi^2\ \rho_{n,p}(\mathbf{r})/2\right]^{\frac{1}{3}} \tag{4.43}$$

where $\rho_n(\mathbf{r})$ and $\rho_p(\mathbf{r})$ are the neutron and proton densities as discussed in section-4.2.2.

While the nucleons inside the nucleus are constrained to have momenta below the Fermi momentum, there is no such constraint on the momentum of the intermediate Δ produced in the medium, it propagates in the medium and experiences all kinds of self-energy (Σ_Δ) interactions. This self-energy is assumed to be the function of the nuclear density $\rho(\mathbf{r})$. This involves the decay of Δ-isobar through $\Delta N \rightarrow NN$ and $\Delta \rightarrow N\pi$ channels in the nucleus. But, their decay, is influenced by the Pauli blocking. The nucleons produced in these decay

processes have to be above the Fermi momentum $\mathbf{k}_F$ of the nucleons in nucleus thus inhibiting the decay as compared to the free decay of the Δ-isobar described by Γ in Eq.3.64. This leads to a modification in the decay width of the Δ resonance which has been studied by many authors [161]-[173]. Further, there are additional decay channels open for the Δ resonance in the nuclear medium. In the nuclear medium the Δ resonance decay through two and three body absorption processes like $\Delta N \rightarrow NN$ and $\Delta NN \rightarrow NNN$ through which Δ disappear in the nuclear medium without producing a pion, while a two body Δ absorption process like $\Delta N \rightarrow \pi NN$ gives rise to some more pions. In the present work, we actually do not include these processes explicitly, instead we use the parametrization of these modifications given by Oset and Salcedo [161], where these nuclear medium effects on the Δ propagation are included by describing the mass and the decay width in terms of the Δ self-energy. The real part of the delta self energy gives the mass of Δ and the imaginary part of the delta seif energy gives the width of Δ. These modifications are parametrizes by making density dependent changes in mass and decay width, in a local density approximation, to the Δ-hole model.

We are interested here in the modification of the free mass and width from the following sources:

(a) The intermediate nucleon state are partly blocked for the Δ decay because some of these states are occupied (Pauli blocking). The nucleon after the Δ decay into pion and a nucleon must be in an unoccupied state, takes into account the Pauli correction by assuming a local Fermi sea at each point of the nucleus of density $\rho(\mathbf{r}) = 2\mathbf{k}_F^3(\mathbf{r})/3\pi^2$, and forcing the nucleon to be above the Fermi sea. This leads to an energy dependent modification in the Δ decay width given as

$$\Gamma \rightarrow \tilde{\Gamma} - 2\mathrm{Im}\Sigma_\Delta \tag{4.44}$$

where $\tilde{\Gamma}$ is the Pauli blocked width of Δ in the nuclear medium and its relativistic form is

$$\tilde{\Gamma} = \frac{1}{6\pi}\left(\frac{f_{\pi N\Delta}}{m_\pi}\right)^2 \frac{M}{\sqrt{s}} |\mathbf{p}'_{cm}|^3 \, F(k_F, E_\Delta, k_\Delta) \tag{4.45}$$

where $F(k_F, E_\Delta, k_\Delta)$, the Pauli correction factor is written as [161]-[162]

$$F(k_F, E_\Delta, k_\Delta) = \frac{k_\Delta |\mathbf{p}'_{cm}| + E_\Delta E'_{p_{cm}} - E_F\sqrt{s}}{2k_\Delta |\mathbf{p}'_{cm}|} \tag{4.46}$$

with $\sqrt{s}$ as the center of mass energy in the Δ decay averaged over the Fermi sea given as

$$\bar{s} = M^2 + m_\pi^2 + 2E_\pi\left(M + \frac{3}{5}\frac{k_F^2}{2M}\right) \tag{4.47}$$

k_F the Fermi momentum, $E_F = \sqrt{M^2 + k_F^2}$, k_Δ is the Δ momentum, $E_\Delta = \sqrt{s + k_\Delta^2}$, and $\mathbf{p}'_{cm}$, $E'_{p_{cm}}$ the nucleon momentum and the relativistic nucleon energy in the final πN center of mass frame.

$$|\mathbf{p}'_{cm}| = \frac{\sqrt{(s - M^2 - m_\pi^2)^2 - 4M^2m_\pi^2}}{2\sqrt{s}} \tag{4.48}$$

In addition the Pauli factor has to replaced by 1 in Eq.4.45, if $F(k_F, E_\Delta, k_\Delta) > 1$ and by zero if $F(k_F, E_\Delta, k_\Delta) < 0$.

b) The intermediate nucleon through the Δ decay inside the nuclear medium feels a single particle potential due to all the other nucleons in the nucleus, known as binding effect, which is taken care by the real part of the Δ self-energy. This effect modifies the mass of Δ in the medium as

$$M_\Delta \rightarrow \tilde{M}_\Delta = M_\Delta + \mathrm{Re}\Sigma_\Delta \tag{4.49}$$

The Δ self-energy plays a very important role in the different pion nuclear reactions. A thorough study of the Δ self-energy is made, using the implicit model for the Δ self-energy by E. Oset and L. L. Salcedo [161]. For the scalar part of the Δ self energy the numerical results are parametrized in the approximate analytical form (excluding the Pauli corrected width), and are given as [161]-[162]:

$$-\mathrm{Im}\Sigma_\Delta = C_Q \left(\frac{\rho}{\rho_0}\right)^\alpha + C_{A2} \left(\frac{\rho}{\rho_0}\right)^\beta + C_{A3} \left(\frac{\rho}{\rho_0}\right)^\gamma \tag{4.50}$$

which is determined mainly by the one pion interactions in the nuclear medium. This includes the two body, three body absorption and the quasi-elastic absorption contributions for the produced pions in the nucleus. The coefficients C_Q accounts for the quasielastic part, the term with C_{A2} for two body absorption and the one with C_{A3} for three body absorption, and are parameterized in the range of energies $80 < T_\pi < 320 MeV$, where T_π is the pion kinetic energy, as [161]-[162]:

$$C(T_\pi) = ax^2 + bx + c, \qquad x = \frac{T_\pi}{m_\pi} \tag{4.51}$$

where C stands for all the coefficients i.e. C_Q, C_{A2}, C_{A3}, α and $\beta(\gamma = 2\beta)$. The different coefficients used above are tabulated in Table.4.1 and Table.4.2 [161].

However, the real part of the Δ self-energy associated with the medium corrections has some energy dependence and near the resonance region where the shift might be more important is approximated as [161]

$$\mathrm{Re}\Sigma_\Delta \simeq -30.0 \left(\frac{\rho}{\rho_0}\right) \mathrm{MeV} \tag{4.52}$$

In the real part of the Δ self-energy $\mathrm{Re}\Sigma_\Delta$ there is one more term associated with the irreducible piece of the optical potential due to the short range piece of the effective spin-isospin interaction [165]-[166]. This may be due to the effective π and ρ meson exchange, then one has to replace the pion optical potential by the π and ρ meson exchange NΔ transition potential. This effect can be taken in the form of the Landau-Migdal short range spin-isospin force

Table 4.1: Coefficients used in Eq.(4.50) for the calculation of $\mathrm{Im}\Sigma_\Delta$ as a function of the energy in the case of pion nuclear scattering.

T_π (MeV)	$C_Q(MeV)$	$C_{A2}(MeV)$	$C_{A3}(MeV)$	α	β	γ
85	9.7	18.9	3.7	0.79	0.72	1.44
125	11.9	17.7	8.6	0.62	0.77	1.54
165	12.0	16.3	15.8	0.42	0.80	1.60
205	13.0	15.2	18.0	0.31	0.83	1.66
245	14.3	14.1	20.2	0.36	0.85	1.70
315	9.8	13.1	14.7	0.42	0.88	1.76

Table 4.2: Coefficients used for an analytical interpolation of $C(T_\pi)$ of Eq.(4.51).

	$C_Q(MeV)$	$C_{A2}(MeV)$	$C_{A3}(MeV)$	α	β
a	-5.19	1.06	-13.46	0.382	-0.038
b	15.35	-6.64	46.17	-1.322	0.204
c	2.06	22.66	-20.34	1.466	0.613

given by $\left(\frac{f_{\pi N\Delta}}{m_\pi}\right)^2 g'_\Delta\ \mathbf{S}\cdot\mathbf{S}^\dagger\ \mathbf{T}\cdot\mathbf{T}^\dagger$ [168], where $g'_\Delta \simeq$0.5-0.6 is the Landau-Migdal parameter. Finally, in the approach of Ref. [162], the correction to $\mathrm{Re}\Sigma_\Delta$ comes out to be

$$\mathrm{Re}\Sigma_\Delta = \frac{4}{9}\left(\frac{f_{\pi N\Delta}}{m_\pi}\right)^2 g'_\Delta\ \rho(\mathbf{r}) \tag{4.53}$$

and taking g'_Δ=0.55 [168], the sum of the two corrections terms to $\mathrm{Re}\Sigma_\Delta$ in Eqs.4.52 and 4.53, get the approximated form as [162]

$$\mathrm{Re}\Sigma_\Delta \simeq 40.0\left(\frac{\rho}{\rho_0}\right)\ \mathrm{MeV} \tag{4.54}$$

With these modifications, which incorporate the various nuclear medium effects on Δ propagation inside the nuclear medium, the differential scattering cross section described in Eq.4.42 modifies to

$$\begin{aligned}\frac{d^2\sigma}{dE_{k'}d\Omega_{k'}} &= \frac{G^2\cos^2\theta_C}{128\pi^3}\int d^3\mathbf{r}\rho(\mathbf{r})\frac{|\mathbf{k}'|}{E_k}\frac{1}{MM_\Delta} \\ &\times\left[\frac{\frac{\tilde{\Gamma}}{2}-\mathrm{Im}\Sigma_\Delta}{(W-M_\Delta-\mathrm{Re}\Sigma_\Delta)^2+(\frac{\tilde{\Gamma}}{2}-\mathrm{Im}\Sigma_\Delta)^2}\right](L_{\mu\nu}J^{\mu\nu})\end{aligned} \tag{4.55}$$

The expressions for $\tilde{\Gamma}$, $\mathrm{Re}\Sigma_\Delta$ and $\mathrm{Im}\Sigma_\Delta$ as defined in Eqs.4.45, 4.50 and 4.54, have been used to numerically evaluate the differential scattering cross section and the total cross sections.

It should be noted from the above expression that the $\mathrm{Im}\Sigma_\Delta$ term in the numerator gives the particle hole excitations and $\tilde{\Gamma}$ term gives the Δ's which produces pions. Use of Eq.4.55 enables us to separate the Δ's which produces pions by using either $\mathrm{Im}\Sigma_\Delta$ or $\tilde{\Gamma}$ in the numerator of Eq.4.55. For example, in case of one π^+ production process $\tilde{\Gamma}$ and C_Q term in $\mathrm{Im}\Sigma_\Delta$ give contribution to the pion production.

The total scattering cross section for the neutrino induced charged current one π^+ production on proton target is given by

$$\frac{d^2\sigma}{dE_{k'}d\Omega_{k'}} = \frac{G^2\cos^2\theta_C}{128\pi^3}\int d^3\mathbf{r}\rho(\mathbf{r})\frac{|\mathbf{k}'|}{E_k}\frac{1}{MM_\Delta} \times \left[\frac{\frac{\tilde{\Gamma}}{2} - C_Q\left(\frac{\rho}{\rho_0}\right)^\alpha}{(W - M_\Delta - \mathrm{Re}\Sigma_\Delta)^2 + (\frac{\tilde{\Gamma}}{2} - \mathrm{Im}\Sigma_\Delta)^2}\right](L_{\mu\nu}J^{\mu\nu}) \quad (4.56)$$

For charged current one π^+ production on the neutron target, $\rho_p(\mathbf{r})$ in the above expression is replaced by $\frac{1}{9}\rho_n(\mathbf{r})$, where the factor $\frac{1}{9}$ with $\rho_n(\mathbf{r})$ comes due to suppression of π^+ production from the neutron target, i.e. $\nu_l + n \rightarrow l^- + \Delta^+$ as compared to the π^+ production from the proton target, i.e. $\nu_l + p \rightarrow l^- + \Delta^{++}$ through process of Δ excitation and decay in the nucleus, i.e. $\Delta^{++} \rightarrow p + \pi^+$ and $\Delta^+ \rightarrow n + \pi^+$ $(\rightarrow p + \pi^0)$.

Therefore, the total scattering cross section for the neutrino induced charged current one π^+ production with the nucleus is given by

$$\frac{d^2\sigma}{dE_{k'}d\Omega_{k'}} = \frac{G^2\cos^2\theta_C}{128\pi^3}\int d^3\mathbf{r}\rho(\mathbf{r})\frac{|\mathbf{k}'|}{E_k}\frac{1}{MM_\Delta}\left[\frac{\frac{\tilde{\Gamma}}{2} - C_Q\left(\frac{\rho}{\rho_0}\right)^\alpha}{(W - M_\Delta - \mathrm{Re}\Sigma_\Delta)^2 + (\frac{\tilde{\Gamma}}{2} - \mathrm{Im}\Sigma_\Delta)^2}\right] \times \left[\rho_p(\mathbf{r}) + \frac{1}{9}\rho_n(\mathbf{r})\right](L_{\mu\nu}J^{\mu\nu}) \quad (4.57)$$

For antineutrino reactions the role of $\rho_p(\mathbf{r})$ and $\rho_n(\mathbf{r})$ are interchanged and $\left[\rho_p(\mathbf{r}) + \frac{1}{9}\rho_n(\mathbf{r})\right]$ in the above expression is replaced by $\left[\rho_n(\mathbf{r}) + \frac{1}{9}\rho_p(\mathbf{r})\right]$ and the antisymmetric term in the leptonic tensor $L_{\mu\nu}$ given in Eq.3.54 change the sign.

4.5 Final State Interactions (FSI)

4.5.1 Final State Interactions effects for Coherent Production

The pions produced in these processes inside the nuclear medium may rescatter or may produce more pions or may get absorbed while coming out from the final nucleus. Even if pion absorption is a relatively small effect at high energies, there is a large number of pions at lower energies which are produced both by the quasielastic rescattering and the pion production on

the nuclear nucleon. The proportion of these pions that eventually comes out of the nucleus is essentially determined by the absorption strength. At low energies, pion absorption has been extensively studied, but there is a little theoretical work at high energies, and not much experimental information is available. In Ref. [174] the effect of pion absorption on the pion nucleus elastic and single charge exchange scattering has been studied in the energy range of 250 to 650 MeV. The absorptive part of the pion nucleus optical potential was calculated within the frame work of many body field theoretical approach. The model agrees with the more complex microscopical model of Oset, Futami and Toki [310] in the Δ resonance region, which contains both two and three body absorption mechanism, and the results show a quite weak absorption at high energies, as was expected. Also, it has been shown that in the Δ resonance region, three body absorption becomes comparable with the two body contribution. As the pion energy increases the effect of two body absorption decreases again, and it becomes dominant, as is the case at low energy. We have considered the final state interaction of the pion by replacing the plane wave pion by a distorted wave pion. The distortion of the pion wave is calculated using the eikonal approximation of Glauber in the impact parameter representation.

The type of problem we consider is the scattering of an incident particle with a nucleus consisting of many particles, which is not an easy to formulate, at any energy. However, the physical conditions which hold at high energies are in a number of ways well suited to the introduction of approximation method. We shall now begin with the method of an approximation which is better suited to many of the purposes of high energy. While this method is not without limitations of its own, however, it allows one to estimate correctly the intensity of a predominant part of the scattering. Let us consider the scattering of a spinless particle of mass m and energy $E = \frac{\hbar k^2}{2m}$ by a static force field which is represented by the interaction potential $V(\mathbf{r})$ of range R. The scattering problem consists of solving the Schrodinger equation

$$\left[\vec{\nabla}^2 + \mathbf{k}^2\right] \psi(\mathbf{r}) = 2mV(\mathbf{r})\psi(\mathbf{r}) \tag{4.58}$$

with the condition that the wave function $\psi(\mathbf{r})$ must have a component that involves an incident plane wave moving in positive z-direction and another component that involves a spherical outgoing wave. It should be emphasized that in scattering problem we do not require $\psi(\mathbf{r})$ to go to zero at $\mathbf{r} \rightarrow \infty$. In fact the scattering amplitude which is the quantity of interest is contained in the $\mathbf{r} \rightarrow \infty$ i.e., asymptotic part of $\psi(\mathbf{r})$. With these conditions the wave function $\psi(\mathbf{r})$ takes the form

$$\psi(\mathbf{r}) \rightarrow e^{i\mathbf{k}\cdot\mathbf{r}} + f(\theta,\phi)\frac{e^{ikr}}{r} \tag{4.59}$$

where $f(\theta,\phi)$ is the scattering amplitude. We know that the eikonal approximation is valid for the processes involving small scattering angle and very large incoming momentum. Therefore, in the high energy approximation, the energy E of the incident particle is much larger than the interaction potential $V(\mathbf{r})$ i.e., $V/E << 1$ and the wavelength $\lambda = k^{-1}$ associated with

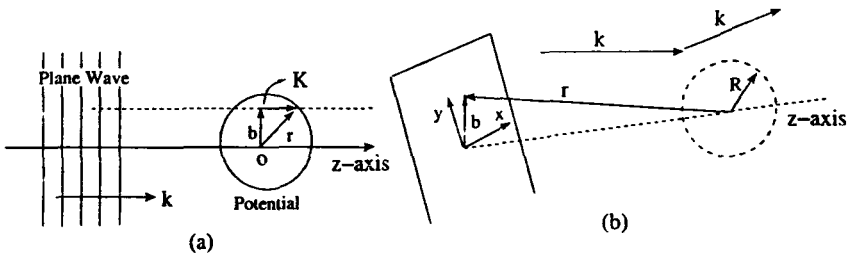

Figure 4.4: Definition of impact parameter in scattering process at high energies.

it is much smaller than the typical size 'a' of the interaction i.e., $ka >> 1$. In this condition, particle traversing through the potential will not get much deflection from its initial direction. hence, the scattering is concentrated at small angles only. Therefore, we can assume the wave function to be of the form

$$\psi(\mathbf{r}) \approx e^{i\mathbf{k}\cdot\mathbf{r}}\phi(\mathbf{r}) \tag{4.60}$$

where $\phi(\mathbf{r})$ is a slowly varying function of $\mathbf{r}$ and satisfies the condition that if $\mathbf{k}$ points along z-axis then $\phi(\mathbf{r}) \to 1$ as $z \to -\infty$. This condition is to reduce the wave function Eq.4.60 to the incident plane wave. Substituting Eq.4.60 into Eq.4.58 with

$$\vec{\nabla}\psi(\mathbf{r}) = e^{i\mathbf{k}\cdot\mathbf{r}}(i\mathbf{k})\phi(\mathbf{r}) + e^{i\mathbf{k}\cdot\mathbf{r}}\vec{\nabla}\phi(\mathbf{r}) \tag{4.61}$$

and

$$\vec{\nabla}^2\psi(\mathbf{r}) = \vec{\nabla}\cdot\vec{\nabla}\psi(\mathbf{r}) = -k^2\psi(\mathbf{r}) + 2ike^{i\mathbf{k}\cdot\mathbf{r}}\vec{\nabla}\phi(\mathbf{r}) + e^{i\mathbf{k}\cdot\mathbf{r}}\vec{\nabla}^2\varphi(\mathbf{r}) \tag{4.62}$$

and our approximation consists in dropping the $\vec{\nabla}^2\phi(\mathbf{r})$ term, since we assume we have $\phi(\mathbf{r})$ varies slowly in a wavelength, we have

$$2ike^{i\mathbf{k}\cdot\mathbf{r}}\vec{\nabla}\phi(\mathbf{r}) = 2nV(\mathbf{r})e^{i\mathbf{k}\cdot\mathbf{r}}\phi(\mathbf{r}) \tag{4.63}$$

We choose z-axis to lie in the direction of propagation $\mathbf{k}$, we have

$$\begin{aligned} \frac{\partial}{\partial z}\phi(\mathbf{r}) &= -\frac{im}{k}V(\mathbf{r})\phi(\mathbf{r}) \\ \phi(x,y,z') &= \exp\left[-\frac{i}{v}\int_{-\infty}^{z} V(x,y,z')dz'\right] \end{aligned} \tag{4.64}$$

where v being the modulus of the particle's initial velocity $v = k/m$. Using Eq.5.64 in Eq.4.60, we have the approximate representation for the scattering wave function as

$$\psi(x,y,z) = \exp\left[ikz - \frac{i}{v}\int_{-\infty}^{z} V(x,y,z')dz'\right] \tag{4.65}$$

Now this expression is missing a good many of the things one looks for in three dimension wave function, e.g., a spherical outgoing wave, but we must remember that the conditions through which it is derived are only intended to hold within the volume occupied by the potential. Fortunately, it is only necessary to know the wave function within the volume of the potential in order to find the scattering amplitude. Therefore, the above expression is fully acceptable approximation to the exact solution for values of argument within the range R of the potential V i.e., for $r \leq R$. Glauber [311] has shown that the impact parameter is a useful concept whenever the motion of the projectile is such that it follows a classical trajectory, such situation is realized in potential scattering at high energies. In high energy scattering the z-axis is chosen parallel to the sum of $\mathbf{K} = \mathbf{k} + \mathbf{k}'$ of the incoming and outgoing momenta as shown in Fig.4.4(b).

Let $\hat{\mathbf{K}}$ is a unit vector, pointing in the incident propagation direction $\mathbf{k}$ which, as before, will also be taken parallel to z-axis shown in Fig.4.4(a), then any position vector $\mathbf{r}$ may be resolved into two components $\mathbf{r} = \mathbf{b} + \hat{\mathbf{K}}z$, where b is a vector lying in a plane perpendicular to $\mathbf{k}$, with this notation $\psi(\mathbf{r})$ may be written as

$$\psi(\mathbf{r}) = \exp\left[i\mathbf{k}\cdot\mathbf{r} - \frac{i}{v}\int_{-\infty}^{z} V(\mathbf{b} + \hat{\mathbf{K}}z')dz'\right] \tag{4.66}$$

Hence, if the potential is concentrated at the origin, then the distance $b = |\mathbf{b}|$ evidently has the interpretation of an impact parameter.

Now we have to take into account the pion absorption effects in the cross section. It is well known that the coherent cross section strongly depends upon the interaction of the produced pion with the nucleus called as final state interaction(FSI). This effect can be taken into account by replacing the plane wave of the outgoing pion described by the nucleon form factor $\mathcal{F}(\mathbf{q} - \mathbf{k}_\pi)$ in Eq.4.20 by the distorted wave in the expression of the nucleon form factor. In this approximation the plane wave of the pion is replaced by the distorted wave as

$$e^{i(\mathbf{q}-\mathbf{k}_\pi)\,\mathbf{r}} \rightarrow \exp\left[i(\mathbf{q} - \mathbf{k}_\pi)\cdot\mathbf{r} - \frac{i}{v}\int_{-\infty}^{z} V(\mathbf{b}, z')dz'\right] \tag{4.67}$$

We will use the fact that the pion self-energy Π is related to the equivalent pion optical potential V_{opt} by means of [162], [169]-[170]

$$\Pi(\rho(\mathbf{r})) = 2\omega\, V_{opt}(\omega, \mathbf{r}) \tag{4.68}$$

where ω is the energy of the pion, using $|\mathbf{v}| = |\mathbf{k}_\pi|/\omega$ Eq.4.67 becomes

$$e^{i(\mathbf{q}-\mathbf{k}_\pi)\,\mathbf{r}} \rightarrow \exp\left[i(\mathbf{q} - \mathbf{k}_\pi)\cdot\mathbf{r} - i\int_{z}^{\infty} \frac{1}{2|\mathbf{k}_\pi|}\Pi(\rho(\mathbf{b}, z'))dz'\right] \tag{4.69}$$

The pion self-energy is calculated in momentum space for the Δ-hole excitations, and given as [161], [162], [169]

$$\Pi(\rho(\mathbf{b}, z')) = \frac{4}{9}\left(\frac{f_{\pi N\Delta}}{m_\pi}\right)^2 \frac{M^2}{\bar{s}}|\mathbf{k}_\pi|^2\, \rho(\mathbf{b}, z')\, G_{\Delta h}(\bar{s}, \rho) \tag{4.70}$$

with $G_{\Delta h}(\bar{s},\rho)$ the Δ-hole propagator given as

$$G_{\Delta h}(s,\rho(\mathbf{b},z')) = \frac{1}{\sqrt{\bar{s}} - M_\Delta + \frac{1}{2}i\tilde{\Gamma}(\bar{s},\rho) - i\mathrm{Im}\Sigma_\Delta(\bar{s},\rho) - \mathrm{Re}\Sigma_\Delta(\bar{s},\rho)} \tag{4.71}$$

Note that we use the non relativistic form of the energy denominator in the Δ propagator for calculating the pion self-energy. Since we are effectively using a pion optical potential derived from the pion self-energy which is calculated in terms of the Δ propagator. In order to be consistent with the potential description, it is desirable that a non relativistic propagator is used even though it is an approximation.

Now the nuclear form factor $\mathcal{F}(\mathbf{q}-\mathbf{k}_\pi)$, in impact parameter representation may be written as

$$\mathcal{F}(\mathbf{q}-\mathbf{k}_\pi) = \int d^2b dz\ \rho(\mathbf{b},z)\ e^{i(\mathbf{q}-\mathbf{k}_\pi)\cdot(\mathbf{b}+\hat{\mathbf{q}}z)} \tag{4.72}$$

where d^2b denotes the integration over the plane of impact vector. $\mathbf{r} = (\mathbf{b},z)$, and $\mathbf{q}$ the momentum transfer is chosen to be along z direction. With this choice, the exponential factor becomes

$$e^{i(\mathbf{q}-\mathbf{k}_\pi)\cdot(\mathbf{b}+\hat{\mathbf{q}}z)} = e^{-i\mathbf{k}_\pi^t\cdot\mathbf{b}}\ e^{i(|\mathbf{q}|-k_\pi^l)z}$$

where $\mathbf{k}_\pi^t$ and $k_\pi^l = \mathbf{k}_\pi\cdot\hat{\mathbf{q}} = \frac{\mathbf{k}_\pi\cdot\mathbf{q}}{|\mathbf{q}|}$ are the transverse and longitudinal components of the pion momentum. Also for the potential with azimuthal symmetry we may carry the integration one step further by noting that $\frac{1}{2\pi}\int_0^{2\pi} e^{i\lambda\cos\phi}d\phi = J_0(\lambda)$ where $J_0(\lambda)$ is the zeroth order Bessels function. Finally, Eq.4.72 takes the form

$$\mathcal{F}(\mathbf{q}-\mathbf{k}_\pi) = 2\pi\int_0^\infty b\ db\int_{-\infty}^\infty dz\ \rho(\mathbf{b},z)\ J_0(k_\pi^t b)\ e^{i(|\mathbf{q}|-k_\pi^l)z} \tag{4.73}$$

When the pion absorption effect is taken into account the nuclear form factor $\mathcal{F}(\mathbf{q}-\mathbf{k}_\pi)$ modifies to $\tilde{\mathcal{F}}(\mathbf{q}-\mathbf{k}_\pi)$ given as

$$\tilde{\mathcal{F}}(\mathbf{q}-\mathbf{k}_\pi) = 2\pi\int_0^\infty b\ db\int_{-\infty}^\infty dz\ \rho(\mathbf{b},z)\ J_0(k_\pi^t b)\ e^{i(|\mathbf{q}|-k_\pi^l)z}\ e^{-if(\mathbf{b},z)} \tag{4.74}$$

where

$$f(\mathbf{b},z) = \int_z^\infty \frac{1}{2|\mathbf{k}_\pi|}\Pi(\rho(\mathbf{b},z'))dz' \tag{4.75}$$

and the pion self-energy Π is defined in Eq.4.70.

4.5.2 Final State Interactions effects for Incoherent Production

The pions which are produced in these processes while traveling inside the nucleus can be absorbed, can change direction, energy, charge, or even produce more pions due to elastic and charge exchange scattering with the nucleons present in the nucleus through strong interactions. Therefore, the production cross sections for the pions from the nuclear targets are affected by the presence of strong interactions of final state pions in the nuclear medium. The effect of final state interaction (FSI) on the weak production cross section for pions are estimated with the help of a Monte Carlo simulation for propagation of pions in the nuclear medium using as the basic input the probabilities per unit length for each of these channels to happens.

In Monte Carlo simulation, pions of a given momentum and charge are generated, and assuming the real part of the pion nuclear potential to be weak compared with their kinetic energies, they are propagated following straight lines till they are out of the nucleus. At the beginning, the pions are placed at a point $(\mathbf{b}, z_{in})$, where $z_{in} = -\sqrt{R^2 - |\mathbf{b}|^2}$, with $\mathbf{b}$ as the random impact parameter, obeying |b| <R. R is upper bound for the nuclear radius, which is chosen to be such that $\rho(R) \approx 10^{-3}\rho_0$, with ρ_0 is the normal nuclear matter density. Then pions are made to move along the z-direction in small steps until it comes out of the nucleus or interact. To take into account the collisions the pion is followed by moving it a short distance dl, along its momentum direction (z-direction), such that $P(p_\pi, r, \lambda)dl << 1$, where $P(p_\pi, r, \lambda)$ is the probability of the interaction per unit length, at the point $\mathbf{r}$ of a pion of momentum $\mathbf{p}_\pi$ and charge λ. A random number $x \in [0, 1]$ is generated such that there are two possibilities:

(a) First possibility is $x > Pdl$, then there is no interaction, and the pion travels a distance dl along the direction of its momentum. Then the procedure is repeated by moving the pion a new step dl.

(b) Second possibility is $x < Pdl$, the interaction has taken place. In this case the channel of interactions are selected according to their respective probabilities, whether it has been absorption, quasielastic scattering, charge exchange, or pion production.

The probabilities of interaction per unit length of a pion is given by

$$P_\pi = \sum_f \left[\sigma_{\pi+n\to f}(\bar{E})\rho_n + \sigma_{\pi+p\to f}(\bar{E})\rho_p\right] \tag{4.76}$$

where f account for all possible final channels, n and p are neutrons and protons and ρ_n, ρ_p are their local densities. The cross section is evaluated at an invariant energy of the neutrino-nucleon system averaged over the local Fermi sea. In Monte Carlo simulation, pions of a given momentum and charge are generated, and assuming the real part of the pion nuclear potential to be weak compared with their kinetic energies, they are propagated following straight lines till they are out of the nucleus. At the beginning, the pions are placed at a point $(\mathbf{b}, z_{in})$, where $z_{in} = -\sqrt{R^2 - |\mathbf{b}|^2}$, with $\mathbf{b}$ as the random impact parameter, obeying |b| <R. R is upper bound for the nuclear radius, which is chosen to be such that $\rho(R) \approx 10^{-3}\rho_0$, with ρ_0

is the normal nuclear matter density. Then pions are made to move along the z-direction in small steps until it comes out of the nucleus or interact. To take into account the collisions the pion is followed by moving it a short distance dl, along its momentum direction (z-direction), such that $P(p_\pi, r, \lambda)dl << 1$, where $P(p_\pi, r, \lambda)$ is the probability of the interaction per unit length, at the point $\mathbf{r}$ of a pion of momentum $\mathbf{p}_\pi$ and charge λ. A random number $x \in [0, 1]$ is generated such that there are two possibilities:

(a) First possibility is $x > Pdl$, then there is no interaction, and the pion travels a distance dl along the direction of its momentum. Then the procedure is repeated by moving the pion a new step dl.

(b) Second possibility is $x < Pdl$, the interaction has taken place. In this case the channel of interactions are selected according to their respective probabilities, whether it has been absorption, quasielastic scattering, charge exchange, or pion production.

The probabilities of interaction per unit length of a pion is given by

$$P_\pi = \sum_f \left[\sigma_{\pi+n\to f}(\bar{E})\rho_n + \sigma_{\pi+p\to f}(\bar{E})\rho_p\right] \tag{4.77}$$

where f account for all possible final channels, n and p are neutrons and protons and ρ_n, ρ_p are their local densities. The cross section is evaluated at an invariant energy of the neutrino-nucleon system averaged over the local Fermi sea.

Finally, once the channel has been selected, for example it has been quasielastic, or charge exchange, the following procedure is used to find the new energy, and direction of the pion, and continue to propagate it along its new direction, checking at every step if new interactions take place. The probability per unit length of quasielastic scattering, or single charge exchange is given by

$$P_{N(\pi^\lambda,\pi^{\lambda'})N'} = \sigma_{N(\pi^\lambda,\pi^{\lambda'})N'} \times \rho_N \tag{4.78}$$

where N is a nucleon, ρ_N is its density and σ is the elementary cross section for the reaction $\pi^\lambda + N \to \pi^{\lambda'} + N'$ obtained from the phase shift analysis. When according to Eq.4.77, a quasielastic scattering took place, the following algorithm is executed to approximately implement Pauli blocking. First, a nucleon is randomly chosen from the local Fermi sea, then the pion and nucleon are boosted to their center of mass system. Assuming isotropic cross sections in the pion-nucleon center of mass system, a random scattering angle is generated (and therefore energy) in that system and the pion and nucleon momenta has been calculated. Finally these momenta are boosted to the lab system. When the momentum of the final nucleon in the lab system is below the Fermi level, the event is considered to be Pauli blocked and therefore, there was no interaction, and the pion initial charge and momentum is unchanged. Otherwise, one have a new pion type and/or a new direction and energy.

For a pion to be absorbed, the probability per unit length is expressed in terms of the imaginary part of the pion self energy Π i.e. $P_{abs} = -\frac{\mathrm{Im}\Pi_{abs}(p_\pi)}{p_\pi}$, where the self energy Π is related to the pion optical potential V given in Eq.4.67 [162], [169]-[170]. The imaginary part

of the pion self energy, related to two-nucleon and three-nucleon pion absorption has been calculated in Ref. [174] [175], which has been used in the simulation [176].

In the case that after moving the step dl the pion gets out of the nucleus, and when the pion is absorbed, if there are some other pions left inside the nucleus (these pions would have been produced previously at some step), then one of them is selected and propagate it from its current position. Finally when there are no pions left, the energy and angles of all pions that got out of the nucleus has been stored, if any, then the full procedure is repeated by generating a new initial pion.

==========*******==========

Chapter 5

Results and Discussions for Pion Production

5.1 Coherent and Incoherent Production of Pions and Leptons

In this section we present the numerical results for the charged current coherent neutrino production of pions and leptons induced by muon type neutrino from ^{12}C and ^{16}O nuclei. We also present the numerical results for the charged current incoherent neutrino production of one π^+ induced by muon type neutrino from ^{12}C and ^{16}O nuclei. We present and discuss the numerical results for the differential cross sections and the Q^2 distributions for the charged current induced incoherent and coherent neutrino production of pions and leptons for ^{12}C and ^{16}O nuclei. The total cross section for the incoherent and coherent production of pions have been presented and discussed.

5.1.1 Coherent Production of Pions and Leptors

A. Charged Current Coherent Pion Production

We have done the numerical calculation for the neutrino energy E_{ν_μ}=1.0 GeV. In Fig.5.1, we show the results of $\left(\frac{d\sigma^{CC}}{d\Omega_{\pi q} d\Omega_{\nu\mu} dE_\pi}\right)$ as a function of the pion angle $\Theta_{\pi q}$ measured with respect to the momentum transfer (q) for lepton angle $\Theta_{\nu\mu}$=0° with respect to the neutrino direction, at q_0=E_ν - E_μ=300 MeV in ^{12}C nuclei, using Eq.4.31. The dotted lines correspond to the result without the nuclear medium effects i.e., with free Δ width and no Δ self energy in the Δ propagator and no pion distortion. One of the major aim of this work is to study the effects of the nuclear medium and the pion final state interactions on coherent weak production of pions. The effects of the nuclear medium have been done considering the renormalization of the Δ properties inside the nuclear medium, through the $Re\Sigma_\Delta$ and $Im\Sigma_\Delta$ modifications in the

nuclear medium according to Eqs.4.50 and 4.54. This has been shown with dashed line, we see that this leads to a strong reduction in the $\left(\frac{d\sigma^{CC}}{d\Omega_{\pi q}d\Omega_{\nu\mu}dE_\pi}\right)$ for all values of $\Theta_{\pi q}$. We find that the reduction in the cross section by incorporating the nuclear medium effects is about 55% at $\Theta_{\pi q}$=0^o and increases with $\Theta_{\pi q}$ as it is about 80% at $\Theta_{\pi q}$=50^o. Further, when both the nuclear medium effects and the pion absorption effect using the eikonal approximation as discussed in section-4.5, for the modified form of the nuclear form factor $\tilde{\mathcal{F}}(\mathbf{q}-\mathbf{k}_\pi)$ are taken into account, there is a further reduction which which is almost 70% in the range $0^o < \Theta_{\pi q} < 20^o$ and then decreases as it is about 67% and 58% at $\Theta_{\pi q}$=30^o and $\Theta_{\pi q}$=40^o.

In Fig.5.2, we present the result $\left(\frac{d\sigma^{CC}}{d\Omega_{\pi q}d\Omega_{\nu\mu}dE_\pi}\right)$ in ^{16}O nuclei, and the effect of the nuclear medium reduces the cross section, as it is around 55% at $\Theta_{\nu\mu}$=0^o and increases with $\Theta_{\pi q}$. It is about 60% and 86% at $\Theta_{\pi q}$=20^o and $\Theta_{\pi q}$=50^o, respectively. The effect of the final state interaction of the pion is almost similar in nature as in case of ^{12}C nuclei.

In Fig.5.3, we show the differential cross section integrated over the lepton angle $\Theta_{\nu\mu}$ i.e., $\left(\frac{d\sigma^{CC}}{d\Omega_{\pi q}dE_\pi}\right)$ for $\Theta_{\pi q} = 0^o$ as a function of q_0, the total pion energy when neglecting the nucleus recoil energy. We observe again the sizable effects of the Δ renormalization and the pion distortion in the nuclear medium. We find the reduction due to nuclear effects decreases with q_0 and in the peak region (q_0=350 MeV of the free) it is about 50%. We see that after the peak reagion it is about 30% and 5% at q_0=400 MeV and 450 MeV, respectively, after which both are approximately same. The final result with the pion absorption also taken into account, the nature of the spectrum is almost flat, and the reduction in the cross section further increases with increase in q_0, as it is about 15%, 55% and 75% at q_0=250, 300 and 350 MeV, respectively. In the peak region (q_0=400 MeV of the nuclear effects) the reduction is about 78% then it starts decreasing, for example, it is about 73%, 58% and 42% at q_0=450 MeV, 600 MeV and 850 MeV, respectively.

In Fig.5.4, we show the result for $\left(\frac{d\sigma^{CC}}{d\Omega_{\pi q}dE_\pi}\right)$ in ^{16}O nuclei, and the nature of the cross section is almost similar as in Fig.5.3 for ^{12}C nuclei.

In Fig.5.5, we present the above result integrated over the pion angle $\Theta_{\pi q}$ i.e., the momentum distribution of pion $\left(\frac{d\sigma^{CC}}{dk_\pi}\right)$ in ^{12}C nuclei. We find that the reduction in the cross section due to the nuclear medium effects increases with the pion momentum $\mathbf{k}_\pi$ and just before the peak region it starts decreasing, in the peak region ($\mathbf{k}_\pi$=310 MeV of free) it is about 60% and decreases further, for example, it is about 45%, 20% and 5% at q_0=350 MeV, 400 MeV and 450 MeV, respectively, after which both are approximately same. The effect of the pion absorption show the further strong reduction in the cross section, as in the peak region ($\mathbf{k}_\pi$=320 - 360 MeV of nuclear effects) which is about 75-80%, accompanied by the shift in the peak towards the lower value of the pion momentum $\mathbf{k}_\pi$, and then decreases further.

In Fig.5.6, we present the momentum distribution $\left(\frac{d\sigma^{CC}}{dk_\pi}\right)$ in ^{16}O nuclei, and the cross section follow the same trend as in Fig.5.5 for ^{12}C nuclei.

In the Fig.5.7 and Fig.5.8, we present the angular distribution of pion $\left(\frac{d\sigma^{CC}}{d\cos\Theta_{\pi q}}\right)$ as a

function of $\cos\Theta_{\pi\vec{q}}$ in ^{12}C and ^{16}O nuclei, respectively. The angular distribution is found to be sharply peaked in the forward direction of the pion angle $\Theta_{\pi q}$. The reduction in the cross section decreases uniformly due to the nuclear medium effects as at $\cos\Theta_{\pi q}$=0.80, 0.90, 0.96 and 1.0 it is about 65%, 50%, 35% and 20%, respectively. The final state interaction of pion with the final nucleus further reduces the cross section and it is about 65-75% in the forward direction. In the inset of these figures, we show explicitly our final results which include both the renormalisation of the Δ properties in the nuclear medium and the final state interaction of the pion with the final nucleus.

B. Charged Current Coherent Lepton Production

In Fig.5.9, we show the differential cross section integrated over the pion angle $\Theta_{\pi q}$ i.e., $\left(\frac{d\sigma^{CC}}{d\Omega_{\nu_\mu} dE_\mu}\right)$ for $\Theta_{\nu\mu} = 0^\circ$ as a function of q_0 in ^{12}C nuclei. We find the reduction due to nuclear effects is approximately 45% for q_0=250 MeV and in the peak region (q_0=320 MeV of the free) it is about 60%. The reduction in the cross section decreases with q_0. We see that it is about 40% and 15% at q_0=350 MeV and 400 MeV. respectively, after which both are approximately same. The final result with the pion absorption also taken into account, the reduction in the cross section further increases with increase in q_0. In the peak region (q_0=330 MeV of the nuclear effects) there is a strong reduction and it is about 85% then it starts decreasing accompained by the slight shift in the peak towards the smaller q_0, for example, it is about 80%, 70% and 60% at q_0=400 MeV, 500 MeV and 600 MeV, respectively. In Fig.5.10, where we have presented our result for $\left(\frac{d\sigma^{CC}}{d\Omega_{\nu_\mu} dE_\mu}\right)$ in ^{16}O nuclei follow the similar trend with nuclear mudium effects and with nuclear medium and pion absorption effects, as discussed in case of Fig.5.9 for ^{12}C nuclei.

In Fig.5.11, we present the result of $\left(\frac{d\sigma^{CC}}{dE_\mu}\right)$ as a function of q_0 in ^{12}C nuclei without the nuclear medium effects, with the nuclear medium effects and with the nuclear medium and pion absorption effects. The reduction due to the nuclear effects increases with q_0 and in the peak region (q_0=340 MeV of the free) it is about 60% then decreases with increase in q_0. For example, it is about 55%, 35% and 8% at q_0=350 MeV, 400 MeV and 450 MeV, respectivley, after which they are same. When including the nuclear medium and pion absorption effects, there is further strong reduction in the peak region (q_0=360 MeV of the nuclear effects) which is about 75% after which it slightly increases and then decrease, along with the shift in the peak towards lower q_0.

In Fig.5.12, we present the result of lepton momentum distribution i.e., $\left(\frac{d\sigma^{CC}}{dk'_\mu}\right)$ as a function of k'_μ in ^{12}C nuclei without the nuclear medium effects, with the nuclear medium effects and with the nuclear medium and pion absorption effects. The cross sections are approximately same up to k'_μ=500 MeV, and then it reduces due to the nuclear effects. In the peak region (k'_μ=660 MeV of the free) the reduction is about 60% then decreases with increase in k'_μ. When including the nuclear medium and pion absorption effects, there is further strong

reduction in the peak region (k'_μ=620 MeV of the nuclear effects) which is about 80% after which it decrease, along with the shift in the peak towards higher k'_μ.

In the Fig.5.13 and Fig.5.14, we present the angular distribution of leptons $\left(\frac{d\sigma^{CC}}{d\cos\Theta_{\nu\mu}}\right)$ as a function of $\cos\Theta_{\nu\mu}$ in ^{12}C and ^{16}O nuclei, respectively. The angular distribution is found to be sharply peaked in the forward direction of the lepton angle $\Theta_{\nu\mu}$. The reduction in the cross section increases uniformly due to the nuclear medium effects as at $\cos\Theta_{\nu\mu}$=0.80, 0.90, 0.96 and 1.0 it is about 15%, 30%, 35% and 37%, respectively. The final state interaction of pion with the final nucleus further reduces the cross section and it is about 60-75% in the forward direction. In the inset of these figures, we show explicitly our final results which include both the renormalisation of the Δ properties in the nuclear medium and the final state interaction of the pion with the final nucleus.

C. Q^2-Distributions and The Total Cross Sections

In Fig.5.15 and Fig.5.16, we have presented the results for the differential cross sections $\left(\frac{d\sigma^{CC}}{dQ^2}\right)$ in ^{12}C and ^{16}O nuclei, respectively, for charged pion production at neutrino energy E_{ν_μ}=1.0 GeV where nuclear medium and final state interaction effects are shown explicitly. We can see from the Fig.5.15 that the reduction in the cross section in the peak region is around 35%, and decreases further uniformaly. The total reduction in the cross section is around 85% in the peak region when pion absorption effect is also taken into account, and decreases further uniformaly. Similar trend is there in case of ^{16}O nuclei shown in Fig.5.16.

In Fig.5.17 and Fig.5.18, we have presented the results for the total scattering cross section σ^{CC} for the coherent charged current reaction induced by ν_μ in ^{12}C and ^{16}O nuclei, respectively. The results for $\sigma^{CC}(E_{\nu_\mu})$ as a function of neutrino energy E_{ν_μ} are shown without nuclear medium effects (dotted line) and with nuclear medium effects (dashed line). When the pion absorption and nuclear medium effects, are both taken into account the results for $\sigma^{CC}(E_{\nu_\mu})$ are shown by the solid lines. We see that the nuclear medium effects lead to a reduction of around 45% for E_ν=0.7 GeV, 25-35% around E_ν=1.0 - 2.0 GeV and it is about 20% at E_ν=3.0 GeV while the reduction due to final state interaction is quite large. This suppression in the cross section due to the nuclear medium and the pion absorption effects is 80% for E_ν around 1.0 GeV, 70% for E_ν around 2.0 GeV and 65% for E_ν around 3.0 GeV.

In Fig.5.19 and Fig.5.20, we have presented the results for the total scattering cross section σ^{NC} for the coherent neutral current reaction induced by ν_μ in ^{12}C and ^{16}O nuclei, respectively. The effect of the nuclear medium, and the nuclear medium and pion absorption effects are same as in case of coherent charged current reactions.

5.1.2 Incoherent Production of Pions

In this section we present the numerical results of incoherent production of one π^+ in ^{12}C and ^{16}O nuclei induced by charged current neutrino interactions using Eq.4.57. We have calculated

the differential and total scattering cross section for the charged current one π^+ production for the incoherent processes with the different N-Δ weak transition form factors given by Schreiner and von Hippel [124], Paschos et al. [146] and Lalakulich et al. [147] as discussed in section-3.3.3.

In Fig.5.21, we show the total cross section for charged current one π^+ production from ^{12}C using the N-Δ transition form factors given by Lalakulich et al. [147] for the incoherent processes. We have presented the results for total scattering cross section $\sigma(E_\nu)$ without the nuclear medium effects, with the nuclear medium modification effects, and with nuclear medium and pion absorption effects. We find that the effect of medium modification of strong interaction properties of the Δ results in an overall reduction of the cross section of around 12-15% for neutrino energies E_ν=0.6-3 GeV (dashed line) as compared to the free Δ (dotted line). However, we find that around 80-85% of these Δ's produce pions and the rest of them produce particle hole excitations. This is calculated by using $\frac{\tilde{\Gamma}}{2}$ and C_Q term in ImΣ_Δ for the production of pion and for medium absorption of Δ, C_{A2} and C_{A3} terms in ImΣ_Δ in Eq.4.56. Therefore, the total effect of the medium modification is an overall reduction of around 30%. These pions, once produced inside the nucleus, rescatter and some of them may be absorbed while coming out of the nucleus. We have estimated this absorption effect in an eikonal aprroximation discussed in section-4.5. When the pion absorption effects are also taken into account along with the nuclear medium effects there is a further reduction in the cross section which is around 20-30% (solid line).

In Fig.5.22, we show the total cross section for charged current one π^+ production from ^{16}O using the N-Δ transition form factors given by Lalakulich et al. [147] for the incoherent processes. We find that the effect of the nuclear medium as well as the effect of the pion absorption are similar in nature as in case of Fig.5.21.

In Fig.5.23, we have shown the charged current one pion production cross section $\sigma(E_\nu)$ vs E_ν induced by neutrinos on ^{12}C target. We have studied the uncertainty in the total cross sections due to the use of various parameterizations of the weak N-Δ transition form factors used in literature. The various theoretical curves show the cross sections for the charged current one π^+ production with nuclear medium and final state interaction effects and calculated by using Schreiner and von Hippel [124](dashed-dotted line), Paschos et al. [146](dashed line) and Lalakulich et al. [147](solid line) weak N-Δ transition form factors. The cross sections obtained with the N-Δ transition form factors given by Paschos et al. [146] and Lalakulich et al. [147] are larger than the cross sections obtained by using the Schreiner and von Hippel [124] parameterization. We find that the cross section obtained by using Paschos et al. [146] and Lalakulich et al. [147] N-Δ transition form factors are respectively 7-8% for neutrino energies E_ν=0.5-3 GeV. The cross sections obtained by using Paschos et al. [146] and Lalakulich et al. [147] N-Δ transition form factor are 10-12% and 10-18% larger than the cross section obtained by using Schreiner and von Hippel [124] N-Δ transition form factors, respectively.

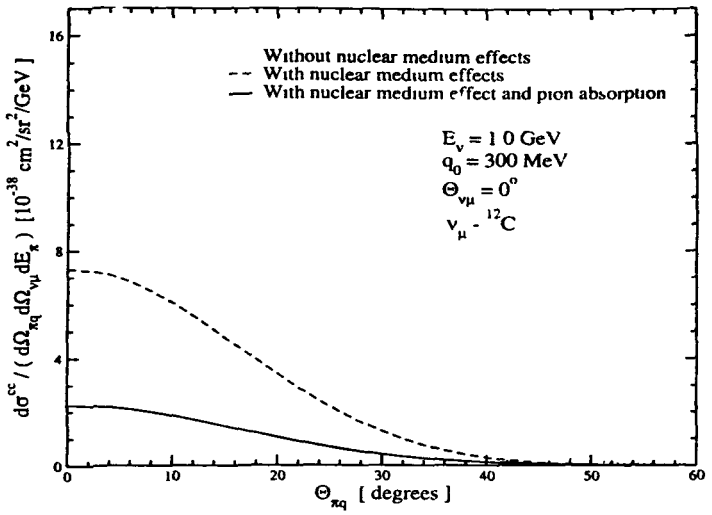

Figure 5.1: $\frac{d^3\sigma}{d\Omega_{\pi q} d\Omega_{\nu\mu} dE_\pi}$ vs pion angle $\Theta_{\pi q}$ for the charged current coherent pion production on ^{12}C nucleus with neutrino beam of E_ν=1.0 GeV.

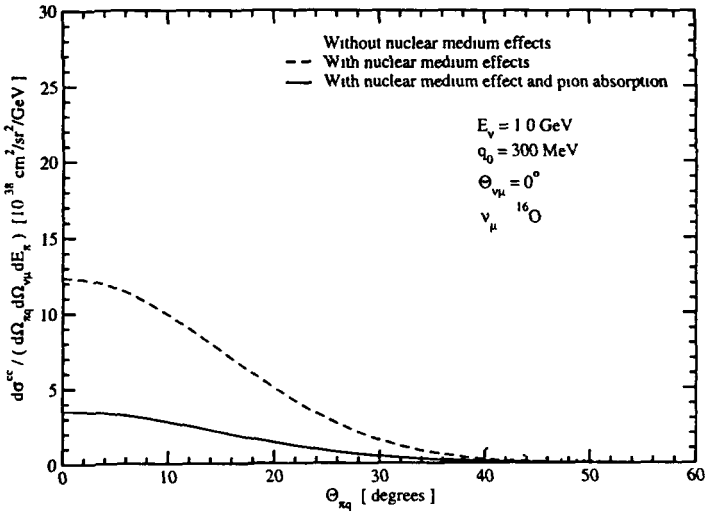

Figure 5.2: $\frac{d^3\sigma}{d\Omega_{\pi q} d\Omega_{\nu\mu} dE_\pi}$ vs pion angle $\Theta_{\pi q}$ for the charged current coherent pion production on ^{16}O nucleus with neutrino beam of E_ν=1.0 GeV

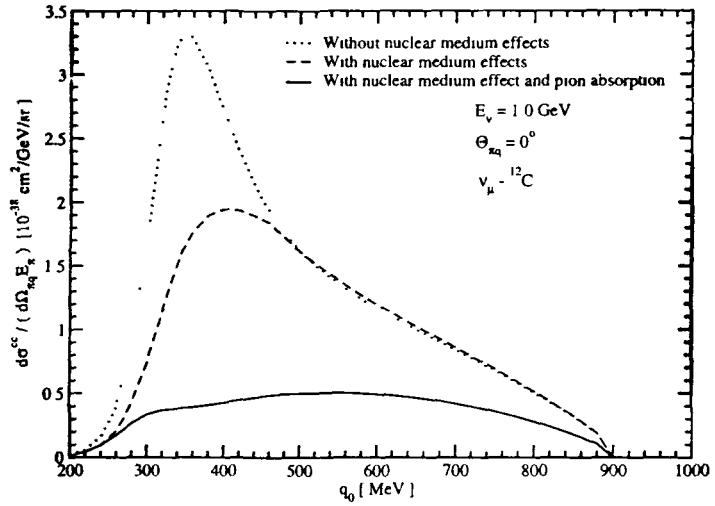

Figure 5.3: $\frac{d^2\sigma}{d\Omega_{\pi q} dE_\pi}$ vs q_0 for the charged current coherent pion production on ^{12}C nucleus with neutrino beam of E_ν=1.0 GeV.

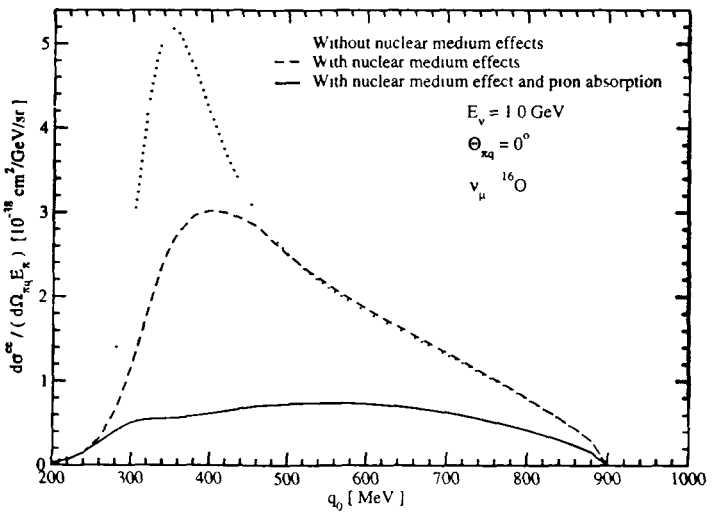

Figure 5.4: $\frac{d^2\sigma}{d\Omega_{\pi q} dE_\pi}$ vs q_0 for the charged current coherent pion production on ^{16}O nucleus with neutrino beam of E_ν=1.0 GeV.

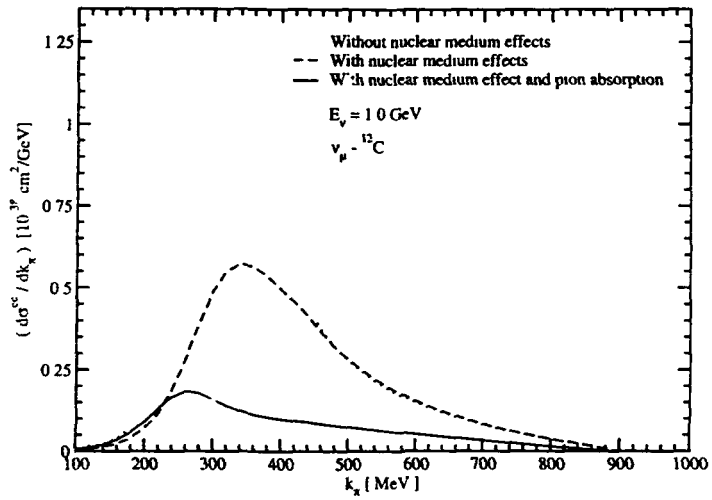

Figure 5 5 Momentum distribution of the pions $\frac{d\sigma}{dk_\pi}$ vs k_π at E_ν=1 0 GeV for the charged current coherent pion production on ^{12}C nucleus

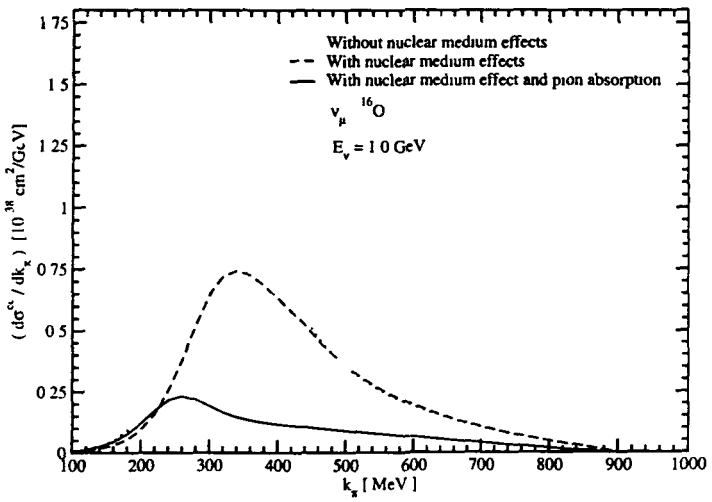

Figure 5 6 Momentum distribution of the pions $\frac{d\sigma}{dk_\pi}$ vs k_π at E_ν=1 0 GeV for the charged current coherent pion production on ^{16}O nucleus

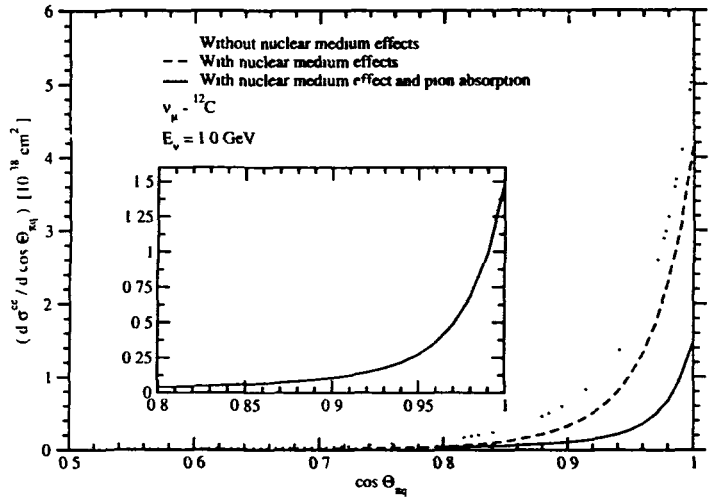

Figure 5.7: Angular distribution of the pions $\frac{d\sigma}{d\cos\Theta_{\pi q}}$ vs $\cos\Theta_{\pi q}$ at E_ν=1.0 GeV for the charged current coherent pion production on ^{12}C nucleus.

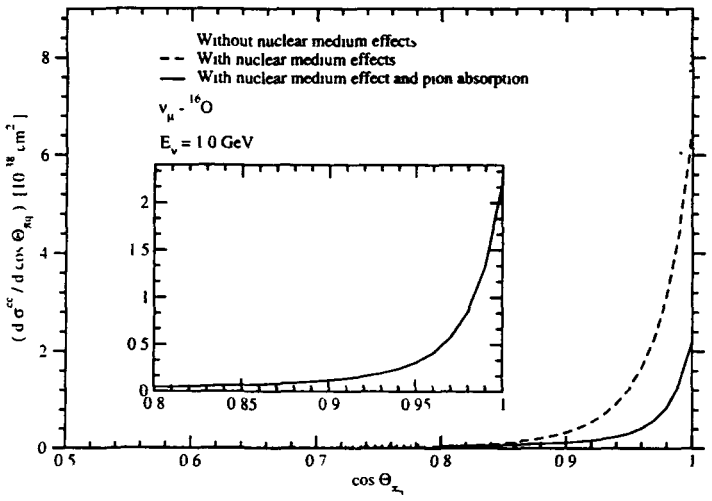

Figure 5.8 Angular distribution of the pions $\frac{d\sigma}{d\cos\Theta_{\pi q}}$ vs $\cos\Theta_{\pi q}$ at E_ν=1.0 GeV for the charged current coherent pion production on ^{16}O nucleus

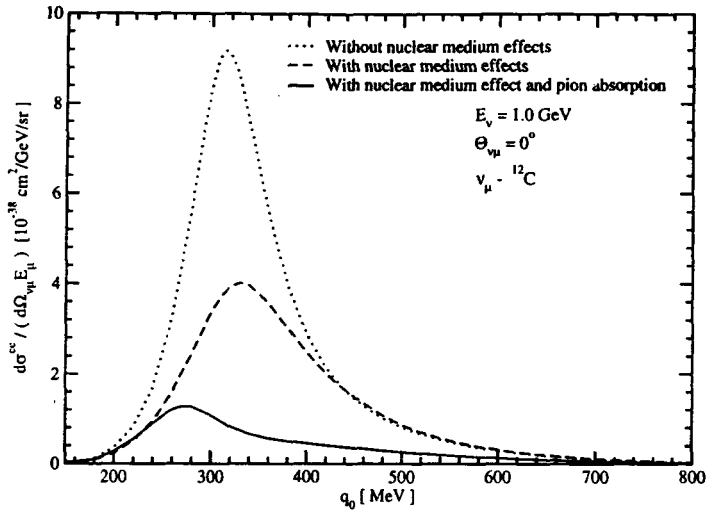

Figure 5.9: $\frac{d^2\sigma}{d\Omega_{\nu\mu}dE_\mu}$ vs q_0 for the charged current coherent lepton production on ^{12}C nucleus with neutrino beam of E_ν=1.0 GeV.

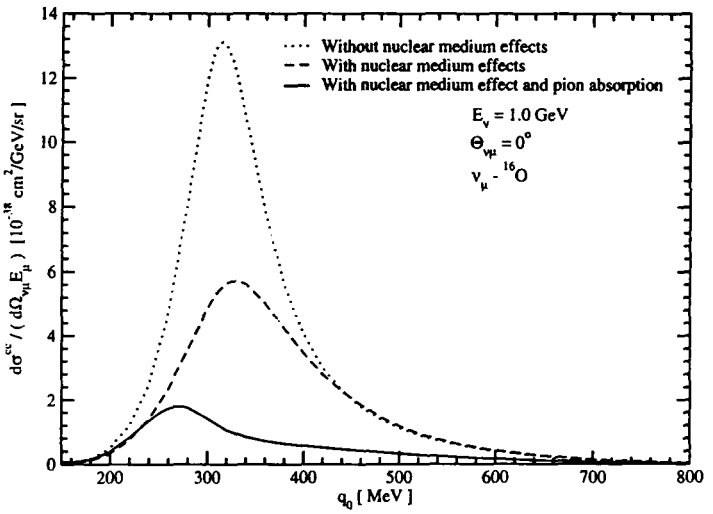

Figure 5.10: $\frac{d^2\sigma}{d\Omega_{\nu\mu}dE_\mu}$ vs q_0 for the charged current coherent lepton production on ^{16}O nucleus with neutrino beam of E_ν=1.0 GeV.

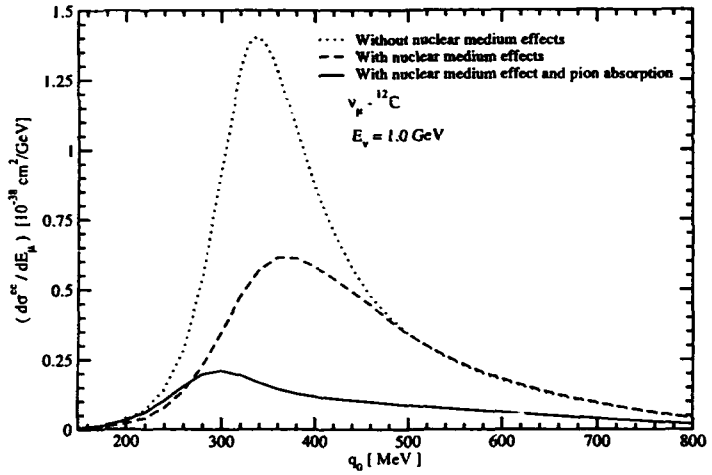

Figure 5.11: Energy spectrum of the leptons $\frac{d\sigma}{dE_\mu}$ vs q_0 at E_ν=1.0 GeV for the charged current coherent lepton production on ^{12}C nucleus.

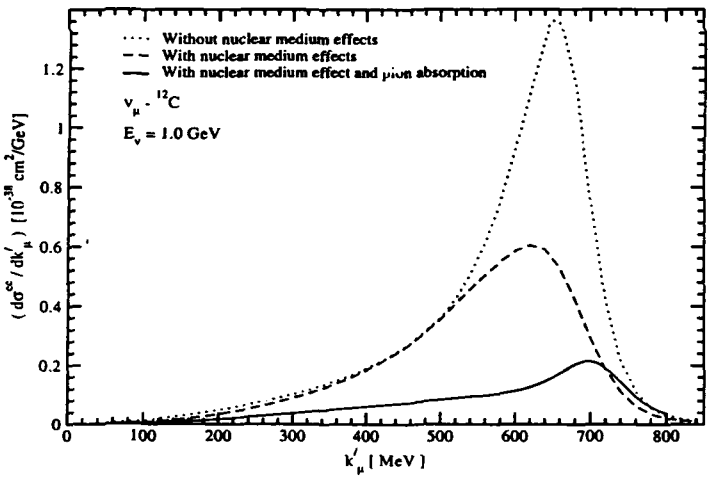

Figure 5.12: Momentum distribution $\frac{d\sigma}{dk'_\mu}$ vs k'_μ at E_ν=1.0 GeV for the charged current coherent lepton production on ^{12}C nucleus.

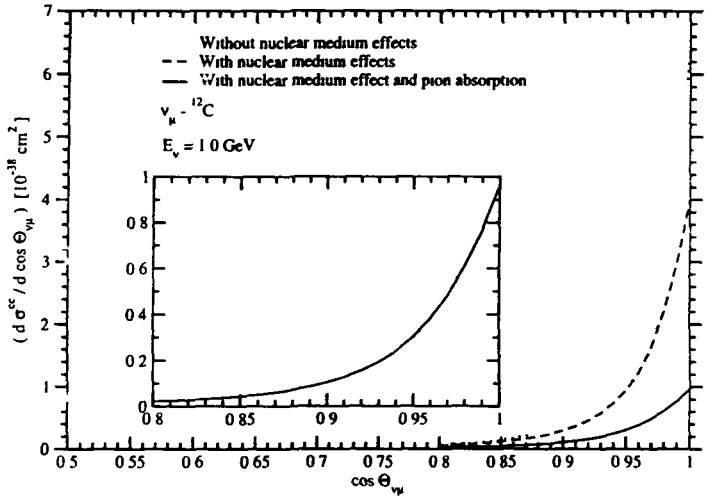

Figure 5.13: Angular distribution of the leptons $\frac{d\sigma}{d\cos\Theta_{\nu\mu}}$ vs $\cos\Theta_{\nu\mu}$ at E_ν=1.0 GeV for the charged current coherent lepton production on ^{12}C nucleus.

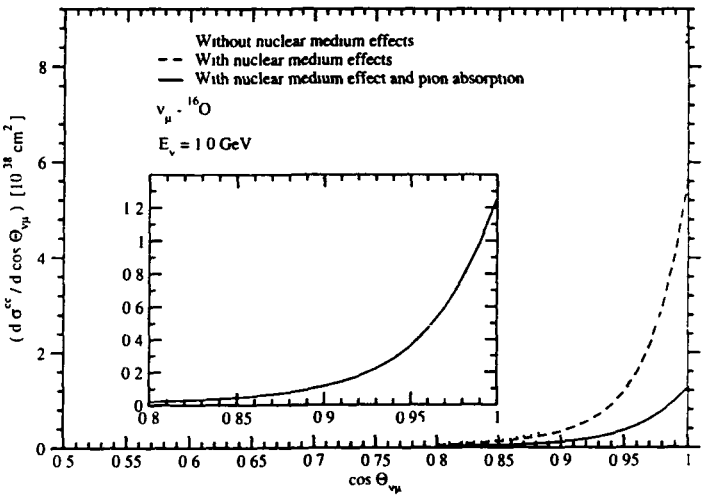

Figure 5.14: Angular distribution of the leptons $\frac{d\sigma}{d\cos\Theta_{\nu\mu}}$ vs $\cos\Theta_{\nu\mu}$ at E_ν=1.0 GeV for the charged current coherent lepton production on ^{16}O nucleus.

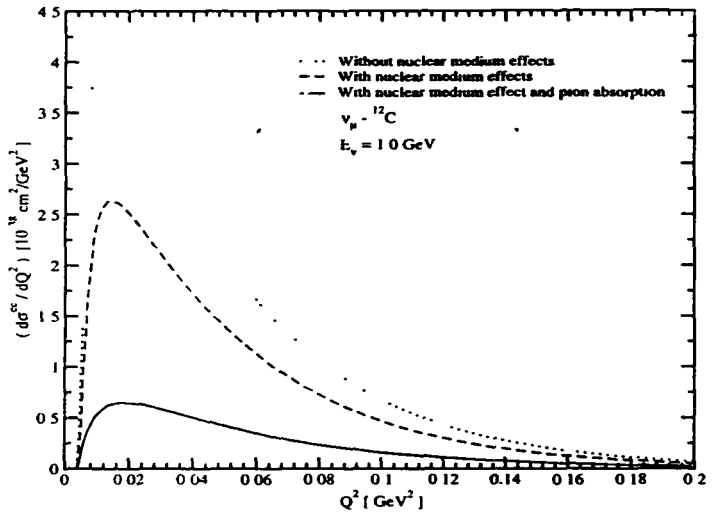

Figure 5.15: Differential cross section $\frac{d\sigma}{dQ^2}$ vs Q^2 at E_ν=1.0 GeV for the charged current coherent pion production on ^{12}C nucleus.

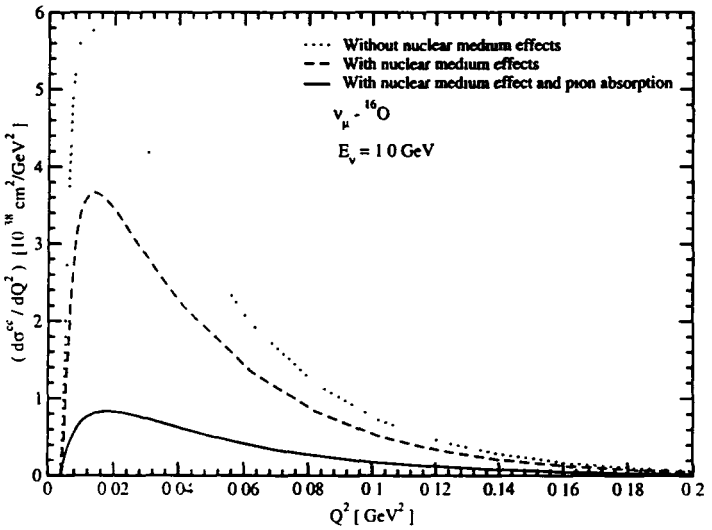

Figure 5.16: Differential cross section $\frac{d\sigma}{dQ^2}$ vs Q^2 at E_ν=1.0 GeV for the charged current coherent pion production on ^{16}O nucleus.

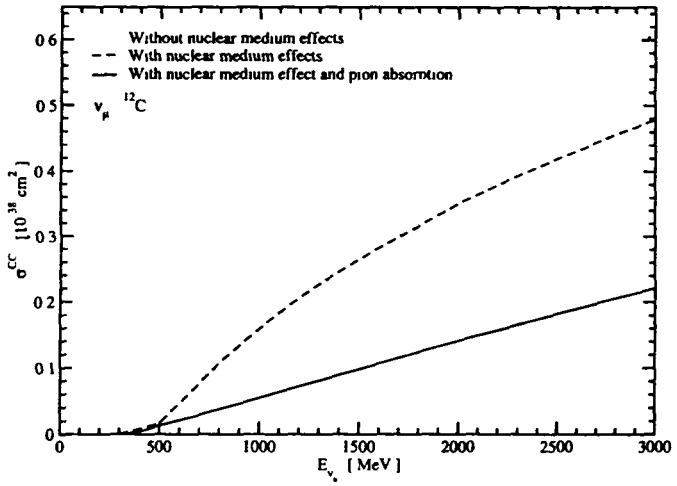

Figure 5 17 Total cross section $\sigma(E_\nu)$ vs E_ν for the charged current coherent pion production in ^{12}C nucleus.

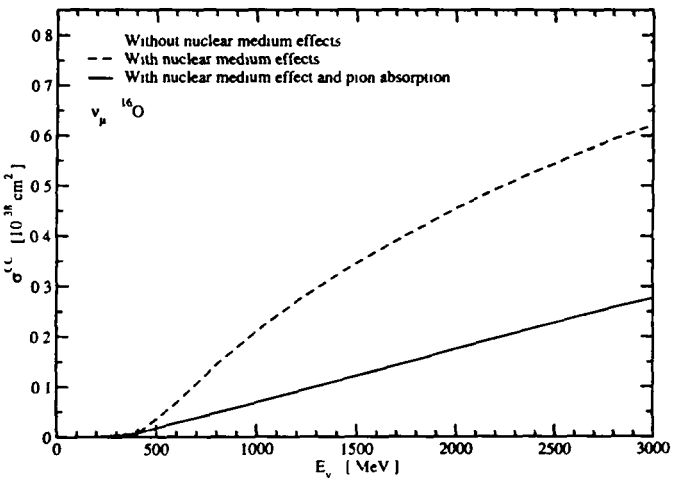

Figure 5 18 Total cross section $\sigma(E_\nu)$ vs E_ν for the charged current coherent pion production in ^{12}C nucleus

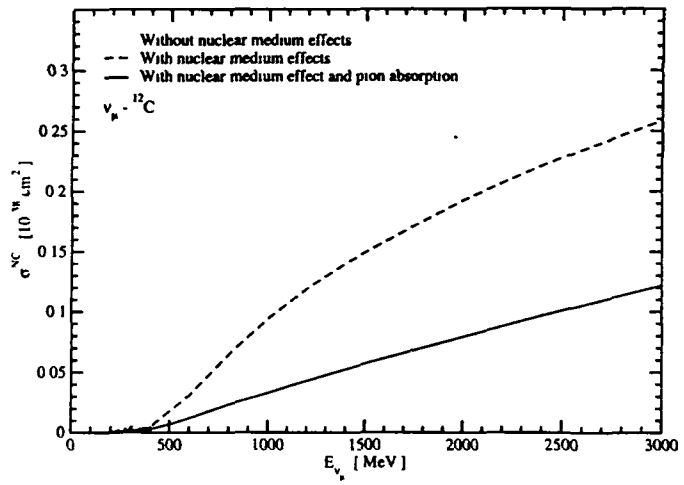

Figure 5 19 Total cross section $\sigma(E_\nu)$ vs E_ν for the neutral current coherent pion production in ^{12}C nucleus

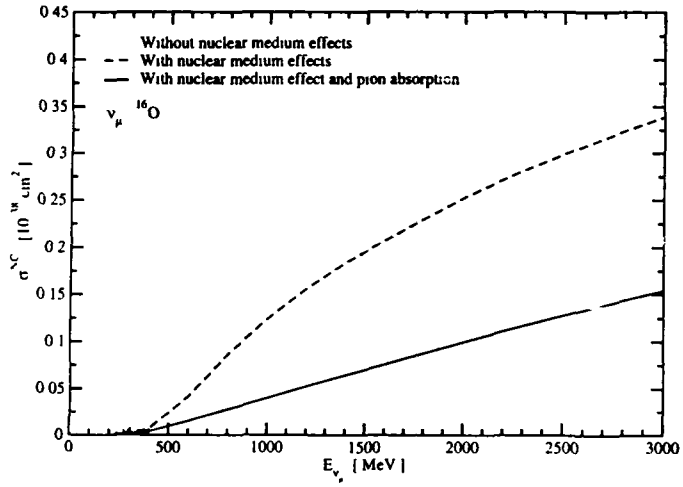

Figure 5 20 Total cross section $\sigma(E_\nu)$ vs E_ν for the neutral current coherent pion production in ^{16}O nucleus

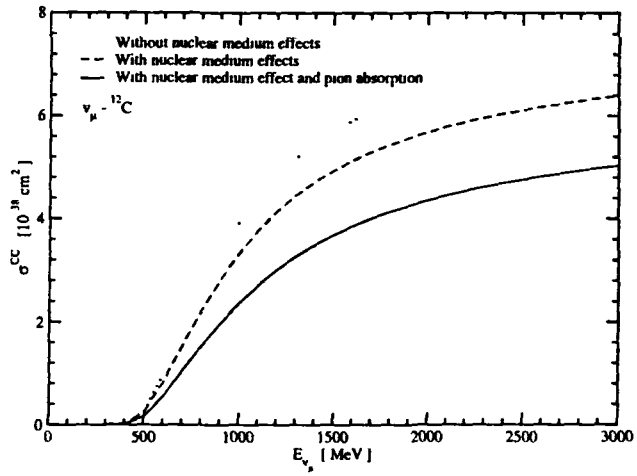

Figure 5.21: Charged current one pion production cross section $\sigma(E_\nu)$ vs E_ν induced by neutrinos on ^{12}C target using the Lalakulich's [147] N-Δ weak transition form factors for the incoherent processes.

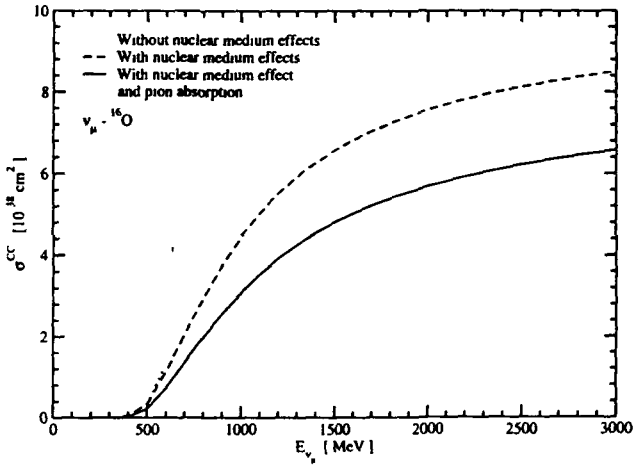

Figure 5.22 Charged current one pion production cross section $\sigma(E_\nu)$ vs E_ν induced by neutrinos on ^{16}O target using the Lalakulich's [147] N-Δ weak transition form factors for the incoherent processes

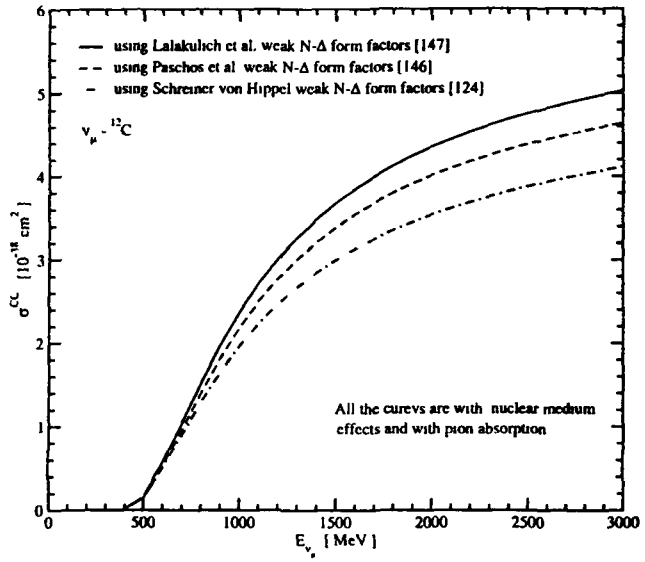

Figure 5.23: Charged current one pion production cross section $\sigma(E_\nu)$ vs E_ν induced by neutrinos on ^{12}C target. The various curves are the cross sections for the charged current one π^+ production with nuclear medium and final state interaction effects and calculated by using Schreiner and von Hippel [124](dashed-dotted line), Paschos et al. [146](dashed line) and Lalakulich et al. [147](solid line) weak N-Δ transition form factors.

5.2 Application to β-Beam Neutrinos at intermediate Energies

For the purpose of future long base line neutrino oscillation experiments, one of the new sources of neutrino beams is the β-beams, provide a source of pure single flavor, well collimated and intense neutrino(antineutrino) beams with a well defined energy spectrum obtained from the β-decay of accelerated radioactive ions boosted by a suitable Lorentz factor γ. The radioactive ion and the Lorentz boost factor γ can be properly chosen to provide the low energy [82]-[90], intermediate and high energy [293], [295], [296], [312]-[316] neutrino beams according to the needs of a planned experiment. In the feasibility study of β-beams, ^{6}He ions with a Q value of 3.5 MeV and ^{18}Ne ions with a Q value of 3.3 MeV are considered to be the most suitable candidates to produce antineutrino and neutrino beams [317].

We have calculated the nuclear response for the β-beam neutrinos (antineutrinos) of intermediate energy corresponding to the various values of γ discussed in the literature. In particular, we study the neutrino nucleus interaction cross sections in ^{16}O for β-beam neutrino(antineutrino) energies corresponding to the Lorentz boost factor γ in the range of $60< \gamma <250$ (150). The energy spectrum of β-beam neutrinos(antineutrinos) from ^{18}Ne(^{6}He)

ion source in the forward angle($\theta = 0^o$) geometry, corresponding to the Lorentz boost factor γ is given by [84], [85]:

$$\Phi_{lab}(E_\nu, \theta = 0) = \frac{\Phi_{cm}(E_\nu \gamma[1 - \beta])}{\gamma[1 - \beta]}$$
$$\Phi_{cm}(E_\nu) = bE_\nu^2 E_e p_e F(Z', E_e)\Theta(E_e - m_e) \quad (5.1)$$

In the above equation $b = ln2/m_e^5 ft_{1/2}$ and $E_e(= Q - E_\nu)$, p_e are the energy and momentum of the outgoing electron, Q is the Q value of the beta decay of the radioactive ion $A(Z, N) \rightarrow A(Z', N') + e^-(e^+) + \bar{\nu}_e(\nu_e)$ and $F(Z', E_e)$ is the Fermi function. In Fig. 5.24, we show the representative spectra for neutrinos(antineutrinos) corresponding to the Lorentz boost factor γ =250 (150).

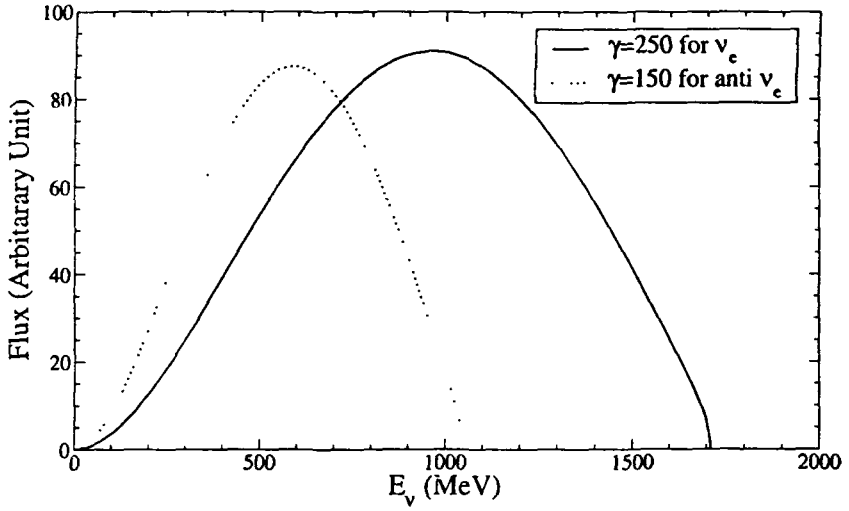

Figure 5.24: Neutrino(solid line) energy spectrum obtained with ^{18}Ne boosted at $\gamma = 250$ and antineutrino(dashed line) energy spectrum obtained with ^{6}He boosted at $\gamma = 150$.

In this energy region the dominant contribution to the charged lepton production cross section comes from the quasielastic reactions. However, the high energy neutrinos corresponding to the tail of an energy spectrum, specially for higher γ (see Fig.5.24), can contribute to the inelastic production of charged leptons through the excitation of the Δ-resonance. In addition to the genuine inelastic production of the charged leptons which will be accompanied by the pions, the neutral current induced inelastic production of π^0 without any charged lepton in the final state can mimic the quasielastic production of charged leptons in which one of the photons from the π^0 decays is misidentified as a signature of the quasielastic electron production. We, therefore, study the quasielastic and the inelastic production of charged leptons induced by the charge current. We also study the neutral current induced production of π^0 which gives

Table 5.1: Cross sections $\langle\sigma\rangle_{\nu_e}$ $(10^{-40}cm^2)$ averaged over the β beam neutrino spectrum for various Lorentz boost factor γ(column I) and corresponding average energies of neutrinos (column II). Columns III and IV give the total cross sections for the quasielastic and the inelastic charged lepton production process and column V gives the the total cross section for the inelastic neutral current production of π^0.

γ	$\langle E_{\nu_e}\rangle$	$\langle\sigma\rangle^{cc}_{qe}$	$\langle\sigma\rangle^{cc}_{inel}$	$\langle\sigma\rangle^{nc}_{inel}$
60	226	131	0.87	0.24
75	282	199	6.3	1.7
100	376	307	33	9
150	564	468	131	35.3
200	752	563	238	64
250	940	617	331	88.7

major contribution to the background of the electron production in the quasielastic reactions induced by neutrinos and antineutrinos.

The numerical results for the total cross section $\sigma(E_{\nu_e})$ induced by neutrino and antineutrino in ^{16}O for the quasielastic, inelastic charged lepton production processes, and inelastic neutral current production of π^0 showing their relative contributions is given in Ref. [138]. Here, we present the flux averaged cross section $\langle\sigma\rangle$, in order to estimate the relative contribution of the quasielastic and the inelastic production of charged leptons and also the background to the quasielastic events due to the neutral current induced neutral pion production at a far detector in a base line experiment, defined as

$$\langle\sigma\rangle = \frac{\int_0^\infty dE_\nu \Phi_{lab}(E_\nu, \theta = 0)\sigma(E_\nu)}{\int_0^\infty dE_\nu \Phi_{lab}(E_\nu, \theta = 0)} \tag{5.2}$$

for the neutrino and the antineutrino energies. This is relevant for the future CERN-FREJUS base line experiments which can be done with the present CERN-SPS and have been discussed in the literature [312]-[314]. The forward angle approximation for the neutrino flux used in Eq.5.9 to calculate the total cross section is quite good for a far detector specially for higher values of the Lorentz factor γ. Quantitatively, we find that the contribution to the total cross section from non-zero θ flux i.e. $\Phi_{lab}(E_\nu, \theta \neq 0)$ is about 5% for $\gamma = 60$ and reduces to less than 1% for $\gamma = 250$. In Tables-5.1 and 5.2, we show the results of the flux averaged cross section $\langle\sigma\rangle$ for neutrino and antineutrino reactions for various values of the Lorentz boost factor γ where we can see the relative contributions of the cross sections for quasielastic and inelastic production of leptons along with the cross sections for neutral current induced production of neutral pions which is the major source of background to the quasielastic events at intermediate energies.

Table 5.2: Cross sections $\langle\sigma\rangle_{\bar{\nu}_e}$ $(10^{-40}cm^2)$ averaged over the β beam antineutrino spectrum for various Lorentz boost factor γ(column I) and corresponding average energies of antineutrinos (column II). Columns III and IV are give the total cross sections for the quasielastic and the inelastic charged lepton production process, while column V gives the total cross section for the inelastic neutral current production of π^0.

γ	$\langle E_{\bar{\nu}_e}\rangle$	$\langle\sigma\rangle^{cc}_{qe}$	$\langle\sigma\rangle^{cc}_{inel}$	$\langle\sigma\rangle^{nc}_{inel}$
60	232	33.2	0.0855	0.028
75	290	46.6	1.2	0.38
100	387	69	7.2	2.2
150	580	111	32	9.5

5.3 Application to Atmospheric Neutrinos in ^{56}Fe

The major sources of uncertainty in the theoretical prediction of the charged leptons of muon and electron flavor produced by the atmospheric neutrinos come from the uncertainties in the calculation of atmospheric neutrino fluxes and neutrino nuclear cross sections. The atmospheric neutrino fluxes at various experimental sites of Kamioka, Soudan and Gransasso have been extensively discussed in literature by many authors [318]-[321]. We have studied the neutrino nuclear cross section in ^{56}Fe nuclei which are relevant for the atmospheric neutrino experiments. The uncertainty in the nuclear production cross section of leptons from ^{56}Fe nuclei by the atmospheric neutrinos are discussed.

The numerical results for the total cross section for the quasielastic processes as a function of energy for neutrino reactions on iron in the energy region relevant to the fully contained events of atmospheric neutrinos i.e E <3 GeV, have been discussed in section-2.7.6, The detail numerical results for the momentum distribution, angular distribution as well as the total cross section for the quasielastic and inelastic production of leptons on iron nuclei for all flavor of neutrinos i.e. ν_μ, $\bar{\nu}_\mu$, ν_e and $\bar{\nu}_e$ have been discussed in Ref. [136].

The energy dependences of the quasielastic and inelastic lepton production cross sections have been used to calculate the lepton production by atmospheric neutrinos after averaging over the neutrino flux corresponding to the two sites of Soudan and Gransasso, where iron based detectors are being used. There are quite a few calculations of atmospheric neutrino fluxes at these two sites. We use the angle averaged fluxes calculated by Honda et al. [319] and Barr et al. [320] for the Soudan site and the fluxes of Barr et al. [320] and Plyaskin [321] for the Gransasso site to calculate the flux averaged cross section $\langle\sigma\rangle$ and also the momentum and the angular distributions for leptons produced by ν_e, $\bar{\nu}_e$, ν_μ and $\bar{\nu}_\mu$ [136].

Here, we present the lepton yields Y_l for lepton of flavor l which we define as

$$Y_l = \int \Phi_{\nu_l}\, \sigma(E_{\nu_l})\, dE_{\nu_l} \tag{5.3}$$

where, Φ_{ν_l} is the atmospheric neutrino flux of ν_l and $\sigma(E_{\nu_l})$ is the total cross section for neutrino ν_l of energy E_{ν_l}. We calculate this yield separately for the quasielastic and inelastic events. We define a relative yield of muon over electron type events by R as $R = R_{\mu/e} = \frac{Y_\mu + Y_{\bar{\mu}}}{Y_e + Y_{\bar{e}}}$ for quasielastic and inelastic events and present our results in Table-5.3. We study the nuclear model dependence as well as the flux dependence of the relative yield R.

Table 5.3: Ratio $R = R_{\mu/e} = \frac{Y_\mu + Y_{\bar{\mu}}}{Y_e + Y_{\bar{e}}}$ corresponding to quasielastic, inelastic and total production of leptons [FG refers to Fermi Gas Model, NM refers to Nuclear Model, FN refers to Free Nucleon, ΔN refers to Δ in Nuclear Model, ΔF refers to Δ Free]. R_F shows the ratio of total lepton yields for muon to electron for the case of free nucleon and R_N shows the ratio of total yields for muon to electron for the case of nucleon in the nuclear medium.

Site	Soudan	Soudan	Soudan	Gransasso	Gransasso
FLUX	Barr et al. [320]	Plyaskin [321]	Honda et al. [319]	Barr et al. [320]	Plyaskin [321]
Quasielastic					
R_{NM}	1.80	1.65	1.89	1.95	2.00
R_{FG}	1.81	1.66	1.89	1.95	2.09
R_{FN}	1.82	1.68	1.90	1.95	2.08
Inelastic					
$R_{\Delta N}$	1.84	1.81	1.95	2.02	2.05
$R_{\Delta F}$	1.82	1.80	1.94	2.01	2.03
Total					
R_N	1.81	1.68	1.90	1.96	2.01
R_F	1.82	1.69	1.90	1.96	2.07

The results for R are presented separately for quasielastic events, inelastic events and the total events in Table-5.3. For quasielastic events $\nu_l(\bar{\nu}_l) + ^{56} Fe \rightarrow l^-(l^+) + X$, the results are presented for the case of free nucleon by R_{FN}, for the nuclear case with Fermi gas model description of Llewellyn Smith [7] by R_{FG} and for the case of nuclear effects within our model by R_{NM}. We see that there is practically no nuclear model dependence on the value of R (compare the values of R_{NM}, R_{FG} and R_{FN} for the same fluxes at each site). This is also true for the inelastic production of leptons i.e. $\nu_l(\bar{\nu}_l) + ^{56} Fe \rightarrow l^-(l^+) + \pi^+(\pi^-) + X$ for which the ratio for free nucleon case (denoted by $R_{\Delta F}$) and the ratio for the nuclear case

Table 5.4: % ratio $r = \frac{Y_\Delta}{Y_{q\,e\,+\Delta}}$ [N refers to Nuclear Model, F refers to free case]

Sites	Soudan	Soudan	Soudan	Gransasso	Gransasso
FLUX	Barr et al. [320]	Plyaskin [321]	Honda et al. [319]	Barr et al. [320]	Plyaskin [321]
$r_\mu(F)$	14	12	14	15	12
$r_e(F)$	14	11	14	14	12
$r_\mu(N)$	22	20	22	23	19
$r_e(N)$	22	19	22	22	19

in our model (denoted by $R_{\Delta N}$) are presented in Table-5.3. It is, therefore, concluded that there is no appreciable nuclear model dependence on the ratio of total lepton yields for the production of muons and electrons(compare the values of R_F and R_N, where R_F shows the ratio of total lepton yields for muon and electron for the case of free nucleon and R_N shows the ratio of total yield for muon and electron for the case of nucleon in the nuclear medium).

However, there is some dependence of the ratio R on the atmospheric neutrino fluxes. The flux dependence of R can be readily seen from Table-5.3, for the two sites of Soudan and Gransasso. At the Gransasso site, we see that there is 4-5% difference in the value of R_N for the total lepton yields for the fluxes of Barr et al. [320] and Plyaskin [321]. At Soudan site, the results for the fluxes of Honda et al. [319] and Barr et al.[320] are within 4-5% but the flux calculation of Plyaskin [321] gives a result which is about 10-11% smaller than the results of Honda et al. [319] and 7-8% smaller than the results of Barr et al. [320]. The flux dependence is mainly due to the quasielastic events. This should be kept in mind while using the flux of Plyaskin [321] for making any analysis of the neutrino oscillation experiments.

In Table-5.4, we present a quantitative estimate of the relative yield of inelastic events r_l defined by $r_l = \frac{Y_l^\Delta}{Y_l}$, where $Y_l^\Delta = Y_l^\Delta + Y_{\bar{l}}^\Delta$ is the lepton yield due to the inelastic events and Y_l is the total lepton yield due to the quasielastic and inelastic events i.e.$Y_l = Y_l^{q\,e} + Y_{\bar{l}}^{q\,e} + Y_l^\Delta + Y_{\bar{l}}^\Delta$. The relative yield for the case of free nucleon is shown by $r_l(F)$ and for the case with the nuclear effects in our model is shown by $r_l(N)$. We see that for free nucleons, the relative yield of the inelastic events due to Δ excitation is in the range of 12-15% for various fluxes at the two sites. The ratio is approximately same for electrons and muons. When the nuclear effects are taken into account this becomes 19-22%. This is due to different nature of the effect of nuclear structure on the quasielastic and inelastic production cross scetions which gives a larger reduction in the cross section for the quasielastic case as compared to the inelastic case.

In all these results presented here, we have not taken into account the final state interactions, which will further lead to the reduction in the cross sections.

5.4 Application to Accelerator Neutrino Cross Sections in ^{12}C and ^{16}O

In section-5.1, we have presented and discussed the differential and the total cross sections for the coherent and incoherent neutrino production of pions and leptons induced by muon type neutrino from ^{12}C and ^{16}O nuclei. In this section, we have applied these results to the atmospheric neutrinos, and the theoretical results have been compared with the experimental results. We see that our results are in good agreement with experimentally observed values. We have obtained the fluxed averaged differential and total cross sections for the K2K and MiniBooNE neutrino spectra, and are compared with the recently inferred value in K2K and MiniBooNE experiments [57], [62]. In view of some new data to be expected soon from K2K and MiniBooNE collaborations, we discuss the implications of our results for K2K and MiniBooNE neutrino energies and other neutrino oscillation experiments in this energy region.

5.4.1 Momentum Distributions

A. Coherent Production

In Fig.5.25 and Fig.5.26, we have presented the results for the momentum distribution of pion $\langle\frac{d\sigma^{CC}}{dk_\pi}\rangle$ as a function of the pion momentum k_π, averaged over the MiniBooNE and K2K spectra for ν_μ induced reaction in ^{12}C. The results have been presented for the differential cross section without the nuclear medium effects, with the nuclear medium effects, and with the nuclear medium modification and final state interaction effects. We find that the effects due to nuclear medium and nuclear medium with final state interaction effects follow the same trend as discussed in case of the the momentum distribution of pion $\left(\frac{d\sigma^{CC}}{dk_\pi}\right)$ in Fig.5.5. Similar is the case we found in the momentum distribution of pion $\langle\frac{d\sigma^{CC}}{dk_\pi}\rangle$ averaged over the K2K spectrum for ν_μ induced reaction in ^{16}O shown in Fig.5.27. In the inset of these figures, we show explicitly our final results which include both the renormalization of the Δ properties in the nuclear medium and the final state interaction of the pion with the final nucleus.

In Fig.5.28, we have presented our final result which include both the nuclear medium modification and final state interaction effects, for the differential cross sections $\langle\frac{d\sigma^{CC}}{dk_\pi}\rangle$ averaged over the MiniBooNE spectrum for ν_μ induced reaction in ^{12}C (solid line), averaged over the K2K spectrum for ν_μ induced reaction in ^{12}C (dotted line) and averaged over the K2K spectrum for ν_μ induced reaction in ^{16}O (dashed line). We see that the peak occurs at the same position but values of the cross sections are different due to the different average energies of the MiniBooNE and K2K spectra, and also due to different nuclei. The average energy of the MiniBooNE spectrum is around $\langle E_{\nu_\mu}\rangle$=750 MeV and of the K2K spectrum is around $\langle E_{\nu_\mu}\rangle$=1.3 GeV.

B. Incoherent Production

In Fig.5.29, we have presented the results for the momentum distribution of lepton $\langle \frac{d\sigma}{dp_\mu} \rangle$, which will decay into pions, as a function of the lepton momentum $\mathbf{p}_\mu$, averaged over the MiniBooNE neutrino spectrum, for ν_μ induced charged current reaction in ^{12}C. The results have been presented for the differential cross section without the nuclear medium effects, with the nuclear medium effects, and with the nuclear medium modification and pion absorption. We find a reduction of about 12-15% around the peak region of the momentum distribution due to the medium modification of strong interaction properties of the Δ, and after the peak region the reduction is almost $\approx$15%. We find a further reduction in the momentum distribution of the lepton spectrum to be around $\approx$25% in the peak region due to the medium modification effects and the pion absorption effect, and it is around 25-30% after the peak region.

In Fig.5.30, we have presented the results for the momentum distribution of lepton $\langle \frac{d\sigma}{dp_\mu} \rangle$ which will be accompanied by the pions, as a function of the lepton momentum $\mathbf{p}_\mu$, averaged over the K2K neutrino spectrum for ν_μ induced charged current reaction in ^{16}O. We can see that the peak region in this case is broader than the momentum distribution averaged over MiniBooNE neutrino spectrum. We find a reduction of about 10-15% in the peak region (p_μ=0.2-0.8 GeV) due to the nuclear medium effects. The effect of the nuclear medium effects and the pion absorption effect give a further reduction in the peak region which is around 20-30%.

In Fig.5.31 and Fig.5.32, we show the results for the lepton momentum distribution $\langle \frac{d\sigma}{dp_\mu} \rangle$ which will be accompanied by the pions, as a function of the lepton momentum $\mathbf{p}_\mu$, averaged over the MiniBooNE and K2K neutrino spectra for ν_μ induced charged current reaction in ^{12}C and ^{16}O, respectively. In Fig.5.31 and Fig.5.32, various theoretical curves show the results with nuclear medium and pion absorption effects and calculated by using Schreiner and von Hippel [124](dotted line), Paschos et al. [146](dashed line) and Lalakulich et al. [147](solid line) weak N-Δ transition form factors. The distribution obtained in both the cases, with the N-Δ transition form factors given by Paschos et al. [146] and Lalakulich et al. [147] are larger than the cross sections obtained by using the Schreiner and von Hippel [124] parameterization. In Fig.5.31, we find that the momentum distribution obtained by using Paschos et al. [146] and Lalakulich et al. [147] N-Δ transition form factors are respectively 6-8% for neutrino energies upto E_ν=2.0 GeV. The distribution obtained by using Paschos et al. [146] and Lalakulich et al. [147] N-Δ transition form factor are 8-12% and 15-20% larger than the distribution obtained by using Schreiner and von Hippel [124] N-Δ transition form factors, respectively. In Fig.5.32, the uncertainty in the momentum distribution due to the use of various parametrisations of the weak N-Δ transition form factors is similar in nature as discussed for Fig.5.31.

5.4.2 Angular Distributions

A. Coherent Production

In Fig.5.33 and Fig.5.34, we have presented the results for the angular distribution of pion $\langle \frac{d\sigma^{CC}}{d\cos\Theta_{\pi q}} \rangle$ as a function of $\cos\Theta_{\pi q}$, averaged over the MiniBooNE and K2K spectra for ν_μ induced reaction in ^{12}C nuclei. The angular distribution is found to be sharply peaked in the forward direction of the pion angle $\Theta_{\pi q}$. The reduction in the differential cross section $\langle \frac{d\sigma^{CC}}{d\cos\Theta_{\pi q}} \rangle$ averaged over the MiniBooNE spectrum for ν_μ induced reaction in ^{12}C decreases uniformly due to the nuclear medium effects as at $\cos\Theta_{\pi q}$=0.80, 0.90, 0.96 and 1.0 it is about 65%, 50%, 35% and 15%, respectively. The final state interaction of pion with the final nucleus further reduces the cross section and it is about 55-75% in the forward direction. In case of the differential cross section $\langle \frac{d\sigma^{CC}}{d\cos\Theta_{\pi q}} \rangle$ averaged over the K2K spectrum for ν_μ induced reaction in ^{12}C, the nuclear medium effects reduces the cross section as 65%, 50%, 30% and 10% at $\cos\Theta_{\pi q}$=0 80, 0.90, 0.96 and 1.0, respectively, and the pion absorption effects further reduces the cross section and it is about 50-75% in the forward direction. Similar is the case for the differential cross section $\langle \frac{d\sigma^{CC}}{d\cos\Theta_{\pi q}} \rangle$ averaged over the K2K spectrum for ν_μ induced reaction in ^{16}O nuclei, as shown in the Fig.5.35. In the inset of these figures, we show explicitly our final results which include both the renormalisation of the Δ properties in the nuclear medium and the final state interaction of the pion with the final nucleus.

In Fig.5.36, we show the result for differential cross sections $\langle \frac{d\sigma^{CC}}{d\cos\Theta_{\pi q}} \rangle$ averaged over the MiniBooNE spectrum for ν_μ induced reaction in ^{12}C (solid line), averaged over the K2K spectrum for ν_μ induced reaction in ^{12}C (dotted line) and averaged over the K2K spectrum for ν_μ induced reaction in ^{16}O (dashed line).

In Fig.5.37 and Fig.5.38, we have presented the results for the angular distribution of lepton $\langle \frac{d\sigma^{CC}}{d\cos\Theta_{\nu\mu}} \rangle$ as a function of $\cos\Theta_{\nu\mu}$, averaged over, the MiniBooNE spectrum for ν_μ induced reaction in ^{12}C nuclei and the K2K spectrum for ν_μ induced reaction in ^{16}O nuclei. The angular distribution is found to be sharply peaked in the forward direction of the lepton angle $\Theta_{\nu\mu}$. The reduction in the differential cross section $\langle \frac{d\sigma^{CC}}{d\cos\Theta_{\nu\mu}} \rangle$ averaged over the MiniBooNE spectrum for ν_μ induced reaction in ^{12}C, due to the nuclear medium effects is in the range of 30-35% in the forward direction. The final state interaction of pion with the final nucleus further reduces the cross section and it is about 55-75% in the forward direction In case of the differential cross section $\langle \frac{d\sigma^{CC}}{d\cos\Theta_{\nu\mu}} \rangle$ averaged over the K2K spectrum for ν_μ induced reaction in ^{16}O, reduction in the cross section lies in the range of 25-30% in the forward direction due to the nuclear medium effects, and the pion absorption effects is same as in case of MiniBooNE average. In the inset of these figures, we show explicitly our final results which include both the renormalisation of the Δ properties in the nuclear medium and the final state interaction of the pion with the final nucleus.

5.4.3 Q^2-Distributions

A. Coherent Production

In Fig.5.39, Fig.5.40 and Fig.5.41, we have presented the differential cross sections $\langle\frac{d\sigma^{CC}}{dQ^2}\rangle$ averaged over the K2K and MiniBooNE neutrino spectra. We have shown explicitly the nuclear medium and final state interaction effects in all these averaged differential cross sections. In Fig.5.39 and Fig.5.40, we have presented the Q^2-distributions averaged over, the MiniBooNE and the K2K neutrino spectra for ν_μ induced reaction in ^{12}C nuclei, respectively. In Fig.5.41, the Q^2-distributions averaged over, the K2K neutrino spectrum for ν_μ induced reaction in ^{16}O nuclei has been shown. In all these averaged cross sections, the effect of the nuclear medium and the nuclear medium with pion absorption effects are almost similar in nature as discussed for the differential cross section $\left(\frac{d\sigma^{CC}}{dQ^2}\right)$.

In Fig.5.42, we have presented our final result which include both the nuclear medium modification and final state interaction effects, for the differential cross sections $\langle\frac{d\sigma^{CC}}{dQ^2}\rangle$ averaged over the MiniBooNE neutrino spectrum for ν_μ induced reaction in ^{12}C (solid line), averaged over the K2K neutrino spectrum for ν_μ induced reaction in ^{12}C (dashed line) and averaged over the K2K neutrino spectrum for ν_μ induced reaction in ^{16}O (dotted line). We see that the peak occurs at the same position but values of the cross sections are different due to the different average neutrino energies of the MiniBooNE and K2K spectra, and also due to the different nuclei.

B. Incoherent Production

In Fig.5.43 and Fig.5.44, we have presented the results for the differential scattering cross section $\langle\frac{d\sigma}{dQ^2}\rangle$ vs Q^2 for charged current one π^+ production for the incoherent process averaged over the MiniBooNE and K2K neutrino spectra for ν_μ induced reaction in ^{12}C (Fig.5.43 for MiniBooNE) and ^{16}O (Fig.5.44 for K2K). The various curves are the results with the nuclear medium modification and final state interaction effects and obtained by using the different N-Δ transition form factors given by Schreiner and von Hippel [124], Paschos et al. [146] and Lalakulich et al. [147]. In Fig.5.43, we find that the nuclear medium effects lead to a reduction in the differential cross section of around 15% in the peak region of $Q^2 \leq 0.2$ GeV^2 and remain almost constant upto $Q^2 \leq 2.0$ GeV^2. When nuclear medium and final state interaction effects are taken into account the total reduction in the cross section is around 38% in the peak region of $Q^2 \leq 0.2$ GeV^2, after which it increases slightly as it becomes around 40% at $Q^2 \leq 2.0$ GeV^2. In Fig.5.44, the effect of the nuclear medium and the nuclear medium with pion absorption effects are similar in nature as discussed for Fig.5.43.

In Fig.5.45 and Fig.5.46, we have presented the results for the Q^2 distribution $\langle\frac{d\sigma}{dQ^2}\rangle$ as a function of Q^2 for charged current one π^+ production for the incoherent process with the nuclear medium modification and final state interaction effects and obtained by using the different N-Δ transition form factors given by Schreiner and von Hippel [124], Paschos et al. [146]

and Lalakulich et al. [147], averaged over the MiniBooNE and K2K spectrum for ν_μ induced reaction in ^{12}C (Fig.5.45 for MiniBooNE) and ^{16}O (Fig.5.46 for K2K). In Fig. 5.45, we find that in the peak region ($Q^2 \leq 0.2$ GeV^2), Q^2 distribution obtained by using Paschos et al. [146] and Lalakulich et al. [147] N-Δ transition form factors are respectively $5-7\%$ and it slightly increases upto 10% at Q^2=2.0 GeV^2. The distribution obtained by using Paschos et al. [146] are about $2-7\%$ (in the peak region $Q^2 \leq 0.2$ GeV^2) larger than the distribution obtained by using Schreiner and von Hippel [124] N-Δ transition form factors, and it further increases, as it becomes 20% at Q^2=1.0 GeV^2 and then decreases to 14% at Q^2=2.0 GeV^2. However, the distribution obtained by using Lalakulich et al. [147] are about $5-15\%$ (in the peak region $Q^2 \leq 0.2$ GeV^2) larger than the distribution obtained by using Schreiner and von Hippel [124] N-Δ transition form factors, and it further increases, as it becomes 25% at Q^2=1.0 GeV^2 and then decreases to 20% at Q^2=2.0 GeV^2. In Fig.5.46, the uncertainty in Q^2 distribution due to the use of various parametrisations of the weak N-Δ transition form factors is similar in nature as discussed for Fig.5.45.

==========*******==========

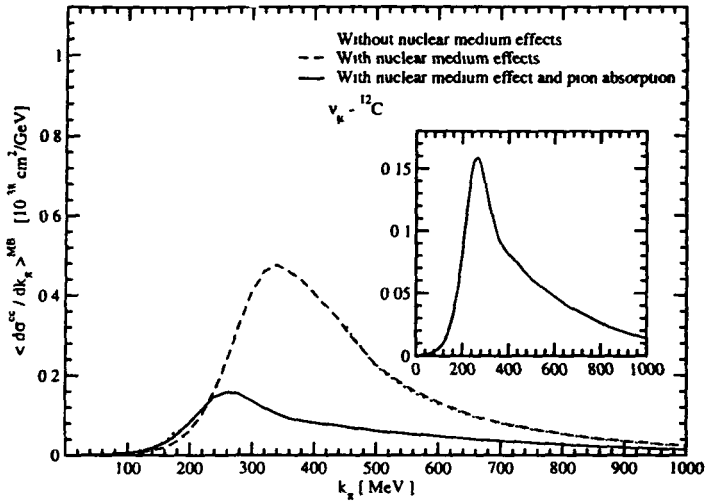

Figure 5 25 Momentum distribution of the pions $\langle \frac{d\sigma}{dk_\pi} \rangle$ vs k_π averaged over the MiniBooNE neutrino spectrum for the coherent charged current reaction induced by ν_μ in ^{12}C nucleus

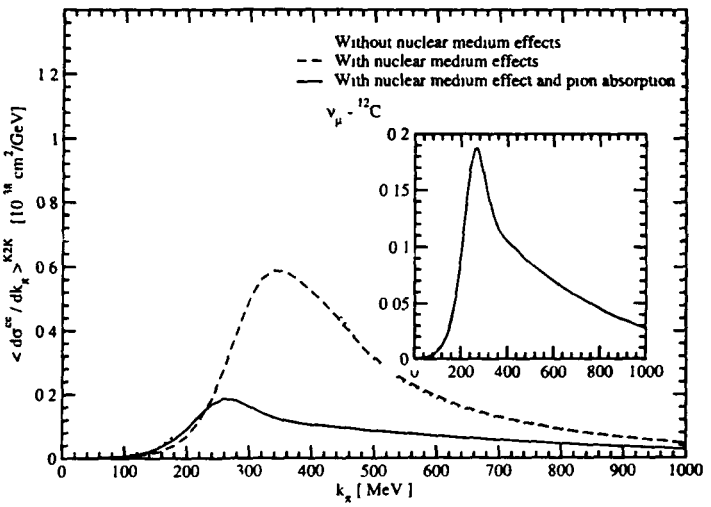

Figure 5 26 Momentum distribution of the pions $\langle \frac{d\sigma}{dk_\pi} \rangle$ vs k_π averaged over the K2K neutrino spectrum for the coherent charged current reaction induced by ν_μ in ^{12}C nucleus

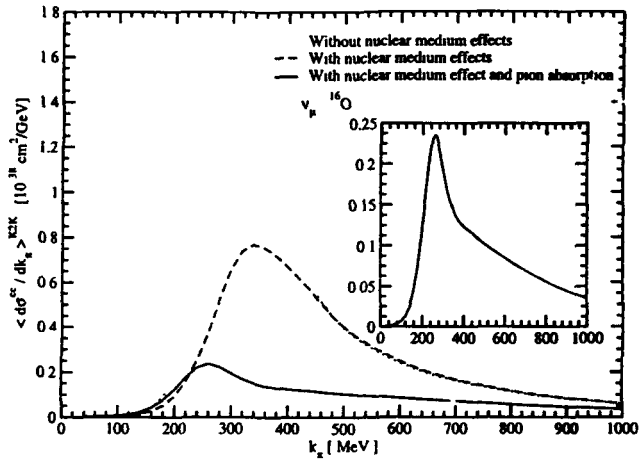

Figure 5.27: Momentum distribution of the pions $\langle \frac{d\sigma}{dk_\pi} \rangle$ vs $\mathbf{k}_\pi$ averaged over the K2K neutrino spectrum for the coherent charged current reaction induced by ν_μ in ^{16}O nucleus

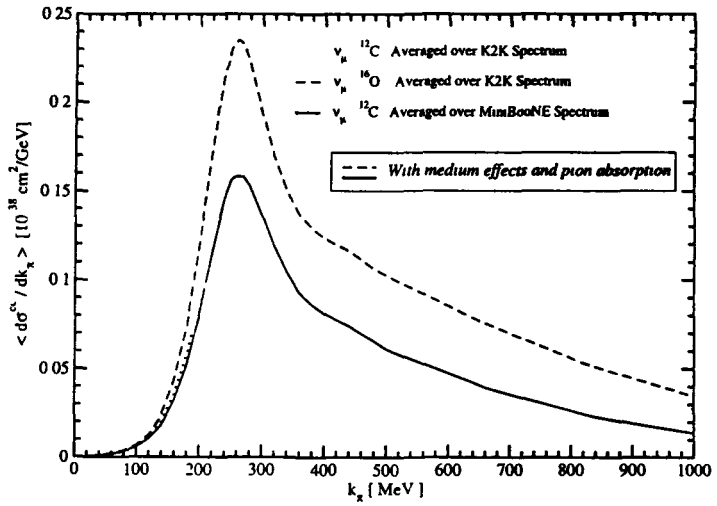

Figure 5.28 Momentum distribution of the pions $\langle \frac{d\sigma}{dk_\pi} \rangle$ vs $\mathbf{k}_\pi$ averaged over the MiniBooNE and the K2K neutrino spectra for the coherent charged current reaction induced by ν_μ in ^{12}C and ^{16}O nuclei

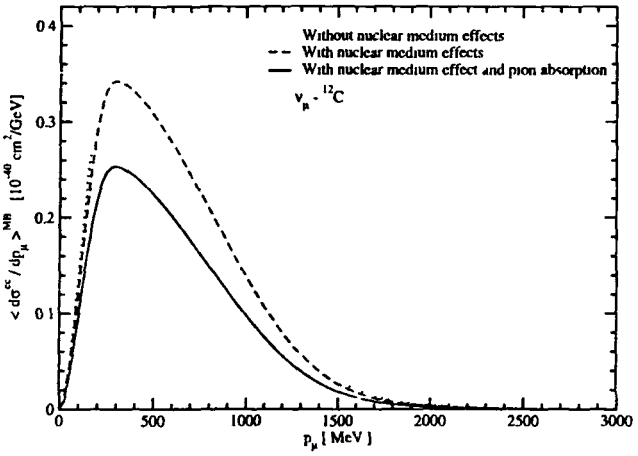

Figure 5 29: Momentum distribution $\langle \frac{d\sigma}{dp_\mu} \rangle$ vs p_μ averaged over the MiniBooNE neutrino spectrum for the incoherent charged current reaction induced by ν_μ on ^{12}C nucleus

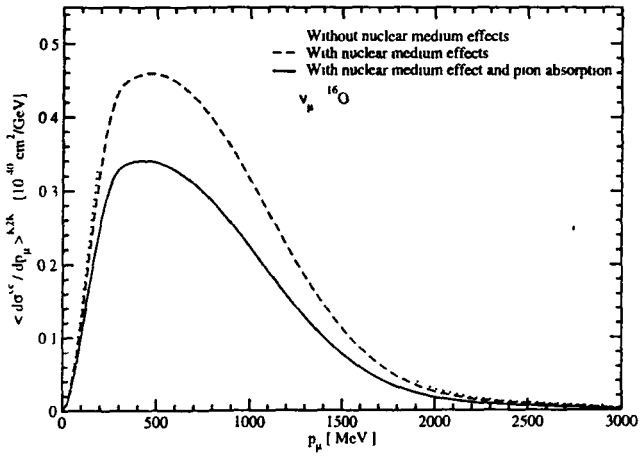

Figure 5 30: Momentum distribution $\langle \frac{d\sigma}{dp_\mu} \rangle$ vs p_μ averaged over the K2K neutrino spectrum for the incoherent charged current reaction induced by ν_μ on ^{16}O nucleus

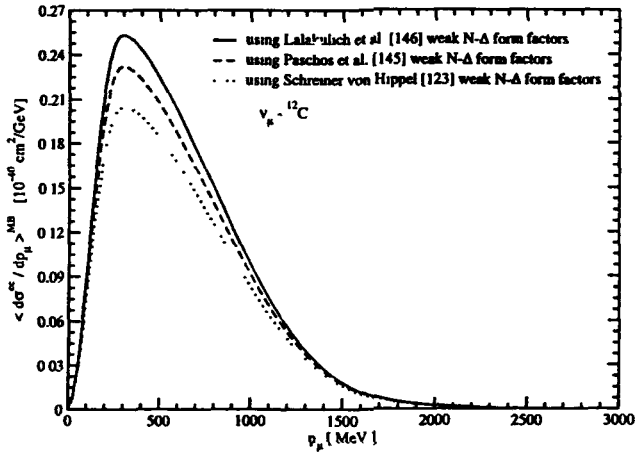

Figure 5.31: Momentum distribution $\langle \frac{d\sigma}{dp_\mu} \rangle$ vs p_μ averaged over the MiniBooNE neutrino spectrum for the incoherent charged current reaction induced by ν_μ on ^{12}C nucleus. The various curves are the final results with nuclear medium and final state interaction effects

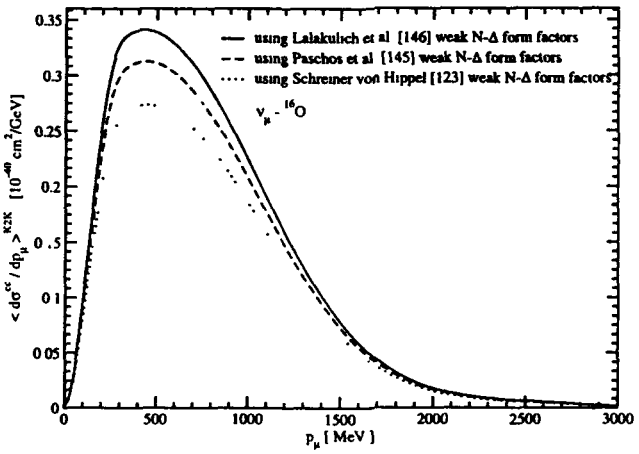

Figure 5.32: Momentum distribution $\langle \frac{d\sigma}{dp_\mu} \rangle$ vs p_μ averaged over the MiniBooNE neutrino spectrum for the incoherent charged current reaction induced by ν_μ on ^{16}O nucleus. The various curves are the final results with nuclear medium and final state interaction effects

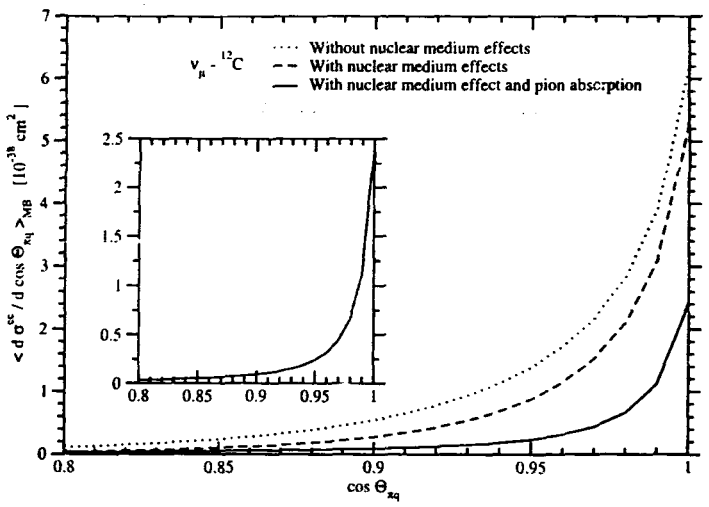

Figure 5.33: Angular distribution of the pions $\langle \frac{d\sigma}{d\cos\Theta_{\pi q}} \rangle$ vs $\cos\Theta_{\pi q}$ averaged over the MiniBooNE neutrino spectrum for the coherent charged current reaction induced by ν_μ in ^{12}C nucleus.

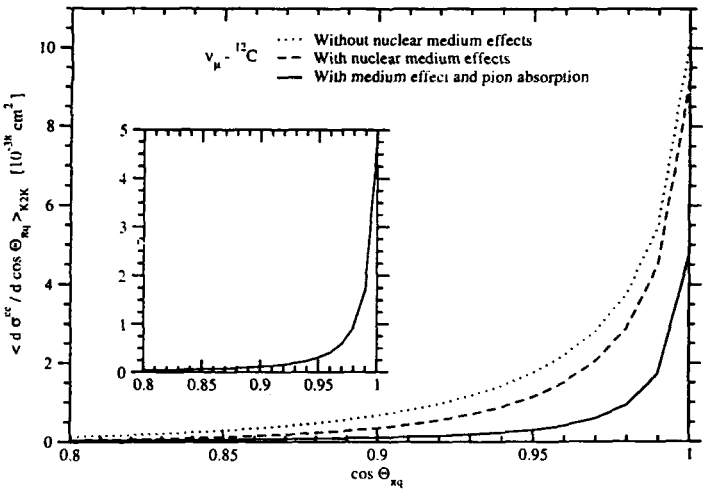

Figure 5.34: Angular distribution of the pions $\langle \frac{d\sigma}{d\cos\Theta_{\pi q}} \rangle$ vs $\cos\Theta_{\pi q}$ averaged over the K2K neutrino spectrum for the coherent charged current reaction induced by ν_μ in ^{12}C nucleus.

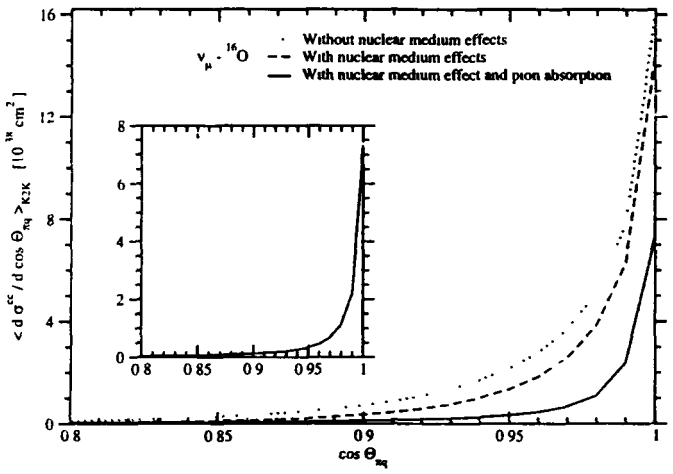

Figure 5.35: Angular distribution of the pions $\langle \frac{d\sigma}{d\cos\Theta_{\pi q}} \rangle$ vs $\cos\Theta_{\pi q}$ averaged over the K2K neutrino spectrum for the coherent charged current reaction induced by ν_μ in ^{16}O nucleus.

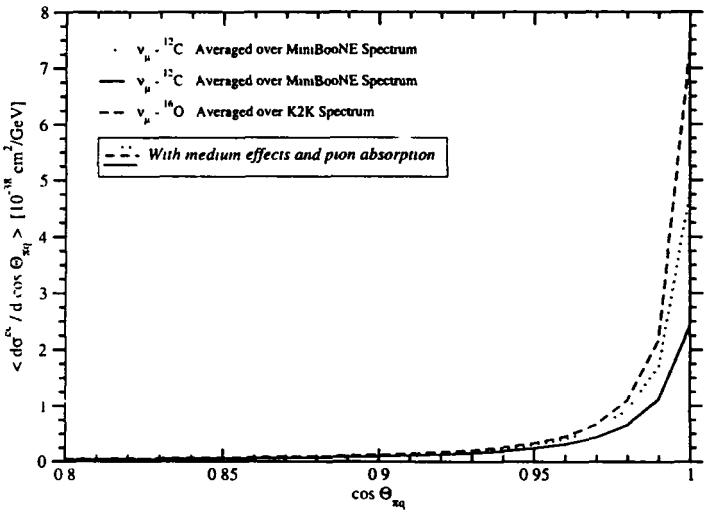

Figure 5.36: Angular distribution of the pions $\langle \frac{d\sigma}{d\cos\Theta_{\pi q}} \rangle$ vs $\cos\Theta_{\pi q}$ averaged over the MiniBooNE and the K2K neutrino spectra for the coherent charged current reaction induced by ν_μ in ^{12}C and ^{16}O nuclei.

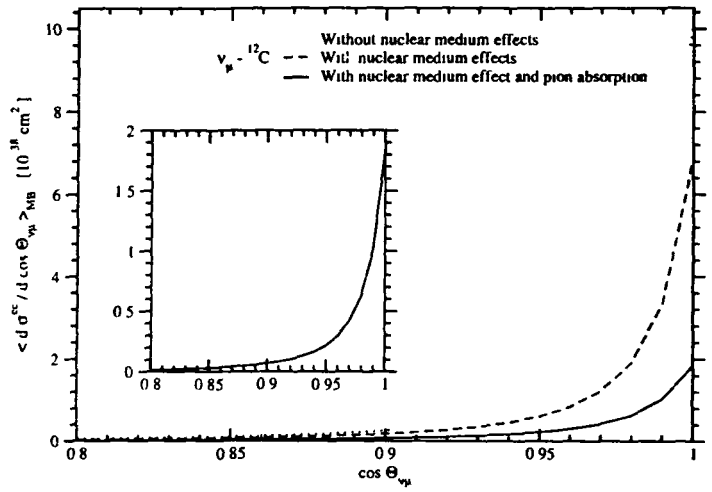

Figure 5 37 Angular distribution of the leptons $\langle \frac{d\sigma}{d\cos\Theta_{\nu\mu}} \rangle$ vs $\cos\Theta_{\nu\mu}$ averaged over the MiniBooNE neutrino spectrum for the ν_μ induced coherent charged current lepton production on ^{12}C nucleus

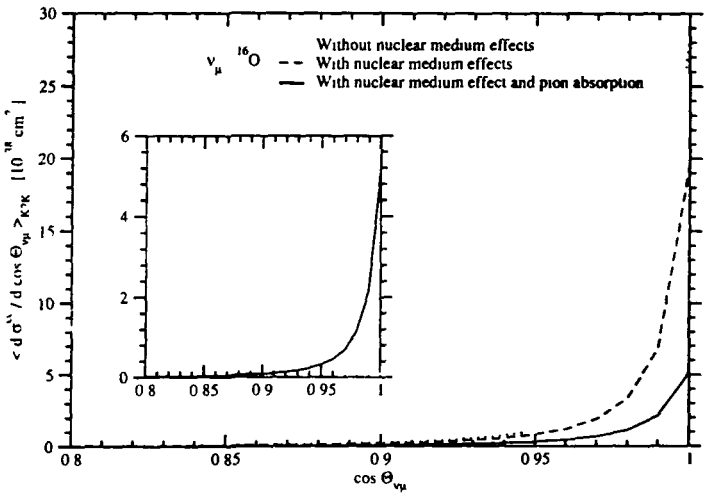

Figure 5 38 Angular distribution of the leptons $\langle \frac{d\sigma}{d\cos\Theta_{\nu\mu}} \rangle$ vs $\cos\Theta_{\nu\mu}$ averaged over the K2K neutrino spectrum for the ν_μ induced coherent charged current lepton production on ^{16}O nucleus

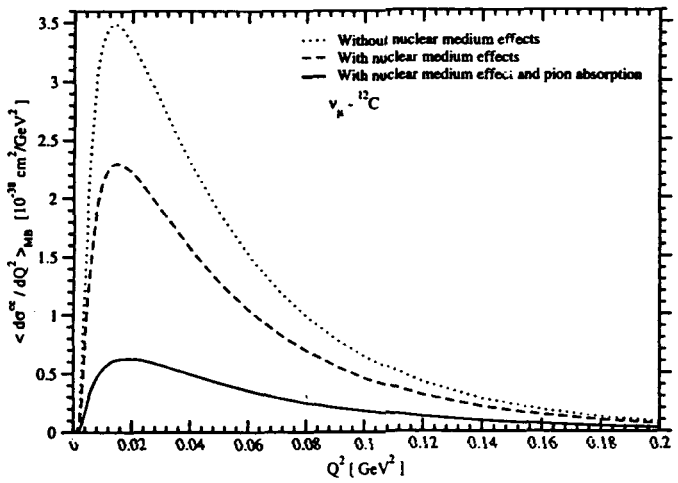

Figure 5.39: Differential cross section $\langle \frac{d\sigma}{dQ^2} \rangle$ vs Q^2 averaged over the MiniBooNE neutrino spectrum for the ν_μ induced coherent charged current pion production on ^{12}C nucleus.

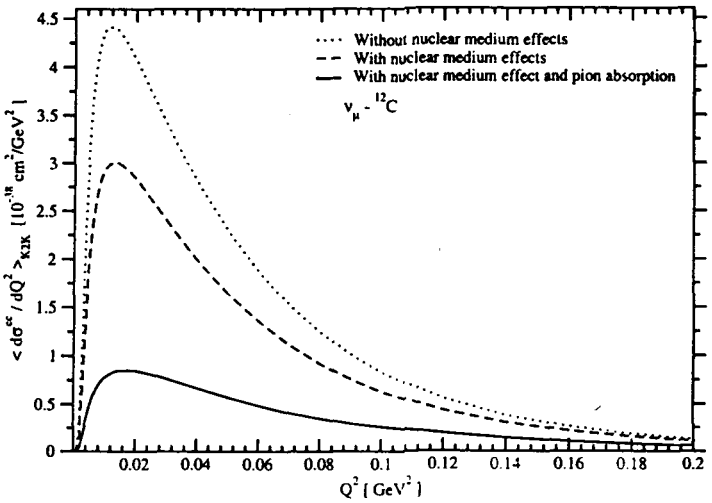

Figure 5.40: Differential cross section $\langle \frac{d\sigma}{dQ^2} \rangle$ vs Q^2 averaged over the k2K neutrino spectrum for the ν_μ induced coherent charged current pion production on ^{12}C nucleus.

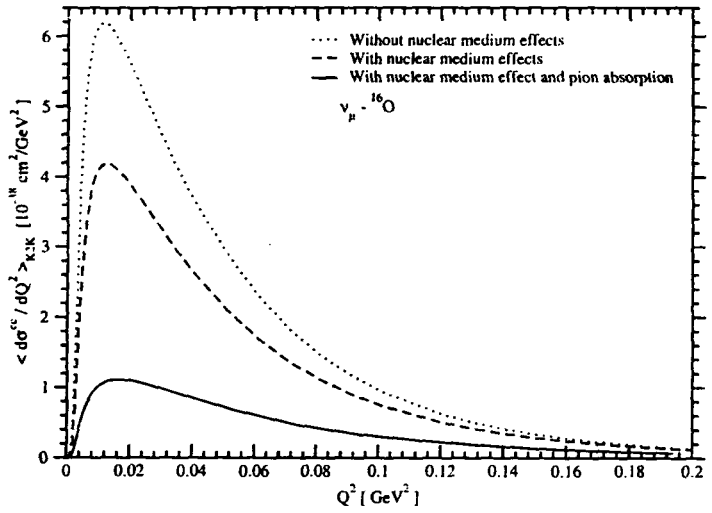

Figure 5.41: Differential cross section $\langle \frac{d\sigma}{dQ^2} \rangle$ vs Q^2 averaged over the k2K neutrino spectrum for the ν_μ induced coherent charged current pion production on ^{16}O nucleus.

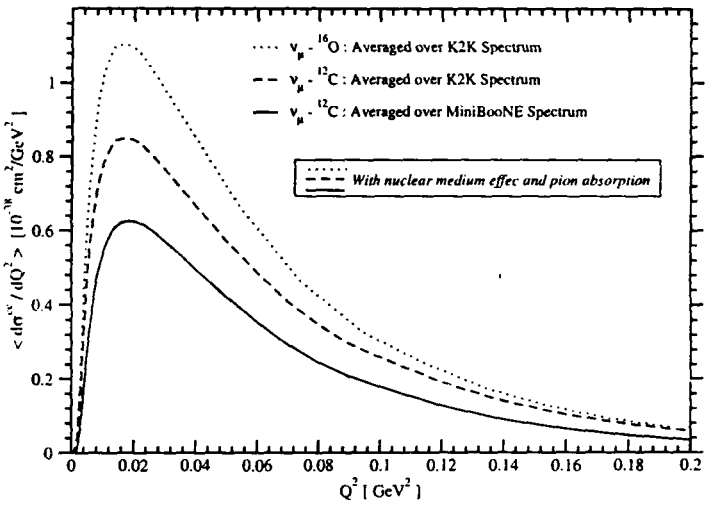

Figure 5.42: Differential cross section $\langle \frac{d\sigma}{dQ^2} \rangle$ vs Q^2 averaged over the MiniBooNE and the k2K neutrino spectra for the ν_μ induced coherent charged current pion production on ^{12}C and ^{16}O nucleus.

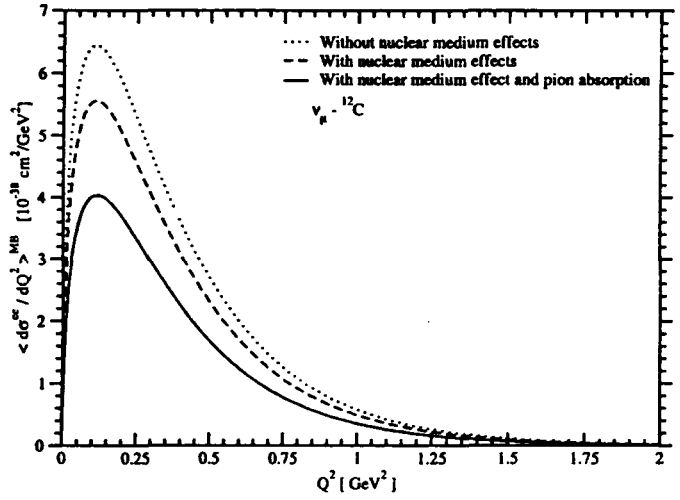

Figure 5.43: Differential cross section $\langle \frac{d\sigma}{dQ^2} \rangle$ vs Q^2 averaged over the MiniBooNE neutrino spectrum for the ν_μ induced charged current incoherent pion production on ^{12}C nucleus.

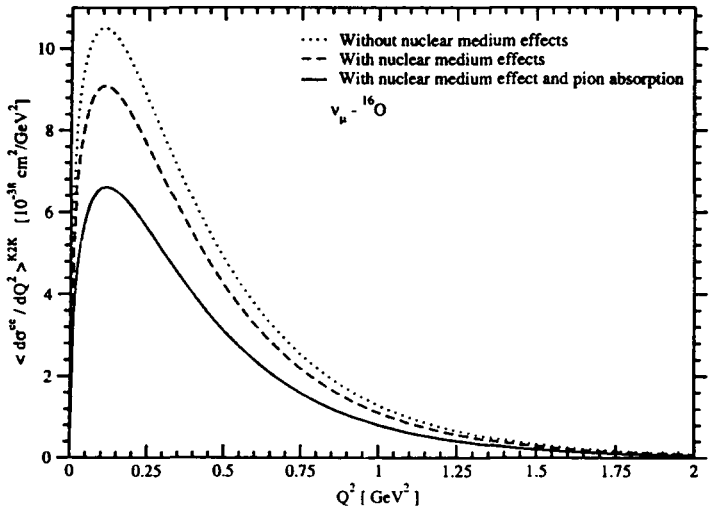

Figure 5.44: Differential cross section $\langle \frac{d\sigma}{dQ^2} \rangle$ vs Q^2 averaged over the K2K neutrino spectrum for the ν_μ induced charged current incoherent pion production on ^{16}O nucleus.

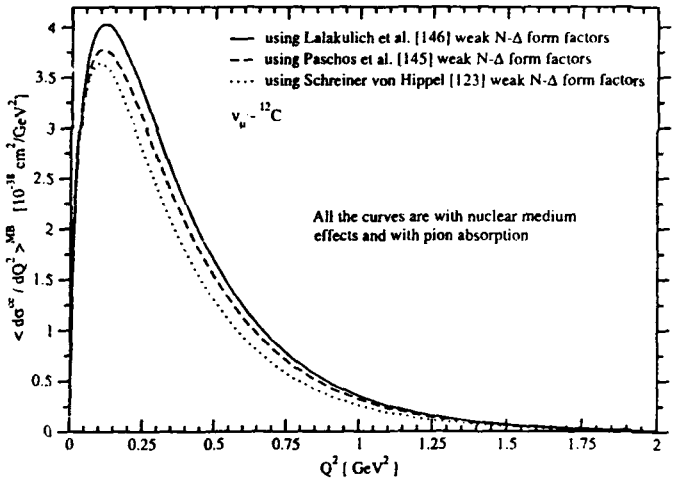

Figure 5.45: Differential cross section $\langle \frac{d\sigma}{dQ^2} \rangle$ vs Q^2 averaged over the MiniBooNE neutrino spectrum for the ν_μ induced charged current incoherent pion production on ^{12}C nucleus.The various curves are the final results with nuclear medium and final state interaction effects.

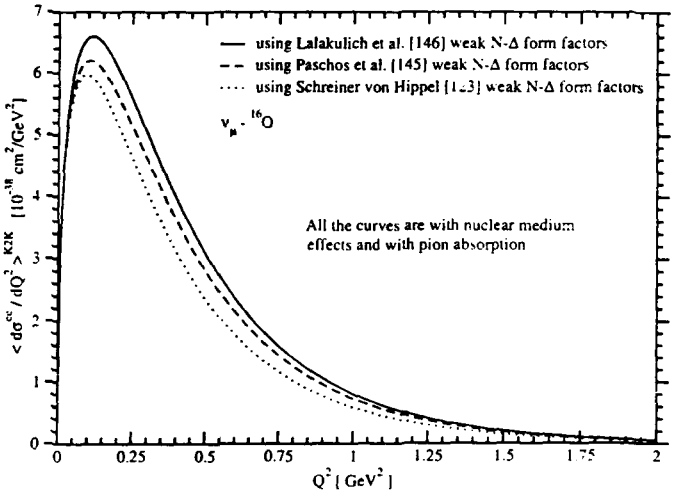

Figure 5.46: Differential cross section $\langle \frac{d\sigma}{dQ^2} \rangle$ vs Q^2 averaged over the K2K neutrino spectrum for the ν_μ induced charged current incoherent pion production on ^{16}O nucleus.The various curves are the final results with nuclear medium and final state interaction effects.

5.4.4 Total Cross Sections

In Fig.5.47, we have shown our final result for the total scattering cross section σ^{CC} for the coherent charged current reaction induced by ν_μ in ^{12}C nuclei. We have shown the result for σ^{CC} (dashed line) when a cut of 450 MeV is applied on the muon momentum i.e., k'_μ >450 MeV as done in the K2K experiment [57]. The solid line is the result without the cut on the muon momentum. We see that due to the cut on the muon momentum the cross section reduces up to $E_\nu \leq 1.5$ GeV after which they are approximately same. We have also shown the predicted coherent charged current cross section induced by ν_μ in ^{12}C nuclei for E_ν=1.3 GeV which is σ^{CC}=7.7×10^{-40} cm^2 with k'_μ >450 MeV cut applied [57].

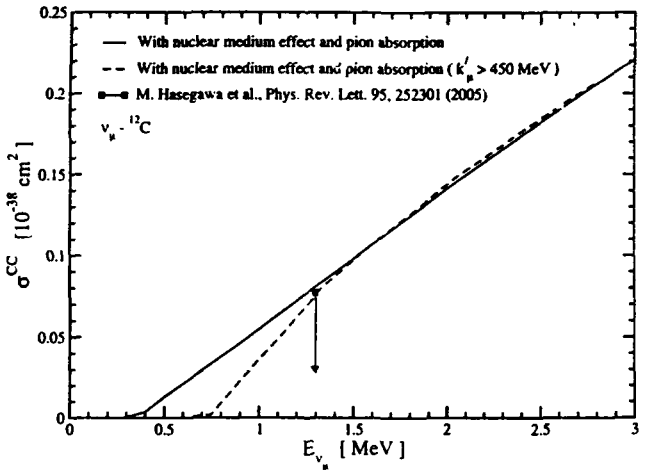

Figure 5.47: Total cross section $\sigma(E_\nu)$ vs E_ν of the coherent pion production by neutrinos in the case of charged current. The dashed line represents the total cross section with a cut on the muon momentum k'_μ >450 MeV. solid line is without any cut. The □ gives the upper bound $\sigma^{CC}_{coh} \leq 7.2\times10^{-40}$ cm^2/C at $\langle E_\nu \rangle$=1.3 GeV [57].

In Fig.5.48, we show the total cross section σ^{NC} for the neutral current induced π^0 production from ^{12}C (solid line), ^{16}O (dashed-dotted line), ^{27}Al (dotted line) and CF_3Br (Freon) (dashed line), along with the experimental results from the MiniBooNE collaboration for ^{12}C [63], from the Aachen collaboration for ^{27}Al [274] and from the Gargamelle collaboration for Freon [276]. We see that the theoretical results for the neutral current induced coherent π^0 production are in reasonable agreement with presently available experimental results in the intermediate energy region.

Using the results for the ν_μ induced coherent charged and neutral current pion production

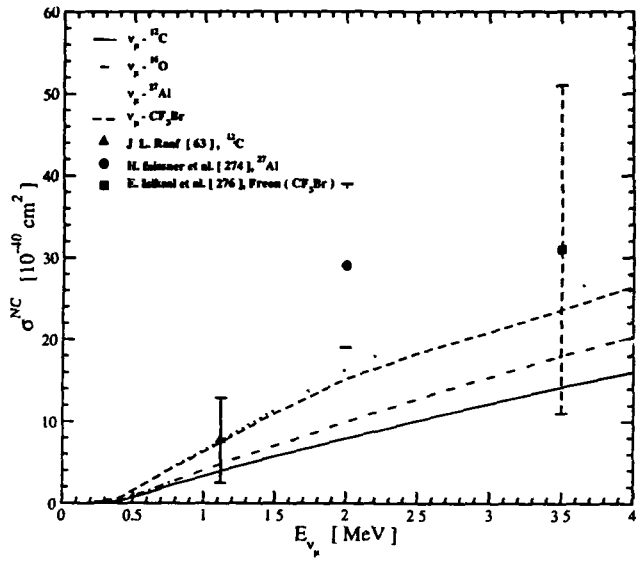

Figure 5.48: Total cross section $\sigma(E_\nu)$ vs E_ν of the coherent pion production by neutrinos in the case of neutral current in ^{12}C (solid line), ^{16}O (dashed-dotted line), ^{27}Al (dotted line) and Freon (CF_3Br) (dashed line) with nuclear medium and pion absorption effects. The experimental points for neutral current are from: △ MiniBooNE [63], • Aachen-Padova [274] and □ Gargamelle [276].

in ^{12}C and ^{16}O nuclei, we have obtained the flux averaged cross section $\langle\sigma\rangle$ for the K2K and the MiniBooNE neutrino spectra.

$$\langle\sigma\rangle = \frac{\int \sigma(E_\nu)\phi(E_\nu)dE_\nu}{\int \phi(E_\nu)dE_\nu} \tag{5.4}$$

The result for the coherent charged current total cross section averaged over the K2K neutrino spectrum with k'_μ >450 MeV cut applied is $\langle\sigma^{CC}\rangle$=0.578×10^{-40} cm^2/nucleon in ^{12}C nuclei, and is consistent with the experimental result of $\langle\sigma^{CC}\rangle$ <0 642×10^{-40} cm^2/nucleon at average neutrino energy $\langle E_\nu\rangle$=1.3 GeV in ^{12}C nuclei reported by the K2K collaboration [57] Since the estimate of coherent neutral current π^0 production is important because it contributes to the major background in the oscillation of ν_μ's to ν_e's, we have calculated the neutral current π^0 production averaged over the K2K and MiniBooNE neutrino spectra. The results are as follows

$$\langle\sigma^{CC}\rangle^{K2K} \text{ in } ^{12}\text{C} = 0\,662 \times 10^{-40}\ cm^2/\text{nucleon (without cut } k'_\mu > 450 \text{ MeV}) \tag{5.5}$$

$$\langle\sigma^{CC}\rangle^{K2K} \text{ in } ^{12}\text{C} = 0.578 \times 10^{-40}\ cm^2/\text{nucleon (with cut } k'_\mu > 450 \text{ MeV}) \tag{5.6}$$

Table 5.5: Charged current incoherent total scattering cross sections for one π^+ production $\langle\sigma^{CC}\rangle$ averaged over the MiniBooNE and K2K neutrino spectra for the different N-Δ transition form factors given by Schreiner and von Hippel [124], Paschos et al. [146] and Lalakulich et al. [147].

N-Δ Transition Form Factors	$\langle\sigma^{CC}\rangle$ in ^{12}C 10^{-38} cm^2	without medium modifications	with medium modifications	with nuclear medium and π-absorption
Lalakulich et al. [147]	MiniBooNE	3.269	2.799	2.034
Paschos et al. [146]	MiniBooNE	3.016	2.582	1.874
Schreiner von Hippel [124]	MiniBooNE	2.701	2.313	1.678
N-Δ Transition Form Factors	$\langle\sigma^{CC}\rangle$ in ^{16}O 10^{-38} cm^2	without medium modifications	with medium modifications	with nuclear medium and π-absorption
Lalakulich et al. [147]	K2K	5.820	5.023	3.639
Paschos et al. [146]	K2K	5.370	4.634	3.358
Schreiner von Hippel [124]	K2K	4.783	4.126	2.988

$$\langle\sigma^{NC}\rangle^{K2K} \text{ in } ^{12}C = 0.395 \times 10^{-40}\ cm^2/\text{nucleon} \quad \text{(without cut)} \tag{5.7}$$

$$\langle\sigma^{NC}\rangle^{K2K} \text{ in } ^{16}O = 0.366 \times 10^{-40}\ cm^2/\text{nucleon} \quad \text{(without cut)} \tag{5.8}$$

$$\langle\sigma^{CC}\rangle^{MB} \text{ in } ^{12}C = 0.461 \times 10^{-40}\ cm^2/\text{nucleon} \quad \text{(without cut)} \tag{5.9}$$

$$\langle\sigma^{NC}\rangle^{MB} \text{ in } ^{12}C = 0.284 \times 10^{-40}\ cm^2/\text{nucleon} \quad \text{(without cut)} \tag{5.10}$$

We can see from these results the important role of the nuclear medium effects which reduces the total cross sections and help to obtain reasonable agreement with the experimental values. The uncertainty in calculating these nuclear effects comes mainly from uncertainties in the value of the Δ-self energy which is calculated [161]-[162] within an accuracy of 15-20%. This leads to an uncertainty of 8-12% in the total cross section. We have also studied the uncertainty in the total cross sections due to the use of various parametrisations of the weak form factors used in literature [132], [146]-[147], [263], which is small (3-5%) as the coherent process is dominated by differential cross sections at very low Q^2. Thus the total uncertainty in the present calculation is estimated to be about 15%.

In our calculation for the coherent process the vector contribution to the cross section is negligibly small and the major contribution comes from the axial current only, leading to the

near equality of neutrino and antineutrino cross sections. The dominant contribution (> 98%) to the cross section comes from $C_5^A(Q^2)$ term. The expression of $C_5^A(Q^2)$ given in Eq.3.49 and used by Paschos et al. [146] and Lalakulich et al. [147] are the same, while using the expression of $C_5^A(Q^2)$ given in Eq.3.48 and used by Schreiner and von Hippel [124] results only a change of a few percent ($\leq$2%) in the differential cross sections beacuse of the low Q^2 dominant nature of the process and these results have not been explicitly shown here. In our calculation we have used the expression of $C_5^A(Q^2)$ used by Schreiner and von Hippel [124].

Using Eq.5.4, we have obtained the flux averaged cross section (σ^{CC}) for the MiniBooNE and K2K neutrino spectra for the charged current muon neutrino induced incoherent π^+ production in ^{12}C and ^{16}O nuclei discussed in section-5.1.1. The results are summarized in table.5.3.

We have also compared our numerical results for the total charged current $1\pi^+$ production cross section with the recent preliminary results from the MiniBooNE collaboration [61]-[62] on ^{12}C. We have calculated the total scattering cross section for the charged current $1\pi^+$ production $\sigma(E_\nu)$ for ν_μ induced reaction on a free proton target i.e. $\nu_\mu + p \rightarrow \mu^- + p + \pi^+$ presented in Fig.5.49 along with the experimental results from the ANL and the BNL experiments [242]-[245].

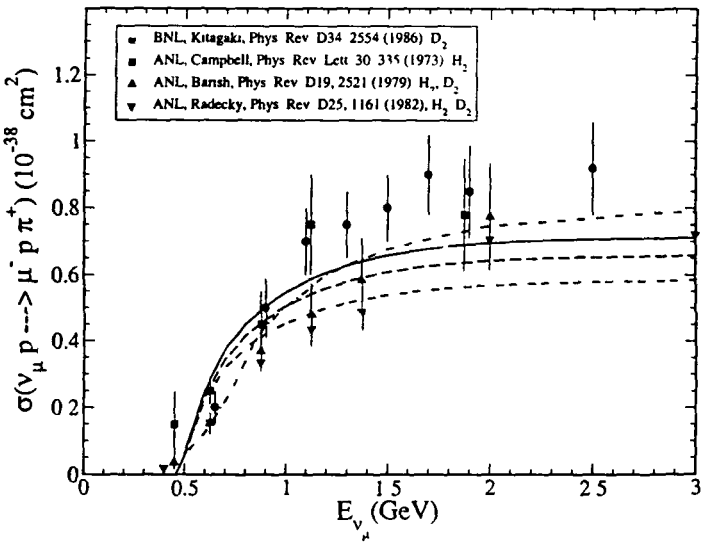

Figure 5.49: Charged current one pion production cross section induced by neutrinos on proton target ($\nu_\mu + p \rightarrow \mu^- + p + \pi^+$). Experimental points are the ANL and the BNL data and dashed-dotted line is the NUANCE cross section taken from Wascko [61]-[62]. The various theoretical curves show the cross section calculated using weak N-Δ transition form factors given by Schreiner and von Hippel [124](double dashed-dotted line), Paschos et al. [146](dashed line) and Lalakulich et al. [147](solid line)

The various theoretical curves show the cross sections calculated using N-Δ transition form factors given by Schreiner and von Hippel [124], Paschos et al. [146] and Lalakulich et al. [147]. We find that in the neutrino energy region of 0.7-2.0 GeV the cross sections obtained with the N-Δ transition form factors given by Paschos et al. [146] and Lalakulich et al. [147] are larger than the cross sections obtained by using the Schreiner and von Hippel [124] parameterization. The uncertainty in the total cross section for $1\pi^+$ production associated due to the uncertainty in the transition form factors is seen from these figures to be about 10-20% in this energy region.

The experimental data from ANL by Campbell et al. [242] are explained satisfactorily in our model. The theoretical results are within 1 standard deviation of the experimental results using weak N-Δ transition form factors of Paschos et al. [146] (χ^2_{pdf}=0.9) and Lalakulich et al. [147] (χ^2_{pdf}=0.8) and within 1.5 standard deviation if Schreiner and von Hippel [124] parameterization is used. The experimental results of Barish et al. [243] (excluding the lowest energy points) are also described satisfactorily by our model within 1 standard deviation if the form factors of Schreiner and von Hippel [124] (χ^2_{pdf}=0.6) and Paschos et al. [146] (χ^2_{pdf}=0.8) are used and within 1.2 standard deviation if the parametrization of Lalakulich et al. [147] is used. On the otherhand the experimental data from BNL by Kitagaki et al. [245] are higher and the experimental data from ANL by Radecky et al. [244] are lower than our theoretical predictions by 2-5 standard deviation depending upon the various N-Δ transition form factors used in this calculation. Clearly, better quality data on neutrino induced pion production is needed in order to determine the N-Δ transition form factors, for which various theoretical predictions exist [253]-[254] in addition to the three models considered in this work.

We have calculated the ratio of the cross sections for inclusive charged current $1\pi^+$ ($CC1\pi^+$) production to charged current quasielastic scattering(CCQE) cross sections. The numerical values of the total cross sections for $1\pi^+$ production shown in Figs.5.17(coherent) and 5.21(incoherent) and the total cross sections for inclusive quasielastic lepton production shown in Fig.2.12 have been used to calculate the ratio $r = \frac{\sigma(CC1\pi^+)}{\sigma(CCQE)}$ which is shown in Fig.5.50, for the various parameterizations for N-Δ transition form factors given by Schreiner and von Hippel [124], Paschos et al. [146] and Lalakulich et al. [147]. We also show in this figure the experimental results for this ratio reported by the MiniBooNE collaboration [61]-[62]. We see that the theoretical predictions for the cross sections in our model are in satisfactory agreement with the experimental results for the ratio and are described within 1 standard deviation for the parameterization of N-Δ transition form factors considered in this work except for the parameterization of Schreiner and von Hippel [124] form factors for which χ^2_{pdf}=1.6. We will like to emphasize that the nuclear medium and pion absorption effects in pion production processes as shown in Fig.5.17 and Fig.5.21, and the nuclear medium effects on the inclusive quasielastic process as shown in Fig.2.12, play an important role in bringing about this agreement. For a given choice of the electroweak nucleon form factors in the quasielastic sector, there is a theoretical uncertainty of 10-20% in this ratio due to use of various parametrisations for the N-Δ transition form factors shown in table.3.1. There is a further uncertainty of 2-3% in this

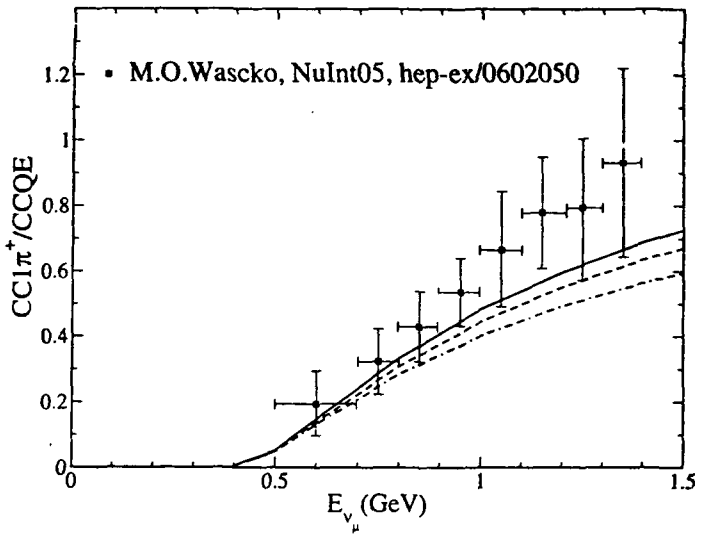

Figure 5.50: $\frac{\sigma(CC1\pi^+)}{\sigma(CCQE)}$ for the ν_μ induced reaction on ^{12}C. The experimental points are taken from Wascko [62]. The theoretical curves are obtained by using Schreiner and von Hippel [124](double dashed-dotted line), Paschos et al. [146](dashed line) and Lalakulich et al. [147](solid line) weak N-Δ transition form factors for C.C.$1\pi^+$ production and Bradford et al. [194] weak nucleon form factors for CCQE.

ratio due to the various electroweak nucleon form factors used in the calculations of the total cross section for the quasielastic production if the world average of M_A=1.05 GeV is used.

In Fig.5.51, we have shown the variation in the total cross section for the charged current $1\pi^+$ production for ν_μ induced reaction in ^{12}C due to the variation in the axial vector dipole mass M_A in the N-Δ transition form factors using the parametrization given by Lalakulich et al. [147]. The results are shown for M_A=1.0 GeV, M_A=1.1 GeV and M_A=1.2 GeV. We find that a 20% change in M_A results in a change of around 20% in the cross section which increases with M_A. In this figure, we have also shown the results predicted by the NUANCE [1] and NEUGEN [2] neutrino event generators. These theoretical results are compared with the experimental results reported by MiniBooNE collaboration. These cross sections are obtained by multiplying the experimental ratio $r = \frac{\sigma(CC1\pi^+)}{\sigma(CCQE)}$ given in Fig.5.50 with the theoretical cross section for quasielastic production given by the model of Smith and Moniz [8] which does not include the effect of nuclear medium modifications due to RPA correlations in the quasielastic cross sections. These results agree quite well with our results for $1\pi^+$ production cross section, shown by dashed-dotted lines, when we do not include the nuclear medium modifications due to RPA correlations in the quasielastic cross sections. However, when the nuclear medium modification effects due to RPA correlations in the quasielastic production cross section shown

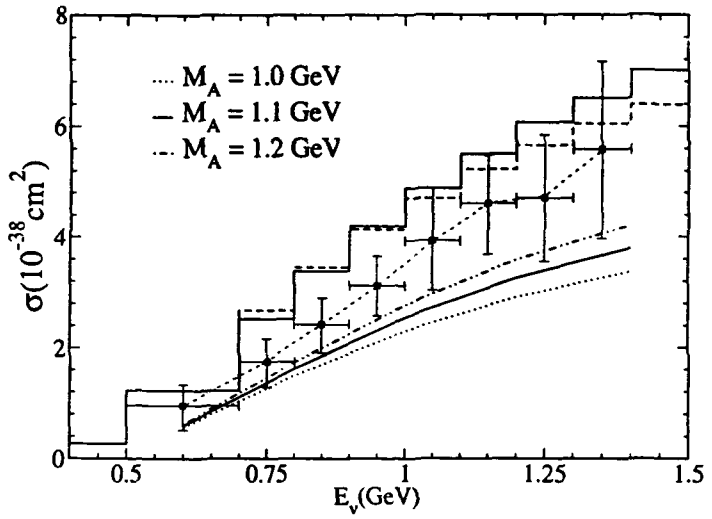

Figure 5.51: $\sigma(CC1\pi^+)$ for ν_μ induced reaction on ^{12}C. The dashed(solid) stairs are the cross sections from NEUGEN(NUANCE) Monte Carlo event simulation and the experimental points shown by solid dot with error bars are the MiniBooNE results [61]-[62]. The theoretical curves show the $CC1\pi^+$ cross section using Lalakulich et al. [147] weak N-Δ transition form factors for the various values of M_A. The dashed-dotted line is $\sigma(CC1\pi^+)$ obtained by using the central value of the experimental results for the ratio $r = \frac{\sigma(CC1\pi^+)}{\sigma(CCQE)}$ [61]-[62](experimental points shown in Fig.5.49) and $\sigma(CCQE)$ calculated in our model without RPA effects.

in Fig.2.12 are used to calculate the total cross section for $1\pi^+$ production by multiplying it by the ratio r (shown in Fig.5.50) the cross sections are reduced. This is shown in Fig.5.52. We see that the experimental results for the total $1\pi^+$ cross sections are now explained satisfactorily with the various parameterizations of N-Δ transition form factors within one standard deviation except for the parametrization of Schreiner and von Hippel for which χ^2_{pdf}=1.4.

It can be seen from Fig.5.51, that the theoretical predictions for the total charged current $1\pi^+$ production cross sections by the neutrino generators like NUANCE [1] and NEUGEN [2] over estimate the experimental cross sections as they do not include the nuclear effects appropriately which are known to reduce the cross sections. For example, the nuclear effects lead to a reduction of 30-40% for the dominant process of incoherent production in this energy region as shown in Fig.5.21 which is large compared to 10% reduction considered in the T=3/2 channel in the NUANCE generator [1].

One may also consider the contribution of higher resonance excitations to $1\pi^-$ production in this energy region, for which there exist very few calculations in literature [137], [146]-[148]. It has been shown by Paschos et al. [146] that the total cross section for neutrino induced

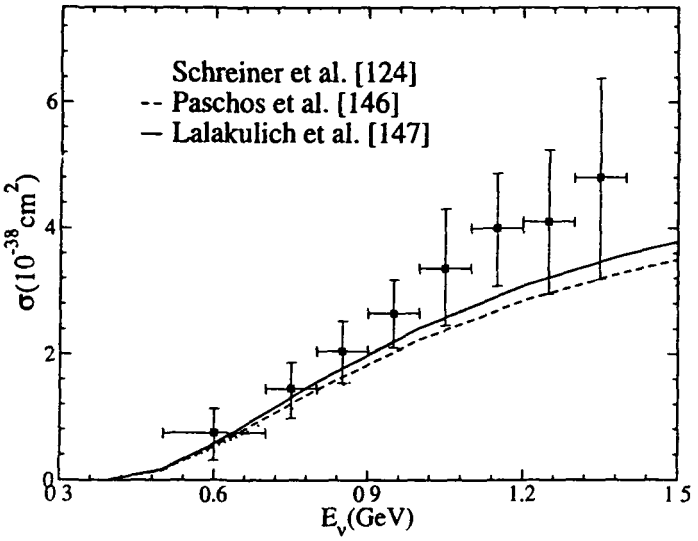

Figure 5.52 $\sigma(CC1\pi^+)$ for ν_μ induced reaction on ^{12}C. The theoretical curves show the cross sections for the various weak N-Δ transition form factors. The experimental points show $\sigma(CC1\pi^+)$ obtained by using the experimental results for the ratio $r = \frac{\sigma(CC1\pi^+)}{\sigma(CCQE)}$ [61]-[62] (experimental points shown in Fig.5.49) and $\sigma(CCQE)$ calculated in our model with RPA effects

excitation of higher resonances like Roper(1440), $S_{11}(1535)$ and $D_{13}(1520)$ is quite small. In an earlier calculation, Alvarez-Ruso et al. [137] have studied weak electro-excitation of Roper and recently Valverde and Vicente Vacas [148] have studied neutrino induced excitation of Roper and consequent pion production processes through excitation of this resonance We have used these results to estimate one pion production in the energy region E_ν <1 5 GeV It is found that the contribution to one pion production through the excitation of Roper resonance is around 2-4% and the contribution of other higher resonance excitations to one pion production is quite negligible. Therefore, higher mass resonances are not expected to make any important contributions to pion production in this energy region

==========*******==========

Chapter 6

Summary and Conclusions

6.1 Quasielastic Inclusive Lepton Production

We have studied the charged current lepton production induced by ν_μ and ν_e neutrinos on various nuclei, in low and intermediate energy region, which are of present interest for atmospheric as well as accelerator neutrino experiments. The calculations have been done for large number of nuclei in the low energy as well as in the intermediate energy region for ^{12}C, ^{16}O and ^{56}Fe. The cross section calculations are performed in a local density approximation taking into account the Pauli blocking, Fermi motion and the renormalization of weak transition strengths in the nuclear medium. The effect of Coulomb distortion for the charged lepton while coming out of the nucleus is taken into account by using the Fermi function as well as the modified momentum approximation(MEMA). In the low energy region, the cross sections are then averaged over the ν_e spectra obtained from the muons decay at rest where the maximum energy of neutrinos is 52.8 MeV.

We find that

(1) The role of nuclear effects like Q_{th} value, Pauli blocking and Fermi motion is to reduce the cross sections. For a given Z, this reduction becomes smaller with the increase in energy. There is a further reduction of the cross section due to the renormalization of weak transition strengths in the nuclear medium. For a given Z, this reduction becomes smaller with the increase in neutrino energy, while for a given neutrino energy E_ν, this reduction increases with Z.

(2) The effect of the Coulomb distortion of the final charged lepton in the total cross section is small except at very low energies and becomes negligible with increase in neutrino energy.

(3) The two methods of treating the Coulomb distortion give similar results for low energy neutrinos in the case of low mass nuclei. For intermediate and heavy mass nuclei the cross sections

with Fermi function are smaller than the cross sections with MEiMA upto certain energy E_{ν_e} after which the the cross sections calculated with Fermi function become larger. At the energy E_{ν_e} where this cross over takes place changes with nuclei. For example it is around 40 MeV for nuclei like ^{56}Fe in the intermediate mass range and around 18 MeV for nuclei in the heavier mass range like ^{208}Pb. This agrees with the results obtained earlier by Engel [156] for ^{208}Pb.

(4) The total cross sections averaged over the neutrino spectrum obtained from the muons decaying at rest is presented for all nuclei considered here. The results for ^{12}C, ^{16}O, ^{56}Fe and ^{208}Pb nuclei are compared with the available experimental results as well as different theoretical calculations. New results have been presented for many other nuclei.

(5) The reduction is larger in the total cross section for quasielastic reactions as compared to the Fermi gas model. The energy dependence of this reduction in cross section is found to be different at threshold energy for ν_μ and ν_e neutrino reactions. However, for E$\geq$500 MeV, the energy dependence is similar in nature.

The numerical results for low energy region presented here can be a very useful benchmark for neutrino nucleus cross section measurements being proposed at SNS facilities using various nuclei as nuclear targets. The numerical results in the intermediate energy region are also useful to analyze the fully contained events of atmospheric neutrino oscillation experiments.

6.2 Coherent and Incoherent Pion Production

We have studied neutrino induced charged current and neutral current one pion production from ^{12}C and ^{16}O target at the intermediate neutrino energies relevant for the MiniBooNE and the K2K experiments. We have done the calculations for the incoherent and coherent production of lepton and/or pions from ^{12}C and ^{16}O nuclear targets. The calculations have been done in a model which takes into account the nuclear medium effects in the weak pion production process through Δ dominance treated in local density approximation, which incorporates the modification of the mass and the width of Δ resonance in the nuclear medium. The effect of the final state interaction of pions with the residual nucleus has also been considered, which has been treated differently for coherent and incoherent processes. In coherent process the final state interaction of pions with the nucleus is described in an eikonal approximation with a pion optical potential derived in terms of the pion self energy in the nuclear medium calculated in the local density approximation, and in incoherent process the final state interaction of pions is calculated with the help of a Monte Carlo simulation for propagation of pions in the nuclear medium using probabilities per unit length as the basic input.

The energy dependence of the total scattering cross sections for the charged current and neutral current one pion production induced by ν_μ is studied. We have also presented and discussed the numerical results for the momentum distribution, angular distribution and Q^2-

distribution for lepton and/or pions. The numerical results for the neutrino nucleus cross sections averaged over the MinibooNE and the K2K neutrino spectra are presented for ^{12}C and ^{16}O nuclei. Specifically, we have presented the results for the total cross section for $1\pi^+$ production from ^{12}C and studied the energy dependence of the ratio of single π^+ production to the quasielastic reaction. The results have been compared with some old experimental results and with the preliminary results available from MiniBooNE experiment.

From this study we conclude that:

(1) In coherent production the contribution to the cross section comes mainly from the s-channel diagram($> 90\%$) which is dominated by on shell Δ, thus making the off shell correction quite small. The inclusion of off shell effects by introducing a form factor at the $\pi N\Delta$ vertex [267]-[268](see Chapter-4, section-4.2.2) leads to a reduction in the cross section which is estimated to be 4-6 % in the energy region of 1-2 GeV.

(2) In coherent production the contribution to the cross section from the vector current is negligibly small (<2 %) and the major contribution comes from the axial current only, leading to near equality of neutrino and antineutrino cross sections.

(3) There is a large reduction due to nuclear effects in the coherent as well as incoherent production cross sections, and there is a further reduction in the cross sections due to the final state interaction of pions with the residual nucleus.

(4) The total cross sections for neutrino induced π^+ production from free proton are closer to the π^+ production cross sections obtained by the ANL experiment and are smaller than the π^+ production cross sections obtained by the BNL experiment in the intermediate energy region. In this energy region, there is a $10-20\%$ theoretical uncertainty in the total cross section due to use of various parameterization of N-Δ transition form factors.

(5) The total cross sections for $1\pi^+$ production is dominated by the incoherent process. The contribution of the coherent pion production is about 4-5% in the energy region of 0.7-1.4 GeV.

(6) In the neutrino energy region of 0.7-1.4 GeV, the results for the ratio of cross section of $1\pi^+$ production to the quasielastic lepton production is described quite well for E_ν <1.0 GeV, when nuclear effects in both the processes are taken into account. However, for energies higher than E_ν >1.0 GeV, the theoretical value of the ratio underestimates the experimental value.

(7) The role of nuclear medium and pion absorption effects is quite important in bringing out the good agreement between the theoretical and experimental results in the energy region of 1.0 GeV. The theoretical and experimental value of the ratio for the total cross sections for

$1\pi^+$ production and quasielastic lepton production are in good agreement for neutrino energies upto 1.0 GeV. We also found that theoretical results for the neutral current induced coherent π^0 production are in reasonable agreement with presently available experimental results in the intermediate energy region.

(8) The results for charged current and neutral current induced total cross sections in ^{12}C and ^{16}O averaged over K2K and MiniBooNE neutrino spectra have been presented for the coherent and incoherent pion production. We have also presented the momentum distribution, angular distribution and Q^2-distribution in ^{12}C and ^{16}O averaged over the MiniBooNE and K2K spectra for the incoherent and coherent charged current one pion production with various N-Δ transition form factors.

The method may be useful to analyze the neutrino induced pion production data at neutrino energies relevant for neutrino osciilation experiments being done by K2K, MiniBooNE and J-PARC collaborations.

==========*********==========

Appendices

Appendix A

Matrix Elements and Spin Sums

Matrix element for the charged current free neutrino nucleon scattering of Eq.2.1 is written as

$$\mathcal{M} = \frac{G_F}{\sqrt{2}} \cos\theta_C \; l^\mu J_\mu \tag{A.1}$$

where the leptonic current l_μ is given in Eq.2.4 and the hadronic current in Eq.2.6. Using this, we can write the matrix element square averaged over the initial and summed over the final spins of the nucleon given by:

$$|\mathcal{M}|^2 = \frac{G_F^2}{2} \cos^2\theta_C \; L^{\mu\nu} J_{\mu\nu} \tag{A.2}$$

The leptonic tensor $L^{\mu\nu}$ is given in Eq.2.9 as

$$\begin{aligned} L^{\mu\nu} = \bar{\Sigma}\Sigma l^{\mu\dagger} l^\nu &= \mathrm{Tr}\left[(\not{k} + m_\nu)\,\gamma^\mu(1-\gamma^5)(\not{k}' + m_l)\,\gamma^\nu(1-\gamma^5)\right] \\ &= 8\left[k^\mu k^{\nu\prime} + k^{\mu\prime}k^\nu - g^{\mu\nu}\; k\cdot k' + i\epsilon^{\mu\nu\alpha\beta}\; k^\alpha k'^\beta\right] \\ &= L_S^{\mu\nu} + iL_A^{\mu\nu} \end{aligned} \tag{A.3}$$

and hadronic tensor $J_{\mu\nu}$ is given in Eq.2.11. Performing the traces in Eq.2.11, we find the hadronic tensor as:

$$\begin{aligned} J_{\mu\nu} \;=\; & \frac{1}{2}\,\frac{1}{4M_pM_n}\left[4(F_1^V)^2(p'_\mu p_\nu + p'_\nu p_\mu - (p\;\; p' - M_pM_n)g_{\mu\nu}) + 4\left(\frac{F_2^V}{2M}\right)^2\right. \\ & [-q^2(p'_\mu p_\nu - p\cdot p' g_{\mu\nu} + p'_\nu p_\mu) + 2q\cdot p(p'_\mu q_\nu - p'\cdot q g_{\mu\nu} + p'_\nu q_\mu) + M_pM_n q^2 g_{\mu\nu} \\ & -q_\nu(p'_\mu p\cdot q - p_\mu q\cdot p' + q_\mu p\cdot p') + M_pM_n q_\mu q_\nu + (p\cdot p' + M_pM_n)q_\mu q_\nu - q_\mu(p\cdot p' q_\nu \\ & -q\cdot p' p_\nu + q\cdot p p'_\nu) + M_pM_n q_\mu q_\nu] + (4F_A^2)\,[(p'_\mu p_\nu + p_\mu p'_\nu) - (p\cdot p' + M_pM_n)g_{\mu\nu}] \\ & + (4F_p^2)\,[q_\mu q_\nu(M_pM_n - p'\cdot p)] + \left(\frac{F_1^V F_2^V}{2M}\right)[(M_n q_\mu p'_\nu + M_p q_\mu p_\nu) - M_n(p'_\mu q_\nu \\ & \left. -q\cdot p' g_{\mu\nu} + p'_\nu q_\mu) + M_p(p_\mu q_\nu - p_\nu q_\mu - p\cdot q g_{\mu\nu}) + (M_n p'_\mu q_\nu + M_p q_\nu p_\mu + M_n q_\mu p'_\nu\right. \end{aligned}$$

$$+M_p q_\mu p_\nu) - M_n(p'_\mu q_\nu - q\cdot p' g_{\mu\nu} + p'_\nu q_\mu) + M_p(p_\nu q_\mu - p_\mu q_\nu + p\cdot q g_{\mu\nu})]$$
$$- (8iF_1^V F_A)\,[\epsilon_{\alpha\mu\delta\nu}\, p'^{\alpha} p^{\delta}] + 8i\left(\frac{F_2^V F_A}{2M}\right)[M_n\,\epsilon_{\alpha\mu\beta\nu}\, p'^{\alpha} q^{\beta} + M_p\,\epsilon_{\mu\beta\delta\nu}\, q^{\beta} p^{\delta}]$$
$$+ (4F_A F_p)\left[-M_n\left(p'_\mu q_\nu + p_\nu q_\mu\right) + M_p\left(p_\mu q_\nu + p_\nu q_\mu\right)\right]] \qquad \text{(A.4)}$$

Finally, contracting the various terms of hadronic tensor $J_{\mu\nu}$ in Eq.A.4 with the leptonic tensor $L^{\mu\nu}$ in Eq.A.3, we get

$$\begin{aligned}
\sum\!\!\!\!\!\!- \sum |\mathcal{M}|^2 \;=\; & \frac{G_F^2\cos\theta_C}{2}\,\frac{1}{2}\left(\frac{1}{4M_pM_n}\right)\left(\frac{1}{4m_l m_\nu}\right)\\
& \times\left\{(F_1^V)^2\,[(k.p)(k'.p') + (k.p')(p.k') - M_pM_n(k.k')]\right.\\
& + (F_A^2)\,[(k.p)(k'.p') + (k.p')(p.k') + M_pM_n(k.k')]\\
& + (2F_1^V F_A)\,[(k.p')(p.k') - (k.p)(k'.p')]\\
& + \left(\frac{F_2}{2M}\right)^2[(k.p)(k'.q)(p'.q) - (k.p)(k'.p')q^2 + (k.p')(p.q)(k'.q)\\
& -(k.p')(p.k')q^2 + \frac{1}{2}(k.k')(p.p')q^2 - \frac{1}{2}(k.k')M_pM_nq^2\\
& -(k.q)(k'.q)(p.p') - (k.q)(k'.q)M_nM_p + (k.q)(p.q)(k'.p')\\
& +(k.q)(p'.q)(p.k')] + \left(\frac{F_1^V F_2^V}{2M}\right)[-M_n(k.k')(p'.q) - M_n(k.q)(k'.p')\\
& -M_n(k'.q)(k.p') + M_p(k.k')(p.q) + M_p(k.q)(k'.p) + M_p(k'.q)\\
& (k.p)] + \left(\frac{2F_AF_2^V}{2M}\right)[-M_p(k'.q)(k.p) + M_p(p.k')(k.q) - M_n(k'.q)\\
& (k.p') + M_n(k'.p')(k.q)] + (F_p^2)\,[(k.q)(k'.q) - \frac{1}{2}q^2(k.k')][(p.p')\\
& -M_pM_n] + (F_AF_p)\,[-M_n(k.p')(k'.q) - M_n(k.q)(k'.p') + M_n(p'.q)\\
& \left.(k.k') + M_p(k.p)(k'.q) + M_p(k.q)(p.k') - M_p(p.q)(k.k')]\right\} \qquad \text{(A.5)}
\end{aligned}$$

where

$$\begin{aligned}
k &= (E_\nu,\ \mathbf{k}), \quad p = (E_n,\ \mathbf{p})\\
k' &= (E_l,\ \mathbf{k}'). \quad p' = (E_p,\ \mathbf{p}')\\
E_n &= \sqrt{\mathbf{p}^2 + M_n^2}, \quad E_p = \sqrt{\mathbf{p}'^2 + M_p^2}\\
q_\mu &= (E_\nu - E_l,\ \mathbf{k} - \mathbf{k}') \qquad \text{(A.6)}
\end{aligned}$$

The same expression can be used for antineutrino scattering by changing sign in the $F_1^V F_A$ and $F_2^V F_A$ terms.

==========**********==========

Appendix B

Lindhard Function

The Lindhard function for the particle hole excitation given in Fig.2.2 is

$$U_N(q_0,\mathbf{q}) = 2\int \frac{d^3p_n}{(2\pi)^3}\frac{M_nM_p}{E_nE_p}\frac{n_n(\mathbf{p})\left[1-n_p(\mathbf{p}+\mathbf{q})\right]}{q_0+E_n(\mathbf{p})-E_p(\mathbf{p}+\mathbf{q})+i\epsilon} \tag{B.1}$$

where q_0=$E_\nu - E_l$, $n_n(\mathbf{p})$ and $n_p(\mathbf{p}+\mathbf{q})$ are occupation numbers for neutrons and protons, respectively, in the Fermi sea. The imaginary part of above Lindhard function is given using following relation

$$\frac{1}{\omega \pm i\eta} = \mathcal{P}\frac{1}{\omega} \mp i\pi\delta(\omega) \tag{B.2}$$

Thus the imaginary part of Eq.B.1 is given as

$$\mathrm{Im}U_N(q_0,\mathbf{q}) = -2\pi\int \frac{d^3p}{(2\pi)^3}\, n_n(\mathbf{p})\,\left[1-n_p(\mathbf{p}+\mathbf{q})\right]\,\delta(q_0+E_n-E_p)\,\frac{M_pM_n}{E_pE_n} \tag{B.3}$$

Since $\mathbf{q}=\mathbf{p}'-\mathbf{p}$, $q_0 = E_\nu - E_l$, we have

$$E_p = \sqrt{(\mathbf{p}+\mathbf{q})^2+M^2} = \sqrt{|\mathbf{p}|^2+|\mathbf{q}|^2+2|\mathbf{p}||\mathbf{q}|cos\theta + M^2} \tag{B.4}$$

Therefore Eq.B.3 can be written as

$$\begin{aligned}\mathrm{Im}U_N(q_0,\mathbf{q}) &= -2\pi\int \frac{d^3p}{(2\pi)^3}\, n_n(\mathbf{p})\,\left[1-n_p(\mathbf{p}+\mathbf{q})\right]\,\frac{M_pM_n}{E_pE_n} \\ &\quad\times\delta\left(q_0+\sqrt{|\mathbf{p}|^2+M^2}-\sqrt{|\mathbf{p}|^2+|\mathbf{q}|^2+2|\mathbf{p}||\mathbf{q}|cos\theta+M^2}\right)\end{aligned} \tag{B.5}$$

The occupation number $n_n(\mathbf{p})$=1 for $p < p_{F_1}$ (p_{F_1} is the local Fermi momenta of neutron), else it is equal to zero. Using this we place the limit on the integral over p from p_{F_1} to 0, and with

$$d^3|\mathbf{p}| = 2\pi d(\cos\theta)|\mathbf{p}|^2 d|\mathbf{p}|$$

Eq.B.5 becomes

$$\begin{aligned} \mathrm{Im}U_N(q_0.\mathbf{q}) &= -(2\pi)^2\, M_p M_n \int_0^{p_{F_1}} \frac{|\mathbf{p}|^2 d|\mathbf{p}|}{(2\pi)^3} \frac{[1-n_p(\mathbf{p}+\mathbf{q})]}{\sqrt{|\mathbf{p}|^2+M^2}} \int_{-1}^{1} d(\cos\theta) \\ &\left(\frac{1}{\sqrt{|\mathbf{p}|^2+|\mathbf{q}|^2+2|\mathbf{p}||\mathbf{q}|cos\theta+M^2}} \right) \delta\left(q_0 + \sqrt{|\mathbf{p}|^2+M^2} \right. \\ &\left. - \sqrt{|\mathbf{p}|^2+|\mathbf{q}|^2+2|\mathbf{p}||\mathbf{q}|cos\theta+M^2} \right) \end{aligned} \tag{B.6}$$

Using the δ function property

$$\int f(x)\delta\left[g(x)\right]dx = \int f(x)\frac{\delta\left[g(x)\right]}{g'(x)}dg(x) = \sum_i \frac{f(x)}{|\partial g(x_i)/\partial x|} \tag{B.7}$$

where the points x_i are the real roots of $g(x)$=0 in the interval of integration. The $cos\theta$ integral can be performed using Eq.B.7, and we get the above equation as

$$\begin{aligned} \mathrm{Im}U_N(q_0,\mathbf{q}) &= -\frac{M_p M_n}{2\pi} \int_0^{p_{F_1}} |\mathbf{p}|^2 d|\mathbf{p}| \frac{[1-n_p(\mathbf{p}+\mathbf{q})]}{\sqrt{|\mathbf{p}|^2+M^2}} \times \qquad \text{(B.8)} \\ &\left[\frac{-|\mathbf{p}||\mathbf{q}|}{\sqrt{|\mathbf{p}|^2+|\mathbf{q}|^2+2|\mathbf{p}||\mathbf{q}|cos\theta+M^2}} \right]^{-1} \\ &= \frac{M_p M_n}{2\pi} \int_0^{p_{F_1}} \frac{|\mathbf{p}|}{|\mathbf{q}|} d|\mathbf{p}| \frac{[1-n_p(\mathbf{p}+\mathbf{q})]}{\sqrt{|\mathbf{p}|^2+M^2}} \left[q_0 + \sqrt{|\mathbf{p}|^2+M^2} \right] \qquad \text{(B.9)} \end{aligned}$$

From the δ integration we have

$$q_0 + \sqrt{|\mathbf{p}|^2+M^2} - \sqrt{|\mathbf{p}|^2+|\mathbf{q}|^2+2|\mathbf{p}||\mathbf{q}|cos\theta+M^2} = 0$$

$$q_0 + \sqrt{|\mathbf{p}|^2+M^2} = \sqrt{|\mathbf{p}|^2+|\mathbf{q}|^2+2|\mathbf{p}||\mathbf{q}|cos\theta+M^2}$$

which implies (B.10)

$$\cos\theta = \frac{q_0^2 - |\mathbf{q}| + 2q_0\sqrt{|\mathbf{p}|^2+M^2}}{2|\mathbf{p}||\mathbf{q}|} \leq 1 \tag{B.11}$$

Further, $[1-n_p(\mathbf{p}+\mathbf{q})] = \Theta(|\mathbf{p}+\mathbf{q}|-p_{F_2}) \Rightarrow (\mathbf{p}+\mathbf{q})^2 > p_{F_2}^2$

Using expression for $\cos\theta$ from Eq.B.10, the above expression becomes

$$\sqrt{q_0^2 - |\mathbf{p}|^2 + 2q_0\sqrt{|\mathbf{p}|^2+M^2}} > p_{F_2} \tag{B.12}$$

Imposing conditions B.10 and B.11 in B.8 gives the factor $\Theta(1-|\cos\theta|)$ and $\Theta(A_1 - p_{F_2})$ where $A_1 = \sqrt{q_0^2 - |\mathbf{p}|^2 + 2q_0\sqrt{|\mathbf{p}|^2 + M^2}}$. With the substitution of these factors Eq.B.8 is given by

$$\begin{aligned} \mathrm{Im}U_N(q_0,\mathbf{q}) &= \frac{M_p M_n}{2\pi}\int_0^{p_{F_1}} \frac{d|\mathbf{p}|}{\sqrt{|\mathbf{p}|^2+M^2}}\,\frac{|\mathbf{p}|}{|\mathbf{q}|}\,\Theta(1-|\cos\theta|)\,\Theta(A_1 - p_{F_2}) \\ &= \frac{M_p M_n}{2\pi}\int_0^{p_{F_1}} \frac{dE}{|\vec{q}|}\,\Theta(1-|\cos\theta|)\,\Theta(A_1 - p_{F_2}) \end{aligned} \tag{B.13}$$

Solving the integral and taking account of the two theta functions gives

$$\mathrm{Im}U_N(q_0,\mathbf{q}) = -\frac{1}{2\pi}\frac{M_p M_n}{|\mathbf{q}|}\,[E_{F_1} - A] \quad \text{with} \tag{B.14}$$

$$q^2 < 0, \quad E_{F_2} - q_0 < E_{F_1} \quad \text{and} \quad \frac{-q_0 + |\mathbf{q}|\sqrt{1-\frac{4M^2}{q^2}}}{2} < E_{F_1}$$

where

$$E_{F_1} = \sqrt{{p_{F_n}}^2 + {M_n}^2}, \quad E_{F_2} = \sqrt{{p_{F_p}}^2 + {M_p}^2} \quad \text{and}$$

$$A = Max\left[M_n,\ E_{F_2} - q_0,\ \frac{-q_0 + |\vec{q}|\sqrt{1-\frac{4M^2}{q^2}}}{2}\right]. \tag{B.16}$$

Otherwise, $\mathrm{Im}U_N(q_0.\mathbf{q})$=0.

==========********==========

Appendix C

Non-relativistic Reduction of Weak Matrix Elements

The most general form of the hadronic current that is Lorentz invariant given in Eq.2.6 in Chapter-2 is

$$J_\mu = \bar{u}(p')\left[F_1^V(q^2)\gamma_\mu + F_2^V(q^2)i\sigma_{\mu\nu}\frac{q^\nu}{2M} + F_A^V(q^2)\gamma_\mu\gamma_5 + F_P^V(q^2)q_\mu\gamma_5\right]u(p) \quad \text{(C.1)}$$

Consider the terms with F_A in the hadronic current J_μ as

$$\bar{u}(p')\ F_A(q^2)\gamma_\mu\gamma_5\ u(p)$$

The spinors $u(p)$ and $\bar{u}(p)$ are represented by

$$u(p) = \sqrt{\frac{E+M}{2E}}\begin{pmatrix} 1 \\ \frac{\vec{\sigma}\cdot\vec{p}}{E+M} \end{pmatrix} \quad \text{(C.2)}$$

$$\bar{u}(p') = u(p')\gamma_0 = \sqrt{\frac{E'+M}{2E'}}\left(1, \quad \frac{-\vec{\sigma}\cdot\vec{p'}}{E'+M}\right) \quad \text{(C.3)}$$

Solving the terms for F_A using Eqs.C.2 and C.3, we get

$$\bar{u}(p')F_A\gamma_\mu\gamma_5 u(p) = F_A(q^2)\left[\bar{u}(p')\gamma_0\gamma_5 u(p),\ \bar{u}(p')\gamma_i\gamma_5 u(p)\right] \quad \text{(C.4)}$$

Using

$$\bar{u}(p')\gamma_0\gamma_5 u(p) = \sqrt{\frac{(E+M)(E'+M)}{4EE'}}\left[\left(1, \quad \frac{-\vec{\sigma}\cdot\vec{p'}}{E'+M}\right)\begin{pmatrix} 1 & 0 \\ 0 & -1 \end{pmatrix}\begin{pmatrix} 0 & 1 \\ 1 & 0 \end{pmatrix}\begin{pmatrix} 1 \\ \frac{\vec{\sigma}\cdot\vec{p}}{E+M} \end{pmatrix}\right]$$

$$= \frac{\vec{\sigma}\cdot(\vec{p}+\vec{p'})}{2E} = \frac{\vec{\sigma}\cdot(2\vec{p}+\vec{q})}{2M} = \frac{\vec{\sigma}\cdot\vec{P}}{2M} \quad \text{(for } E = E' = M\text{)} \quad \text{(C.5)}$$

and

$$\bar{u}(p')\gamma_i\gamma_5 u(p) = \sqrt{\frac{(E+M)(E'+M)}{4EE'}}\left[\left(1,\ \frac{-\vec{\sigma}\cdot\vec{p'}}{E'+M}\right)\begin{pmatrix} 0 & \sigma_i \\ -\sigma_i & 0 \end{pmatrix}\begin{pmatrix} 0 & I \\ I & 0 \end{pmatrix}\begin{pmatrix} 1 \\ \frac{\vec{\sigma}\cdot\vec{p}}{E+M} \end{pmatrix}\right]$$

$$= \left(\vec{\sigma} - \frac{\sigma_i(\vec{\sigma}\cdot\vec{p})(\vec{\sigma}\cdot\vec{p'})}{4E^2}\right) \qquad \text{(for } E = E' = M\text{)} \tag{C.6}$$

Neglecting second order term, we get term with $F_A(q^2) \propto F_A\ \vec{\sigma}$.

Similarly, considering the term

$$\bar{u}(p')\ F_2^V(q^2)\ i\sigma_{\mu\nu}\frac{q^\nu}{2M}\ u(p)$$

We have

$$\sigma_{i\nu}\ q^\nu = \sigma_{i0}\ q^0 - \sigma_{ii}\ q^i$$

Since $q^0 = E - E' = 0$ for $E = E'$, only $\nu = i$ will contribute, i.e.,

$$\begin{aligned} \sigma_{\mu\nu}\ q^\nu &= -\sigma_{ii}\ q^i = -\left[\sigma_{0i}\ q^i,\ \sigma_{ji}\ q^i\right] \\ &= -i\begin{pmatrix} 0 & \vec{\sigma}\cdot\vec{q} \\ \vec{\sigma}\cdot\vec{q} & 0 \end{pmatrix},\ \begin{pmatrix} \vec{\sigma}\times\vec{q} & 0 \\ 0 & \vec{\sigma}\times\vec{q} \end{pmatrix} \end{aligned} \tag{C.7}$$

Hence,

$$i\frac{F_2}{2M}\ \bar{u}(p')\ \sigma_{\mu\nu}\ q^\nu u(p) = -i\frac{F_2}{2M}\left[\bar{u}(p')\ \sigma_{0i}\ q^i\ u(p),\ \bar{u}(p')\ \sigma_{ji}\ q^i\ u(p)\right] \tag{C.8}$$

We have

$$\begin{aligned} -i\frac{F_2}{2M}\ \bar{u}(p')\ \sigma_{0i}\ q^i u(p) &= -\frac{F_2}{2M}\left[\sqrt{\frac{(E+M)(E'+M)}{4EE'}}\left(1,\ \frac{-\vec{\sigma}\cdot\vec{p'}}{E'+M}\right)\begin{pmatrix} 0 & \vec{\sigma}\cdot\vec{q} \\ \vec{\sigma}\cdot\vec{q} & 0 \end{pmatrix}\right. \\ &\quad \left.\begin{pmatrix} 1 \\ \frac{\vec{\sigma}\cdot\vec{p}}{E+M} \end{pmatrix}\right] \\ &= -\frac{F_2}{2M}\left[\frac{(\vec{\sigma}\cdot\vec{q})(\vec{\sigma}\cdot\vec{q})}{2E}\right] \end{aligned} \tag{C.9}$$

and

$$\begin{aligned} -i\frac{F_2}{2M}\ \bar{u}(p')\ \sigma_{ji}\ q^j u(p) &= -\frac{F_2}{2M}\left[\sqrt{\frac{(E+M)(E'+M)}{4EE'}}\left(1,\ \frac{-\vec{\sigma}\cdot\vec{p'}}{E'+M}\right)\begin{pmatrix} \vec{\sigma}\times\vec{q} & 0 \\ 0 & \vec{\sigma}\times\vec{q} \end{pmatrix}\right. \\ &\quad \left.\begin{pmatrix} 1 \\ \frac{\vec{\sigma}\cdot\vec{p}}{E+M} \end{pmatrix}\right] \\ &= -i\frac{F_2}{2M}\left[\frac{E+M}{2E}\ \left(\vec{\sigma}\times\vec{q} - \frac{(\vec{\sigma}\times\vec{q})(\vec{\sigma}\cdot\vec{p})(\vec{\sigma}\cdot\vec{p'})}{(E+M)^2}\right)\right] \end{aligned} \tag{C.10}$$

Neglecting the second order term, we get term with $F_2(q^2) \propto F_2(q^2)\ \vec{\sigma} \times \vec{q}$.

Similarly, considering the term

$$\bar{u}(p')\ F_1^V(q^2)\ \gamma_\mu\ u(p)$$

we get

$$F_1^V(q^2)\ \bar{u}(p')\ \gamma_0\ u(p) = F_1^V(q^2)\left[1 + \frac{|\vec{p}|^2 + i\epsilon_{ijk}\ p_i p_j \sigma_k + \vec{p}\cdot\vec{q} + i\epsilon_{ijk}\ q_i p_j \sigma_k}{(2M)^2}\right] \quad \text{(C.11)}$$

and

$$F_1^V(q^2)\ \bar{u}(p')\ \gamma_i\ u(p) = F_1^V(q^2)\frac{1}{2M}\left[(2p_i + q_i) - i\epsilon_{ijk}\ q_i \sigma_k\right] \quad \text{(C.12)}$$

Considering the term

$$\bar{u}(p')\ F_p(q^2)\ q_\mu \gamma_5\ u(p)$$

we get only

$$F_p(q^2)\ q_i\ \bar{u}(p')\ \gamma_5\ u(p) = -F_p(q^2)\frac{q_i q_j}{2M}\sigma_j \quad \text{(C.13)}$$

Now collecting J_0 and J_i terms together of the hadronic current J_μ, we get

$$J_0 = \frac{F_A(q^2)}{2M}\ \sigma_i P_i + F_1^V(q^2)\left[1 + \frac{\vec{p}\cdot\vec{p'} + i\epsilon_{ijk}\ p'_i p_j \sigma_k}{(2M)^2}\right] + \frac{F_2^V(q^2)}{(2M)^2}\ \sigma_l q_l \sigma_m q_m \quad \text{(C.14)}$$

and

$$J_i = F_A(q^2)\left[\vec{\sigma}_i - \frac{\sigma_i(\vec{\sigma}\cdot\vec{p})(\vec{\sigma}\cdot\vec{p'})}{(2M)^2}\right] + \frac{F_1^V(q^2)}{2M}\left[P_i - i\epsilon_{ijk}\ q_j \sigma_k\right] - \iota\frac{F_2^V(q^2)}{2M}\ \epsilon_{jkl}\sigma_k q_l \quad \text{(C.15)}$$

Now we find J_{00}

$$J_{00} = \tilde{\sum}\sum\left\{\frac{F_A(q^2)}{2M}\ \sigma_i P_i + F_1^V(q^2)\left[1 + \frac{\vec{p}\cdot\vec{p'} + i\epsilon_{ilm}\ p'_i p_l \sigma_m}{(2M)^2}\right] + \frac{F_2^V(q^2)}{(2M)^2}\ \sigma_l q_l \sigma_m q_m\right\}$$
$$\times\left\{\frac{F_A(q^2)}{2M}\sigma_j P_j + F_1^V(q^2)\left[1 + \frac{\vec{p}\cdot\vec{p'} + i\epsilon_{jl'm'}\ p'_j p_{l'}\sigma_{m'}}{(2M)^2}\right] + \frac{F_2^V(q^2}{(2M)^2}\sigma_{l'} q_{l'}\sigma_{m'} q_{m'}\right\} \quad \text{(C.16)}$$

Neglecting the terms with $1/(2M)^3$, $1/(2M)^4$ or higher power and using the trace relations

$$\begin{aligned}
\mathrm{Tr}(I) &= 2 && \text{(C.17)}\\
\mathrm{Tr}(\sigma^l) &= 0 && \text{(C.18)}\\
\mathrm{Tr}(\sigma^i\sigma^j) &= 2\delta^{ij} && \text{(C.19)}\\
\mathrm{Tr}(\sigma^i\sigma^j\sigma^k) &= 2i\epsilon^{ijk} && \text{(C.20)}\\
\mathrm{Tr}(\sigma^i\sigma^j\sigma^k\sigma^l) &= 2\left[\delta^{ij}\delta^{kl} - \delta^{ik}\delta^{jl} + \delta^{il}\delta^{jl}\right] && \text{(C.21)}
\end{aligned}$$

we get finally

$$\begin{aligned}
J_{00} &= \bar{\sum}\sum\left[\left(\frac{F_A(q^2)}{2M}\right)^2 \sigma_i P_i \sigma_j P_j + (F_1^V(q^2))^2\left\{1+\frac{2\vec{p}\cdot\vec{p'}}{(2M)^2}\right\}\right.\\
&\quad \left.+2\frac{F_1^V(q^2)F_2^V(q^2)}{(2M)^2}\sigma_l q_l \sigma_l \sigma_m\right]\\
&= \bar{\sum}\sum\left[\left(\frac{F_A(q^2)}{2M}\right)^2 (\delta_{ij}+i\epsilon_{ijk}\,\sigma_k)\,P_i P_j + (F_1^V(q^2))^2\left\{1+\frac{2\vec{p}\cdot\vec{p'}}{(2M)^2}\right\}\right.\\
&\quad \left.+2\frac{F_1^V(q^2)F_2^V(q^2)}{(2M)^2}\,(\delta_{lm}+i\epsilon_{lmn}\,\sigma_n)\,q_l q_m\right]\\
&= \left[2\left(\frac{F_A(q^2)}{2M}\right)^2 \vec{P}^2 + 2(F_1^V(q^2))^2\left\{1+\frac{2\vec{p}\cdot(\vec{p}+\vec{q})}{(2M)^2}\right\} + 4\frac{F_1^V(q^2)F_2^V(q^2)}{(2M)^2}|\vec{q}|^2\right]
\end{aligned} \qquad \text{(C.22)}$$

Similarly, we find J_{ij} as follows

$$\begin{aligned}
J_{ij} &= \bar{\sum}\sum\left\{F_A(q^2)\left[\vec{\sigma}_i + \frac{(\vec{\sigma}\cdot\vec{p'})\sigma_i(\vec{\sigma}\cdot\vec{p})}{(2M)^2}\right] + \frac{F_1^V(q^2)}{2M}\,[P_i - i\epsilon_{ilm}\,q_l\sigma_m]\right.\\
&\quad \left.-i\frac{F_2^V(q^2)}{2M}\,\epsilon_{ilm}\,\sigma_l q_m\right\} \times \left\{F_A(q^2)\left[\vec{\sigma}_j + \frac{(\vec{\sigma}\cdot\vec{p'})\sigma_j(\vec{\sigma}\cdot\vec{p})}{(2M)^2}\right] + \frac{F_1^V(q^2)}{2M}\right.\\
&\quad \left.[P_j - i\epsilon_{jl'm'}\,q_{l'}\sigma_{m'}] - i\frac{F_2^V(q^2)}{2M}\,\epsilon_{jl'm'}\,\sigma_{l'}q_{m'}\right\}
\end{aligned} \qquad \text{(C.23)}$$

Neglecting the terms with $1/(2M)^3$, $1/(2M)^4$ or higher power and using the trace relations given in Eq.C.17-21, we get

$$\begin{aligned}
J_{ij} &= \bar{\sum}\sum\left[F_A^2(q^2)\sigma_i\sigma_j + \left(\frac{F_1^V(q^2)}{2M}\right)^2 P_i P_j + 2\frac{F_1^V(q^2)F_2^V(q^2)}{(2M)^2}\epsilon_{il'l}\epsilon_{jl'm'}\,q_l q_{m'}\right.\\
&\quad \left.-\left(\frac{F_2^V(q^2)}{2M}\right)^2 \epsilon_{lim}\epsilon_{ljm'}\,q_m q_{m'}\right]
\end{aligned}$$

$$
\begin{aligned}
&= F_A^2(q^2)\left[(\delta_{ij}-\hat{q}_i\hat{q}_j)+\hat{q}_i\hat{q}_j\right]+\left(\frac{F_1^V(q^2)}{2M}\right)^2 P_iP_j+2\frac{F_1^V(q^2)F_2^V(q^2)}{(2M)^2}\\
&\quad (\delta_{ij}|\vec{q}|^2-q_iq_j)-\left(\frac{F_2^V(q^2)}{2M}\right)^2\left(\delta_i^j\delta_m^{m'}-\delta_i^{m'}\delta_m^j\right)q_mq_{m'}\\
&= 2\Bigg\{F_A^2(q^2)\left[(\delta_{ij}-\hat{q}_i\hat{q}_j)+\hat{q}_i\hat{q}_j\right]+\left(\frac{F_1^V(q^2)}{2M}\right)^2 P_iP_j+2\frac{F_1^V(q^2)F_2^V(q^2)}{(2M)^2}\\
&\quad |\vec{q}|^2(\delta_{ij}-\hat{q}_i\hat{q}_j)-|\vec{q}|^2\left(\frac{F_2^V(q^2)}{2M}\right)^2(\delta_{ij}-\hat{q}_i\hat{q}_j)\Bigg\} \qquad \text{(C.24)}
\end{aligned}
$$

Now we find J_{0i}

$$
\begin{aligned}
J_{0i} &= \bar{\sum}\sum\Bigg\{\frac{F_A(q^2)}{2M}\sigma_iP_i+F_1^V(q^2)\left[1+\frac{\vec{p}\cdot\vec{p'}+i\epsilon_{ilm}\,p'_ip_l\sigma_m}{(2M)^2}\right]\\
&\quad +\frac{F_2^V(q^2)}{(2M)^2}\sigma_lq_l\sigma_mq_m\Bigg\}\Bigg\{F_A(q^2)\left[\vec{\sigma}_j+\frac{(\vec{\sigma}\cdot\vec{p'})\sigma_j(\vec{\sigma}\cdot\vec{p})}{(2M)^2}\right]+\frac{F_1^V(q^2)}{2M}\\
&\quad \left[P_j-i\epsilon_{jl'm'}\,q_{l'}\sigma_{m'}\right]-i\frac{F_2^V(q^2)}{2M}\,\epsilon_{jl'm'}\,\sigma_{l'}q_{m'}\Bigg\} \qquad \text{(C.25)}
\end{aligned}
$$

$$
\begin{aligned}
J_{0i} &= \bar{\sum}\sum\Bigg[\frac{F_A^2(q^2)}{2M}(\delta_{ij}+i\epsilon_{ijk}\,\sigma_k)\,P_i-\frac{F_1^V(q^2)F_A(q^2)}{(2M)^2}i\epsilon_{jl'm'}q_{l'}P_i\\
&\quad (\delta_{im'}+i\epsilon_{imn}\,\sigma_n)-i\frac{F_2^V(q^2)F_A(q^2)}{(2M)^2}\epsilon_{jl'm'}q_{l'}P_i\,(\delta_{im'}+i\epsilon_{im'n}\,\sigma_n)\\
&\quad +i\frac{F_1^V(q^2)F_A(q^2)}{(2M)^2}\epsilon_{ilm}P'_ip_l\,(\delta_{mj}+i\epsilon_{mjn}\,\sigma_n)+\frac{(F_1^V(q^2))^2}{2M}P_j\Bigg] \qquad \text{(C.26)}
\end{aligned}
$$

Neglecting all the terms with $O(1/M^3)$ or higher powers and using trace relations, we get

$$
\begin{aligned}
J_{0i} &= 2\left[\frac{F_A^2(q^2)}{2M}\delta_{ij}P_i+\frac{(F_1^V(q^2))^2}{2M}P_j\right]\\
&= 2\frac{F_A^2(q^2)}{2M}\left[(\delta_{ij}-\hat{q}_i\hat{q}_j)+\hat{q}_i\hat{q}_j\right](2p_i+q_i)+2\frac{(F_1^V(q^2))^2}{2M}(2p_i+q_i) \qquad \text{(C.27)}
\end{aligned}
$$

Using Eq C.24 and Eq C.27, we get the nonvanishing components as

$$
\begin{aligned}
J_{zz} &= 2\left[F_A^2(q^2)U_L+\left(\frac{F_1^V(q^2)}{2M}\right)^2(p_z^2+2p_z|\vec{q}|+|\vec{q}|^2)\right] \qquad \text{(C.28)}\\
J_{xx} &= 2\left[F_A^2(q^2)U_T\delta_{xx}+\left(\frac{F_1^V(q^2)}{2M}\right)^2p_x^2+2\frac{F_1^V(q^2)F_2^V(q^2)}{(2M)^2}|\vec{q}^{\,2}U_T\right.
\end{aligned}
$$

$$-|\vec{q}|^2 \left(\frac{F_2^V(q^2)}{2M}\right)^2 U_T\Bigg] \tag{C.29}$$

$$J_{oz} = 2\frac{F_A^2(q^2)}{2M}[(2p_z + q_z)U_L] + 2\frac{(F_1^V(q^2))^2}{2M}(2p_z + q_z) \tag{C.30}$$

$$J_{z0} = J_{0z} \tag{C.31}$$

==========********==========

Appendix D

Hadronic and Leptonic Tensors $J_{\mu\nu}$ and $L^{\mu\nu}$

D.1 Component Form

D.1.1 Leptonic Tensor

$$L^{\mu\nu} = 8\left[k^{\mu}k^{\nu\prime} + k^{\mu\prime}k^{\nu} - g^{\mu\nu}\ k\cdot k' + i\epsilon^{\mu\nu\alpha\beta}\ k^{\alpha}k'^{\beta}\right] \tag{D.1}$$

$$L^{00} = 8\left[k^0k^{0\prime} + \vec{k}\cdot\vec{k'}\right] \tag{D.2}$$

$$L^{0i} = 8\left[k^0k^{i\prime} + k^ik^{0\prime}\right] \tag{D.3}$$

$$L^{ij} = 8\left[k^ik^{j\prime} + k^{i\prime}k^j + k\cdot k'\delta^{ij}\right] \tag{D.4}$$

D.1.2 Hadronic Tensor

I. $(F_1^V)^2$-Term: $8\ \left(\frac{1}{2}\right)\left(\frac{1}{4M_pM_n}\right)\cdot(F_1^V)^2$

$$J_{\mu\nu} = \left[p'_{\mu}p_{\nu} + p'_{\nu}p_{\mu} - (p\cdot p' - M_pM_n)g_{\mu\nu}\right] \tag{D.5}$$

$$J_{\mu\nu} = \left[p_{\mu}p_{\nu} + \frac{(q_{\mu}p_{\nu} + q_{\nu}p_{\mu})}{2} + \frac{q^2}{4}g_{\mu\nu}\right] \tag{D.6}$$

$$J_{00} = E^2(\vec{p}) + q_0E(\vec{p}) + \frac{q^2}{4} \tag{D.7}$$

$$J_{ij} = p_ip_j + \frac{(q_ip_j + p_iq_j)}{2} - \frac{q^2}{4}\delta_{ij} \tag{D.8}$$

$$J_{0i} = \left[p_0p_i + \frac{(q_0p_i + q_ip_0)}{2}\right] \tag{D.9}$$

$$J_{0z} = \frac{2E(\vec{p})p_z + q_0 p_z + |\vec{q}|E(\vec{p})}{2} \tag{D.10}$$

$$J_{zz} = p_z^2 + |\vec{q}|p_z - \frac{q^2}{4} \tag{D.11}$$

$$J_{xx} = p_x^2 - \frac{q^2}{4} \tag{D.12}$$

II. $(F_2^V)^2$-Term: $\left(\frac{1}{2}\right)^2 \left(\frac{1}{2}\right)\left(\frac{1}{4M_pM_n}\right) (F_2^V)^2$

$$J_{\mu\nu} = 2q^2\left[4g_{\mu\nu} - 4\frac{p_\mu p_\nu}{M^2} - 2\frac{(p_\mu q_\nu + q_\mu p_\nu)}{M^2} - q_\mu q_\nu\left(\frac{4}{q^2} + \frac{1}{M^2}\right)\right] \tag{D.13}$$

$$J_{00} = 8q^2\left[1 - \frac{E^2(\vec{p})}{M^2} - \frac{E(\vec{p})q_0}{M^2} - \frac{q_0^2}{q^2} - \frac{q_0^2}{4M^2}\right] \tag{D.14}$$

$$J_{ij} = -8q^2\left[\delta_{ij} + \frac{p_i pj}{M^2} + \frac{(p_i q_j + q_i p_j)}{2M^2} + \frac{q_i q_j}{q^2} + \frac{1}{4M^2}q_i q_j\right] \tag{D.15}$$

$$J_{0i} = -8q^2\left[\frac{p_0 pi}{M^2} + \frac{(p_0 q_i + q_0 p_i)}{2M^2} + \frac{q_0 q_i}{q^2} + \frac{1}{4M^2}q_0 q_i\right] \tag{D.16}$$

$$J_{0z} = -4q^2\left[2\frac{E(\vec{p})p_z}{M^2} + \frac{E(\vec{p})|\vec{q}|}{M^2} + 2\frac{q_0|\vec{q}|}{q^2} + \frac{2q_0 p_z}{M^2} + \frac{q_0|\vec{q}|}{2M^2}\right] \tag{D.17}$$

$$J_{zz} = -2q^2\left[\frac{4p_z^2}{M^2} + \frac{4p_z|\vec{q}|}{M^2} + \frac{q_0^2}{q^2} + \frac{|\vec{q}|^2}{M^2}\right] \tag{D.18}$$

$$J_{xx} = -8q^2\left[1 - \frac{p_x^2}{M^2}\right] \tag{D.19}$$

III. (F_A^2)-Term: $8\left(\frac{1}{2}\right)\left(\frac{1}{4M_pM_n}\right)(F_A)^2$

$$J_{\mu\nu} = \left[p_\mu p_\nu + \frac{(p_\mu q_\nu + q_\mu p_\nu)}{2} + g_{\mu\nu}\left(\frac{q^2}{4} - M^2\right)\right] \tag{D.20}$$

$$J_{00} = \left[\vec{p}^2 + q_0 E(\vec{p}) + \frac{q^2}{4}\right] \tag{D.21}$$

$$J_{ij} = \left[p_i p_j + \frac{(p_i q_j + q_i p_j)}{2} - \delta_{ij}\left(\frac{q^2}{4} - M^2\right)\right] \tag{D.22}$$

$$J_{0i} = \left[p_0 p_i + \frac{(p_0 q_i + q_0 p_i)}{2}\right] \tag{D.23}$$

$$J_{0z} = \left[E(\vec{p})p_z + \frac{1}{2}\left(E(\vec{p})|\vec{q}| + q_0 p_z\right)\right] \tag{D.24}$$

$$J_{zz} = \left[M^2 + p_z^2 + |\vec{q}|p_z - \frac{q^2}{4}\right] \tag{D.25}$$

$$J_{xx} = \left[p_x^2 + M^2 - \frac{q^2}{4}\right] \tag{D.26}$$

IV. $(F_1^V F_2^V)/2M$**-Term:** $8\ \left(\frac{1}{2}\right)\left(\frac{1}{4M_p m_n}\right)\ (F_1^V F_2^V)/2$

$$J_{\mu\nu} = \left[-q_\mu q_\nu + q^2 g_{\mu\nu}\right] \tag{D.27}$$
$$J_{00} = -|\vec{q}|^2 \tag{D.28}$$
$$J_{ij} = \left[-q_i q_j - q^2\delta_{ij}\right] = -\left[q_i q_j + q^2\delta_{ij}\right] \tag{D.29}$$
$$J_{0z} = \left[-q_0|\vec{q}|\right] \tag{D.30}$$
$$J_{zz} = -q_0^2 \tag{D.31}$$
$$J_{xx} = -q^2 \tag{D.32}$$

V. $(F_1^V F_A)$**-Term:** $i8\ \left(\frac{1}{2}\right)\left(\frac{1}{4M_p M_n}\right)\ (F_1^V F_A)$

$$J_{\mu\nu} = -\epsilon_{\alpha\mu\delta\nu}\ p'^\alpha p^\delta = \epsilon_{\mu\nu\alpha\delta}\ p'^\alpha p^\delta = \epsilon_{\mu\nu\alpha\delta}\ \left(p^\alpha p^\delta + q^\alpha p^\delta\right) \tag{D.33}$$
$$J_{ij} = \epsilon_{ij\alpha\delta}\ \left(p^\alpha p^\delta + q^\alpha p^\delta\right) \tag{D.34}$$
$$J_{xy} = \left[q_0 p_z - E(\vec{p})|\vec{q}|\right] \tag{D.35}$$

VI. $(F_2^V F_A)$**-Term:** $i8\ \left(\frac{1}{2}\right)\left(\frac{1}{4M_p M_n}\right)\ (F_2^V F_A)$

$$J_{\mu\nu} = \frac{1}{2}\left[\epsilon_{\alpha\mu\beta\nu}\ p'^\alpha q^\beta + \epsilon_{\mu\beta\delta\nu}\ q^\beta p^\delta\right] = \frac{1}{2}\left[-\epsilon_{\mu\nu\alpha\beta}\ p^{\alpha\prime} q^\beta + \epsilon_{\mu\nu\beta\delta}\ q^\beta p^\delta\right] \tag{D.36}$$
$$J_{\mu\nu} = \frac{1}{2}\left[-\epsilon_{\mu\nu\alpha\beta}\ \left(p^\alpha q^3 + q^\alpha q^\beta\right) + \epsilon_{\mu\nu\beta\delta}\ q^\beta p^\delta\right] \tag{D.37}$$
$$J_{ij} = \frac{1}{2}\left[-\epsilon_{ij\alpha\beta}\ \left(p^\alpha q^\beta + q^\alpha q^\beta\right) + \epsilon_{ij\beta\delta}\ q^\beta p^\delta\right] \tag{D.38}$$
$$J_{xy} = \left[q_0 p_z - E(\vec{p})|\vec{q}|\right] \tag{D.39}$$

D.2 RPA Corrections

$$\begin{aligned}\frac{J_{00}^{RPA}}{M^2} = {} & \left(F_1^V(q^2)\right)^2\left[\left(\frac{E(\vec{p})}{M}\right)^2 + \left(\frac{q_0 E(\vec{p}) + q^2/4}{M^2}\right)\right] - \frac{q^2}{M^2}\left(\frac{F_2^V(q^2)}{2}\right)^2 \\ & \left[\frac{\vec{p}^2 + q_0 E(\vec{p}) + q_0^2/4}{M^2} + \frac{q_0^2}{q^2}\right] - \frac{1}{2}\left(F_1^V(q^2)F_2^V(q^2)\right)\left(\frac{|\vec{q}|}{M}\right)^2 \\ & + F_A^2(q^2)\left[\frac{\vec{p}^2 + q_0 E(\vec{p}) + q^2/4}{M^2} - U_L\left(\frac{q_0^2}{m_\pi^2 - q^2}\right)\left(\frac{q^2}{m_\pi^2 - q^2}\right)\right]\end{aligned} \tag{D.40}$$

$$\frac{J_{0z}^{RPA}}{M^2} = \frac{1}{2}\left(F_1^V(q^2)\right)^2\left[\frac{E(\vec{p})}{M}\left(\frac{2p_z+|\vec{q}|}{M}\right)+\frac{q_o p_z}{M^2}\right]-\frac{1}{2}\frac{q^2}{M^2}\left(\frac{F_2^V(q^2)}{2}\right)^2 \left[\frac{E(\vec{p})}{M}\left(\frac{2p_z+|\vec{q}|}{M}\right)+\frac{2q_0|\vec{q}|}{q^2}+\frac{q_0\left(2p_z+|\vec{q}|\right)}{2M^2}\right]-\frac{1}{2}\left(F_1^V(q^2)F_2^V(q^2)\right) \left[\frac{q_0|\vec{q}|}{M^2}\right]+F_A^2(q^2)\left[U_L\frac{E(\vec{p})}{M}\left(\frac{2p_z+|\vec{q}|}{2M}\right)+\frac{q_o p_z}{2M^2}-U_L\left(\frac{q_0|\vec{q}|}{m_\pi^2-q^2}\right) \left(\frac{q^2}{m_\pi^2-q^2}\right)\right] \tag{D.41}$$

$$\frac{J_{zz}^{RPA}}{M^2} = \left(F_1^V(q^2)\right)^2\left[\frac{p_z^2+|\vec{q}|p_z-q^2/4}{M^2}\right]-\frac{1}{4}\frac{q^2}{M^2}\left(\frac{F_z^V(q^2)}{2}\right)^2\left[\left(\frac{2p_z+|\vec{q}|}{M}\right)^2 +\frac{q_0^2}{q^2}\right]-\frac{1}{2}\left(F_1^V(q^2)F_2^V(q^2)\right)\left(\frac{q_0}{M}\right)^2+F_A^2(q^2)\left[U_L+\frac{p_z^2+|\vec{q}|p_z-q^2/4}{M^2} -U_L\left(\frac{|\vec{q}|}{m_\pi^2-q^2}\right)\left(\frac{q^2}{m_\pi^2-q^2}\right)\right] \tag{D.42}$$

$$\frac{J_{RPA}^{xx}}{M^2} = \left(F_1^V(q^2)\right)^2\left[\frac{p_x^2-q^2/4}{M^2}\right]-\frac{q^2}{M^2}\left(\frac{F_2^V(q^2)}{2}\right)^2\left[U_T+\frac{p_x^2}{M^2}\right] -\frac{1}{2}\left(F_1^V(q^2)F_2^V(q^2)\right)U_T\left(\frac{q^2}{M^2}\right)+F_A^2(q^2)\left[U_L+\frac{p_x^2-q^2/4}{M^2}\right] \tag{D.43}$$

$$\frac{J_{xy}^{RPA}}{M^2} = iF_A(q^2)\left[F_1^V(q^2)+F_2^V(q^2)\right]\left[\frac{q_0p_z}{M^2}-U_T\frac{|\vec{q}|E(\vec{p})}{M^2}\right] \tag{D.44}$$

D.3 Contractions of $L^{\mu\nu}$ and $J_{\mu\nu}$ in Component Form

I. $(F_1^V)^2$-Term: $8\ \left(\frac{1}{2}\right)\left(\frac{1}{4M_pM_n}\right)\ 8\ \left(\frac{1}{4m_lm_\nu}\right)\ (F_1^V)^2$

$$L^{00}J_{00} = \left[E^2(\vec{p})+q_0E(\vec{p})+\frac{q^2}{4}\right]\left[k_0k_0'+\vec{k}\cdot\vec{k}'\right] \tag{D.45}$$

$$L^{0i}J_{0i}+L^{i0}J_{i0} = E(\vec{p})\left[k_0(\vec{q}\cdot\vec{k}')+k_0'(\vec{q}\ \ \vec{k})\right] \tag{D.46}$$

$$L^{ij}J_{ij} = \left[k\cdot k'|\vec{p}|^2-\frac{q^2}{4}\left(3k_0k_0'-\vec{k}\ \ \vec{k}'\right)\right] \tag{D.47}$$

II. $(F_2^V)^2$-Term: $\left(\frac{1}{2}\right)^2 \left(\frac{1}{2}\right) \left(\frac{1}{4M_pM_n}\right) 8 \left(\frac{1}{4m_lm_\nu}\right) (F_2^V)^2$

$$L^{00}J_{00} = 8q^2\left[1 - \frac{E^2(\vec{p})}{M^2} - \frac{E(\vec{p})q_0}{M^2} - \frac{q_0^2}{q^2} - \frac{q_0^2}{4M^2}\right]\left[k_0k_0' + \vec{k}\cdot\vec{k'}\right] \tag{D.48}$$

$$L^{0i}J_{0i} = -8q^2\left[\left\{\frac{p_0}{2M^2} + q_0\left(\frac{1}{q^2} + \frac{1}{M^2}\right)\right\}\left(k_0(\vec{q}\cdot\vec{k'}) + k_0'(\vec{q}\cdot\vec{k})\right)\right] \tag{D.49}$$

$$L^{ij}J_{ij} = -8q^2\left[2\vec{k}\cdot\vec{k'} + 3k\cdot k' + \frac{k\cdot k'}{M^2}\vec{p}^2 + \left(\frac{1}{4M^2} + \frac{1}{q^2}\right)\left(2(\vec{k}\cdot\vec{q})(\vec{k'}\cdot\vec{q}) + k\cdot k'|\vec{q}|^2\right)\right] \tag{D.50}$$

III. (F_A^2)-Term: $8 \left(\frac{1}{2}\right) \left(\frac{1}{4M_pM_n}\right) 8 \left(\frac{1}{4m_lm_\nu}\right) (F_A)^2$

$$L^{00}J_{00} = \left[E^2(\vec{p}) - M^2 + q_0E(\vec{p}) + \frac{q^2}{4}\right]\left[k_0k_0' + \vec{k}\cdot\vec{k'}\right] \tag{D.51}$$

$$L^{0i}J_{0i} = E(\vec{p})\left[k_0(\vec{q}\cdot\vec{k'}) + k_0'(\vec{q}\cdot\vec{k})\right] \tag{D.52}$$

$$L^{ij}J_{ij} = \left[k\cdot k'|\vec{p}|^2 - \left(\frac{q^2}{4} - M^2\right)\left(3k_0k_0' - \vec{k}\cdot\vec{k'}\right)\right] \tag{D.53}$$

IV. $(F_1^VF_2^V)/2M$-Term: $8 \left(\frac{1}{2}\right) \left(\frac{1}{4M_pm_n}\right) 8 \left(\frac{1}{4m_lm_\nu}\right) (F_1^VF_2^V)/2$

$$L^{00}J_{00} = -|\vec{q}|^2\left[k_0k_0' + \vec{k}\cdot\vec{k'}\right] \tag{D.54}$$

$$L^{0i}J_{0i} = -\left[q_0k_0(\vec{q}\cdot\vec{k'}) + q_0k_0'(\vec{q}\cdot\vec{k})\right] \tag{D.55}$$

$$L^{ij}J_{ij} = -\left[2(\vec{q}\cdot\vec{k})(\vec{q}\cdot\vec{k'}) + 3q^2k_0k_0' - q^2\vec{k}\cdot\vec{k'} + |\vec{q}|^2q\cdot k\right] \tag{D.56}$$

V. $(F_1^VF_A)$-Term: $8 \left(\frac{1}{2}\right) \left(\frac{1}{4M_pM_n}\right) 8 \left(\frac{1}{4m_lm_\nu}\right) (F_1^VF_A)$

$$L^{00}J_{00} = 2\left[(p\cdot k')(q\cdot k) - (p\cdot k)(q\cdot k')\right] \tag{D.57}$$

$$L^{ij}J_{ij} = 2\left[(p\cdot k')(q\cdot k) - (p\cdot k)(q\cdot k')\right] \tag{D.58}$$

VI. $(F_2^VF_A)/2M$-Term: $8 \left(\frac{1}{2}\right) \left(\frac{1}{4M_pM_n}\right) 8 \left(\frac{1}{4m_lm_\nu}\right) (F_2^VF_A)/2M$

$$L^{00}J_{00} = 2M\left[(p\cdot k')(q\cdot k) - (p\ \ k)(q\cdot k')\right] \tag{D.59}$$

$$L^{ij}J_{ij} = 2M\left[(p\cdot k')(q\cdot k) - (p\ \ k)(q\cdot k')\right] \tag{D.60}$$

Appendix E

Rarita Schwinger Field

E.1 Spin-$\frac{3}{2}$ Spinors

The Rarita Schwinger spin-$\frac{3}{2}$ field can be constructed from the coupling of spin-$\frac{1}{2}$ and spin-1 field

$$u^{\mu}(\mathbf{p}, S_{\Delta}) = [\epsilon^{\mu}(\mathbf{p}, \lambda) \otimes u(\mathbf{p}, s)]^{\frac{3}{2}}_{S_{\Delta}} \tag{E.1}$$

$$= \sum_{\lambda, s} \left(\begin{array}{cc|c} 1 & \frac{1}{2} & \frac{3}{2} \\ \lambda & s & S_{\Delta} \end{array} \right) \epsilon^{\mu}(\mathbf{p}, \lambda)\, u(\mathbf{p}, s) \tag{E.2}$$

where $u(\mathbf{p}, s)$ and $\epsilon^{\mu}(\mathbf{p}, \lambda)$ are spin-$\frac{1}{2}$ ans spin-1 polarisation vector, respectively. Evaluating the Clebsch-Gordan coefficients, for example,

$$u^{\mu}(\mathbf{p}, 3/2) = \left(\begin{array}{ccc} 1 & \frac{1}{2} & \frac{3}{2} \\ 1 & \frac{1}{2} & \frac{3}{2} \end{array} \right) \epsilon^{\mu}(\mathbf{p}, 1)\, u(\mathbf{p}, 1/2) = \epsilon^{\mu}(\mathbf{p}, 1)\, u(\mathbf{p}, 1/2) \tag{E.3}$$

$$u^{\mu}(\mathbf{p}, -3/2) = \left(\begin{array}{ccc} 1 & \frac{1}{2} & \frac{3}{2} \\ -1 & -\frac{1}{2} & -\frac{3}{2} \end{array} \right) \epsilon^{\mu}(\mathbf{p}, -1)\, u(\mathbf{p}, -1/2)$$

$$= \epsilon^{\mu}(\mathbf{p}, -1)\, u(\mathbf{p}, -1/2) \tag{E.4}$$

this leads to the following explicit form of the spinors

$$u^{\mu}(\mathbf{p}, \pm 3/2) = \epsilon^{\mu}(\mathbf{p}, \pm 1)\, u(\mathbf{p}, \pm 1/2) \tag{E.5}$$

$$u^{\mu}(\mathbf{p}, \pm 1/2) = \sqrt{\frac{2}{3}}\, \epsilon^{\mu}(\mathbf{p}, 0)\, u(\mathbf{p}, \pm 1/2) + \sqrt{\frac{1}{3}}\, \epsilon^{\mu}(\mathbf{p}, \pm 1)\, u(\mathbf{p}, \mp 1/2) \tag{E.6}$$

Rarita-Schwinger spinor for a spin-$\frac{3}{2}$ particle may be written down in the following form [308], [309]

$$u^{\mu}(\mathbf{p}, s) = \sqrt{\frac{E_{\Delta} + M_{\Delta}}{2M_{\Delta}}} \left(\begin{array}{c} \mathbf{I} \\ \frac{\sigma \cdot \mathbf{p}}{E_{\Delta} + M_{\Delta}} \end{array} \right) S^{\mu}_{\Delta N}\, \chi_s \tag{E.7}$$

where χ_s is the four components spin states for spin-$\frac{3}{2}$ particle:

$$\chi_{+\frac{3}{2}} = \begin{pmatrix} 1 \\ 0 \\ 0 \\ 0 \end{pmatrix}, \quad \chi_{+\frac{1}{2}} = \begin{pmatrix} 0 \\ 1 \\ 0 \\ 0 \end{pmatrix} \quad \chi_{-\frac{1}{2}} = \begin{pmatrix} 0 \\ 0 \\ 1 \\ 0 \end{pmatrix} \quad \chi_{-\frac{3}{2}} = \begin{pmatrix} 0 \\ 0 \\ 0 \\ 1 \end{pmatrix}$$

and $S^{\mu}_{\Delta N}$ is the four components coupling matrices containing the Clebsch-Gordan coefficients for the coupling $1 \otimes \frac{1}{2} = \frac{3}{2}$:

$$\begin{aligned} S_0 &= \frac{\mathbf{p}}{M_\Delta} \begin{pmatrix} 0 & \sqrt{2/3} & 0 & 0 \\ 0 & 0 & \sqrt{2/3} & 0 \end{pmatrix}, \quad S_1 = \begin{pmatrix} -\sqrt{1/2} & 0 & \sqrt{1/6} & 0 \\ 0 & -\sqrt{1/6} & 0 & \sqrt{1/2} \end{pmatrix} \\ S_2 &= i \begin{pmatrix} \sqrt{1/2} & 0 & \sqrt{1/6} & 0 \\ 0 & \sqrt{1/6} & 0 & \sqrt{1/2} \end{pmatrix}, \quad S_3 = \frac{E_\Delta}{\mathbf{p}} S_0 \end{aligned} \tag{E.8}$$

The spinor $u^{\mu}(\mathbf{p}, s)$ for spin-$\frac{3}{2}$ massive particle is subjected to the Rarita Schwinger field equations:

$$(i\gamma_\nu \partial^\nu - M_\Delta)\, \psi^\mu = 0 \tag{E.9}$$

with the constraint equations

$$\gamma_\mu \psi^\mu = 0, \quad \text{and} \quad \partial_\mu \psi^\mu = 0. \tag{E.10}$$

Note that ψ^μ is a vector spinor, means it transforms, under Lorentz transformation, like a product of a four vector and a Dirac spinor.

E.2 Δ-Propagator

The free Lagrangian for the massive spin-$\frac{3}{2}$ field is given as [266]

$$\mathcal{L} = \bar{\psi}^\alpha \, \Lambda_{\alpha\beta} \, \psi^\beta \tag{E.11}$$

with

$$\begin{aligned} \Lambda_{\alpha\beta} &= -\Big[(-i\partial_\mu \gamma^\mu + M) g_{\alpha\beta} - iA(\gamma_\alpha \partial_\beta + \gamma_\beta \partial_\alpha) - \frac{i}{2}(3A^2 + 2A + 1) \gamma_\alpha \partial^\mu \gamma_\mu \gamma_\beta \\ &\quad - M(3A^2 + 3A + 1) \gamma_\alpha \gamma_\beta \Big] \end{aligned} \tag{E.12}$$

where M is the mass of the spin-$\frac{3}{2}$ baryon and A is an arbitrary parameter subjected to the restriction $A \neq -\frac{1}{2}$. In Eqs.E.11 and E.12, α, β, and μ are Lorentz indices. Physical properties of the free field, such as energy-momentum tensor, do not depend on the parameter A.

The propagator for the massive spin-$\frac{3}{2}$ particle satisfies the following equation in momentum space

$$\Lambda_{\alpha\beta}(p) \; G^\beta_\delta(p) = g_{\alpha\delta} \tag{E.13}$$

where $g_{\alpha\delta}$ is the metric tensor, and the Eq.E.12 in momentum space becomes

$$\begin{aligned}\Lambda_{\alpha\beta} &= -\Big[(-\not{p}+M)g_{\alpha\beta} - A(\gamma_\alpha p_\beta + \gamma_\beta p_\alpha) - \frac{1}{2}(3A^2+2A+1)\gamma_\alpha \not{p}\gamma_\beta \\ &\quad -M(3A^2+3A+1)\gamma_\alpha\gamma_\beta\Big] \end{aligned} \tag{E.14}$$

Solving for G using Eq.E.13, we get

$$\begin{aligned}G_{\alpha\beta}(p) &= \frac{\not{p}+M}{p^2-M^2}\left[g_{\alpha\beta} - \frac{1}{3}\gamma_\alpha\gamma_\beta - \frac{1}{3M}(\gamma_\alpha p_\beta - \gamma_\beta p_\alpha) - \frac{2}{3M^2}p_\alpha p_\beta\right] \\ &\quad - \frac{1}{3M^2}\frac{A+1}{2A+1}\left[\gamma_\alpha p_\beta + \frac{A}{2A+1}\gamma_\alpha p_\beta + \left(\frac{1}{2}\frac{A+1}{2A+1}\not{p} - \frac{AM}{2A+1}\right)\gamma_\alpha\gamma_\beta\right] \end{aligned} \tag{E.15}$$

Since the physical properties of the free filed are independent of the parameter A, taking a particular choice A=-1, yields the expression often found in literature for the spin-$\frac{3}{2}$ propagator

$$P^{\mu\nu} = \frac{\not{p}+M}{p^2-M^2}\left[g^{\mu\nu} - \frac{1}{3}\gamma^\mu\gamma^\nu - \frac{2}{3M^2}p^\mu p^\nu + \frac{1}{3}(p^\mu\gamma^\nu - p^{\nu\mu})\right] \tag{E.16}$$

Introducing the decay width this modifies to

$$P^{\mu\nu} = \frac{\not{p}+M}{p^2-M^2+i\Gamma M}\left[g^{\mu\nu} - \frac{1}{3}\gamma^\mu\gamma^\nu - \frac{2}{3M^2}p^\mu p^\nu + \frac{1}{3}(p^\mu\gamma^\nu - p^{\nu\mu})\right] \tag{E.17}$$

Eq.E.16 may be written in terms of the spin projection operators

$$P^{\mu\nu} = \frac{\not{p}+M}{p^2-M^2}(P^{3/2})_{\mu\nu} - \frac{2}{3M^2}(\not{p}+M)(P_{22}^{1/2})_{\mu\nu} + \frac{1}{\sqrt{3}M}\left[(P_{12}^{1/2})_{\mu\nu} + (P_{21}^{1/2})_{\mu\nu}\right] \tag{E.18}$$

these projectors are given by:

$$\begin{aligned}(P^{3/2})_{\mu\nu} &= g^{\mu\nu} - \frac{1}{3}\gamma_\mu\gamma_\nu - \frac{1}{3p^2}(\not{p}\gamma_\mu p_\nu + p_\mu\gamma_\nu\not{p}) \\ (P_{11}^{1/2})_{\mu\nu} &= \frac{1}{3}\gamma_\mu\gamma_\nu - \frac{p_\mu p_\nu}{p^2} + \frac{1}{3p^2}(\not{p}\gamma_\mu p_\nu + p_\mu\gamma_\nu\not{p}) \\ (P_{22}^{1/2})_{\mu\nu} &= \frac{p_\mu p_\nu}{p^2} \\ (P_{12}^{1/2})_{\mu\nu} &= \frac{1}{\sqrt{3}p^2}(p_\mu p_\nu - \not{p}p_\nu\gamma_\mu) \\ (P_{21}^{1/2})_{\mu\nu} &= \frac{1}{\sqrt{3}p^2}(\not{p}p_\mu\gamma_\nu - p_\mu p_\nu) \end{aligned} \tag{E.19}$$

here $(P^{3/2})_{\mu\nu}$ is the spin-$\frac{3}{2}$ and $(P_{22}^{1/2})_{\mu\nu}$, $(P_{12}^{1/2})_{\mu\nu}$, $(P_{21}^{1/2})_{\mu\nu}$ are the spin-$\frac{1}{2}$ projector part of the theory. These satisfy the orthonormality conditions

$$(P_{ij}^I)_{\mu\nu}(P_{kl}^J)^{\nu\sigma} = \delta^{IJ}\delta_{jk}(P_{il}^J)_\mu^\sigma \tag{E.20}$$

and the sum rule for the projection operators

$$(P^{3/2})_{\mu\nu} + (P_{11}^{1/2})_{\mu\nu} + (P_{22}^{1/2})_{\mu\nu} = g_{\mu\nu} \tag{E.21}$$

Since the projectors fulfill the completeness relation Eq.E 21, $(P_{11}^{1/2})_{\mu\nu}$ projects onto those states for which $1 \otimes \frac{1}{2} = \frac{1}{2}$. Following properties are also useful

$$\not{p} P_{ij}^{1/2} = \pm P_{ij}^{1/2} \not{p}, \quad + \text{ for } i = j, \quad - \text{ for } i \neq j \tag{E.22}$$

$$\not{p} P^{3/2} = \pm P^{3/2} \not{p} \tag{E.23}$$

==========********==========

Appendix F

Matrix Element for Coherent Weak Pion Production

The amplitude for the charged current weak pion production from the nuclei in case of delta pole term corresponding to the Feynman diagrams shown in Fig.4.2, is in general given by Eq.4.13, with l^μ as the leptonic current given in Eq.3.18 and the hadronic current $\mathcal{J}_\mu = (J^s_\mu + J^u_\mu)$ as the sum of direct (s-channel) and crossed (u-channel) diagram, which has been separated into its vector (V^μ) and axial vector part (A^μ) as $J^s_\mu = (V^s_\mu + A^s_\mu)$ and $J^u_\mu = (V^u_\mu + A^u_\mu)$, given in Eq.4.15

$$J^s_\mu = \sqrt{3}\,\frac{f_{\pi N\Delta}}{m_\pi}\,k_{\pi\sigma}\sum_r \bar{u}_r(p')\,\Delta^{\sigma\lambda}\,\mathcal{O}_{\lambda\mu}\,u_r(p) \tag{F.1}$$

$$J^u_\mu = \sqrt{3}\,\frac{f_{\pi N\Delta}}{m_\pi}\sum_r \bar{u}_r(p')\,k_{\pi\sigma}\,\mathcal{O}^{\sigma\lambda}\,\Delta_{\lambda\mu}\,u_r(p) \tag{F.2}$$

where $\Delta^{\sigma\lambda}$ or $\Delta_{\lambda\mu}$ is the relativistic Δ propagator modified by a phenomenological constant decay width given as in Eq.4.10 and $\mathcal{O}^{\sigma\lambda}$ or $\mathcal{O}_{\lambda\mu}$ is the weak N-Δ transition vertex given as the sum of vector(V^μ) and axial part (A^μ) in Eqs.3.56 and 4.16 for charged current and neutral current respectively.

We find the leptonic tensor $\mathcal{L}^{\mu\nu}$ given as

$$\begin{aligned}\mathcal{L}^{\mu\nu} &= \mathrm{Tr}\left[(\not{k}' + m_{l'})\gamma^\mu(1-\gamma^5)(\not{k} + m_l)\gamma^\nu(1-\gamma^5)\right] \\ &= 8\left[k^\mu k'^\nu + k'^\mu k^\nu - (k\cdot k')\,g^{\mu\nu} + i\epsilon^{\mu\nu\rho\sigma}k^\rho k'^\sigma\right]\end{aligned} \tag{F.3}$$

and $\mathcal{J}_{\mu\nu}$ as the hadronic tensor given as

$$\begin{aligned}\mathcal{J}_{\mu\nu} &= \frac{1}{2}\,\mathcal{J}_\mu\mathcal{J}^\dagger_\nu \\ &= \frac{1}{2}\left(J^s_{\mu\nu} + J^u_{\mu\nu} + |J^s_\mu J^{u\dagger}_\nu| + |J^u_\mu J^{s\dagger}_\nu|\right)\end{aligned} \tag{F.4}$$

For the coherent process, we write the spinors in the rest frame of the nucleus in the following form

$$u_r(\mathbf{p}) = \frac{\not{p} + M}{\sqrt{2M(E+M)}} u,(0) \tag{F.5}$$

$$\bar{u}_r(\mathbf{p}') = \bar{u}_r(0) \frac{\not{p}' + M}{\sqrt{2M(E'+M)}} \tag{F.6}$$

$$\sum_r u_r(0)\bar{u}_r(0) = \frac{1+\gamma_0}{2} \tag{F.7}$$

For example, we can find, the $J^s_{\mu\nu}$ part of the hadronic tensor of Eq.F.4. Using the spinor representation in Eqs.F.5-F.7 and Eq.4.10, with Eq.3.56 for the Δ propagator and effective N-Δ transition vertex, respectively, the Eq.F.1 comes out to be in the form

$$J^s_\mu = \chi \, \mathrm{Tr}\Big[(1+\gamma_0)\,(\not{p}+M)\,(\not{p}'+M)\,k^\pi_\sigma\,(\not{P}+M_\Delta)\Big(g^{\sigma\lambda} - \frac{1}{3}\gamma^\sigma\gamma^\lambda - \frac{2}{3M^2_\Delta}P^\sigma P^\lambda + \frac{P^\sigma\gamma^\lambda - \gamma^\sigma P^\lambda}{3M_\Delta}\Big)\, g_{\lambda\mu}\Big] \tag{F.8}$$

with

$$\chi = \sqrt{3}\left(\frac{f_{\pi N\Delta}}{m_\pi}\right)\left(\frac{1}{2}\right)^2\left(\frac{1}{2M}\right)^2 \frac{C^A_5(Q^2)}{(P^2 - M^2_\Delta) + i\Gamma M_\Delta}$$

Here we have given the expression considering only the $C^A_5(Q^2)$ term of the axial part. Using

$$(\not{p}+M)(1+\gamma_0) = (M\gamma_0 + M)(1+\gamma_0) = 2M(1+\gamma_0)$$

and

$$2M(1+\gamma_0) = 2M\left(1 + \frac{\not{p}}{M}\right) = 2(\not{p}+M)$$

we get Eq.F.8 in the following form

$$J^s_\mu = 2\,\chi\,\mathrm{Tr}\Big[(\not{p}+M)\,(\not{p}'+M)\,(\not{P}+M_\Delta)\Big(k^\pi_\mu - \frac{1}{3}\not{k}_\pi\gamma_\mu - \frac{2}{3M^2_\Delta}k_\pi\cdot P P_\mu + \frac{k_\pi\cdot P\gamma_\mu - \not{k}_\pi P_\mu}{3M_\Delta}\Big)\Big] \tag{F.9}$$

Using the trace algebra, we find the final expression as

$$J^s_\mu = 8\,\chi\,\left[\alpha_s\,k^\pi_\mu + \beta_s\,P_\mu + \gamma_s\,p_\mu\right] \tag{F.10}$$

Using Eq.F.10 and $J^{s\dagger}_\nu$, we can find the $J^s_{\mu\nu}$ part of the hadronic tensor of Eq.F.4,

$$J^s_{\mu\nu} = 64\,\chi^2\,\left[\alpha^2_s\,k^\pi_\mu\,k^\pi_\nu + \beta^2_s\,P_\mu\,P_\nu + \gamma^2_s\,p_\mu\,p_\nu + \alpha_s\,\beta_s\,(k^\pi_\mu\,P_\nu + P_\mu\,k^\pi_\nu) + \beta_s\,\gamma_s\,(P_\mu\,p_\nu + p_\mu\,P_\nu) + \alpha_s\,\gamma_s\,(k^\pi_\mu\,p_\nu + p_\mu\,k^\pi_\nu)\right] \tag{F.11}$$

Using Eq.F.3 and F.11 we can find the amplitude square for the weak charged current induced pion production from a nucleus, corresponding to direct (s-channel) process, and it comes out to be in the form

$$\begin{aligned}|\mathcal{A}^s_\Delta|^2_{CC} &= \chi_a^2\,\chi_b^2\,\left[\alpha_s^2\left(2k\cdot k_\pi k'\cdot k_\pi - m_\pi^2 k\cdot k'\right) + \beta_s^2\left(2P\cdot kP\cdot k' - P^2 k\cdot k'\right)\right.\\ &\quad +\gamma_s^2\left(2p\cdot kp\cdot k' - M^2 k\cdot k'\right) + 2\alpha_s\beta_s\left(k\cdot k_\pi P\cdot k' + k'\cdot k_\pi P\cdot k\right.\\ &\quad \left.-k\cdot k'P\cdot k_\pi\right) + 2\beta_s\gamma_s\left(P\cdot kp\cdot k' + P\cdot k'p\cdot k - P\cdot pk\cdot k'\right)\\ &\quad \left.+2\alpha_s\gamma_s\left(k\cdot k_\pi p\cdot k' + k'\cdot k_\pi p\cdot k - k\cdot k'p\cdot k_\pi\right)\right] \qquad \text{(F.12)}\end{aligned}$$

with

$$\begin{aligned}\chi_a &= 16\sqrt{3}\,G\cos\theta_C\left(\frac{1}{2}\right)^2\left(\frac{1}{2M}\right)^2\left(\frac{f_{\pi N\Delta}}{m_\pi}\right)\\ \chi_b &= C_5^A(Q^2)\,\frac{1}{\left(P^2 - M_\Delta^2\right) + i\Gamma M_\Delta}\,\mathcal{F}_{CC}(\mathbf{q}-\mathbf{k}_\pi) \qquad \text{(F.13)}\end{aligned}$$

and the variables k and k' represents the four momenta of the incident and scattered particle, p, k_π and $P = (p+q)$ correspond to the four momenta of the nucleon, emitted pion and the intermediate Δ produced respectively. M and M_Δ represent the mass of the nucleon and Δ. The variables α_s, β_s and γ_s are defined as follow

$$\begin{aligned}\alpha_s &= \frac{2}{3}M\left(P^2 + MM_\Delta\right) - \frac{2}{3}MP\cdot k_\pi + \frac{2}{3}\left(M + M_\Delta\right)p\cdot P - M_\Delta p\cdot k_\pi\\ &\quad +\frac{1}{3M_\Delta}P\cdot k_\pi p\cdot P \qquad \text{(F.14)}\\ \beta_s &= -\frac{2P\cdot k_\pi}{3M_\Delta^2}\left[M\left(P^2 + MM_\Delta\right) + \left(M + M_\Delta\right)P\cdot p - MP\cdot k_\pi - M_\Delta p\cdot k_\pi\right]\\ &\quad -\frac{1}{3M_\Delta}\left(P^2 + MM_\Delta\right)p\cdot k_\pi + \frac{1}{3}\left(M + M_\Delta\right)pk_\pi\\ &\quad -\frac{1}{3M_\Delta}\left(m_\pi^2 p\cdot P - p\cdot k_\pi P\cdot k_\pi\right) \qquad \text{(F.15)}\\ \gamma_s &= \frac{1}{3M_\Delta}\left[\left(P^2 - M_\Delta^2\right)P\cdot k_\pi - \left(P\cdot k_\pi\right)^2 + m_\pi^2 M_\Delta^2\right] \qquad \text{(F.16)}\end{aligned}$$

Similarly in the same manner using Eq.F.2, we can find the $J^u_{\mu\nu}$ part of the hadronic tensor of Eq.F.4. and Δ crossed (u-channel) term of the matrix element square comes out to be

$$\begin{aligned}\mathcal{A}^u_\Delta|^2_{CC} &= \chi_a^2\,\chi_b^2\,\left\{\alpha_u^2\left(2k\cdot k_\pi k'\cdot k_\pi - m_\pi^2 k\cdot k'\right) + \beta_u^2\left(2P\cdot kP\cdot k' - P^2 k\cdot k'\right)\right.\\ &\quad +\gamma_s^2\left[\left(2p\cdot kp\cdot k' - M^2 k\cdot k'\right) + \left(2q\cdot kq\cdot k' - q^2 k\cdot k'\right)\right.\\ &\quad \left.+2\left(p\cdot kq\cdot k' + p\cdot k'q\cdot k - q\cdot pk\cdot k'\right)\right] + 2\alpha_u\beta_u\left(k\cdot k_\pi P\cdot k'\right.\\ &\quad \left.+k'\cdot k_\pi P\cdot k - k\cdot k'P\cdot k_\pi\right) + 2\alpha_u\gamma_u\left[\left(k\cdot k_\pi p\cdot k' + k'\cdot k_\pi p\cdot k\right.\right.\\ &\quad \left.\left.-k\cdot k'p\cdot k_\pi\right) + \left(k\cdot k_\pi q\cdot k' + k'\cdot k_\pi q\cdot k - k\cdot k'q\cdot k_\pi\right)\right]\\ &\quad +2\beta_u\gamma_u\left[\left(P\cdot kp\cdot k' + P\cdot k'p\cdot k - P\cdot pk\cdot k'\right) + \left(P\cdot kq\cdot k'\right.\right.\\ &\quad \left.\left.\left.+P\cdot k'q\cdot k - q\cdot Pk\cdot k'\right)\right]\right\} \qquad \text{(F.17)}\end{aligned}$$

where χ_a and χ_b are same as in Eq.F.13 with $P = (p - k_\pi)$ as the four momentum of the Δ produced. The variables α_u, β_u and γ_u are defined as follow

$$\alpha_u = \frac{2}{3}M\left(P^2 + MM_\Delta\right) + \frac{2}{3}Mq\cdot P + \frac{2}{3}\left(M + M_\Delta\right)P\cdot p + \frac{2}{3}M_\Delta q\cdot p \tag{F.18}$$

$$\begin{aligned}\beta_u = & -\frac{2P\cdot k_\pi}{3M_\Delta^2}\left[M\left(P^2 + MM_\Delta\right) + \left(M + M_\Delta\right)P\cdot p + Mq\cdot P + M_\Delta q\cdot p\right] \\ & -\frac{1}{3M_\Delta}\left(P^2 + MM_\Delta\right)p\cdot k_\pi + \frac{1}{3}\left(M + M_\Delta\right)p\cdot k_\pi \\ & +\frac{1}{3M_\Delta}\left(p\cdot Pq\cdot k_\pi - p\cdot k_\pi q\cdot P\right)\end{aligned} \tag{F.19}$$

$$\begin{aligned}\gamma_u = & \frac{1}{3M_\Delta}\left(P^2 + MM_\Delta\right)P\cdot k_\pi - \frac{1}{3}\left(M + M_\Delta\right)P\cdot k_\pi - \frac{1}{3}M_\Delta q\cdot k_\pi \\ & +\frac{1}{3M_\Delta}P\cdot k_\pi q\cdot p + \frac{1}{3}M_\Delta p\cdot k_\pi - \frac{1}{3M_\Delta}P\cdot k_\pi p\cdot P\end{aligned} \tag{F.20}$$

The interference terms of the matrix element square are given as

$$\begin{aligned}&|\mathcal{A}^s_\Delta\mathcal{A}^{u\,\dagger}_\Delta|_{CC} = |\mathcal{A}^u_\Delta\mathcal{A}^{s\,\dagger}_\Delta|_{CC} = \chi_a^2\,\chi_b^2\,\{\alpha_s\alpha_u(2k\cdot k_\pi k'\cdot k_\pi - m_\pi^2 k\cdot k') \\ &\alpha_s\beta_u(k\cdot k_\pi P_u\cdot k' + k'\cdot k_\pi P_u\cdot k - k\cdot k'P_u\cdot k_\pi) + \alpha_s\gamma_u(k\cdot k_\pi P_s\cdot k' \\ &+k'k_\pi P_s\cdot k - k\cdot k'P_s\cdot k_\pi) + \beta_s\gamma_u(P_s\cdot kk'\cdot k_\pi + P_s\cdot k'k\cdot k_\pi \\ &-k\cdot k'P_s\cdot k_\pi) + \beta_s\beta_u(P_s\cdot kP_u\cdot k' + P_s\cdot k'P_u\cdot k - k\cdot k'P_s\cdot P_u) \\ &+\beta_s\gamma_u(2P_s\cdot kP_s\cdot k' - k\cdot k'P_s^2) + \gamma_s\alpha_u(k\cdot k_\pi p\cdot k' + k'\cdot k_\pi p\cdot k \\ &-k\cdot k'p\cdot k_\pi) + \gamma_s\beta_u(P_u\cdot kp\cdot k' + P_u\cdot k'p\cdot k - P_u\cdot pk\cdot k') \\ &+\gamma_{su}(p\cdot k'P_s\cdot k + p\cdot kP_s\cdot k' - k\cdot k'p\cdot P_s)\end{aligned} \tag{F.21}$$

where χ_a and χ_b are same as in Eq.F.13 with $P_s = (p + q)$ and $P_u = (p - k_\pi)$ as the four momentum of the intermediate Δ produced in s-channel and u-channel respectively. The variables $\alpha_{s,u}$, $\beta_{s,u}$ and $\gamma_{s,u}$ are same as defined in Eqs.F.14-16 and F.18-20.

The matrix element square in the neutral current process for Δ-direct (s-channel) and crossed (u-channel) diagrams are related with the charged current matrix elements as:

$$|\mathcal{A}^s_\Delta|^2_{NC} = \left(\xi_A^{I=1}\right)^2|\mathcal{A}^s_\Delta|^2_{CC}, \qquad |\mathcal{A}^u_\Delta|^2_{NC} = \left(\xi_A^{I=1}\right)^2|\mathcal{A}^u_\Delta|^2_{CC} \tag{F.22}$$

$$|\mathcal{A}^s_\Delta\mathcal{A}^{u\,\dagger}_\Delta|_{NC} = \left(\xi_A^{I=1}\right)^2|\mathcal{A}^s_\Delta\mathcal{A}^{u\,\dagger}_\Delta|_{CC}, \quad |\mathcal{A}^u_\Delta\mathcal{A}^{s\,\dagger}_\Delta|_{NC} = \left(\xi_A^{I=1}\right)^2|\mathcal{A}^u_\Delta\mathcal{A}^{s\,\dagger}_\Delta|_{CC} \tag{F.23}$$

with

$$\begin{aligned}\chi_a &= 16\sqrt{3}\,G\left(\frac{1}{2}\right)^2\left(\frac{1}{2M}\right)^2\left(\frac{f_{\pi N\Delta}}{m_\pi}\right) \\ \chi_b &= C_5^A(Q^2)\,\frac{1}{\left(P^2 - M_\Delta^2\right) + i\Gamma M_\Delta}\,\mathcal{F}_{NC}(\mathbf{q} - \mathbf{k}_\pi)\end{aligned} \tag{F.24}$$

and $\xi_A^{I=1}$ defined in Eq.3.15.

Appendix G

Differential Cross Sections

General expression of the differential cross section for the interaction of two particle ($i = 1, 2$) and N outgoing particles ($f = 1, ..., N$) can be written as

$$d\sigma = (2\pi)^4 \, \delta^4 \left[\sum_f p'_f - \sum_i p_i \right] \frac{1}{4\sqrt{(p_1 \cdot p_2)^2 - m_1^2 m_2^2}} \prod_f \frac{d^3\mathbf{p}'_f}{(2\pi)^3 \, 2E'_f} \sum' |\mathcal{M}_{fi}|^2 \quad \text{(G.1)}$$

The amplitude $\mathcal{M}$ is the invariant matrix element for the process under consideration. For particles with non zero spin, unpolarized cross sections are calculated by averaging over initial spin components and summing over final states. For the neutrinos there is no averaging over initial neutrino helicities since they occurs only left-handed. However, for convenience of calculation, one can formally sum over both helicity states, as the factor $(1 - \gamma_5)$ guarantees that right-handed neutrinos do not contribute to the cross section.

G.1 Differential Cross Section for Δ Production

The differential cross section for the reaction $\nu(k) + p(p) \rightarrow \mu^-(k') + \Delta^{++}(p')$ can be written as

$$d\sigma = \frac{1}{2} \, \frac{(2\pi)^4 \delta^4(k + p - p' - k')}{4\sqrt{(k \cdot k')^2 - m_\nu^2 M^2}} \frac{d^3\mathbf{k}'}{(2\pi)^3 2E_{k'}} \frac{d^3\mathbf{p}'}{(2\pi)^3 2E_{p'}} \, |\bar{\mathcal{M}}|^2 \quad \text{(G.2)}$$

where $k + p = k' + p'$, and $q = k - k'$. Using the relation

$$4\sqrt{(k \cdot k')^2 - m_\nu^2 M^2} \; = \; 4p \cdot k \; = \; 4ME_\nu \quad \text{(G.3)}$$

and

$$s = (p + k)^2 = M^2 + 2p \cdot k \Rightarrow 4p \cdot k = 2(s - M^2) \quad \text{(G.4)}$$

we have

$$d\sigma = \frac{1}{2}\,\frac{(2\pi)^4\delta^4(k+p-p'-k')}{2(s-M^2)}\,\frac{d^3\mathbf{k}'}{(2\pi)^3 2E_{k'}}\,\frac{d^3\mathbf{p}'}{(2\pi)^3 2E_{p'}}\,|\bar{\mathcal{M}}|^2 \tag{G.5}$$

Using the following relation

$$d^3\mathbf{k}' = |\mathbf{k}'|^2\, d|\mathbf{k}|\, d\Omega_{k'} \;=\; E_{k'}\,|\mathbf{k}'|\, dE_{k'}\, d\Omega_{k'} \tag{G.6}$$

we get after integrating over Δ momentum

$$\frac{d\sigma}{dE_{k'}d\Omega_{k'}} = \frac{1}{16\pi^2}\,\frac{1}{2(s-M^2)}\,|\mathbf{k}'|\,\frac{1}{2E_{p'}}\,\delta(E_p+q_0-E_{p'})\,|\bar{\mathcal{M}}|^2 \tag{G.7}$$

In order to take into account the width of the Δ, we must replace in Eq.G.7

$$\delta(E_p+q_0-E_\Delta) \to -\frac{1}{\pi}\,\mathrm{Im}\left[\frac{1}{E_p+q_0-E_\Delta+\imath\frac{\Gamma}{2}}\right] \tag{G.8}$$

where we have used the relation

$$\frac{1}{x-x_0\mp\imath\epsilon} = P\frac{1}{x-x_0} \pm \imath\pi\delta(x-x_0) \tag{G 9}$$

and then

$$\frac{M_\Delta}{E_\Delta}\,\delta(p^0_\Delta-E_\Delta) \to -\frac{1}{\pi}\,\mathrm{Im}\left[\frac{1}{W-M_\Delta+\imath\frac{1}{2}\Gamma(W)}\right] \to \frac{1}{\pi}\left[\frac{\frac{\Gamma(W)}{2}}{(W-M_\Delta)^2+\frac{\Gamma^2(W)}{4}}\right] \tag{G 10}$$

using

$$\delta(W-M_\Delta) = \frac{1}{p^0_\Delta/W}\delta(p^0_\Delta-E_\Delta) \simeq \frac{M_\Delta}{E_\Delta}\delta(p^0_\Delta-E_\Delta) \tag{G.11}$$

where $W=\sqrt{p'^2}=\sqrt{{p^0_\Delta}^2-\vec{p}^2_\Delta}$ is the invariant mass of Δ and $\Gamma(W)$ is the rest width of Δ. Using Eq.G.10 in Eq.G.7, we get

$$\frac{d\sigma}{dE_{k'}d\Omega_{k'}} = \frac{1}{128\pi^3}\,\frac{1}{(s-M^2)}\,\frac{|\mathbf{k}'|}{M_\Delta}\left[\frac{\Gamma(W)}{(W-M_\Delta)^2+\frac{\Gamma^2(W)}{4}}\right]|\bar{\mathcal{M}}|^2 \tag{G.12}$$

Using the relation $Q^2=-q^2=(k-k')=-2k\cdot k'$ and Eq G.4, with

$$\frac{d\sigma}{dQ^2} = \frac{\pi}{E_\nu E_{k'}}\,\frac{d\sigma}{d\Omega_{k'}} \tag{G.13}$$

we obtain

$$\frac{d\sigma}{dE_{k'}dQ^2} = \frac{1}{64\pi^2}\,\frac{1}{(s-M^2)^2}\,\frac{M}{M_\Delta}\,\frac{|\mathbf{k}'|}{E_{k'}}\left[\frac{\Gamma(W)}{(W-M_\Delta)^2+\frac{\Gamma^2(W)}{4}}\right]|\bar{\mathcal{M}}|^2 \tag{G.14}$$

Finally neglecting muon mass so that $|\mathbf{k}'|\,d|\mathbf{k}'| = E_{k'}\,dE_{k'}$ and integrating over lepton energy we get

$$\frac{d\sigma}{dQ^2} = \frac{G^2\cos^2\theta_C}{128\pi^2}\,\frac{1}{(s-M^2)^2}\,\frac{M}{M_\Delta}\int_{E^{min}_{k'}}^{E^{max}_{k'}} dE_{k'}\,L_{\mu\nu}j^{\mu\nu}\left[\frac{\Gamma(W)}{(W-M_\Delta)^2+\frac{\Gamma^2(W)}{4}}\right] \tag{G.15}$$

G.2 Charged Current Weak Pion Production

The differential cross section for charged current weak pion production from nucleon i.e., for

$$\nu_l(k) + N(p) \rightarrow l'(k') + N'(p') + \pi(k_\pi)$$

can be written as

$$d\sigma = \frac{(2\pi)^4\delta^4(q+p-p'-k_\pi)}{4\sqrt{(k\cdot k')^2 - m_l^2M^2}} \frac{d^3\mathbf{k}'}{(2\pi)^3 2E_{l'}} \frac{d^3\mathbf{p}'}{(2\pi)^3 2E_{p'}} \frac{d^3\mathbf{k}_\pi}{(2\pi)^3 2E_\pi} \prod_f (2m_f) \sum{}' |\mathcal{M}|^2 \quad \text{(G.16)}$$

where

$$q = k - k' \quad \text{and} \quad q + p = p' + k_\pi$$

In the lab frame (target at rest) i.e. $|\mathbf{p}| = 0$ and $E_p = M$ therefore from energy momentum relation

$$|\mathbf{p}| + |\mathbf{q}| = |\mathbf{p}'| + |\mathbf{k}_\pi| \Rightarrow |\mathbf{q}| = |\mathbf{p}'| + |\mathbf{k}_\pi|$$

Then

$$4\sqrt{(k\cdot k')^2 - m_l^2M^2} = 4ME_l \quad \text{(G.17)}$$

Using above relations, integrating over the final nucleon momentum and taking a factor of $2M^2$ outside from the matrix element square $|\mathcal{M}|^2$ the differential cross section reduces to

$$d\sigma = \frac{1}{(2\pi)^5} \frac{M}{E_l} \frac{1}{2E_{p'}} \frac{d^3\mathbf{k}'}{2E_l'} \frac{d^3\mathbf{k}_\pi}{2E_\pi} \delta^0(q_0 + p_0 - p_0' - k_\pi^0) \sum{}' |\mathcal{M}|^2 \quad \text{(G.18)}$$

Using the following relations

$$d^3\mathbf{k}' = |\mathbf{k}'|^2\, d|\mathbf{k}|\, d\Omega_{ll'} = E_{l'}\, |\mathbf{k}'|\, dE_{l'}\, d\Omega_{ll'} \quad \text{(G.19)}$$

$$d^3\mathbf{k}_\pi = |\mathbf{k}_\pi|^2\, d|\mathbf{k}_\pi|\, d\Omega_{\pi q} = E_\pi\, |\mathbf{k}_\pi|\, dE_\pi\, d\Omega_{\pi q} \quad \text{(G.20)}$$

we get

$$\frac{d^5\sigma}{dE_\pi\, d\Omega_\pi\, d\Omega_{ll'}} = \frac{1}{8} \frac{1}{(2\pi)^5} \frac{M}{E_l} \frac{|\mathbf{k}_\pi|}{E_{p'}} |\mathbf{k}'|\, dE_{l'}\, \delta^0(M + q_0 - E_{p'} - E_\pi) \sum{}' |\mathcal{M}|^2 \quad \text{(G.21)}$$

Now doing the energy integration over $dE_{l'}$ i.e. $\int dE_{l'}\, \delta^0(M + q_0 - E_{p'} - E_\pi)$ and using the property of standard delta function defined as

$$\delta(f(x)) = \sum_i \delta(x - x_i) / \left|\frac{\partial f}{\partial x}\right|_{x=x_i} \quad \text{(G.22)}$$

$$f(E_{p'}) = M + q_0 - E_{p'} - E_\pi = M + E_l - E_{l'} - E_{p'} - E_\pi$$

Then

$$\left|\frac{\partial f(E_{p'})}{\partial E_{l'}}\right| = 1 + \frac{\partial E_{p'}}{\partial E_{l'}} \quad \text{with} \quad E_{p'} = M + E_l - E_{l'} - E_{p'} - E_\pi$$

Evaluating

$$\frac{\partial E_{p'}}{\partial E_{l'}} = \frac{\partial}{\partial E_{l'}}\sqrt{|\mathbf{q}|^2 + |\mathbf{k}_\pi|^2 - 2|\mathbf{k}_\pi||\mathbf{q}|\cos\theta_{\pi q} + M^2}$$

$$\frac{\partial E_{p'}}{\partial E_{l'}} = \frac{|\mathbf{q}|\,(E_{l'} - E_l\cos\theta_{ll'}) - |\mathbf{k}_\pi|\,(E_{l'} - E_l\cos\theta_{ll'})\cos\theta_{\pi q}}{E_{p'}|\mathbf{q}|}$$

then

$$\left|\frac{\partial f(E_{p'})}{\partial E_{l'}}\right|^{-1} = \frac{E_{p'}|\mathbf{q}|}{|\mathbf{q}|\,(E_{p'} + E_{l'} - E_l\cos\theta_{ll'}) - |\mathbf{k}|\,(E_{l'} - E_l\cos\theta_{ll'})\cos\theta_{\pi q}}$$

Thus the differential cross section in the laboratory frame where pion has to be seen comes out to be in the following form

$$\frac{d^5\sigma}{dE_\pi\, d\Omega_\pi\, d\Omega_{ll'}} = \frac{1}{8}\frac{1}{(2\pi)^5}\frac{M}{E_l}|\mathbf{k}'|\,|\mathbf{k}_\pi|\,\frac{1}{\mathcal{R}}\sum{}'|\mathcal{M}|^2 \tag{G.23}$$

Using $Q^2 = -q^2 = -2E_lE_{l'} - 2E_l|\mathbf{k}'|\cos\theta_{ll'}$ and $dQ^2 = -\frac{E_l|\mathbf{k}'|}{\pi}d\Omega_{ll'}$ we get

$$\frac{d^5\sigma}{dE_\pi\, d\Omega_\pi\, dQ^2} = \frac{\pi}{8}\frac{1}{(2\pi)^5}\frac{M}{E_l^2}\,|\mathbf{k}_\pi|\,\frac{1}{\mathcal{R}}\sum{}'|\mathcal{M}|^2 \tag{G.24}$$

where

$$\mathcal{R} = \left[(E_{p'} + E_{l'} - E_l\cos\theta_{ll'}) - \frac{|\mathbf{k}_\pi|}{|\mathbf{q}|}(E_{l'} - E_l\cos\theta_{ll'})\cos\theta_{\pi q}\right] \tag{G.25}$$

In the above expression for the differential cross section the recoil of the nucleus has been considered We have also calculated the differential cross section where the recoil of the nucleus has been neglected and we find that considering the recoil of the nucleus gives less than $(3-4\%)$ correction in the energy range which we have considered. The differential cross section for the charged current weak pion production where the recoil of the nucleus has been neglected i.e. $E_{p'} = M$ and keeping in mind that in the coherent reaction the energy transfer to the nucleus is directly taken away by the emitted pion i.e. $q_0 = E_l - E_{l'} = E_\pi$, this implies $q_0 + p_0 - p_0' - k_0 = q_0 - k_0$ and Eq.G.23 becomes

$$\frac{d^5\sigma}{dE_\pi\, d\Omega_\pi\, d\Omega_{ll'}} = \frac{1}{8}\,\frac{1}{(2\pi)^5}\,\frac{|\mathbf{k}_\pi|}{E_l}\,|\mathbf{k}'|\,dE_{l'}\,\delta^0(q_0 - E_\pi)\sum{}'|\mathcal{M}|^2 \tag{G.26}$$

Finally integrating over $E_{l'}$ we get the differential cross section as

$$\frac{d^5\sigma}{dE_\pi\, d\Omega_\pi\, d\Omega_{ll'}} = \frac{1}{8}\frac{1}{(2\pi)^5}\,\frac{|\mathbf{k}'|}{E_l}|\mathbf{k}_\pi|\sum{}'|\mathcal{M}|^2 \tag{G.27}$$

G.3 Neutral Current Weak Pion Production

Considering the neutral current process where pion has to be seen

$$\nu(k) + N(p) \rightarrow \nu'(k') + N(p') + \pi(k_\pi)$$

the general form of the differential cross section will be given by the Eq.G.16. Using the Eq.G.17 and neglecting the recoil of the nucleus i.e. $E_{p'} = M$ the differential cross section becomes

$$d\sigma = \frac{1}{8}\frac{1}{(2\pi)^5}\frac{1}{E_\nu E_{\nu'}}\frac{1}{E_\pi} d^3\mathbf{k}' d^3\mathbf{k}_\pi d^3\mathbf{p}' \delta^4(q + p - p' - k_\pi) \sum' |\mathcal{M}|^2$$

Integrating over the final nucleon momentum the differential cross section reduces to

$$d\sigma = \frac{1}{8}\frac{1}{(2\pi)^5}\frac{1}{E_\nu E_{\nu'}}\frac{1}{E_\pi} d^3\mathbf{k}' d^3\mathbf{k}_\pi \delta^0(q_0 + p_0 - p_0' - k_0) \sum' |\mathcal{M}|^2 \tag{G.28}$$

Using the following relations

$$d^3\mathbf{k}' = |\mathbf{k}'|^2 d|\mathbf{k}'|\, d\Omega_{\nu\nu'} = E_{\nu'}^2\, dE_{\nu'}\, d\Omega_{\nu\nu'} \tag{G.29}$$

$$d^3\mathbf{k}_\pi = |\mathbf{k}_\pi|^2 d|\mathbf{k}_\pi|\, d\Omega_{\pi q} = E_\pi |\mathbf{k}_\pi|\, dE_\pi\, d\Omega_{\pi q} \tag{G.30}$$

we get

$$\frac{d^5\sigma}{d\Omega_\pi dE_\pi d\Omega_{\nu\nu'}} = \frac{1}{8}\frac{1}{(2\pi)^5}\frac{E_{\nu'}}{E_\nu}|\mathbf{k}_\pi|\, dE_{\nu'}\, \delta^0(q_0 - k_0) \sum' |\mathcal{M}|^2 \tag{G.31}$$

Finally integrating over $E_{\nu'}$ we get the differential cross section for neutral current pion production as

$$\frac{d^5\sigma}{d\Omega_\pi dE_\pi d\Omega_{\nu\nu'}} = \frac{1}{8}\frac{1}{(2\pi)^5}\left(1 - \frac{E_\pi}{E_\nu}\right)|\mathbf{k}_\pi| \sum' |\mathcal{M}|^2 \tag{G.32}$$

G.4 Charged Current Weak lepton Production

Similarly, the differential cross section for the charged current process where lepton has to be seen

$$\nu(k) + N(p) \rightarrow l'(k') + N(p') + \pi(k_\pi)$$

using Eq.G.16 and Eq.G.17, we have the expression as

$$\frac{d^5\sigma}{d\Omega_\pi\, d\Omega_{ll'}\, dE_l} = \frac{1}{8}\frac{1}{(2\pi)^5}\frac{M}{E_l}\frac{|\mathbf{k}_\pi|}{E_{p'}}|\mathbf{k}'|\, dE_\pi\, \delta^0(M + q_0 - E_{p'} - E_\pi) \sum' |\mathcal{M}|^2 \tag{G.33}$$

Now doing the energy integration over dE_π i.e. $\int dE_\pi\ \delta^0(M + q_0 - E_{p'} - E_\pi)$ and using Eq.G.22, with

$$f(E_{p'}) = M + q_0 - E_{p'} - E_\pi = M + E_l - E_{l'} - E_{p'} - E_\pi$$

Then

$$\left|\frac{\partial f(E_{p'})}{\partial E_\pi}\right| = 1 + \frac{\partial E_{p'}}{\partial E_\pi} \quad \text{with} \quad E_{p'} = M + E_l - E_{l'} - E_{p'} - E_\pi$$

Evaluating

$$\begin{aligned}\frac{\partial E_{p'}}{\partial E_\pi} &= \frac{\partial}{\partial E_\pi}\sqrt{|\mathbf{q}|^2 + |\mathbf{k}_\pi|^2 - 2|\mathbf{k}_\pi||\mathbf{q}|\cos\theta_{\pi q} + M^2} \\ \frac{\partial E_{p'}}{\partial E_\pi} &= \frac{E_\pi|\mathbf{k}_\pi| - E_\pi|\mathbf{q}|\cos\theta_{\pi q}}{E_{p'}|\mathbf{k}_\pi|}\end{aligned}$$

then

$$\left|\frac{\partial f(E_{p'})}{\partial E_\pi}\right|^{-1} = \frac{E_{p'}|\mathbf{k}_\pi| + E_\pi|\mathbf{k}_\pi| - E_\pi|\mathbf{q}|\cos\theta_{\pi q}}{E_{p'}|\mathbf{k}_\pi|}$$

Thus the differential cross section in the laboratory frame where lepton has to be seen comes out to be in the following form

$$\frac{d^5\sigma}{dE_l\ d\Omega_\pi\ d\Omega_{ll'}} = \frac{1}{8}\frac{1}{(2\pi)^5}\frac{|\mathbf{k}'|\ |\ \mathbf{k}_\pi|}{E_l}\ \mathcal{R}\ \sum{}' |\mathcal{M}|^2 \tag{G.34}$$

$$\mathcal{R} = \left[\frac{M\ |\mathbf{k}_\pi|}{E_{p'}|\mathbf{k}_\pi| + E_\pi(|\mathbf{k}_\pi| - |\mathbf{q}|\cos\theta_\pi)}\right] \tag{G.35}$$

Finally, integrating over the respective lepton and pion solid angles, we can find the differential cross sections, for example,

$$\frac{d\sigma}{dQ^2} = \int_{-1}^{+1} d\cos\theta_{\pi q}\int_0^{2\pi} d\phi_{\pi q} \times \left[\frac{d^5\sigma}{d\Omega_\pi\ dE_\pi\ dQ^2}\right] \tag{G.36}$$

==========********==========

Appendix H

Kinematics for Weak Pion Production

The weak pion production process shown in Fig.H.1 is:

$$l(k) + N(p) \rightarrow l'(k') + N'(p') + \pi^{\alpha}(k_{\pi}) \tag{H.1}$$

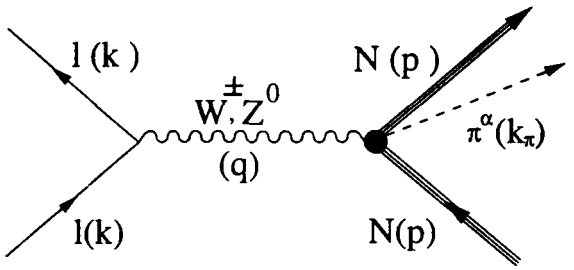

Figure H.1: Kinematic variables for weak pion production.

Where l is neutrino and l' is a neutrino in the case of neutral current reactions and an electron or a muon in the case of charged current reactions with initial momenta k and final momenta k' respectively. N can be a proton or neutron and π^{α} are the different possible charged states $(\pi^{+}, \pi^{-}, \pi^{0})$ of the pion produced and are determined by the lepton number and charge conservation in the charged and neutral current reactions. The four momentum of each particle is indicated in parenthesis. We consider an incoming neutrino with four momentum k =(E_l, $\mathbf{k}$) which scatters from a nucleon N =(p, n) of four momentum p =(p_0=M, $\mathbf{p}$) (mass M) via $W^{\pm}$, Z^0 boson exchange producing a charged lepton with four momentum k' =($E_{l'}$, $\mathbf{k'}$) and a final nucleon of four momentum p' =(p'_0, $\mathbf{p'}$) along with a pion of four momentum k_{π} =(E_{π}, $\mathbf{k}_{\pi}$) (mass m_{π}). The four momentum transfer $q = (q_0, \mathbf{q}) = k - k'$, exchanged between the leptonic and hadronic vertices is fixed by the four momenta of incident and outgoing leptons.

The conservation of energy and momentum for above reactions are given by

$$\left.\begin{array}{l} k + p = k' + p' + k_\pi \Rightarrow (k - k') + p = p' + k_\pi \\ q + p = P_X = p' + k_\pi \quad \text{where} \quad q = k - k' \end{array}\right\} \tag{H.2}$$

where P_X is the four momentum of the intermediate recoiling hadron πN system, which decays into a pion and a nucleon and the square of the momentum transfer $q = k - k'$, is given by

$$q^2 = (k - k')^2 = -2\, k \cdot k' = -4\, E_l E_{l'} \sin^2\left(\frac{\theta_{ll'}}{2}\right) \tag{H.3}$$

Where the angle $\theta_{ll'}$ is the scattering angle of the scattered lepton from the direction of the incident one, and hence q^2 can be fixed by the lepton kinematics. The other useful kinematical variables are the Lorentz invariant Mendelstam variables(s,t,u=$\bar{s}$) defined as

$$\left.\begin{array}{l} s = W^2 = (p+q)^2 = (p' + k_\pi)^2 = M^2 + m_\pi^2 + 2\,(p' \cdot k_\pi) \\ t = (q - k_\pi)^2 = (p' - p)^2 = 2M^2 - 2\,(p \cdot p') \\ u = \bar{s} = (p' - q)^2 = (k_\pi - p)^2 = M^2 + m_\pi^2 - 2\,(p \cdot k_\pi) \end{array}\right\} \tag{H.4}$$

which satisfy the well known relation

$$s + t + u = \sum m_i^2 = 2M^2 + q^2 + {m_\pi}^2 \tag{H.5}$$

The t-variable can also be written in the following form

$$\begin{aligned} t &= t_{min} - 4\,|\mathbf{k}_\pi|\,|\mathbf{q}| \sin^2\left(\frac{\theta_\pi}{2}\right) \\ t_{min} &= (q_0 - E_\pi)^2 - (|\mathbf{q}| - |\mathbf{k}_\pi|)^2 \end{aligned} \tag{H.6}$$

and θ_π is the pion angle with the momentum transfer. Other useful Lorentz invariant variables are

$$P = \frac{1}{2}(p + p'),\quad \Delta = p' - p,\quad \kappa = \frac{1}{2}(k + k')$$

$$\text{such that } P \cdot \Delta = 0,\quad \nu_A = q \cdot P = \kappa \cdot P,\quad \nu_B = -\frac{1}{2}(q \cdot \kappa) \tag{H.7}$$

In terms of these variables, the Mendelstam variables can be written in the following form

$$s = M^2 + 2\,(\nu_A - \nu_B),\quad u = \bar{s} = M^2 - 2\,(\nu_A + \nu_B) \tag{H.8}$$

The most significant variables are invariant momentum transfer square (Q^2 = -q^2) and the angles (θ_π, ϕ_π) defining the direction of motion of the pion in center of mass frame.

Five particles are appearing in the weak pion production of a single pion i.e. neutrino and nucleon in the initial state and three particles namely neutrino (in neutral current reactions), electron or muon (in charged current reactions), nucleon and the produced pion in the final state. These correspond to the fifteen degrees of freedom. Out of these, three refer to the

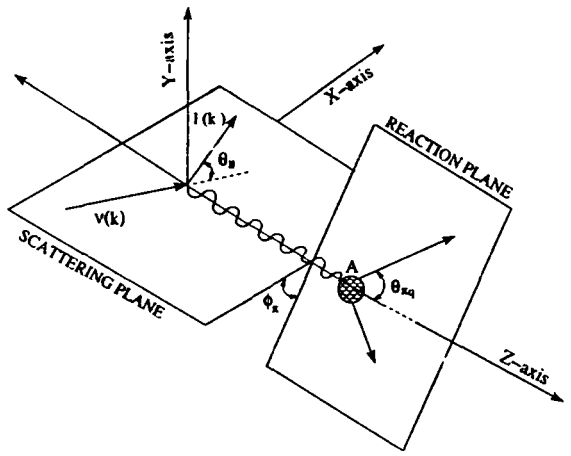

Figure H.2: Kinematics and angles for weak pion production.

rotation and three to the translations of the system as a whole. In the remaining nine degrees of freedom, only five correspond to the independent variables because of the four relations (conservation of the energy and momentum) given in Eq.H.2. In the laboratory frame, these five variables are the energies E_l and $E_{l'}$ of the incident and scattered particles respectively, where l correspond to the neutrino and l' correspond to the neutrino in neutral current reactions and electron or muon in charged current reactions, the scattering angle $\theta_{ll'}$ of the scattered lepton from the direction of the incident one, pion angle $\theta_{\pi q}$ with the momentum transfer and the azimuthal angle ϕ_π is the angle between the scattering plane defined by $\mathbf{k}$ and $\mathbf{k}'$, and the reaction plane spanned by pion 3-momentum $\mathbf{k}_\pi$ and momentum transfer $\mathbf{q}$, which can be expressed as

$$\begin{aligned} (\mathbf{k}\times\mathbf{k}')\cdot(\mathbf{q}\times\mathbf{k}_\pi) &= |(\mathbf{k}\times\mathbf{k}')|\,|(\mathbf{q}\times\mathbf{k}_\pi)|\,\cos\phi_\pi \\ \Rightarrow \cos\phi_\pi &= \frac{(\mathbf{k}\times\mathbf{k}')\cdot(\mathbf{q}\times\mathbf{k}_\pi)}{|(\mathbf{k}\times\mathbf{k}')|\,|(\mathbf{q}\times\mathbf{k}_\pi)|} \end{aligned} \tag{H.9}$$

Also

$$|\mathbf{q}\times\kappa| = |\mathbf{k}\times\mathbf{k}'| = E_l\,E_{l'}\,\sin\theta_{ll'} \tag{H.10}$$

and

$$(\mathbf{q}\times\kappa)\cdot(\mathbf{q}\times\mathbf{k}_\pi) = \begin{vmatrix} |\mathbf{q}^2| & \kappa\cdot\mathbf{q} \\ \mathbf{q}\cdot\mathbf{k}_\pi & \kappa\cdot\mathbf{k}_\pi \end{vmatrix} \tag{H.11}$$

so that the angle ϕ_π can be defined as

$$\cos\phi_\pi = \frac{|\mathbf{q}^2|\,(\kappa\cdot\mathbf{k}_\pi) - (\mathbf{q}\cdot\kappa)\,(\mathbf{q}\cdot\mathbf{k}_\pi)}{|\mathbf{q}|\,|\mathbf{k}_\pi|\,\sin\theta_{ll'}\,\sin\theta_{\pi q}} \tag{H.12}$$

The recoil nucleon carry the four momenta p' and energy $E_{p'}$. This ϕ_π symmetry provides a check for the coherent π^0 production. It can also be used to separate the coherent part from some background of incoherent contribution since the ϕ_π dependence is quite different for the two processes and known.

==========*******==========

Bibliography

Bibliography

[1] D. Casper, NUANCE, Nucl. Phys. **B (Proc. Suppl.) 112**, 161 (2002); G. P. Zeller, talk presented in NuINT02, Irvine, California, 12-15 Dec. (2002); arXiv:hep-ex/0312061, (2003).

[2] H. Gallagher, NEUGEN, Nucl. Phys. **B (Proc. Suppl.) 112**, 188 (2002).

[3] Y. Hayato, NEUT, Nucl. Phys. **B (Proc. Suppl.) 112**, 171 (2002).

[4] A. Rubbia, NUX, talk presented in NuINT01, Tsukuba, Japan, 13-16 Dec. (2001).

[5] F. Cavanna and O. Palamara, GENEVE, Nucl. Phys. **B (Proc. Suppl.) 112**, 183 (2002).

[6] A. Ferrari, P. R. Sala, A. Fasso and J. Ranft, Report No. **CERN-2005-010**; G. Battistoni, A. Ferrari, T. Montaruli and P. R. Sala, Nucl. Phys. **B (Proc. Suppl.) 145**, 128 (2005); G. Battistoni, P. R. Sala and A. Ferrari, Acta. Phys. Polon. **B37**, 2361 (2006).

[7] C. H. Llewellyn Smith, Phys. Rep. **3**, 261 (1972).

[8] R. A. Smith and E. J. Moniz, Nucl. Phys. **B43**, 605 (1972).

[9] D. Rein, L. M. Sehgal, Ann. Phys. (N.Y.) **133**, 79 (1981).

[10] P. Lipari, Nucl. Phys. **B (Proc. Suppl.) 112**, 274 (2002); A. Bodek and U. K. Yang, Nucl. Phys. **B (Proc. Suppl.) 112**, 70 (2002); M. Gluck, E. Reya and A. Vogt, Z. Phys. **C67**, 433 (1995).

[11] R. Davis, Jr., D. S. Harmer and K. C. Hoffman, Phys. Rev. Lett. **20**, 1205 (1986).

[12] K. S. Hirata et al., Phys. Rev. Lett. **65**, 1297 (1990).

[13] A. I. Abazov et al., Phys. Rev. Lett. **67**, 3332 (1991).

[14] S. Fukuda et al., Phys. Rev. Lett. **86**, 5651 (2001).

[15] Q. R. Ahmed et al., Phys. Rev. Lett. **87**, 071301 (2001).

[16] Q. R. Ahmed et al., Phys. Rev. Lett. **89**, 011301 (2002).

[17] Q. R. Ahmed et al., Phys. Rev. Lett. **89**, 011302 (2002).

[18] S. N. Ahmad et al., Phys. Rev. Lett. **92**, 181301 (2004).

[19] J. Hosaka et al., Phys. Rev. **D73**, 112001 (2006).

[20] K. Eguchi et al., KamLAND Collaboration, Phys. Rev. Lett. **90**, 021802 (2003).

[21] M. Apollonio, et al., Eur. Phys. J. **C27**, 331 (2003).

[22] C. V. Achar et al., Phys. Lett. **B18**, 196 (1965).

[23] C. V. Achar et al., Phys. Lett. **B19**, 78 (1965).

[24] F. Reines et al., Phys. Rev. Lett. **15**, 429 (1965).

[25] Y. Ashie et al. Phys. Rev. **D71**, 112005 (2005).

[26] T. J. Haines et al., Phys. Rev. Lett. **57**, 1986 (1986).

[27] D. Casper et al., Phys. Rev. Lett. **66**, 2561 (1991).

[28] R. Becker-Szendy et al., Phys. Rev. **D46** 3720 (1992).

[29] K. S. Hirata et al., Phys. Lett. **B205**, 416 (1988).

[30] K. S. Hirata et al., Phys. Lett. **B280**, 146 (1992).

[31] Y. Fukuda et al., Phys. Lett. **B335**, 237 (1994).

[32] Y. Fukuda et al., Phys. Lett. **433**, 9 (1998).

[33] Y. Fukuda et al., Phys. Rev. Lett. **81**, 1562 (1998).

[34] E. W. Beir et al., Phys. Lett. **B283**, 446 (1992).

[35] W. W. M. Allison et al., Phys. Lett. **B391**, 491 (1997).

[36] W. W. M. Allison et al., Phys. Lett. **B427**, 217 (1998).

[37] W. W. M. Allison et al., Phys. Lett. **B449**, 137 (1999).

[38] W. A. Mann, Nucl. Phys. **B(Proc. Suppl.) 91**, 134 (2000).

[39] W. W. M. Allison et al., Phys. Lett. **D71**, 052005 (2005).

[40] T. Kafka, Nucl. Phys. **B(Proc. Suppl.) 87**, 186 (2000).

[41] M. Sanchez et al., Phys. Rev. **D68**, 113004 (2003).

[42] T. Kajita and Y. Totsuka, Rev. Mod. Phys. **73**, 85 (2001).

[43] K. Kaneyuki, Nucl. Phys. **B(Proc.Suppl.)112**, 24 (2002).

[44] S. Fukuda et al., Phys. Rev. Lett. **86**, 5651 and 5656 (2001).

[45] G. Giacomelli and A. Margiotta, Eur. Phys. J. **C33**, S826 (2004).

[46] M. Ambrosio et al., Phys. Lett. **B566**, 35 (2003).

[47] M. Ambrosio et al., Phys. Lett. **B517**, 59 (2001).

[48] P. Adamson et al., Phys. Rev. **D73**, 072002 (2006).

[49] M. H. Ahn, et al., Submitted to Phys. Rev. **D74**, 072003 (2006); arXive:hep-ex/0606032.

[50] D. G. Michael, et al., (MINOS), Submitted to Phys. Rev. Lett., (2006); arXive:hep-ex/0607088.

[51] S. Yamamoto, et al., Phys. Rev. Lett. **96**, 181801 (2006).

[52] Y. Hayato, *Workshop on interactions of nuclear physics with neutrino and electron*, Jefferson Lab., Newport News, 4-5 May 2006.

[53] E. Aliu, et al., Phys. Rev. Lett. **94**, 081802 (2005).

[54] T. Araki, et al., (KamLAND), Phys. Rev. Lett. **94**, 081801 (2005).

[55] S. Nakayama, Nucl. Phys. **B139**, 41 (2005).

[56] Y. Oyama, et al., arXiv:hep-ex/0512041 (2005).

[57] M. Hasegawa et al., Phys. Rev. Lett. **95**, 252301 (2005).

[58] M. H. Ahn, et al., Phys. Rev. Lett. **93**, 051801 (2004).

[59] M. H. Ahn, et al., Phys. Rev. Lett. **90**, 041801 (2003).

[60] C. M. Mauger, *A Study of $\nu_\mu \leftrightarrow \nu_\tau$ vs $\nu_\mu \leftrightarrow \nu_s$ Neutrino Oscillation In Atmospheric Neutrinos Using a K2K near detector Measurement*, Ph.D. Thesis, SUNY at Stony Brook (2002).

[61] S. Zeller, *NOVE Workshop*, Venice, Italy 7-10 Feb., (2006).

[62] M. O. Wascko, **NuInt 05**, Nucl. Phys. **(Proc. Suppl.) 159**, 50 (2006); arXiv:hep-ex/0602050.

[63] J. L. Raaf, *A Measurement of the Neutral Current π^0 Cross Section at MiniBooNE*, Ph.D. Thesis, University of Cincinnati, Fermilab-Thesis, (2005).

[64] J. Monroe, Nucl. Phys. **B (Proc. Suppl.) 139**, 59 (2005):arXiv:hep-ex/0408019.

[65] H. A. Tanaka, Nucl. Phys. **B (Proc. Suppl.) 149**, 122, 227 (2005).

[66] S. Geer, Phys. Rev. **D57**, 6989 (1998).

[67] A. De Rujula, M. B. Gavela and P. Hernandez, Nucl. Phys. **B547, 21 (1999).**

[68] M. Apollonio, et al., arXive:hep-ph/0210192.

[69] J. J. Gomez-Cadenas and D. A. Haris, Ann. Rev. Nucl. Part. Sci. **52**, 53 (2002).

[70] M. Aoki, Y. Iwashitaa and M. Kuze, **B(Proc.Suppl.)149**, 411 (2005).

[71] A. Blondel, Eur. Phys. J. **A 24S2**, 183 (2005).

[72] Y. Itow, et al., **B(Proc.Suppl.)111**, 146 (2002).

[73] A. Para and M. Szleper, arXive:hep-ex/0110032.

[74] D. Ayres, et al., arXive:hep-ex/0210005.

[75] Milind V. Diwan, *Heavy Quarks and Leptons*, San Juan, 89-109 (2004); arXive:hep-ex/0407047.

[76] P. Zucchelli, Phys. Lett. **B532**, 166 (2002).

[77] L. B. Auerbach et al. Phys. Rev. **D66**, 015501 (2002).

[78] L. B. Auerbach et al. Phys. Rev. **C64**, 065501 (2001).

[79] B. Armbruster et al., Phys. Rev. **D65**, 112001 (2002).

[80] Study Report, **ν-SNS Collaboration**, *Neutrino Program at the SNS*, (2004).

[81] C. Volpe, Nucl. Phys. **A752**, 38 (2005).

[82] C. Volpe, J. Phys. **G30**, L1 (2004).

[83] C. Volpe, J. Phys. **G34**, R1 (2007); arXive:hep-ph/0605033.

[84] J. Serreau and C. Volpe, Phys. Rev. **C70**, 055502 (2004).

[85] C. Volpe, **B(Proc.Suppl.)155**, 97 (2006).

[86] G. C. McLaughlin, Phys. Rev. **C70**, 045804 (2004).

[87] G. C. McLaughlin and C. Volpe, Phys. Lett. **B591**, 229 (2004).

[88] N. Jachowicz and G. C. McLaughlin, Phys. Rev. Lett. **96**, 172301 (2006).

[89] N. Jachowicz and G. C. McLaughlin, Eur. Phys. J. **A 27S1**, 41 (2006).

[90] C. Volpe, J. Phys. **G31**, 903 (2005).

[91] J. S. O'Connell, T. W. Donnelly and J. D. Walecka, Phys. Rev. **C6**, 719 (1972).

[92] H. Uberall, B. A. Lamers, J. D. Langworthy and F. J. Kelly, Phys. Rev. **C6**, 1911 (1972).

[93] T. W. Donnelly and J. D. Walecka, Phys. Lett. **B41**, 275 (1972).

[94] T. W. Donnelly, Phys. Lett. **B43**, 93 (1973).

[95] J. B. Longworthy, B. A. Lamers and H. Uberall, Nucl. Phys. **A280**, 351 (1977).

[96] W. C. Haxton, Phys. Rev. **D36**, 2283 (1983).

[97] C. Maieron, M. C. Martinez, J. A. Caballero and J. M. Udias, Phys. Rev. **C68**, 048501 (2003).

[98] B. Goulard and H. Primakoff, Phys. Rev. **135B**, 1139 (1964).

[99] J. S. Bell and C. H. Llewllynsmith, Nucl. Phys. **B28**, 317 (1971).

[100] E. V. Bugaev, G. S. Bisnovatyi-Kogan, M. A. Rudzsky and Z. F. Seidov, Nucl. Phys. **A324**, 350 (1979).

[101] T. K. Gaisser and J. S. O'Connell, Phys. Rev. **D34**, 822 (1986).

[102] A. C. Hayes and I. S. Towner, Phys. Rev. **C61**, 044603 (2000).

[103] T. Kuramoto, M. Fukugita, Y. Kohyama and K. Kubodera, Nucl. Phys. **A512**, 711 (1990).

[104] A. K. Mann, Phys. Rev. **D48**, 422 (1993).

[105] G. Co, C. Bleve, I. De Mitri and D. Martello, Nucl.Phys. **(Proc.Suppl.)112**, 210 (2002).

[106] J. M. Udias and P. J. Mulders, Phys. Rev. Lett. **74**, 4993 (1995).

[107] H. Nakamura and R. Seki, Nucl. Phys. **(Proc.Suppl.)112**, 197 (2002).

[108] H. Kim, J. Piekarewicz and C. J. Horowitz, Phys. Rev. **C51**, 2739 (1995).

[109] J. Engel, E. Kolbe, K. Langanke and P. Vogel, Phys. Rev. **D48**, 3048 (1993).

[110] N. Auerbach, N. Van Giai and O. K. Vorov, Phys. Rev. **C56**, 2368 (1997).

[111] E. Kolbe, K. Langanke, F. K. Thielmann and P. Vogel, Phys. Rev. **C52**, 3437 (1995).

[112] E. Kolbe, K. Langanke and S. Krewald, Phys. Rev. **C51**, 1122 (1995).

[113] D. A. Krakauer et al., Phys. Rev. **C45**, 2450 (1992).

[114] J. Marteau, Nucl. Phys. **(Proc.Suppl.)112**, 203 (2002); Eur. Jour. **A5**, 183 (1999).

[115] T. S. Kosmas and E. Oset, Phys. Rev. **C53**, 1409 (1996).

[116] S. K. Singh and E. Oset, Phys. Rev. **C48**, 1246 (1993).

[117] M. Sajjad Athar, Shakeb Ahmad and S. K. Singh, Phys. Rev. **C71**, 045501 (2005).

[118] M. Sajjad Athar and S. K. Singh, Phys. Lett. **B591**, 69 (2004).

[119] M. Sajjad Athar, Shakeb Ahmad and S. K. Singh, Nucl. Phys. **A764**, 551 (2006).

[120] S. K. Singh and M. Sajjad Athar, Nucl. Phys. **B(Proc. Suppl.) 215**, 219 (2002).

[121] M. Sajjad Athar and S. K. Singh, Phys. Rev. **C61**, 028501 (2000).

[122] S. L. Adler, Ann. Phys. (N.Y.) **50**, 189 (1968).

[123] P. A. Zucker, Phys. Rev. **D4**, 3350 (1971).

[124] P. A. Schreiner and F. von Hippel, Nucl. Phys. **B58**, 333 (1973).

[125] P. Andreadis, A. Baltas, A. Le Yaouanc, L. Oliver, O. Pene and J. C. Raynal, Ann. Phys. 88, 242 (1974).

[126] G. L. Fogli and G. Nardulli, Nucl. Phys. **B160**, 116 (1979).

[127] G. L. Fogli and G. Nardulli, Nucl. Phys. **B165**, 162 (1980).

[128] S. Rai Choudhary and H. K. Dewan, Phys. Rev. **D28**, 79 (1983).

[129] E. A. Paschos, L. Pasquali and J. Y. Yu, Nucl.Phys **B588**, 263 (2000).

[130] E. A. Paschos, Nucl. Phys. **B (Proc. Suppl.) 112**, 89 (2002).

[131] E. A. Paschos and J. Y. Yu, Phys.Rev. **D65**, 033002 (2002).

[132] T. Sato and T. S. H. Lee, Phys. Rev. **C63**, 055201 (2001); T. Sato, D. Uno and T. S. H. Lee, Phys. Rev. **C67**, 065201 (2003), arXiv:nucl-th/0303050.

[133] O. Lalakulich and E. A. Paschos, Phys. Rev. **D71**, 074003 (2005), arXiv:hep-ph/0501109.

[134] H. Kim, S. Schramm and C. J. Horowitz, Phys. Rev. **C53**, 2468 (1996).

[135] S. K. Singh, M. J. Vicente Vacas and E. Oset, Phys. Lett. **B416**, 23 (1998).

[136] M. Sajjad Athar, S. Ahmad and S. K. Singh, Eur. J. of Phys. **A24**, 459 (2005).

[137] L. Alvarez-Ruso, S. K. Singh and M. J. Vicente Vacas, Phys. Rev. **C57**, 2693 (1998); L. Alvarez-Ruso, *Excitation of Baryonic Resonances Induced by Nucleons and leptons*, Ph.D. Thesis, Departmento de Fisica Teorica, University de valencia, (1999).

[138] S.K.Singh, M.Sajjad Athar and Shakeb Ahmad, Phys. Rev. Lett. **96** 241801 (2006), arXiv:nucl-th/0601045,

[139] S. K. Singh, M. Sajjad Athar and Shakeb Ahmad, Pramana- J. Phys., **Vol. 66**, 689 (2006), arXiv:nucl-th/0507016.

[140] S. L. Adler, S. Nussinov and E.A.Paschos, Phys. Rev. **D9**, 2125 (1974).

[141] H. Kim, S. Schramm and C. J. Horowitz, Phys. Rev. **C53**, 3131 (1996).

[142] J. Marteau, J. Delorme and M. Ericson, Nucl. Instrum. Meth. **A451**, 76 (2000).

[143] S. K. Singh, M. Sajjad Athar and Shakeb Ahmad, Phys. Lett. **B641**, 159 (2006); arXiv:nucl-th/0603001.

[144] W. Cassing, M. Kant, K. Langanke and P. Vogel, arXiv:nucl-th/060109, (2006).

[145] J. Y. Yu, E. A. Pashos, D. P. Roy and I. Scheinbein, J. Korean Phys. Soc. **45**, S335, (2004); arXiv:hep-ph/03121230.

[146] E. A. Paschos, M. Sakuda, I. Scheinbein and J. Y. Yu, Nucl. Phys. **B139**, 125 (2005); E. A. Paschos, J. Y. Yu and M. Sakuda, Phys. Rev. **D69**, 014013 (2004), arXiv:hep-ph/0308130.

[147] O. Lalakulich, E. A. Paschos and G. Piranishvili, Phys. Rev. **D74**, 014009 (2006), arXiv:hep-ph/0602210.

[148] M. Valverde and M. J. Vicente Vacas, Private communication.

[149] S. K. Singh and E. Oset, Nucl. Phys. **A542**, 587 (1992).

[150] S. K. Singh, N. C. Mukhopadhyay and E. Oset, Phys. Rev. **C57**, 2687 (1998).

[151] J. Nieves, J. E. Amaro, M. Valverde, Phys. Rev. **C70**, 055503 (2004).

[152] A. Gill, J. Nieves and E. Oset, Nucl. Phys. **A627**, 543 (1997).

[153] R. C. Carrasco and E. Oset, Nucl. Phys. **A536**, 445(1992).

[154] E. Oset, D. Strottman, H. Toki and J. Navarro, Phys. Rev. **C48**, 2395 (1993).

[155] E. Oset, P. Fernandez de Cordoba, L. L. Salcedo and R. Brockmann, Phys. Rep. **188**, 79 (1990).

[156] J. Engel, Phys. Rev. **C57**, 2004 (1998).

[157] E. Kolbe, K. Langanke, G. Martinez-Pinedo and P. Vogel, J. Phys. **G29**, 2569 (2003).

[158] J. Engel, G. C. McLaughlin and C. Volpe, Phys. Rev. **D67**, 013005 (2003).

[159] E. Kolbe and K. Langanke, Phys. Rev. **C63**, 025802 (2001).

[160] C. Volpe, N. Auerbach, G. Colo and N. Van Giani, Phys. Rev. **C65**, 044603 (2002).

[161] E. Oset and L. L. Salcedo, Nucl. Phys., **A468**, 631 (1987).

[162] C. Garcia Recio, E. Oset, L. L. Salcedo, D. Strottman and M. J. Lopez, Nucl. Phys., **A526**, 685 (1991).

[163] H. Hirenzaki, J. Nieves, E. Oset and M. J. Vicente Vacas, Phys. lett. **B304**, 198 (1993).

[164] R. C. Carrasco, J. Nieves and E. Oset, Nucl. Phys. **A565**, 797 (1993).

[165] E. Oset and W. Weise, Phys. Lett., **B77**, 159 (1978).

[166] E. Oset and W. Weise, Nucl. Phys., **A319**, 477 (1979).

[167] E. Oset and W. Weise, Nucl. Phys., **A448**, 597 (1986).

[168] E. Oset, H. Toki and W. Weise, Phys. Rep., **83**, 282 (1982).

[169] E. Oset, L. L. Salcedo and D. Strottman, Phys. Lett., **B165**, 13 (1985).

[170] J. Nieves, E. Oset and C. Garcia Recio, Nucl. Phys. **A443**, 570 (1985)

[171] M. Hirata, F. Lenz and K. Yazaki, Ann. Phys. (N.Y.) **120**, 205 (1979)

[172] J. H. Koch, E. J. Moniz and N. Ohtsuka, Ann. of Phys. **154**, 99 (1984).

[173] H. M. Hofmann, Z. Phys. **A289**, 273 (1979).

[174] E. Oset and D. Strottman, Phys. Rev. **C42**, 2454 (1990).

[175] L. L. Salcedo, E. Oset, M. J. Vicente Vacas and C. Garcia-Recio, Nucl. Phys. **A 484**, 557 (1988).

[176] M. J. Vicente Vacas, Private Communication; M. J. Vicente Vacas, M. Kh Khankhasaev and S. G. Mashnik, nucl-th/9412023.

[177] Jean-Eric Campagne, Nucl. Phys. **B (Proc. Suppl.) 155**, 185 (2006); Jean-Eric Campagne and A. Cazes, Eur. Phys. J., **C45**, 643 (2006); Jean-Eric Campagne, NuFact05, Capri, Italy, 12-20 Jun 2005; arXive:hep-ex/0510029.

[178] W. A. Mann et al., **ANL**, Phys. Rev. Lett. **31**, 844 (1973).

[179] S. J. Barish et al., **ANL**, Phys. Rev. **D16**, 3103 (1977).

[180] N. J. Baker et al., **BNL**, Phys.Rev. **D23**, 2499 (1981).

[181] T. Kitagaki et al., **FANL**, Phys.Rev. **D26**, 436 (1983).

[182] L. B. Auerbach et al., **LSND**, Phys. Rev. **C66**, 015501 (2002).

[183] M. Pohl et al., **GGM**, Lett. Nuovo Cimento **26**, 332 (1979).

[184] S. Bonetti et al., **GGM**, Nuovo Cimento **38**, 260 (1977).

[185] J. Brunner et al., **SKAT**, Z. Phys. **C45**, 551 (1990).

[186] S. V. Belikov et al., **Serpukov**, Z. Phys. **A320**, 260 (177).

[187] N. Armenise et al., **GGM**, Nucl. Phys. **B152**, 365 (1979).

[188] G. Fanourakis et al., **BNL**, Phys. Rev. **D21**, 562 (1980).

[189] V. Bernard, L. Elouadrhiri and U. G. Meissner, J. Phys. **G28**, R1 (2002); arXive:hep-ph/0107088.

[190] P. E. Bosted, Phys. Rev. **C51**, 409 (1995).

[191] H. Budd, A.Bodek and J. Arrington, **NuInt02**; arXive:hep-ex/0308005.

[192] H. Budd, A.Bodek and J. Arrington, Nucl. Phys. **B(Proc. Suppl.)139**, 90 (2005); arXive:hep-ex/0410055.

[193] J. J. Kelly, Phys. Rev. **C70**, 068202 (2004).

[194] R. Bradford, A.Bodek, H. Budd and J. Arrington, **NuInt05**, Nucl. Phys. **(Proc. Suppl.)159**, 127 (2006); arXive:hep-ex/0602017.

[195] M. K. Jones et al., Phys. Rev. Lett. **84**, 1398 (2000).

[196] A. F. Krutov and V. E. Troitsky, Eur. Phys. J. **A16**, 285 (2003); arXive:hep-ph/0202183.

[197] S. Galster et al. Nucl. Phys. **B32**, 221 (1971).

[198] E. Oset, in *SERC School in Nuclear Physics*, Ed. by B. K. Jain, World Sceintific, Singapore (1987).

[199] A. L. Fetter and J. D. Walecka, *Quantum Theory of Many Particle Systems*, McGraw Hill (1971).

[200] E. Oset, in *Quarks, Mesons and Isobars*, Ed. by R. Guardiola and A. Polls, World Sceintific, Singapore.

[201] E. Oset and A. Planques-Mestre, Nucl. Phys. **A359**, 289 (1981).

[202] C. Gracia Recio, E. Oset and L. L. Salcedo, Phys. Rev. **C37**, 194 (1988).

[203] G. A. Cowan and W. C. Haxton, Science, **216**, 51 (1982).

[204] C. M. Lederer and V. S. Shirley, Ed *Table of Isotopes*, John Wiley and Sons., New York (1978).

[205] R. Machleidt, in *Advances in Nuclear Physics*, Ed. by J. W. Negele and E. Vogt, **Vol.19**, p189, Plenum, New York (1989).

[206] H. Behrens and W. Buhring, *Electron Radial Wave Functions and Nuclear Beta Decay*, Clarendon Press, Oxford, (1982).

[207] G. Co and J. Heisenberg, Phys. Lett. **B197**, 489 (1987).

[208] Y. Jin, D. S. Onley and L. E. Wright, Phys. Rev. **C50**, 168 (1994).

[209] D. R. Yennie, F. L. Boos and D. G. Ravenhall, Phys. Rev. **137**, B882 (1965).

[210] F. Lenz and R. Rosenfelder, Nucl. Phys. **A176**, 513 (1971).

[211] K. S. Kim and L. E. Wright, (2002);arXive:nucl-th/0208039.

[212] C. Giusti and P. D. Pacati, Nucl. Phys. **A473**, 717 (1987).

[213] P. Gueye et al., Phys. Rev. **C60**, 044308 (1999).

[214] F. T. Avignone III and Y. V. Efremenko, J. of Phys. **G29**, 2615 (2003).

[215] H. de Vries, C. W. de Jager and C. de Vries, At. Data Nucl. Data Tables **36**, 495 (1987)C; W. de Jager, H. de Vries and C. de Vries At. Data Nucl. Data Tables **14**, 479 (1974).

[216] C. Volpe, N. Auerbach, G. Colo, T. Suzuki and N. Van Giai, Phys. Rev. C **62** (2000) 015501.

[217] T. Suzuki and H. Sagawa, Nucl. Phys. A **718** (2003) 446c.

[218] E. Kolbe, K. Langanke and P. Vogel, Nucl. Phys. **A652**, 91 (1999).

[219] C. Athanassopoulos et al., Phys. Rev. **C55**, 2078 (1997).

[220] R. Maschuw, Prog. Part. Nucl. Phys. **40**, 183 (1998).

[221] S. L. Mintz, J. of Phys. **G28**, 451 (2002).

[222] G. C. McLaughlin, Phys. Rev. **C70**, 045804 (2004).

[223] N. Jachowicz, K. Heyde and J. Ryckebusch, Phys. Rev. **C66**, 055501 (2002).

[224] M. Pourkaviani and S. L. Mintz, J. of Phys. **G16**, 569 (1990).

[225] M. Fukugita, Y. Kohyama and K. Kubodera, Phys. Lett. **B212**, 139 (1988).

[226] D. S. Miller, J. R. Wilson and R. W. Mayle, Astrophys. J. **415**, 278 (1993); H. T. Janka and W. Hillebrandt, Astron. Astrophys. **224**, 49 (1989).

[227] T. Totani, K. Sato, H. E. Dalhed and J. R. Wilson, Astrophys. J. **496**, 216 (1998); H. T. Janka and E. Muller, Phys. Rep. **256**, 135 (1995); T. A. Thomson, A. D. Burrows and P. A. Pinto, Astrophys. J. **592**, 434 (2003).

[228] M. T. Keil, G. G. Raffelt and H. T. Janka, Astrophys. J. **590**, 971 (2003); G. G. Raffelt, M. T. Keil, R. Buras, H. T. Janka and M. Rampp, arXive:astro-ph/0303226(2003); G. G. Raffelt, *Stars as Laboratories for Fundamental Physics* (The University of Chicago Press, Chicago, 1996), pp.395-411.

[229] R. N. Boyd, G. C. McLaughlin, A. St. J. Murphy and P. F. Smith, J. Phys. **G29**, 2543 (2003); J. J. Zach et al, Nucl. Instr. Methods **A484**, 194 (2002).

[230] M. Aglietta et al., Nouvo Cimento **A105**, 1793 (1992); M. Selvi, Nucl. Phys. (**Proc. Suppl.**)**138**, 115 (2005); arXive:hep-ph/0307287 (2003).

[231] D. Michael, Nucl. Phys. **B (Proc. Suppl.) 112**, 1(2003).

[232] E. Kolbe, K. Langanke and G. Martinez-Pinedo Phys. Rev. **C60**, 052801(R) (1999).

[233] J. Toivanen, E. Kolbe, K. Langanke, G. Martinez-Pinedo and P. Vogel, Nucl. Phys. **A694**, 395 (2001).

[234] S. E. Woosley, D. H. Hartmann, R. D. Hoffman and W. C. Haxton, Astrophys. J. **356**, 272 (1990).

[235] K. L. Miller et al. Phys. Rev. **D26**, 537 (1982).

[236] T. Kitagaki et al. Phys. Rev. **D28**, 4366 (1983); ibid **D34** 2554 (1986); ibid **D42** 1331 (1990).

[237] W. Lee et al., Phys. Rev. Lett. **38**, 202 (1977).

[238] J. Bell et al., Phys. Rev. Lett. **41**, 1008 (1978).

[239] P. Allen et al., Nucl. Phys. **B176**, 269 (1980).

[240] P. Allen et al., Nucl. Phys. **B264**, 221 (1986).

[241] D. Allasia et al., Nucl. Phys. **B343**, 285 (1990).

[242] J. Campbell et al., Phys. Rev. Lett. **30**, 335 (1973).

[243] S. J. Barish et al., Phys. Rev. **D19**, 2521 (1979).

[244] G. M. Radecky et al., Phys. Rev. **D25**, 1161 (1982).

[245] T. Kitagaki et al., Phys.Rev. **D34**, 2554 (1986).

[246] H. W. Hammer and D. Drechsel, Z. Phys. **A353**, 321 (1995).

[247] M. J. Dekker, P. J. Brussaard and J. A. Tjon, Phys. Rev. **C49**, 2650 (1994).

[248] A. W. Thomas and W. Weise, *The Structure of the Nucleon*, Wiley-VCH, Berlin, (2001).

[249] S. L. Adler, Phys. Rev. **D12**, 2644 (1975).

[250] J. Bijtebier, Nucl. Phys. **B21**, 158 (1970).

[251] S. K. Singh, Nucl. Phys. **B (Proc. Suppl) 112**, 77 (2002).

[252] N C. Mukhopadhyay et al., Nucl. Phys. **A633**, 481 (1998).

[253] T. R. Hemmert, B. R. Holstein and N. C. Mukhopadhyay, Phys. Rev. **D51**, 158 (1995).

[254] J. Liu, N. C. Mukhopadhyay and L. Zhang, Phys. Rev. **C52**, 158 (1995).

[255] J. Liu and N. C. Mukhopadhyay, Phys. Rev. **C52**, 1630 (1995).

[256] R. P. Feynman, M. Kislinger and F. Ravndal, Phys. Rev. **D3**, 2706 (1971).

[257] V. D. Burkert and T. S. H. Lee, Int. J. Mod. Phys. **E13**, 1035 (2004).

[258] Th. Wilbois, P. Wilhelm and H. Arenhovel, Phys. Rev. **C57**, 295 (1998).

[259] R. Beck, Phys. Rev. Lett. **78**, 606 (1997).

[260] A. J. Buchmann, E. Hernandez and A. Faessler, Phys. Rev. **C55**, 448 (1997).

[261] O. Hanstein, D. Drecshel and L. Tiator, Phys. Lett. **B385**, 45 (1996).

[262] M. Benmerouche and N. C. Mukhopadhyay, Phys. Rev. **D46**, 101 (1992).

[263] T. Leitner, L. Alvarez-Ruso and U. Mosel, **PANIC 05, AIP**, Conf. Proc. **842**, (2006); arXiv:nucl-th/0601021.

[264] L. Alvarez-Ruso, S. K. Singh and M. J. Vicente Vacas, Phys. Rev. **C59**, 3386 (1999).

[265] P. A. Schreiner and F. von Hippel, Phys. Rev. Lett. **30**, 339 (1973).

[266] M. Benmerrouche, R. M. Davidson and N. C. Mukhopaghyay, Phys. Rev. **C39**, 2339 (1989).

[267] M. Post, *Hadronic Spectral Functions in Nuclear Matter*, PhD thesis, Universitat Giessen, 2003.

[268] G. Penner and U. Mosel, Phys. Rev. **C66**, 055211 (2002).

[269] W. Lerche et al., Phys. Lett. **B78**, 510 (1978).

[270] T. Bolognese, J. P. Engel, J. L. Guyonnet and J. L. Riester, Phys. Lett. **B81**, 393 (1979).

[271] H. J. Grabosch et al., Z. Phys. **C41**, 527 (1989).

[272] V. V. Ammosov, Sov. J. Nucl. Phys. **50**, 57 (1988).

[273] V. V. Ammosov, Sov. J. Nucl. Phys. **50**, 67 (1989).

[274] H. Faissner et al., (Aachen-Padova), Phys. Lett. **B125**, 230 (1983).

[275] F. Bergsma et al , CHARM Coll., Phys. Lett. **B157**, 469 (1985).

[276] E. Isiksal, D. Rein and J. G. Morfin, (Gargamelli), Phys. Rev. Lett. **52**, 1096 (1984).

[277] C. Baltay et al., Phys. Rev. Lett. **57**, 2629 (1986).

[278] H. J. Grabosch et al., SKAT Coll., Z. Phys.**C31**, 203 (1986).

[279] P. Marage et al., BEBC (WA59) Coll., Phys. Lett. **B140**, 137 (1984).

[280] P. Marage et al., BEBC (WA59) Coll., Z. Phys. **C31**, 191 (1986).

[281] P. Marage et al., BEBC (WA59) Coll., Z. Phys. **C43**, 523 (1989).

[282] P. P. Allport et al., BEBC (WA59) Coll., Z. Phys. **C43**, 523 (1989).

[283] V. V. Ammosov et al., E180 Coll., Sov. J. Nucl. Phys. **45**, 1029 (1987).

[284] M. Aderholz et al., E632 Coll., Phys. Rev. Lett. **63**, 2349 (1989).

[285] S. Willocq et al., E632 Coll., Phys. Rev. **D47**, 2661 (1993).

[286] P. Vilain et al., CHARM-II Coll., Phys. Lett. **B313**, 267 (1993).

[287] D. Drechsel and L. Tiator, Ed. **NSTAR 2001**, World Scientific, New Jersey (2001).

[288] F. Vissani and A. Yu Smirnov, Phys. Lett. **B432**, 376 (1998).

[289] W. Winter, *Neutrino Oscillations*, **Venice 2006, 165**, (2006); arXiv:hep-ph/0603012, (2006).

[290] A. Donini, E. Fernandez-Martinez, D. Meloni and S. Rigolin, Nucl. Phys. **B743**, 41 (2006).

[291] P. Strolin, Nucl. Phys. **B (Proc. Suppl.) 155**, 148 (2006).

[292] C. Albright et al., **FERMILAB-FN-0692**; arXiv:hep-ex/0008064, (2000).

[293] M. Mezzetto, J. Phys. G: Nucl. Part. Phys. **29**, 1781 (2003).

[294] A. Donini, E.Fernandez-Martinez, P. Migliozzi, S. Rigolin,, L. Scotto Lavina, T. Tabarelli de Fatis and F. Terranova, arXiv:hep-ph/0604229, (2006).

[295] J. Burguet Castell, D. Casper, J. J. Gomez-Cadenas, P. Hernandez and F. Sanchez, Nucl. Phys. **B695**, 217 (2004).

[296] P. Huber, M. Lindner, M. Rolinec and W. Winter, Phys. Rev. **D73**, 053002 (2006).

[297] K. S. McFarland, Nucl. Phys. **(Proc. Suppl.)159**, 107 (2006); arXiv:physics/0605088.

[298] D Naples et al., Intl. J. Mod. Phys. **A20**, 3078 (2005).

[299] D. S. Ayres et al., arXiv:hep-ex/0503053, (2005).

[300] S. Brice et al., Nucl. Phys. **B (Proc. Suppl.) 139**, 317 (2005).

[301] M. Benedikt et al., EURISOL-DS-TASK12-TN-06-01 (2006).

[302] D. Rein, L. M. Sehgal, Nucl. Phys. **B223**, 29 (1983).

[303] K. S. Lackner, Nucl. Phys. **B153**, 571 (1970).

[304] A. A. Belkov and B. Z. Kopeliovich, Sov. J. Nucl. Phys. **46**, 449 (1987).

[305] S. L. Adler, Phys. Rev. **135**, B963 (1964).

[306] E. A. Paschos, A. kartavtsev and G. J. Gounaris, Phys. Rev. **D74**, 054007 (2006); arXiv:hep-ph/0512139.

[307] N. G. kelkar, E. Oset and P. Fernandez de Cordoba, Phys. Rev. bf C55, 1964 (1997).

[308] W. Rarita and J. Schwinger, Phys. Rev. **C60**, 61 (1941).

[309] T. Ericson and W. Weise, *Pion and Nuclei*, Claredon Press, Oxfors, (1988).

[310] E. Oset, Y. Futami and H. Toki, Nucl. Phys. **A448**, 597 (1986).

[311] R. J. Glauber, *Lectures in Theoretical Physics*, ed. by W. E. Brittin and L. G. Dunham, Interscience Publishers, Inc., New York, **Volume I**, 315 (1959).

[312] M. Mezzetto, Nucl. Phys. **B (Proc. Suppl.) 149**, 179 (2005).

[313] M. Mezzetto, Nucl. Phys. **B (Proc. Suppl.) 155**, 214 (2006), arXive:hep-ex/0511005.

[314] J. Burguet-Castell, D. Casper, E. Couce, J. J. Gomez-Cadenas and P. Hernandez, Nucl. Phys. **B725**, 306(2005), arXive:hep ph/0503021.

[315] A. Donini, et al., Nucl. Phys. **B710**, 402 (2005).

[316] F. Terranova, A. Marotta, P. Migliozzi and M. Spinetti, Eur. Phys. J. **C38**, 69 (2004).

[317] B. Autin, et al., J. Phys. **G29**, 1785 (2003).

[318] M. Honda, T. Kajita, K. Kasahara and S. Midorikawa, Phys. Rev. **D70**, 043008 (2004); arXive:astro-ph/0404457; G. Battistoni, A. Ferrari, T. Montaruli and P. R. Sala, Astroparicle Phy. **19**, 269 (2003); T. K. Gaisser and M. Honda, Ann. Rev. Nucl. Part. Sci. **52**, 153 (2002).

[319] M. Honda, T. Kajita, K. Kasahara and S. Midorikawa, Phys. Rev. **D52**, 4985 (1995).

[320] G. Barr, T. K. Gaisser and T. Stanev, Phys. Rev. **D39**, 3532 (1989).

[321] V. Plyaskin, arXive:hep-ph/0303146(2003).